PhD Thesis

Design and development of synthetic anion transporters: Towards therapeutic prospects

A dissertation submitted to the

Indian Institute of Technology Guwahati

as partial fulfilment for the Degree of
Doctor of Philosophy in Chemistry

By

Sribash Das

Department of Chemistry
Indian Institute of Technology Guwahati
Guwahati 781039, Assam, India

To
My Beloved Family

Declaration

13th March, 2024

I declare that the thesis titled "Design and development of synthetic anion transporters: Towards therapeutic prospects" submitted to the Department of Chemistry, Indian Institute of Technology Guwahati, for the degree of Doctor of Philosophy, is a concise research contribution. I adhere to standard scientific reporting practices, duly acknowledging the work of other investigators where applicable.

Additionally, I affirm that this work has not been submitted elsewhere for any degree, diploma, associateship, or membership, to the best of my knowledge.

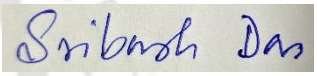

(**Sribash Das**)

भारतीय प्रौद्योगिकी संस्थान गुवाहाटी
Indian Institute of Technology Guwahati
Prof. Debasis Manna
Department of Chemistry
Phone: +91-0361-258-2325
Fax: +91-0361-258-2349
E-mail: dmanna@iitg.ac.in

13th March, 2024

To whom it may concern

This certifies that Mr. Sribash Das (Roll No. 186122049) is the sole researcher behind the thesis titled "Design and development of synthetic anion transporters: Towards therapeutic prospects," submitted for the Ph.D. degree in Chemistry at the Indian Institute of Technology Guwahati. All information and data presented in the thesis are his original findings. Mr. Sribash Das conducted meticulous scientific investigations and adhered to laboratory guidelines throughout his Ph.D. tenure. This thesis, or any part thereof, has not been previously submitted for any degree or diploma.

Debasis Manna

(**Prof. Debasis Manna**)

Contents

Chapter 2

Development of tryptophan-based ion transporter for efficient chloride ion transport across lipid membranes

Chapter 4

Development multi-stimuli controlled release of a transmembrane chloride ion carrier from a sulfonium-linked procarrier

Acknowledgements

I humbly express my deep gratitude to the Supreme Being, whose kind favour bestowed on me the necessary inspiration to successfully complete this task.

First and foremost, I would like to sincerely thank my supervisor, Prof. Debasis Manna, for his consistent mentoring and valuable ideas throughout my Ph.D. journey. His meticulous counsel has greatly enhanced my scientific understanding. Since the beginning of my research journey, I have been surrounded by a stimulating atmosphere that has greatly facilitated my understanding of this remarkable journey, distinguished by several educational experiences. His unwavering advice, encouragement, and active engagement significantly enhanced my scientific understanding to a higher degree. I am very fortunate to have a mentor like him who always endeavours to provide assistance for the betterment of pupils. I feel very privileged and fortunate to be affiliated with his study group. In addition to his studies, his opinions and beliefs about life greatly assist me in navigating the challenges that arise in my own life as well. I express my gratitude to you, sir, for serving as my guide, mentor, and philosopher.

I would like to express my gratitude to my doctorate committee members, Prof. Manish Kumar, Dr. Animesh Das, Dr. Kalyan Raidongia, Prof. Kalyanasis Sahu, and Prof. Tarun K. Panda for their ongoing guidance and thorough assessment of my research endeavours.

I like to convey my appreciation to the faculties and staff of the Department of Chemistry for their unwavering assistance and support. I am very grateful to the Department of Chemistry and CIF (IIT Guwahati) for granting me access to a wide range of advanced instrument facilities, which have greatly enhanced the quality of my study. I am really grateful to CSIR for awarding me the scholarship that enabled me to do my studies.

I would like to acknowledge all of my past and present lab members, including Dr. Ashalata Roy, Dr. Subhankar Panda, Dr. Abhishek Saha, Dr. Nirmalya Pradhan, Dr. Nasim Akhtar, Dr. Oindrila Biswas, Dr. Subhasis Dey, Dr. Anjali Patel, Dr. Shitaljit Sharma, Ms. Priyanka Mazumder, Mr. Gunanka Hazarika, Mr. Biswa Mohan Prusty, Ms. Soumya Srimayee, Ms. Nikumoni Das, Ms. Rama Karn, Mr. Mrinal Kanti Kar, Mr. Rahul Kumar, Dr. Md. Intekhab Alam, and Ms. Suravi Chauhan. They have created a supportive and amicable environment in the lab, which has greatly alleviated the stress of my research and personal life. I am grateful to every one of you for being an integral part of my family, and your presence will undoubtedly be etched in my heart forever.

I would like to express my heartfelt gratitude to all of my friends, particularly Mr. Somnath Paik, Mr. Koushik Sarkar, Mr. Anirban Mandol, Mr. Ajnabiul Hoque, and my love Dr. Kakoli Malakar, for their unwavering support and encouragement.

Finally, I must acknowledge that my Ph.D. achievements would not have been possible without recognizing the contributions of my parents. In order to achieve my aspirations, they have made significant sacrifices that I am unable to adequately articulate. The assistance and blessings of others have been important to my achievements so far in life. Additionally, I would like to express my gratitude for the boundless affection, assistance, and well wishes bestowed upon me by my grandma, grandfather, maternal uncles, aunties, and all my brothers.

I express my gratitude to each and every one of you for being a significant and unforgettable presence in my life.

Mr. Sribash Das

Abstract

The thesis, titled "***Design and development of synthetic anion transporters: Towards therapeutic prospects***," provides a brief description of several kinds of novel anionophores that exhibit significant promise for therapeutic applications. This thesis includes insights on the recognition, transportation across cell membranes, and potential therapeutic applications. The thesis is divided into four chapters, based on experimental findings obtained during the research periods.

Chapter 1 primarily explored the many possible applications of anionophores in addressing a wide variety of therapeutic diseases. It additionally reviewed their probable mode of action by a comprehensive review of current research.

Chapter 2 we developed a new class of amino acid (tryptophan) based derivatives. The tryptophan based receptors selectively transport the Cl^- ions across the lipid bilayer. Detailed transport activity and mechanistic study of the receptors are discussed.

Chapter 3 explores the synthesis and characterization of a 4-aminoquinazoline analogue, which is an anion-induced molecular switch and pH-responsive anionophore. The compound's pH-switchable nature is crucial in the acidic microenvironment of cancer cells. Its transport activity is assessed under various physiological conditions, showing increased efficacy in facilitating chloride ion transport under acidic conditions. Further exploration includes antibacterial studies on gram-positive and gram-negative bacterial cell lines.

Chapter 4 this work focuses on designing and synthesizing multi-stimuli responsive proanionophore molecules using a novel class of sulphonium-based water-soluble proanionophores. The aim is to improve the efficiency and specificity of anion transport mechanisms by addressing conventional challenges such as poor deliverability, selectivity, and uptake.

List of Abbreviation

ATP	Adenosine triphosphate
YFP	Yellow fluorescent protein
FRT	Fisher rat thyroid
RVD	Regulatory volume decrease
CHOL	Cholesterol
PARP	Poly(ADP-ribose) polymerase
DFT	Density Functional Theory
HPTS	8-Hydroxypyrene-1,3,6-trisulfonate
Lucigenin	*N*,*N*′-Dimethyl-9,9′-biacridinium dinitrate
AVD	Apoptotic Volume Decline
VRACs	Certain volume-regulated anion channels
GLUT	Glucose transporter
VSOR	Volume-sensitive outwardly rectifying
GSH	Glutathione
ROS	Reactive oxygen species
RGD	Arginyl-glycyl-aspartic acid
NQO1	NAD(P)H quinone oxidoreductase 1
DNA	Deoxyribonucleic acid
Calcein	4',5'-Bis(*N*,*N*-bis(carboxymethyl)aminomethyl)fluorescein acetoxymethyl ester
BLM	Black lipid membrane
MTT	3-(4,5-dimethylthiazol-2-yl)-2,5-diphenyltetrazolium bromide
NMR	Nuclear Magnetic Resonance
UV	Ultraviolet
DMSO	Dimethyl sulfoxide
DMF	Dimethylformamide
DCM	Dichloromethane
DCC	Dicyclohexyl carbodiimide

TFA	Trifluoroacetic acid
HBTU	Hexafluorophosphate Benzotriazole Tetramethyl Uronium
Et_3N	Triethyl amine
EtOH	Ethanol
FTIR	Fourier-transform infrared spectroscopy
H_2O	Water
IC_{50}	The concentration of an inhibitor which causes 50% inhibition of a maximal activity
EC_{50}	Half maximal effective concentration
KCl	Potassium chloride
K_a	Association constant
LUV	Large unilamellar vesicles
KCl	Potassium chloride
LUV	Large unilamellar vesicles
m/z	Mass to charge ratio
M.P	Melting point
MeOH	Methanol
λ_{ex}	Excitation wavelength
λ_{em}	Emission wavelength
TBACl	Tetrabutylammonium chloride
TBABr	Tetrabutylammonium bromide
$TBANO_3$	Tetrabutylammonium nitrate
TBAF	Tetrabutylammonium fluoride
TBAI	Tetrabutylammonium iodide
EYPC	Egg-yolk phosphatidylcholine
CHOL	Cholesterol
THF	Tetrahydrofuran
ISE	Ion selective electrode
FCCP	4-(trifluoromethoxy)phenylhydrazone
Val	Valinomycin

HPLC	High-performance liquid chromatography
HRMS	High-resolution mass spectra
NOESY	Nuclear Overhauser Effect Spectroscopy
IF	Fractional emission intensity
PBS	Phosphate buffered saline
MALDI-TOF	Matrix-Assisted Laser Desorption/Ionization-Time Of Flight
ESI	Electrospray ionization
CFTR	Cystic fibrosis transmembrane conductance regulator
CF	Cystic fibrosis
CaCC	Ca^{2+}-activated Cl^- channel
CDC	Centers for Disease Control and Prevention
MIC	Minimum inhibitory concentration
MQAE	*N*-(Ethoxycarbonylmethyl)-6-methoxyquinolinium bromide
LUVs	Large unilamellar vesicles
LB	Luria Bertani
HEPES	4-(2-Hydroxyethyl)-1-piperazineethanesulfonic acid
DPPS	1,2-Dipalmitoyl-sn-glycero-3-phosphoserine
POPS	Palmitoyl-oleoyl phosphatidylserine
DPPC	1,2-Dipalmitoylphosphatidylcholine
MRSA	Methicillin-resistant *S. aureus*
S. aureus	Staphylococcus aureus
E. Coli.	Escherichia coli
FESEM	Field emission scanning electron microscopy
QTOF	Quadrupole Time-of-Flight

For symbols/units

Å	Angstrom
atm	Atmosphere
β	Beta
C	Celsius
J	Coupling constant
°	Degree
δ	Delta
Hz	Hertz
K	Kelvin
MHz	Megahertz
m	Meta
µg	Micro gram
µM	Micro mole
mL	Millilitre
mV	Mili Volt
min	Minute
h	Hour
nM	Nano mole
o	Ortho
p	Para
%	Percent
s	Second

Chapter 1

Introduction of anion transportation and its biological implications towards therapeutics

The cell membrane's semipermeable nature allows only a limited number of substances to cross the membrane by diffusion pathways. Due to the substantial thermodynamic energy barrier that the hydrophobic region of the lipid bilayer and polar substances, such as big macromolecules, proteins, DNA, and ions, cannot diffuse through the membrane. Non-polar molecules like natural gases, H_2O, ethanol and small hydrophobic molecules can cross the hydrophobic barrier. Membrane-spanning transport molecules, such as proteins, polysaccharides, and their complexes, play a vital role in maintaining the ionic homeostasis of polar species by transporting ions across the phospholipid bilayer through channel or carrier formation.[1]

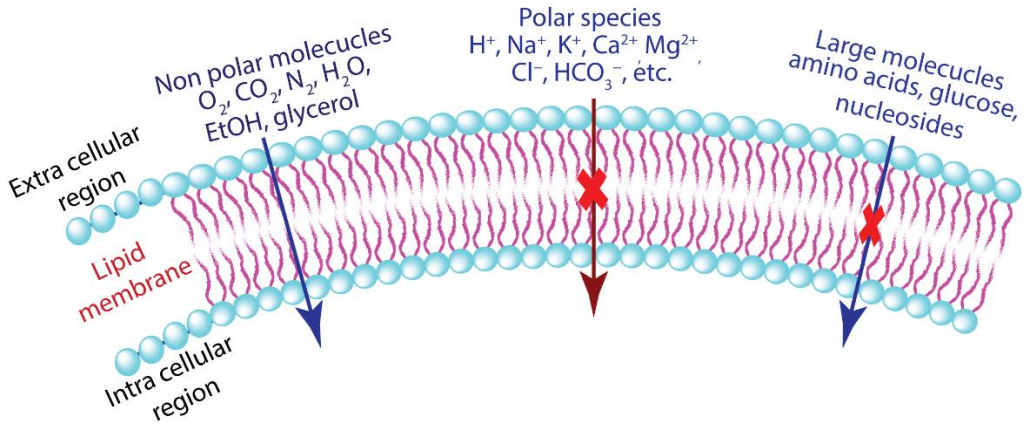

Figure 1.1. Transport of species across a semipermeable lipid bilayer.

The translocation of ions through the cell membrane is crucial for various physiological processes, including ion homeostasis, signal transduction, cell volume regulation, migration, hormone secretion, blood pressure regulation, pH regulation, and the induction of programmed cell death.[2] The Cl^- ion, which is the most abundant anion found outside of cells, plays a vital role across the normal functioning of cells.[3] Numerous disorders, including Bartter's syndrome, osteopetrosis, Dent's disease, cystic fibrosis, and even cancer, have been linked to the presence of defective Cl^- ion channels.[4,5,6,7] Cystic fibrosis (CF), a disease caused by the failure of cystic fibrosis transmembrane conductance regulator (CFTR) proteins, can result in channelopathies that have malfunctioned ion transport activity, formed due to genetic mutations.[8] The study of anionophores has expanded beyond its initial focus on channelopathies like cystic fibrosis, where dysregulated anion transport is crucial. The development of non-toxic anionophores has

been turned, as an alternative approach, to restore anion transport in CFTR-defective cells, providing a potential therapeutic avenue for cystic fibrosis.[9]

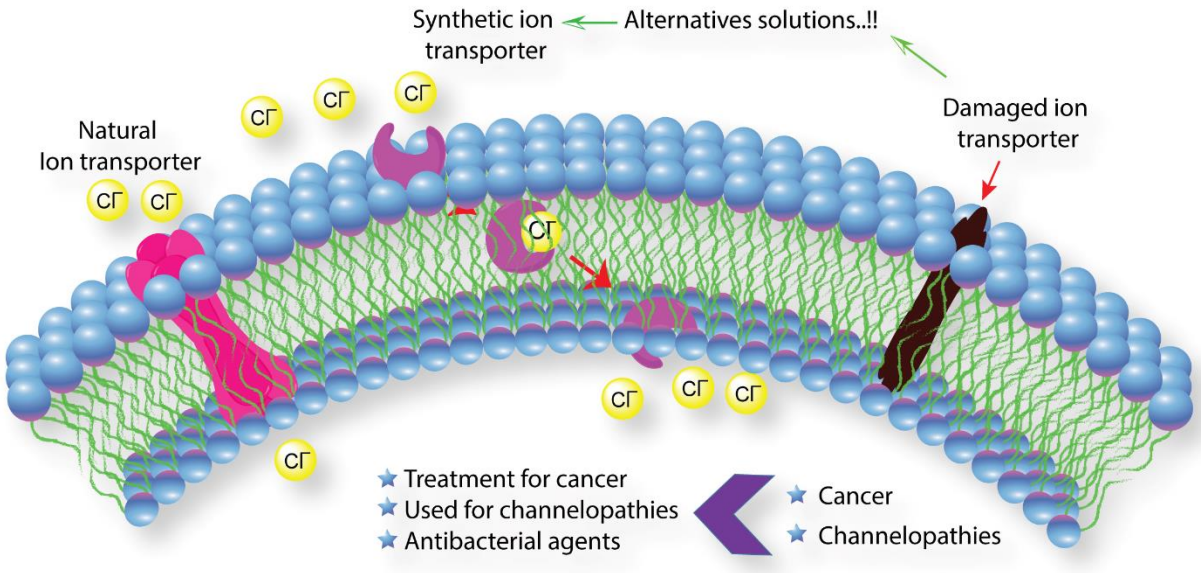

Figure 1.2. Several potential therapeutic applications of anionophore.

Recent studies indicate that ion transporters embedded in the lipid bilayer of cancer cells promote the efflux of Cl^- ions, leading to cell death. Ion transporters, stationed in the lipid bilayer of the membrane, facilitate the movement of ions across the hydrophobic membrane, therefore initiating apoptosis, autophagy, and other cellular death processes that kill cancer cells. Anionophores also show promising therapeutic applications in antimicrobial treatment, addressing the global challenge of antibacterial resistance. Regulating ion equilibrium to reduce extracellular acidity shows potential in combating multidrug resistance arising from protein overexpression or genetic material mutations. The controlling of the equilibrium of ions has a tendency to minimize the acidity of outside of cells and counter multidrug resistance caused by the overexpression or mutation of proteins or genetic materials.[10,11,12] Researchers have directed their efforts towards developing anionophores with inherent antibacterial activity, which must exhibit low cytotoxicity against human cells. Membrane depolarization is the primary mode of action for the antibacterial properties of anionophores, making it challenging for bacteria to develop resistance against them.[13] Scientists worldwide are working to develop novel ideas, leading to the development of artificial ion transporter systems. These synthetic ion carriers hold promise for treating diseases taken on by inadequate anion transport, offering potential solutions for healthcare in various medical fields.

In this thesis work, the primary objective was to design and synthesize a wide range of potential anion-transporting molecules. Additionally, the therapeutic applications of these molecules were investigated. The research work is divided into four chapters; each chapter develops a new class of anionophores and proposes their potential therapeutic applications. Furthermore, we sought to minimize the drawbacks associated with recognized anionophores and proposed alternative methodologies to overcome these barriers.

Chapter 1: primarily explored the many possible applications of anionophore in addressing a wide variety of therapeutic diseases. It additionally reviewed their probable mode of action by a comprehensive review of current research.

Chapter 2: we developed a new class of amino acid based (mainly tryptophan) derivatives and hypothesized that the amino acid scaffold, which is already a biologically relevant molecule, may mute the toxicity towards the normal cells. The tryptophan based receptors selectively transport the Cl^- ions across the lipid bilayer. They have valuable insights into the development of novel therapeutic agents, especially in addressing ion transport-related challenges. We proposed that these tryptophan-based transporters hold significant promise for designing innovative solutions to ion transport-related disorders.

Chapter 3: discusses the synthesis and characterization of a 4-aminoquinazoline analogue, which has the unique capability to function as an anion-induced molecular switch and a pH-responsive anionophore. The compound, which has a quinazoline moiety, exhibits intricate interactions with H^+/Cl^- ions and is particularly responsive under acidic conditions. This pH-responsive quinazoline-based anionophore is a promising candidate for anticancer drug due to the acidic nature of cancer cell microenvironments and other channelophthaies-related diseases. The compound showed bactericidal activity against gram-positive bacteria demonstrates its versatility, making it a potential candidate for antibiotic development. This innovative and stimuli-responsive molecular entity offers multifaceted therapeutic applications.

Chapter 4: in this chapter we have developed multi-stimuli responsive proanionophore molecules featuring a novel class of sulphonium-based water-soluble proanionophores. The main focus of this work was to address conventional challenges associated with synthetic anionophores, including issues related to poor deliverability, selectivity, and uptake, which were encountered in the molecules presented in earlier chapters. The research focused on

overcoming these hurdles through the design and synthesis of proanionophores responsive to GSH, ROS, and light aiming to enhance the efficiency and specificity of anion transport mechanisms.

Chapter 2

Development of tryptophan-based ion transporter for efficient chloride ion transport across lipid membranes

Over the past two decades, researchers have developed anionophores to overcome limitations in natural ion transporters. These artificial molecules were non-selective towards cancerous and non-cancerous cells, as well as showed toxicity towards healthy mammalian cells. These molecules have shown effectiveness in targeting cancerous and non-cancerous cells, but they also have toxicity. To reduce toxicity, we selected the amino acid (tryptophan) scaffold as the anion receptors due to its biocompatibility in physiological systems. By incorporating anion-binding cavities, these amino acids can utilize their beneficial biological features while reducing toxicity to healthy cells. This approach improves the compatibility of anionophores with living organisms, providing an efficient method for developing less toxic and more suitable ion transporters in biological systems.

A new class of tryptophan analogues containing thiourea and amide functionalized were synthesized (***2.3a-i*** and ***2.4***) (Scheme 2.1). We hypothesized that the tryptophan derivatives could introduce multivalent NH bond interactions within the binding cavity, thereby affording the opportunity to develop a novel class of anion transporters rooted in thiourea-amide-based tryptophan derivatives. To check the role of the tryptophan indole ring, two derivatives of leucine and phenylalanine were also synthesized (***2.5a*** and ***2.5b***) (Scheme 2.1).

The initial anion binding property of the tryptophan derivatives (**2.3f** and **2.3i**) was primarily confirmed by the ^{1}H NMR titration and the DFT analysis. This initial anion binding ability encouraged us to validate its anion transport efficacy across the model lipid membrane having EYPC/CHOL (6:4). Additionally, the potent compound **2.3i** revealed distinctly greater selectivity for Cl^- ion in comparison with other tested biologically relevant anions such as Br^-, I^-, NO_3^-, ClO_4^- and SCN^-. Transport mechanistic experiment showed that potent compound **2.3i** follow OH^-/Cl^- antiport pathway through the carrier mechanism.

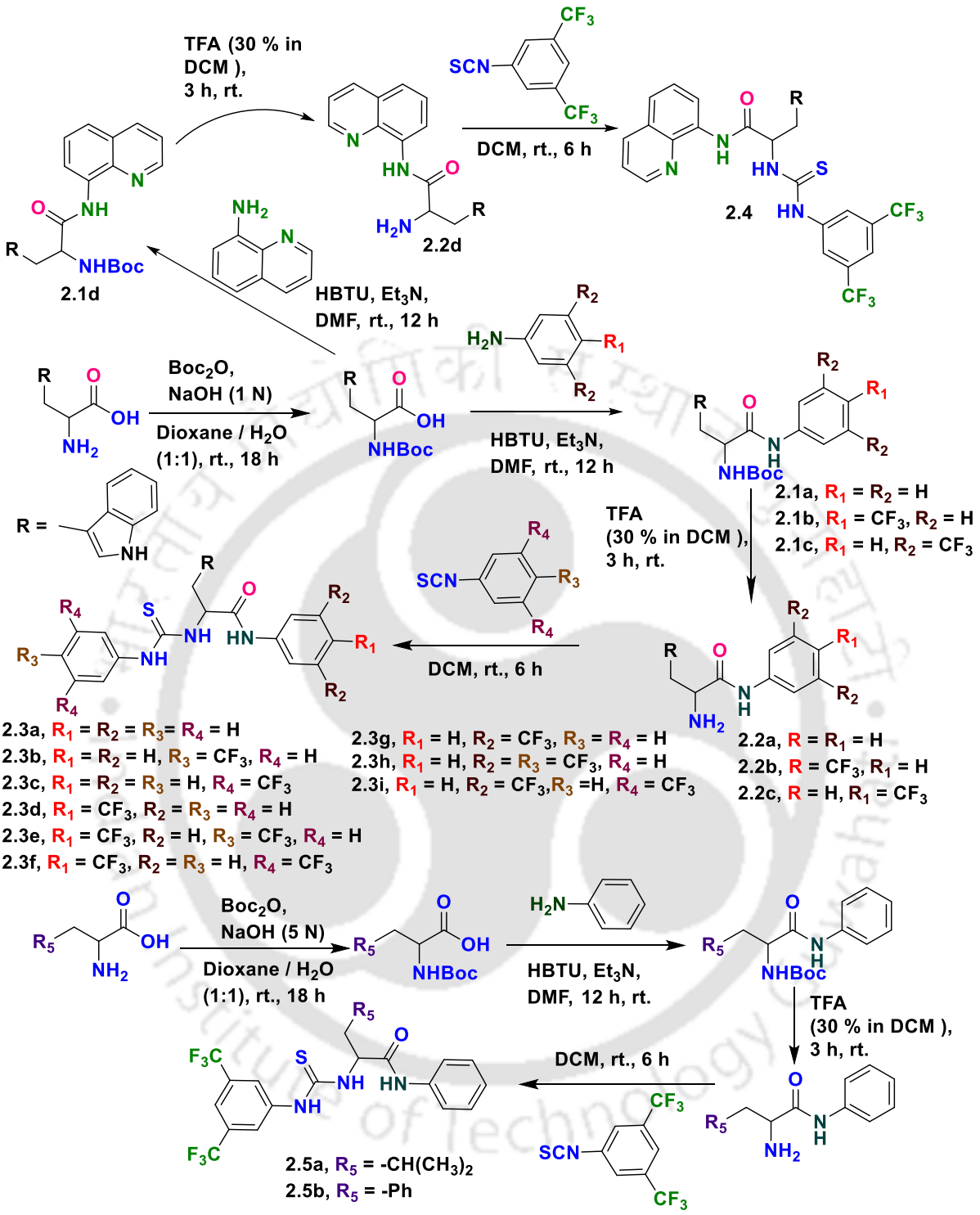

Scheme 2.1. Synthetic steps for tryptophan analogs (2.3a-2.3i and 2.4) and leucine (2.5a) and phenylalanine (2.5b) derivatives.

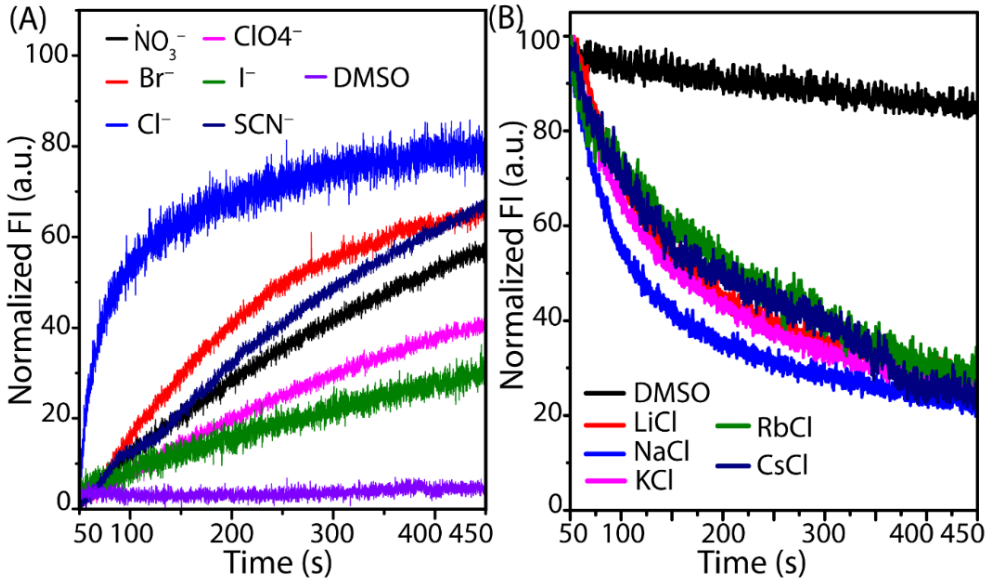

Figure 2.1. The anion transport selectivity of **2.3i** (5 μM) across the EYPC/CHOL-LUVs⊃HPTS (8:2 molar ratio) was measured at pH 7.2 (A). Cation selectivity of **2.3i** (5 μM) determined by changing the external cations (M^+ = Li^+ , Na^+ , K^+ , Rb^+ , Cs^+) across EYPC/CHOL-LUVs⊃lucigenin (B).

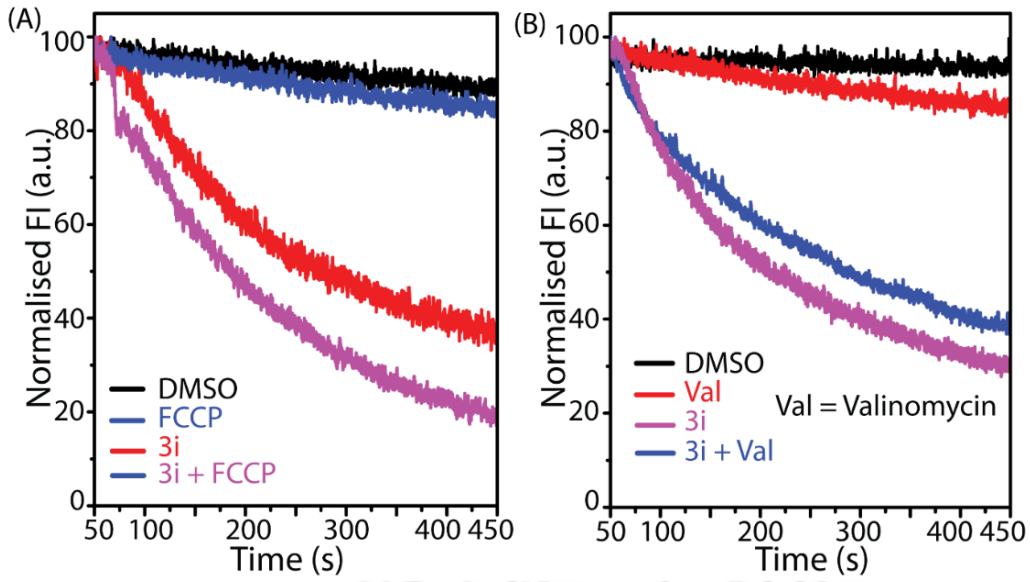

Figure 2.2. The Cl^- transport activity of **2.3i (**2.5 μM**)** in the absence and presence of FCCP (A) and valinomycin (Val) (B).

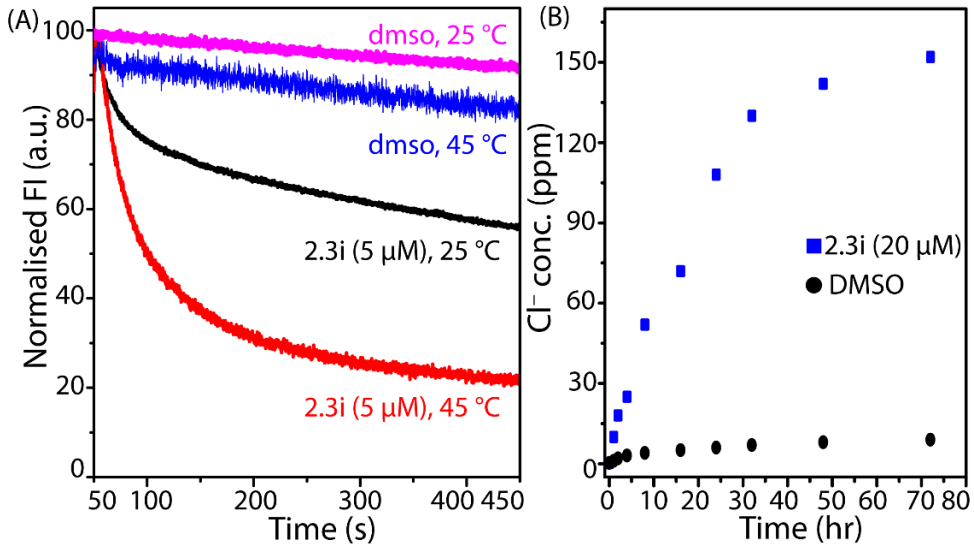

Figure 2.3. Temperature-dependent Cl^- transport by **2.3i** (5 μM) using DPPC-LUV⊃lucigenin (A). The Cl^- ion transport activity of compound **2.3i** (20 μM) was recorded across a U-tube by using the Cl^- ion gradient, using a chloride ion-selective electrode (B).

Therefore, tryptophan-based transporters have valuable insights into the development of novel therapeutic agents, especially in addressing ion transport-related challenges. In this chapter we propose that these tryptophan-based transporters hold significant promise for designing innovative solutions to ion transport-related disorders.

Chapter 3

Development of chloride-responsive molecular switch: driving ion transport and empowering antibacterial activities

The transmembrane transport of Cl^- by synthetic ion transporters can induce antibacterial activities, which are crucial in combating drug-resistant bacterial strains. Membrane-directing molecules with ion transport properties are considered a novel class of antibacterial agents, as they minimize drug resistance against most bacterial strains. However, developing stimuli-responsive synthetic ion transporters with properties like natural ones remains challenging. Several stimuli-responsive synthetic ion transporters have been developed to regulate ion transport properties, but little effort has been made in utilizing biologically active moiety for stimuli-responsive ion transport properties.[14] However, little effort has been made in utilizing biologically active moiety for stimuli-responsive ion transport properties. This approach would provide stimuli-responsive antibacterial, anticancer, or other therapeutic activities to the

compounds due to the presence of biologically active moiety and additional ion recognition and transport moiety.

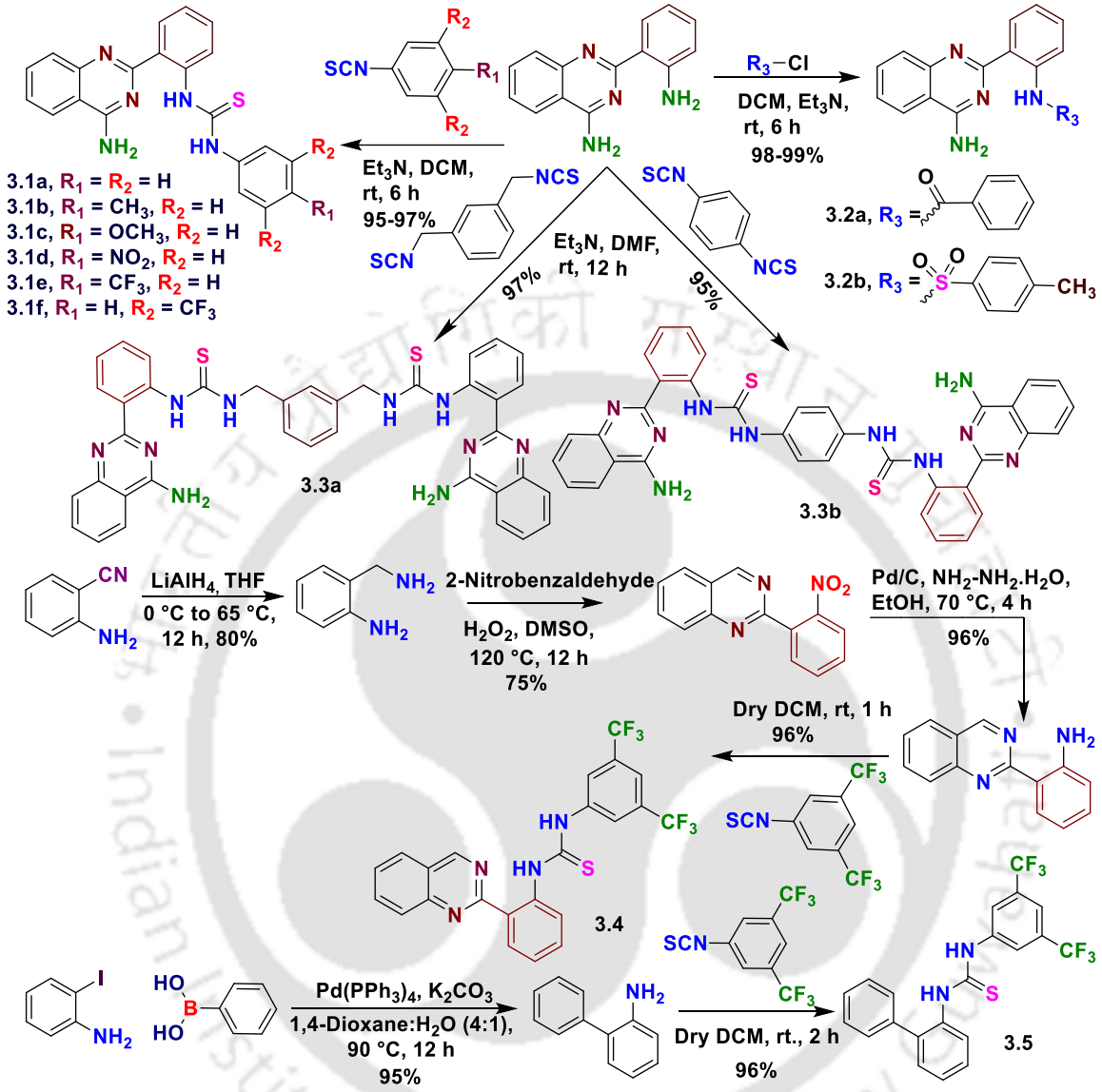

Scheme 3.1. Synthetic routes to 4-aminoquinazoline analogs and controlled compounds.

In in this chapter we explore the biological active moiety used as a synthetic ion transporter, specifically the transmembrane H^+/Cl^- cotransport and antimicrobial activity of 4-aminoquinazoline-based compounds against Gram-positive and Gram-negative bacterial strains. The study hypothesizes that the potent molecule would adopt an open or closed conformation in the absence and presence of an anion, leading to the formation of an anion-induced molecular switch that recognizes and transports anion across the membrane. The presence of a free amine group would offer additional pH-responsive anion transport properties under an acidic environment. The study suggests that the anion-recognition and transport

properties of 4-aminoquinazoline analogues have never been explored as pH-responsive Cl^- transporters. This presents a dynamic and adaptable system for anion recognition and transmembrane transport. The 4-aminoquinazoline thiourea derivatives (**3.1a-f** and **3.3a-b**) were synthesized additionally two controlled compounds **(3.4 and 3.5)** were synthesized to check the role of free amine group and the quinazoline scaffold.

The X-ray solid-state structures of the potent compound 3.1f showed that the amine and thiourea moieties adopt anti-conformation, after Cl^- binding the thiourea groups adopt syn-conformation with the amine group due to strong hydrogen bonding (Figure 3.1A). A significant chemical shift of N-Ha and N-H_b protons suggests the compound interacts with Cl^- via hydrogen bonding. The polarization of N-H_b and N-H_c protons is prompted by the through-space effect due to Cl^-, generating a partial positive charge on the proton. The N-H_a proton shows an upfield chemical shift due to structural switching upon Cl^- coordination. The binding analysis of concentration-dependent chemical shifts reveals a 1:1 host-guest interaction-based complex with a binding affinity of 159.74 ± 7.81 M^{-1}, suggesting the Cl^- recognition aptitude of 3.1f in the solution (Figure 3.1B).

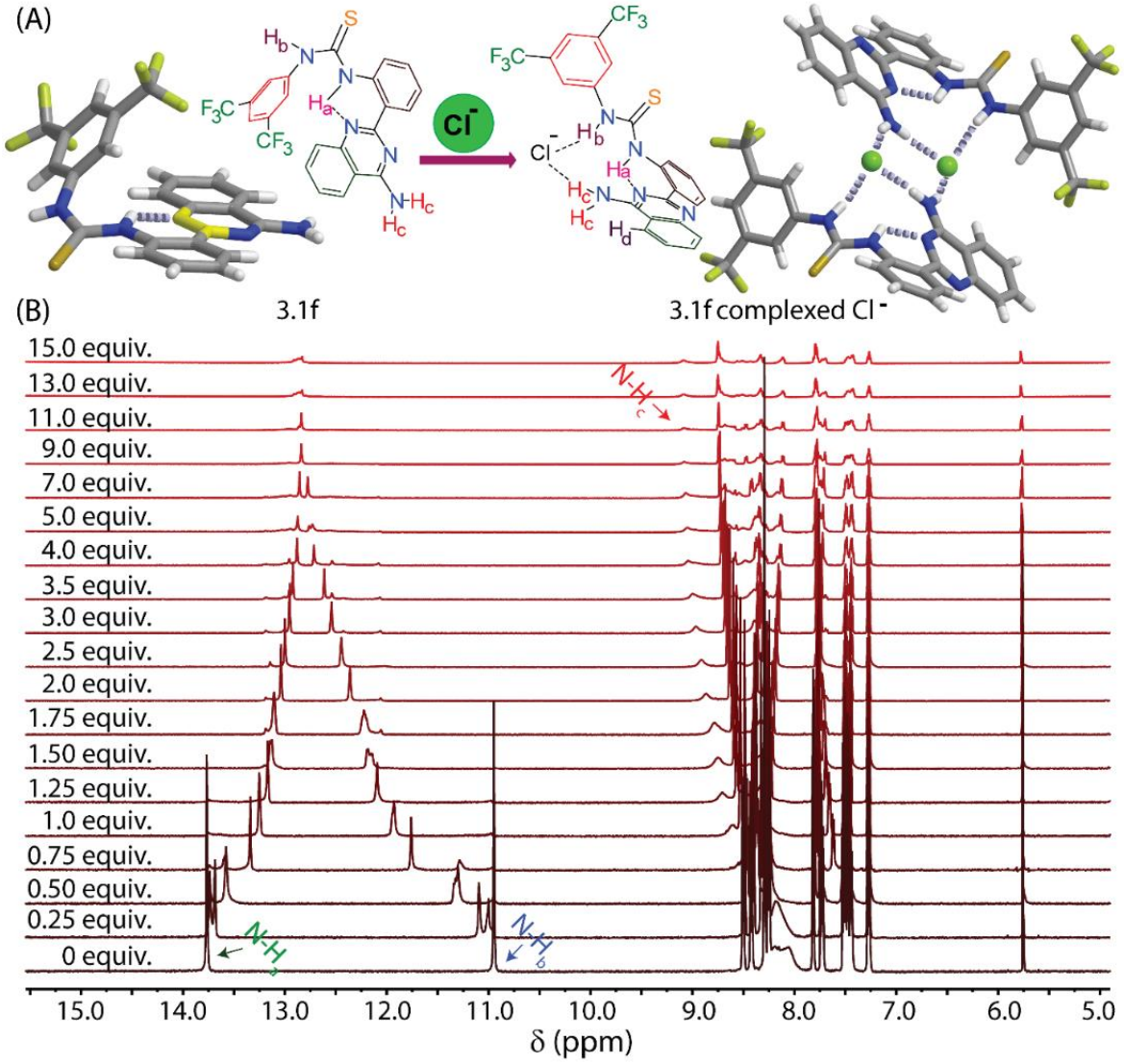

Figure 3.1. XRD-crystal structure of 3.1f and 3.1f complexed with Cl^- (A). The partially stacked plot of ^1H NMR titration experiment of 3.1f (10.0 mM) with successive addition of TBACl in DMSO-d_6 solvent (B).

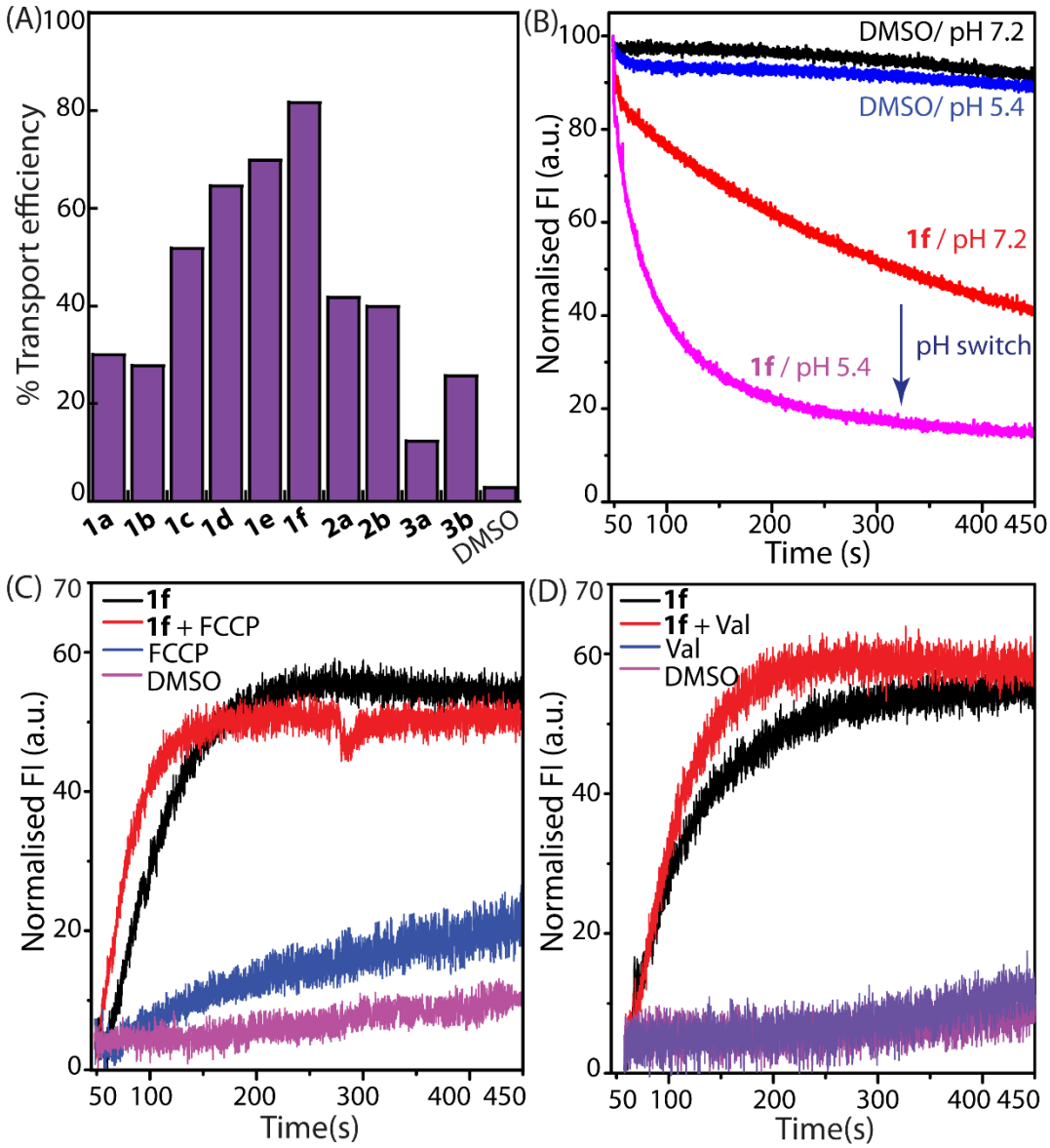

Figure 3.2. Assessment of Cl^- transport activity of the synthesized compounds (A). The pH-dependent Cl^- transport activity of **1f** (B). The Cl^- transport activity of **1f** in the absence and presence of FCCP (C) and valinomycin (Val) (D).

Several fluorescence-based anion transport experiment was performed using the Lucigenin, HPTS encapsulated dye across the model DPPC/POPS/CHOL-LUVs. All these biophysical experiments showed that the potent compounds (**3.1f**) could transport the chloride anions over the model lipid membrane through the carrier mechanism (Figure 3.2A). Furthermore, a pH-dependent transportation aptitude was as well observed for potent compound as the 4-aminoquinazoline nitrogen atom develops protonated at acidic pH and gives to strong anion interactions (Figure 3.2B). For mechanism, both FCCP and valinomycin assays indicate the

cotransport of H^+/Cl^- by the compound at physiological pH (Figure 3.3 A-B). The DPPC and U-tube assay confirmed that the compound follows the carrier transport pathways (Figure 3.3C-D).

The potent Cl^- transporter 3.1f was exhibited strong antibacterial activity against the gram positive bacteria such as Staphylococcus aureus (S. aureus; MIC value of 2.34 ± 0.39 μM) and methicillin-resistant S. aureus (MRSA; MIC value of 2.50 ± 0.50 μM). The minimal bactericidal concentration (MBC) calculation revealed that 3.1f showed a bactericidal effect at a concentration as low as the MIC. The S. aureus cells were also treated with MQAE dye, a cell-permeable fluorescence indicator of Cl^-. The addition of 3.1f resulted in a time-dependent drop in fluorescence intensity of MQAE dye, suggesting the 3.1f-mediated Cl^- transport activity could modify the biological processes that rely on Cl^- cofactors, potentially resulting in bacterial cell death.

So overall in this chapter we have developed a biologically active molecule which applied in the anion transport field to improve the drawbacks of classical anionophores and it would give the promising application for antibiotics as an anionophore research.

Chapter 4

Development of multi-stimuli controlled release of a transmembrane chloride ion carrier from a sulfonium-linked procarrier

The distribution of anionophores in cells can be challenging due to their lipophilic nature. Controlling their solubility could enhance their therapeutic efficacy. A multi-stimuli-responsive anion transport strategy could be beneficial in targeting different types of cancer cells. Higher intracellular levels of GSH and ROS in cancer cells would preferentially release anionophores, leading to apoptosis by perturbing ion homeostasis. In this chapter we have installed a 4-carboxy-2-nitrobenzyl sulfonium moiety to the active anionophore which would increase the aqueous solubility of the corresponding anionophore and allow its removal at high GSH and ROS concentrations or in the presence of light. Substituted aryl groups were attached at the other end of the 1, 3-phenylenedimethanamine scaffold to optimize ion transport efficiency. The water-soluble proanionophore successfully released the membrane active ionophore in the

presence of stimuli like GSH, ROS, and light, and transported Cl^- ion across the model lipid bilayers.

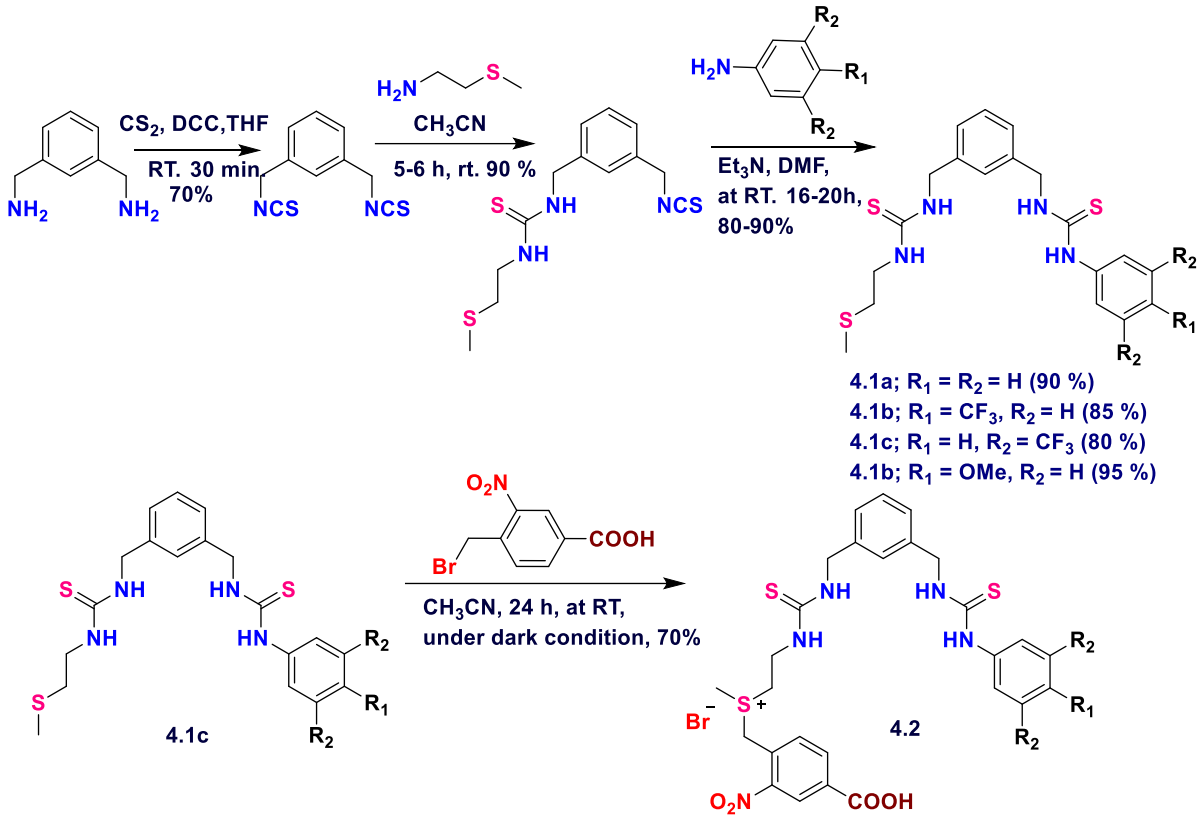

Scheme 4.1. Synthesis of anionophores **4.1a-4.1b** and proanionophore **4.2.**

The ^1H NMR titration experiments confirmed the binding of dithiourea derivative to the Cl^- ion. The fluorescence-based assay confirmed that the dithiourea derivative selectively transports Cl^- ion across the lipid bilayer. The U-tube and cholesterol concentration-dependent assays suggest the transport of Cl^- ion via carrier pathway (Figure 4.1C-D). The FCCP and valinomycin assays showed that Cl^-/ OH^- antiport mechanism is the operative pathway of Cl^- ion transport (Figure 4.1A-B). The regenerated active carrier also successfully transports Cl^- ion under similar experimental conditions.

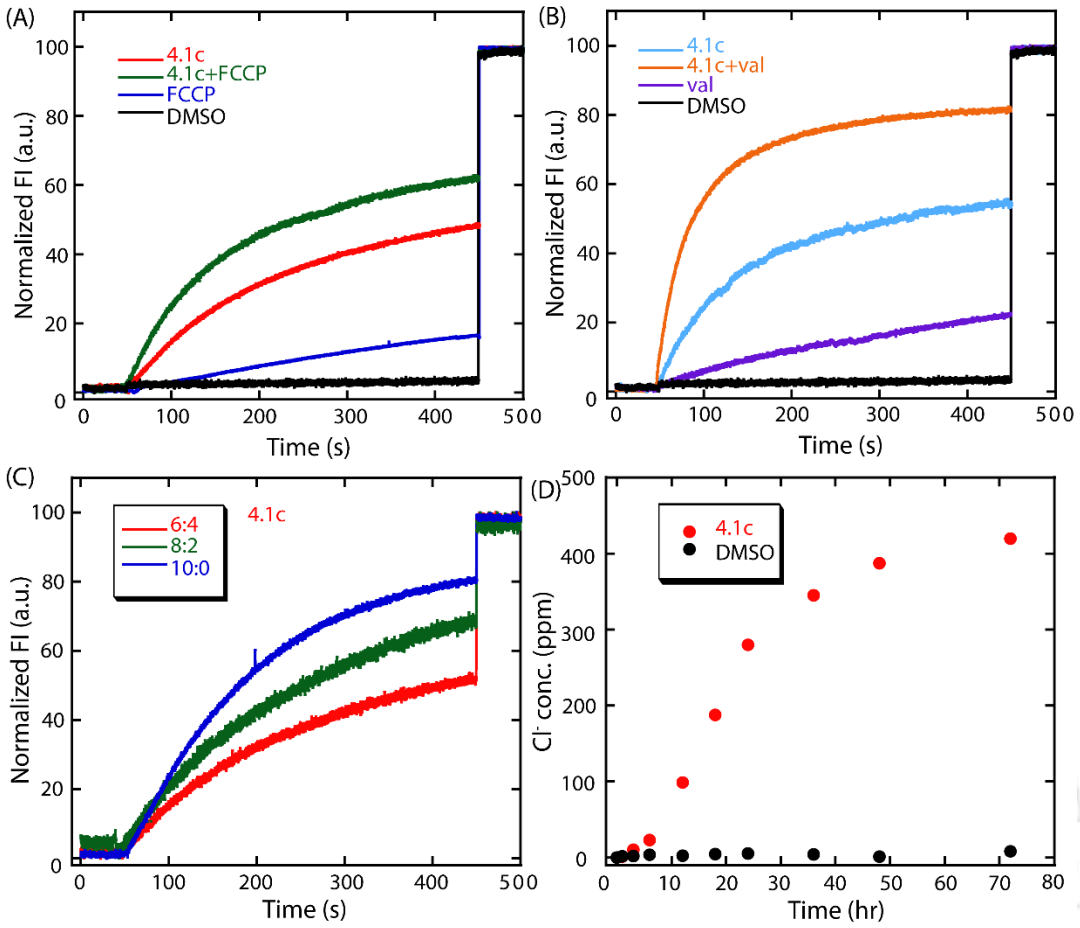

Figure 4.1. Assessment of ion transport activity of compound **4.1c** (0.038 μM) in the absence and presence of FCCP (4 μM) (A) and valinomycin (Val; 2.5 pM) (B). A pH gradient (pHin = 7.2, pHout = 7.8) was applied to initiate the transport of Cl^- ion. The effect of cholesterol concentration on the transport of Cl^- ion in the presence of compound **4.1c** (0.038 μM) (C). The Cl^- ion transport efficacy of compound **4.1c** (2 mM) was recorded across a U-tube by utilizing the Cl^- ion gradient, using chloride ion-selective electrode (D).

The successful regeneration of active lipophilic carrier **4.1c** from water-soluble proanionophore **4.2** in the presence of GSH, ROS, and light encouraged us to study stimuli-activated transmembrane ion transport efficiency.[15] The time-dependent improvement of the Cl^- ion transport aptitude also proved the generation of the active carrier **4.1c** in the presence of GSH, ROS, and light (Figure 4.6 A-C). The photo-irradiation rate of dealkylation was quite faster in comparison with that in the presence of GSH and ROS, which is advantageous for their bio-applicability. The photo-activated strategy can be applied for only surface phenomena due to the lack of tissue penetration ability of the light. The higher levels of intracellular GSH and ROS in cancer cells could be sufficient enough to release the active carrier and promote

ion transport mediated apoptosis. However, the structural integrity of proanionophore **4.2** was intact in the absence of GSH, ROS, and light.

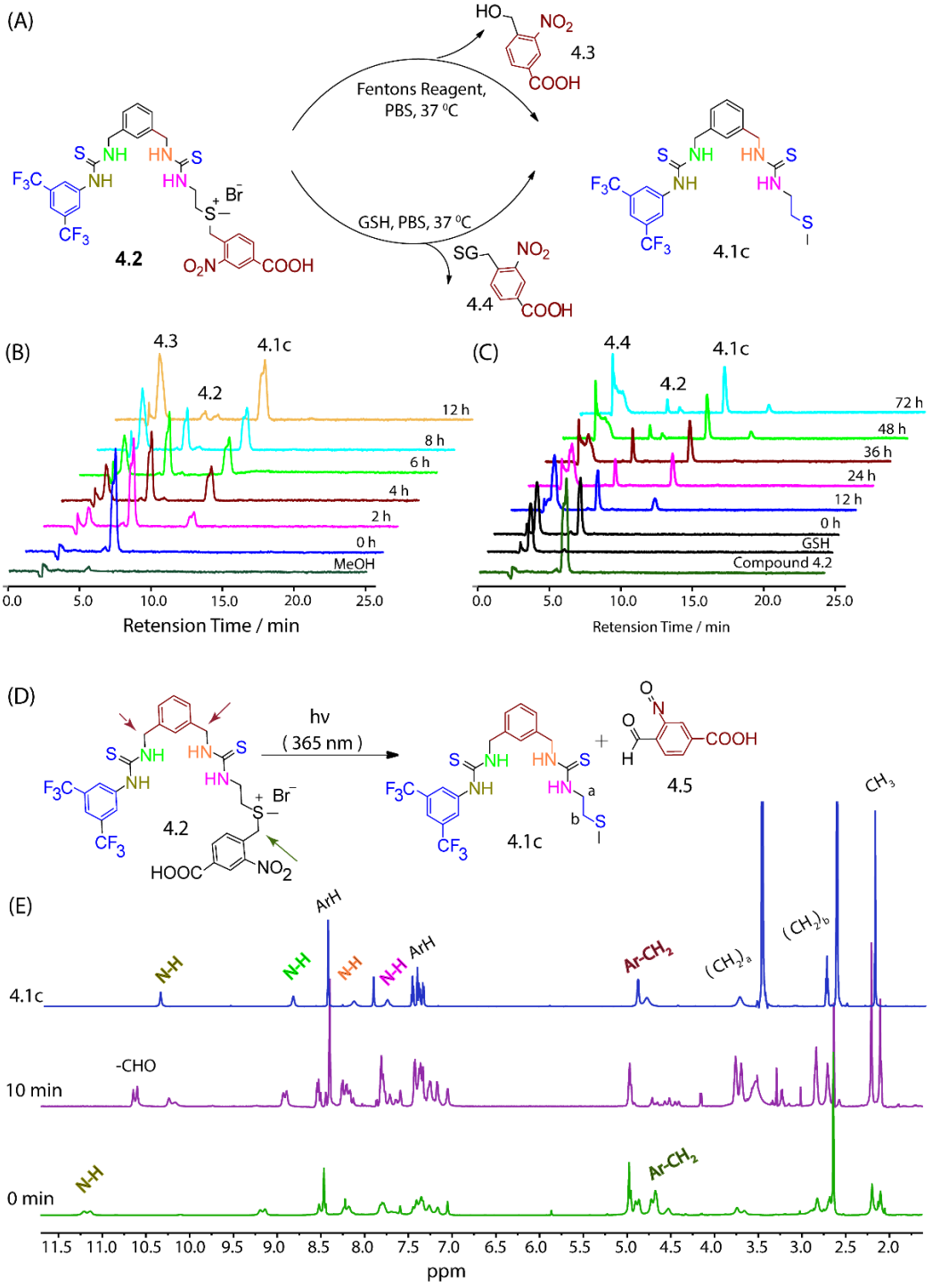

Figure 4.2. Proposed mechanisms of ROS and GSH mediated cleavage of proanionophore **4.2** (A). HPLC traces at different time intervals in the absence and presence of Fenton's Reagent (B) and GSH (C). Proposed mechanism of photo-mediated cleavage of proanionophore **4.2** (D). ^{1}H NMR spectra of proanionophore **4.2** at different time intervals (E).

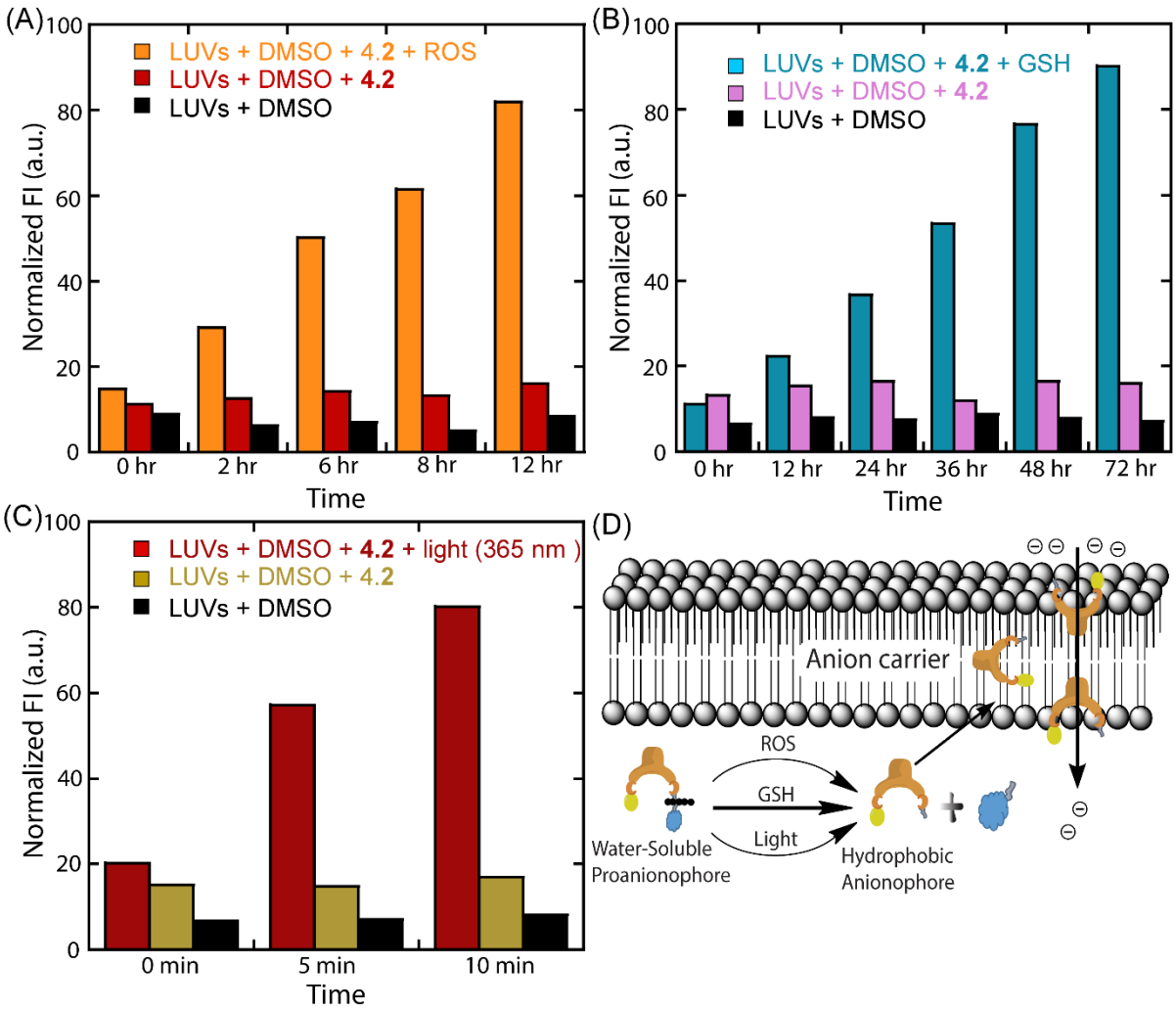

Figure 4.3. Chloride ion transport measurement of the Fenton's reagent (A), glutathione (B) and light (365 nm) (C) mediated release of the active transporter **4.1c** from proanionophore **4.2** in the presence of LUVs. Schematic diagram representing the stimuli-mediated regeneration of the active anionophore from its proanionophore and its transmembrane anion transport properties (D).

Overall in this chapter, we have developed a water soluble proanionophore which release the active anionophore by multi stimuli like GSH. ROS and 365 nm light. This investigation revealed that the multistimuli-responsive strategy could be applied for the treatment of ion transport associated diseases.

Conclusions

In this thesis, we have fruitfully defined various prospects of anionophore research. Additionally, concise literature on the biologically active anionophores has also been

documented in **Chapter 1**. Inspired by the numerous prospects of anionophore, the artificial anionophores have shown effectiveness in specifically targeting both cancerous and non-cancerous cells, in **Chapter 2** we developed a new class of amino acid based (tryptophan-based) derivatives and we hypothesize that the amino acid scaffold already a biologically relevant molecule which may mute the toxicity towards the normal cells. The tryptophan based receptors selectively transport the Cl^- ions across the lipid bilayer. The tryptophan-based transporters have valuable insights into the development of novel therapeutic agents, especially in addressing ion transport-related challenges. We propose that these tryptophan-based transporters hold significant promise for designing innovative solutions to ion transport-related disorders. In **Chapter 3**, to overcome the limitation of classical anionophores we developed a 4-aminoquinazoline analogue selectively transports Cl^- across the lipid bilayers via a carrier pathway. The outcomes also revealed that the quinazoline moiety has cooperative interactions of H^+ and Cl^- ions with the thiourea moiety, resulting in the transport of H^+/Cl^- across the membranes. The pH-dependent analysis revealed that the transport of Cl^- by the potent compound increased in the acidic environment. We hypothesize that such anion-induced molecular switch could be beneficial in exploring ion transport-mediated biological activities. But still, the classical anionophores are having the problems such as deliverability and cellular uptake due to the lipophilic nature of the anionophore. So in this regard, in chapter 4, the primary motivation has been given to overcome all these traditional difficulties related with anionophore and we came up with the concept of sulphonium-based proanionophore, where the sulphonium-based proanionophore compound have been synthesized and explored their transport activity, and release studies.

Future Perspectives

Research on anion transport has made significant progress in the last two decades, with potential therapeutic applications in treating cancer, cystic fibrosis, and channelopathies. However, conventional anionophores face challenges such as inadequate transportability, cellular absorption, and discrimination between cancerous and healthy cells. Scientists are now working on stimuli-responsive proanionnophores to overcome these challenges. Extensive research has been conducted on molecules that transport chloride anions for potential therapeutic applications. However, it is crucial to focus on creating and investigating additional molecules that transport other ions to explore their biological functions and discover more

therapeutic possibilities. It is possible for monovalent anions to fight different viruses, and it is also possible for artificial chloride ion transporter molecules to help with diseases like arrhythmogenesis, cardiac ischemia preconditioning, and heart failure. Artificial molecules that transport anions could manage anionic imbalances and prevent chronic kidney disease. Changes in the genes of some cation-chloride cotransporters (CCCs) channels can throw off the balance of chloride ions, which can cause health problems like ischemia, newborn seizures, temporal lobe epilepsy, and neuropathic pain.

References

1. Davis, J. T.; Gale, P. A.; Quesada, R., Advances in anion transport and supramolecular medicinal chemistry. Chem. Soc. Rev. 2020, 49 (16), 6056-6086.

2. Saha, T.; Hossain, M. S.; Saha, D.; Lahiri, M.; Talukdar, P., Chloride-mediated apoptosis-inducing activity of bis (sulfonamide) anionophores. J. Am. Chem. Soc. 2016, 138 (24), 7558-7567.

3. Turner, K. L.; Sontheimer, H., Cl− and K+ channels and their role in primary brain tumour biology. Philos. Trans. R. Soc. B 2014, 369 (1638), 20130095.

4. Hladky, S.; Haydon, D., Ion movements in gramicidin channels. In Current topics in membranes and transport, Elsevier: 1984; Vol. 21, pp 327-372.

5. Vaughan-Jones, R. D.; Spitzer, K. W.; Swietach, P., Intracellular pH regulation in heart. J. Mol. Cell. Cardiol. 2009, 46 (3), 318-331.

6. Dworakowska, B.; Dołowy, K., Ion channels-related diseases. Acta Biochim. Pol. 2000, 47 (3), 685-703.

7. Jentsch, T. J.; Hübner, C. A.; Fuhrmann, J. C., Ion channels: function unravelled by dysfunction. Nat. Cell Biol. 2004, 6 (11), 1039-1047.

8. Anderson, K. J.; Cormier, R. T.; Scott, P. M., Role of ion channels in gastrointestinal cancer. World J. Gastroenterol. 2019, 25 (38), 5732.

9. Sheppard, D. N.; Davis, A. P., Pore-forming small molecules offer a promising way to tackle cystic fibrosis. Nature Publishing Group UK London: 2019.

10. Akhtar, N.; Saha, A.; Kumar, V.; Pradhan, N.; Panda, S.; Morla, S.; Kumar, S.; Manna, D., Diphenylethylenediamine-based potent anionophores: transmembrane chloride ion

transport and apoptosis inducing activities. ACS Appl. Mater. Interfaces 2018, 10 (40), 33803-33813.

11. Ko, S.-K.; Kim, S. K.; Share, A.; Lynch, V. M.; Park, J.; Namkung, W.; Van Rossom, W.; Busschaert, N.; Gale, P. A.; Sessler, J. L., Synthetic ion transporters can induce apoptosis by facilitating chloride anion transport into cells. Nat. Chem. 2014, 6 (10), 885-892.

12. Van Rossom, W.; Asby, D. J.; Tavassoli, A.; Gale, P. A., Perenosins: a new class of anion transporter with anti-cancer activity. Org. Biomol. Chem. 2016, 14 (9), 2645-2650.

13. Ventola, C. L., The antibiotic resistance crisis: part 1: causes and threats. Pharm. Ther. 2015, 40 (4), 277.

14. Harvey, A. L.; Edrada-Ebel, R.; Quinn, R. J., The re-emergence of natural products for drug discovery in the genomics era. Nat. Rev. Drug Discov. 2015, 14 (2), 111-129.

15. Akhtar, N.; Pradhan, N.; Saha, A.; Kumar, V.; Biswas, O.; Dey, S.; Shah, M.; Kumar, S.; Manna, D., Tuning the solubility of ionophores: glutathione-mediated transport of chloride ions across hydrophobic membranes. Chem. comm. 2019, 55 (58), 8482-8

भारतीय प्रौद्योगिकी संस्थान गुवाहाटी
Indian Institute of Technology Guwahati

Chapter 1

Introduction of anion transportation and its biological implications towards therapeutics

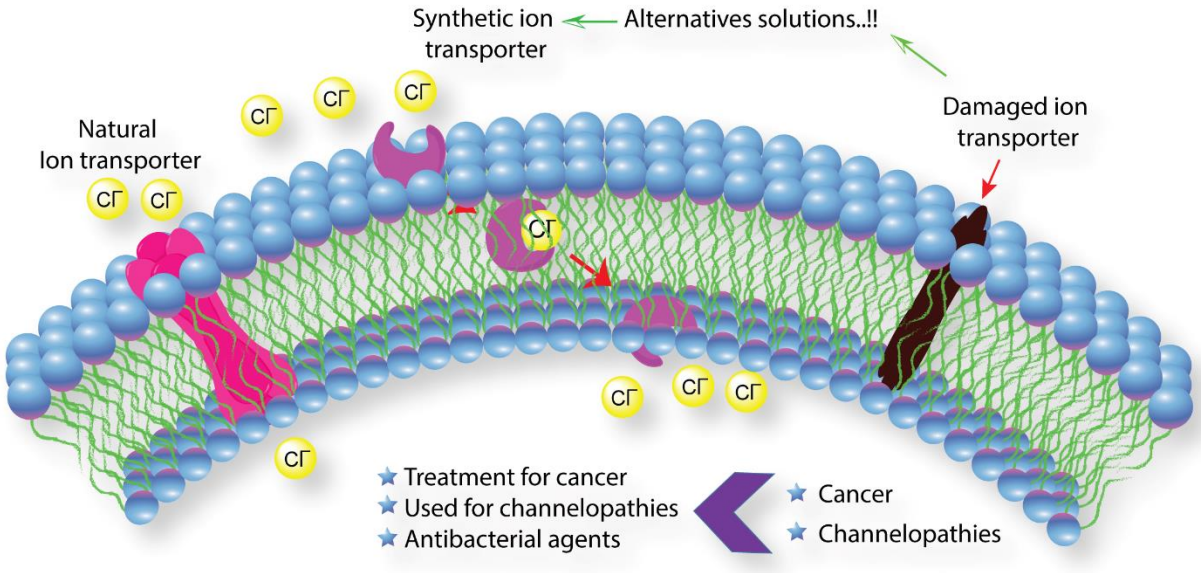

भारतीय प्रौद्योगिकी संस्थान गुवाहाटी
Indian Institute of Technology Guwahati

1.1. Introduction

The translocation of ions through the cell membrane is essential for several physiological processes such as proliferation of cells, sensory transmission, and regulation of pH and maintaining the osmotic pressure. The cell membrane is semipermeable in nature, caused by the specific arrangement of hydrophobic tail and hydrophilic head groups of the lipid bilayer, allowed mainly a limited number of particular substances cross the cell membrane by diffusion pathways. Non polar molecules of small sizes, such as natural gases (O_2, CO_2, and N_2), H_2O, EtOH, and small hydrophobic molecules, are able to pass across the membrane by diffusion process, towards the concentration gradient. However, polar substances such as glucose and nucleotides, big macromolecules like proteins and DNA, and ions are unable to pass through the lipid bilayer by simple diffusion due to the large thermodynamic energy barrier formed by the hydrophobic region of the lipid bilayer (Figure 1.1). Normally, the maintenance of ionic homeostasis of polar species are helped by several membrane spanning transport molecules, which include proteins, polysaccharides, and their complexes that serve as crucial for the transmembrane transport of biologically relevant ions. Specific types of proteins found in membranes play a vital role in transporting ions across the phospholipid bilayer by forming channels or carriers.

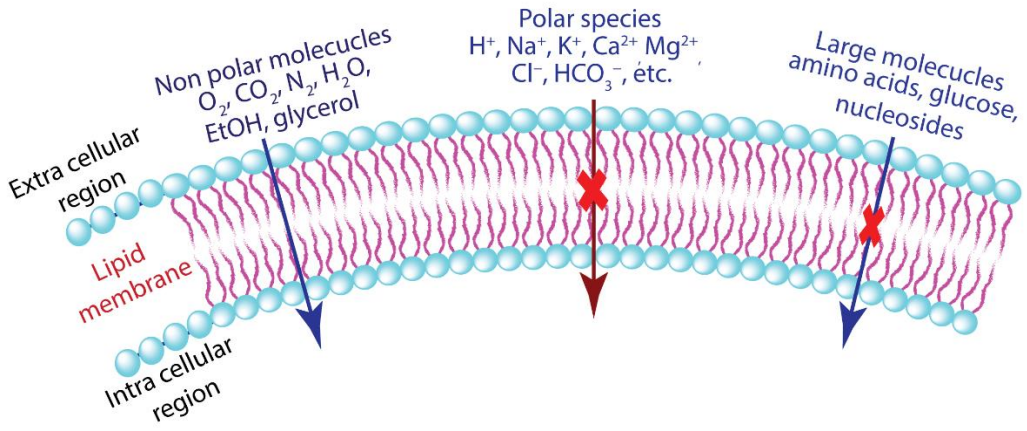

Figure 1.1. Transport of species across a semipermeable lipid bilayer.

1.2. Importance of ion transport

Transporting ions across the membranes of living organisms is a vital process in life that is precisely controlled by membrane-embedded pumps, channels, and carriers.[1] It is necessary for the preservation of cellular ion and pH equilibrium. Cystic fibrosis (CF), which affects regular ion flow due to the failure of the cystic fibrosis transmembrane conductance regulator (CFTR) proteins, can result in a group of diseases known as channelopathies. Genetic mutations may

lead to malfunctioning of ion transport, which may eventually give rise to channelopathies (Figure 1.2). Chloride (Cl^-), which is the most abundant anion found outside of cells, plays a vital role throughout the normal functioning of cells. Numerous disorders, including Bartter's syndrome, osteopetrosis, Dent's disease, cystic fibrosis, and even cancer, have been linked to the presence of defective Cl^- ion channels.[2 3]

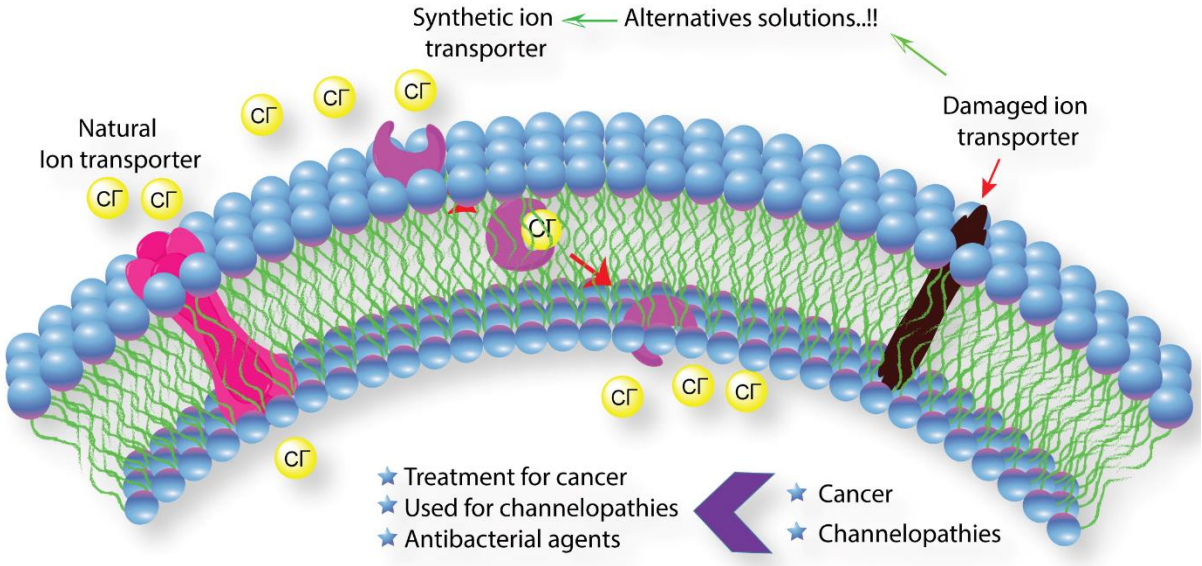

Figure 1.2. Several potential therapeutic applications of anionophore.

Recent investigations have highlighted the significance of ion homeostasis, specifically Cl^- ion, in the regulation of cellular death.[4] Another factor that contributes to antibacterial resistance is the presence of mutations in membrane protein machinery.[5] In order to address these issues, scientists from all over the globe have been working to develop novel indies, which have ultimately led to the development of artificial ion transporter systems. A possible breakthrough in the treatment of channelopathies, cancer, and bacterial infections might be achieved via the use of anionophore molecules, which try to replicate the activities of natural transport proteins that are dysfunctional. The development of organic molecucles that are proficient of selectively binding anions and enabling their transport properties across cell membranes constitutes a wonderful footstep forward in the direction of revolution in the healthcare sectors. The promise of these synthetic ion carriers lies in their potential to treat diseases caused by inadequate anion transport. Recent advancements in the development of small organic molecules as synthetic carriers have provided optimism for innovative therapeutic approaches. The possible applications include a wide range of medical fields, which have the promise of bringing out advancement solutions for healthcare. This novel approach

demonstrates the advancement that has been achieved in the development of fundamental organic molecules for the purpose of targeted anion transport. The idea of artificial ion transporter molecules provides a unique path. The purpose of this chapter is to dive into the scientific foundations of anion transportation. It highlights current breakthroughs and their possible impact on the treatment of disorders linked with abnormal ion homeostasis, therefore opening the way for innovative approaches to healthcare.

1.3. Transport pathways and mechanism

Ion transport pathways is mainly characterized by two pathways either ion carriers or ion channels (Figure 1.3).

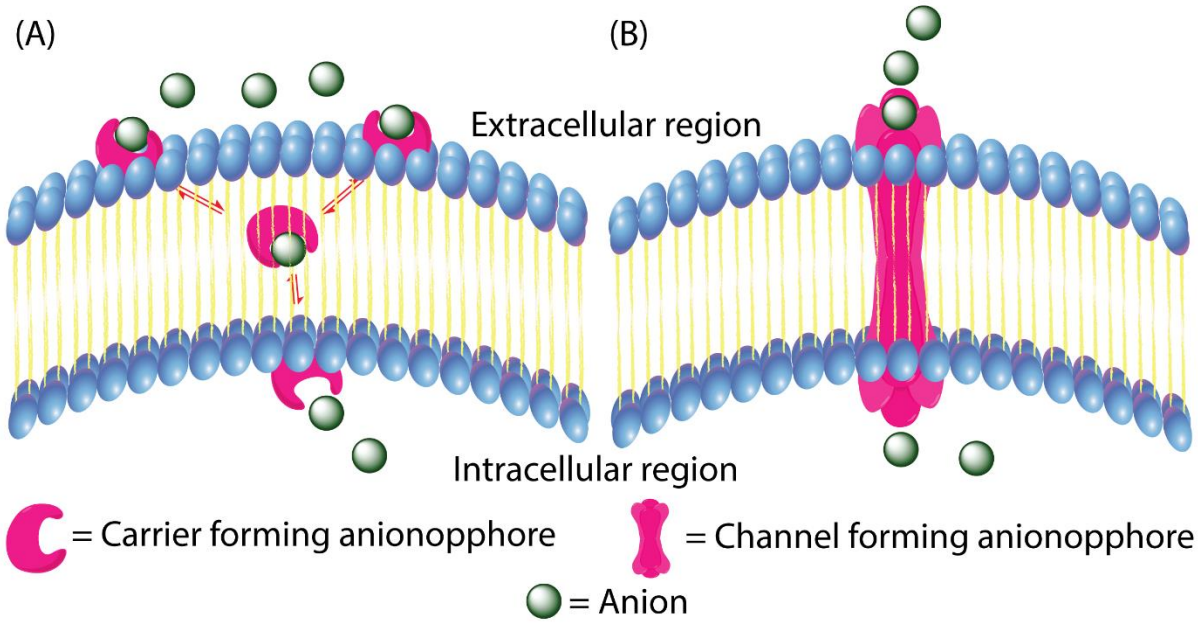

Figure 1.3. Transport pathways. (A) Ion carriers (B) Ion channels.

Ion carriers are small biomolecules that facilitate the passage of ions across a membrane by gripping them from one side and releasing them on the other side by three mechanistic pathways which are uniport, symport and antiport mechanism (Figure 1.4).

- **Uniport mechanism:** When the charge molecucles are transported in a single direction across the lipid membrane is called uniport process. One well known example is Glucose transporter (GLUT) is found in erythrocytes.
- **Symport mechanism:** This is a co-transport mode transport process in which two separate ions or substances are transported in the same direction across the lipid

membrane. One example is Na/glucose transporter proteins exemplify symport pathways.

- **Antiport mechanism:** This one is also a co-transport process where the two different substances have been sent in different ways. One example is Na^+/H^+ antiporter proteins channels.

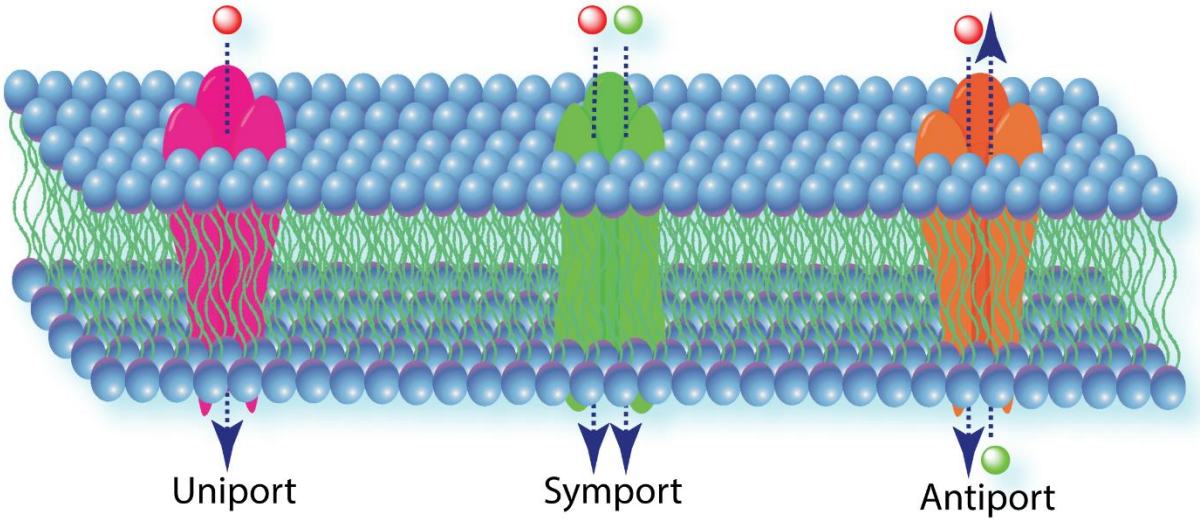

Figure 1.4. Transport mechanism.

1.4. Therapeutic significance of ion transport

It is widely known that natural ion transporter has connections to many physiological processes that regulate cell growth and programmed cell death. Therefore, any changes in their role often coincide with apoptosis. Apoptosis involves a genetically programmed cell death that is defined by specific physical characteristics, including cell shrinkage, membrane blabbing, nuclear breakdown, chromatin condensation, the formation of smaller apoptotic bodies with a disordered cell membrane, and rapid engulfment by neighbouring cells. Apoptosis is responsible for maintaining the equilibrium between cell growth and cell demise by removing harmful, impaired, aging, or contaminated cells from the organism. Any disruption of this regulated system might result in an excessive accumulation of non-functional cells, potentially leading to various pathological states such as tumor formation, viral infections, and autoimmune illnesses. An important characteristic of cancer is the reduction of programmed cell death (apoptosis) in tumor cells. This enables them to grow to more severe stages of malignancy, initiate invasion and spread to other parts of the body (metastasis), and gain tolerance to various treatments. Tumor development is mostly attributed to the suppression of

apoptosis, because it hampers the normal functioning of apoptotic signaling pathways and allows the tumor to evade the immune response. Hence, the targeted reactivation of apoptosis is seen as a promising therapeutic strategy to battle cancer. Apoptosis in cancer cells may be triggered by specifically targeting either the extrinsic route, including the death receptor, or the intrinsic pathway, involving the mitochondria.[6] Apoptosis is often characterized by a reduction in cell size, whereas an elevation in cell volume corresponds to cell proliferation.[7]

Ion channels are essential for controlling cell growth and programmed cell death by facilitating the movement of ions across cell membranes. Proteinaceous ion channels, such as Ca^{2+} channels, K^+ channels, and Cl^- channels, are essential for a wide range of cellular functions. Pro- and anti-apoptotic proteins maintain the maintenance of transmembrane Ca^{2+} ion balance, allowing the Ca^{2+} signalling mechanism to control several physiological processes, including apoptosis.[8] Diverse apoptotic triggers that rely on Ca^{2+} ions, such as oxidative stress, ceramide, and arachidonic acid, induce the liberation of Ca^{2+} ions from the endoplasmic reticulum. This, in turn, initiates the triggering of apoptosis processes, involving the discharge of cytochrome c from the mitochondria.[9] The transport of K^+, Na^+, and Cl^- ions is the cause of cell shrinkage, and several investigations have shown that this ion movement is necessary for apoptosis. Intracellular concentrations of Cl^- and Na^+ ions are typically lower (from 5 to 40mM and 10 to 30mM, respectively) compared to the extracellular levels (120mM and 142mM, accordingly). In contrast, the intracellular concentration of K^+ ions are far greater (140 mM) than their external value (4 mM). The preservation of concentration gradients of these single-charged ions across each layer of the cell's membrane maintains the size of the cell and controls the survival of the cells. Potassium (K^+) channels play a crucial role in apoptosis due to their significant impact on membrane potential and their ability to modulate cell volume in an isotonic environment, which are important characteristics of apoptosis. Recent investigations have shown that the release of K^+ ions and decreased levels of K^+ ions within cells might trigger apoptosis. The activation of caspases and the apoptotic nuclease activity is influenced by the concentration of K^+ ions. However, once they are active, their activity is not regulated by fluctuations in K^+ ion concentration.[10] Na^+ ions, along with other monovalent ions, participate in the apoptotic volume reduction process, leading to the breakdown of genetic material and ultimately causing cell death. Nevertheless, the outflow of K^+ ions does not exclusively determine the inflow of Na^+ ions, indicating the presence of distinct ionic routes for K^+ and Na^+ ions during apoptosis. Saxitoxin, a sodium ion channel blocker, prevents apoptotic cell death by inhibiting the function of sodium ions. This demonstrates that sodium ions not only

help maintain ion balance and regulate cell size, but also play a crucial role in initiating signals for cell death. The Cl^- ion is present in large quantities in all organisms. The efflux of K^+ ions is closely linked to apoptotic volume decline (AVD). It has been shown that the efflux of water, which causes cell shrinkage, is driven by K^+ ions. In this process, Cl^- ions typically follow the efflux of K^+ ions to preserve charge neutrality. When exposed to different triggers that cause cell death, certain volume-regulated anion channels (VRACs) are also activated. This activation leads to the release of Cl^- ions during the period before cell death occurs. The AVD, occurring under normal tonicity, is followed by regulatory volume drop (RVD), which is facilitated by both potassium (K^+) and chloride (Cl^-) channels. Consequently, as anticipated, it was shown that inhibiting the volume regulating K^+ and Cl^- channels prevented the cells from exhibiting any morphological traits associated with apoptosis, such as caspase activation, cytochrome c release, and DNA laddering. As a result, the cells were saved from undergoing cell death (Figure 1.4).[11, 12] The VRACs may be activated by both cellular edema and heightened generation of reactive oxygen species (ROS).[13] During anion volume decrease, these volume-regulated anion channels (VRACs) become active and initiate a range of cellular actions, even in non-enlarged cells. Pharmacologically inhibiting these channels prevents AVD in several cell types. Apoptosis involves many additional channel-mediated Cl^- flow mechanisms. It is shown that the regulation of Cl^- flow may harm the internal mechanisms that start apoptosis, but it has a little impact on the external route of apoptosis. VSOR chloride channels play a key role in the movement of Cl^- ions for the duration of apoptosis.[14]

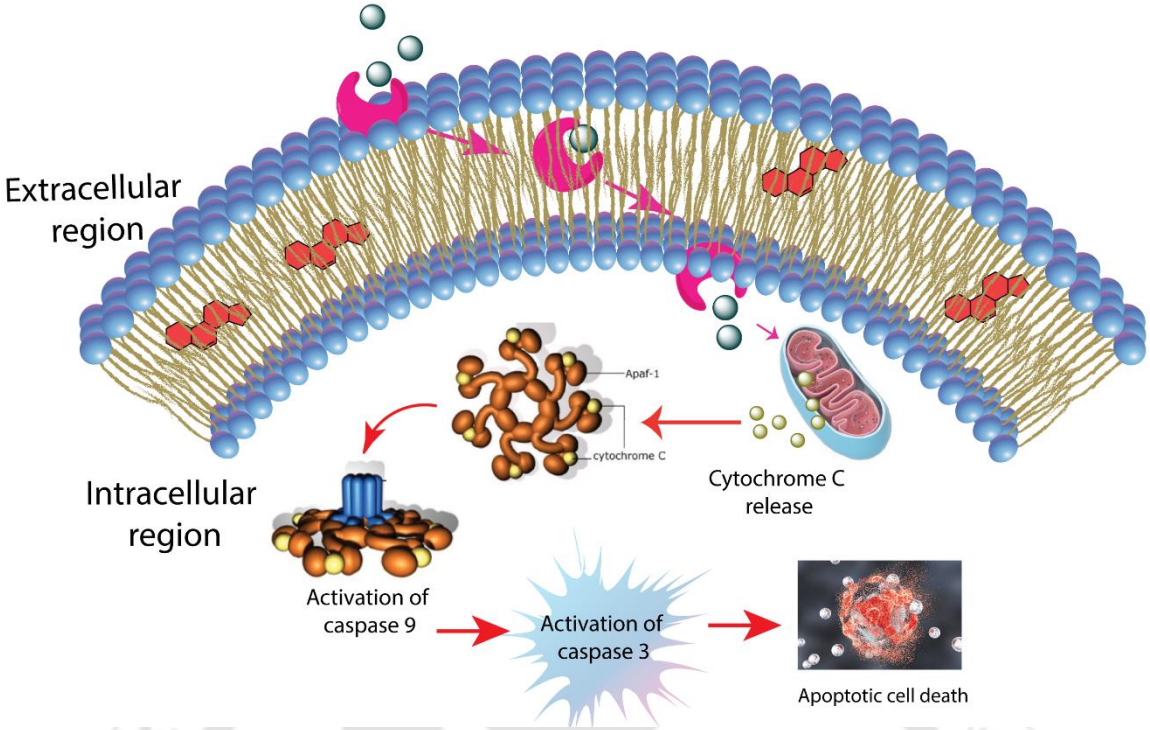

Figure 1.4. Schematic presentation of chloride transport mediated apoptosis.

Cells have developed a protective mechanism to regulate cell volume and ion balance across their membranes in response to variations in ion concentration in the inside and outside of the cell. Hence, the absence of control in the normal ion transport mechanism results in the emergence of several disorders associated with ion channels, such as cystic fibrosis and cancer. To address dysregulated ion transport-related disorders, synthetic ion channels and carriers have been developed. Since, last two decades, several research groups have investigated the ion transport characteristics of artificial ionophores inside the cellular milieu.[15] Several studies have also shown the effects of synthetic ionophores on living organisms. Despite being at its nascent stage of development, the exploration of ionophore-mediated biological processes has immense therapeutic promise. The synthesized ionophores exhibited effective Cl^- ion transportation across the epithelial cell membranes that had dysfunctional CFTR channels. The administration of synthetic ionophores also resulted in the initiation of programmed cell death in cancer cells. Therefore, synthetic ionophores has the capacity to combat cancer, cystic fibrosis, and other disorders associated with ion transport. Ionophores are typically hydrophobic and operate inside the lipid bilayer. They do not interact with bio-macromolecules such as DNA, proteins, or enzymes. Instead, they control ion transport to trigger apoptosis. Synthetic ionophores have the ability to overcome disruptions caused by genetic mutations and

over-expression of genetic material, proteins, and enzymes. They have emerged as an unconventional technique for treating many pathological disorders. Scientists worldwide have been extensively studying various natural and artificial anion transporter molecules due to their significant relevance to the healthcare system. Their aim is to investigate the diverse pharmacological effectiveness of these molecules. This chapter provides a summary of several anionophores derived from natural products and their use as anti-proliferative agents in biological applications. In addition, other synthetic anionophores with potential therapeutic applications are also scrutinized.

1.5. Natural compound based anionophores

1.5.1. Prodigiosin-based anionophores

Prodigiosin, the first alkaloid-based transmembrane an anion carrier (Figure 1.5), dissipates the pH gradient in liposomes and cells.[16] Prodigiosin transports the H^+/Cl^- ion-pair via electrostatic contact and the formation of hydrogen bonds. Most recently conducted studies have connected prodigiosin's immunosuppressive, antibacterial, antifungal, and anticancer characteristics to its ions transport activities. Prodigiosin's cytotoxicity led to the invention of obatoclax, a synthetic counterpart. Different biophysical study proved that the obatoclax follow the Cl^-/HCO_3^- antiport mechanism. Quesada and co-workers synthesized a class of obatoclax compounds (**1.1c-e**).[17]

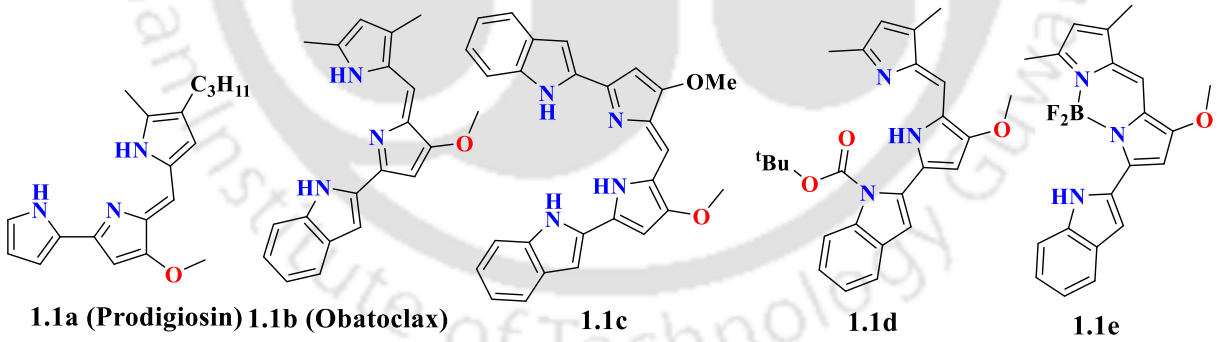

Figure 1.5. Prodigiosin-based anionophores.

1.5.2. Tambjamine-based anionophores

Tamjamines, marine alkaloids, have anion transport-adjusted anticancer properties. The tambjamine 2, 2'-bipyrrolic ring structure resembles prodigiosin structurally. Several tamjamine derivatives were developed (**1.2a-q**) (Figure 1.6).[18] Bio-physical investigations show that tambjamines move via the Cl^-/HCO_3^- exchange channel and do not deprotonate fast

under physiological circumstances. Cellular activity investigations showed that *2,2′*-bipyrrole-based potential anion transporters deacidify acidic organelles to kill cancer cells.[19 20 21 22]

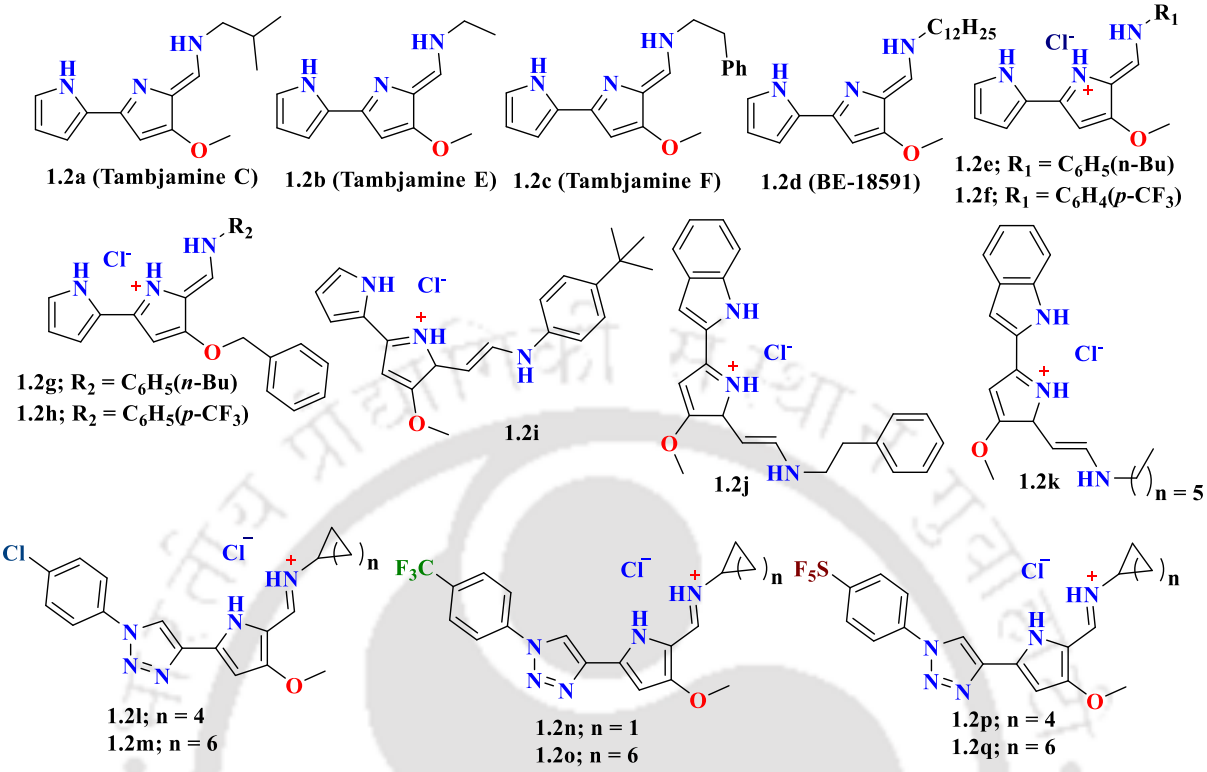

Figure 1.6. Tambjamine-based anionophores.

1.5.3. Perenosin-based anionophores

Based on the biological activities of natural product-based ionophores, Gale and colleagues synthesized perenosins and studied their ion transport-mediated cell killing effects. The imine bond links the abundant pyrrole-based anion binding moiety to the indole, benzimidazole, or indazole scaffold (**1.3a-n**) (Figure 1.7).[23] Using ISE and fluorescence study showed that perenosins transport anions via the Cl^-/ NO_3^- antiport mechanism. Structure–activity relationship investigations showed that perenosin anion transport is controlled by N–H proton acidity and molecule lipophilicity. Benzimidazole and indazole-containing perenosins lacked effective transmembrane Cl^- ion transport. Studies on pH-dependent anion transport showed that powerful perenosins exhibited greater Cl^- ion transport in acidic environments (pH 6.2) than in physiological settings, perhaps owing to increased protonation. Further research shows that perenosins act as HCl cotransporters in acidic environments and Cl^-/ NO_3^- antiporters in physiological settings. Cell viability experiments employing normal and malignant cell lines examined perenosins' anticancer properties.

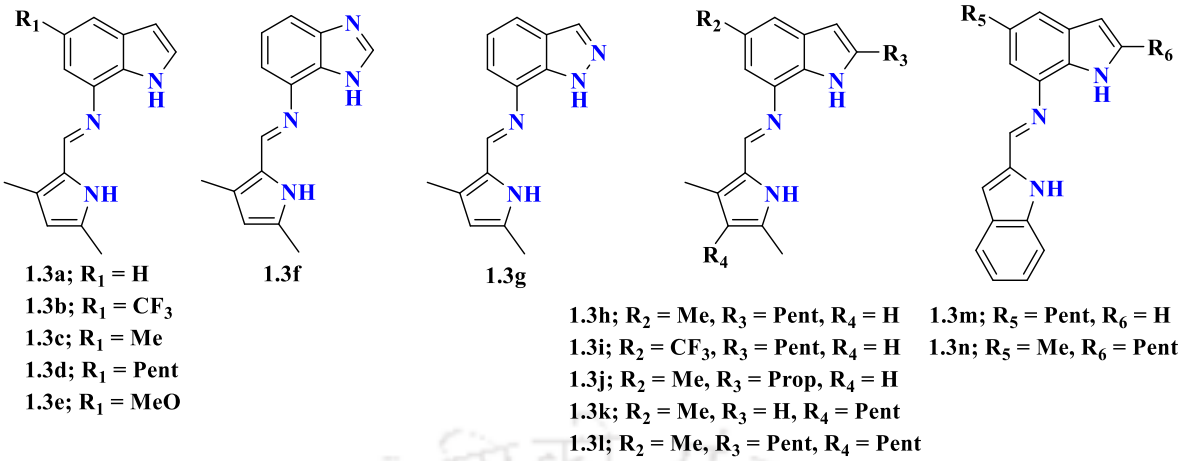

Figure 1.7. Perenosin-based anionophores.

1.6. Synthetic anion transporters

1.6.1. Amide functionalised anionophores

Neutral binding sites with amide bonds are being widely employed owing to their simple making and the ability to recognize anions via hydrogen bonding. Various amide groups, including simple amides (CONH), thioamides (CSNH), sulfonamide (SO_2NH), and cyclic squaramide, are often used as receptors for anions. In 1997, Crabtree and coworkers published an investigation revealing simple and inflexible amide receptors (**1.4a-d**) (Figure 1.8).[24] Those compounds have binding affinity towards halide ions in solution, as demonstrated by ^{1}H NMR and FT-IR analyses. X-ray diffraction utilizes showed that compound **1.4a** forms a 1:1 combination with bromide ion. Compound **1.4a** adopts a syn-syn configuration in order to connect with a halide ion. Compound **1.4a** exhibits limited solubility in $CDCl_3$ as a result of self-association. The solubility in substance **1.4b** is enhanced by the inclusion of alkyl chains. They also documented the presence of dipodal receptors **1.4c** and **1.4d** (Figure).[24] Compound **1.4c** has lower affinity towards halide ions compared to compound **1.4b** because the NH groups have decreased acidity. In compound **1.4d**, the existence of unshared electron pairs on the pyridyl nitrogen atom enables it to form bonds with smaller ions, such as fluoride. Gale and his colleagues synthesized compounds **1.4e** and **1.4f** (Figure 1.8), which are similar to compound **1.4a** but have increased acidity in the NH group. They achieved this by adding nitro and dinitrophenyl groups having electron-withdrawing properties at the m- position. The crystal structure of compound **1.4e** exhibits a binding mechanism with the Cl^- ion in the solid state that is similar to that seen in compound **1.4a**. Gale and co-workers synthesized a set of dipodal amide and thioamide receptors **1.4g-k** (Figure 1.8).[25] that were formed from furan and

thiophene components. Analysis using **1.4g**, ^{1}H NMR in DMSO-d_6 / 0.5% water indicates that oxamide derivatives **1.4h** and **1.4i** primarily attach to oxoanions. On the other hand, the more acidic thioamide **1.4j** exhibits increased affinity for anion binding, including towards Cl^{-}, benzoate, and dihydrogen phosphate. Thiophene receptor **1.2k** has a higher degree of selectivity towards dihydrogen phosphate compared to other anions. Talukdar and co-workers have shown that pyrrole-2-carboxamides are very adaptable transmembrane ion transport systems that can be readily adjusted to achieve a broad variety of characteristics via minor structural modifications. Four pyrrole-2-carboxamides series 1 (**1.4l-o**) were synthesized (Figure 1.8), with two alkyl (hexyl and octyl) and two aryl (4-bromophenyl and 4-(tert-butyl)phenyl) substituents. The 4-acetyl group on these molecules, namely pyrrole, was converted to ethyl in order to produce a second series of transporters series 2 (**1.4p-s**) (Figure 1.8). The synthesized compounds exhibited a broad range of logP and N–H pKa values. The ion transport assay was performed on EYPC-LUVs⊃HPTS demonstrated that the derivatives were effective in transporting anions. Series 2 exhibited more activity compared to their equivalent members in series 1, and compound **1.4r** had the highest ion transport activity. Analysis of the compounds' activities at different doses revealed that the formation of the active ion transport complex involves two to four molecules of the transporter, as indicated by the Hill coefficient (n = 2-4). This suggests that the transporter can be finely adjusted with minor changes in its structure, demonstrating its high degree of tunability. The predominant method of ion transport was determined to be anion antiport via mechanistic investigations using **1.4r** across HPTS and lucigenin entrapped vesicles. The anion binding mechanism was confirmed using crystallization, NMR titration tests, and theoretical calculations. The active transporter complexes [(**1.4r**)$_2$ + Cl^{-}] (aryl substituted) and [(**1.4q**)$_4$ + Cl^{-}] (alkyl substituted) were expected using CONFLEX 8 software and then optimized using DFT geometry optimization using GAUSSIAN 09.[26] Talukdar and colleagues discovered a chloride carrier, (**1.4t-w**) (Figure 1.8), which is chemically uncomplicated. This carrier efficiently transports Cl^{-} ions across the lipid bilayer by an antiport mechanism. Additionally, **1.4w** was shown to possess electrogenic properties. The U-tube experiment demonstrated that the 1-dimensional carrier functions as a carrier, rather than a channel. The MQAE experiment demonstrated that **1.4w** efficiently transfers Cl^{-} ions into the cells. Based on the MTT experiment, it was shown that **1.4w** exhibited no toxicity towards cells, even at high doses, when compared to the control compound **1.4y**. The discovery of the chloride transporting and non-toxic 3-(1H-1,2,3-triazol-

1-yl)benzamide system has provided an opportunity to investigate its potential use in treating channelopathies.[27]

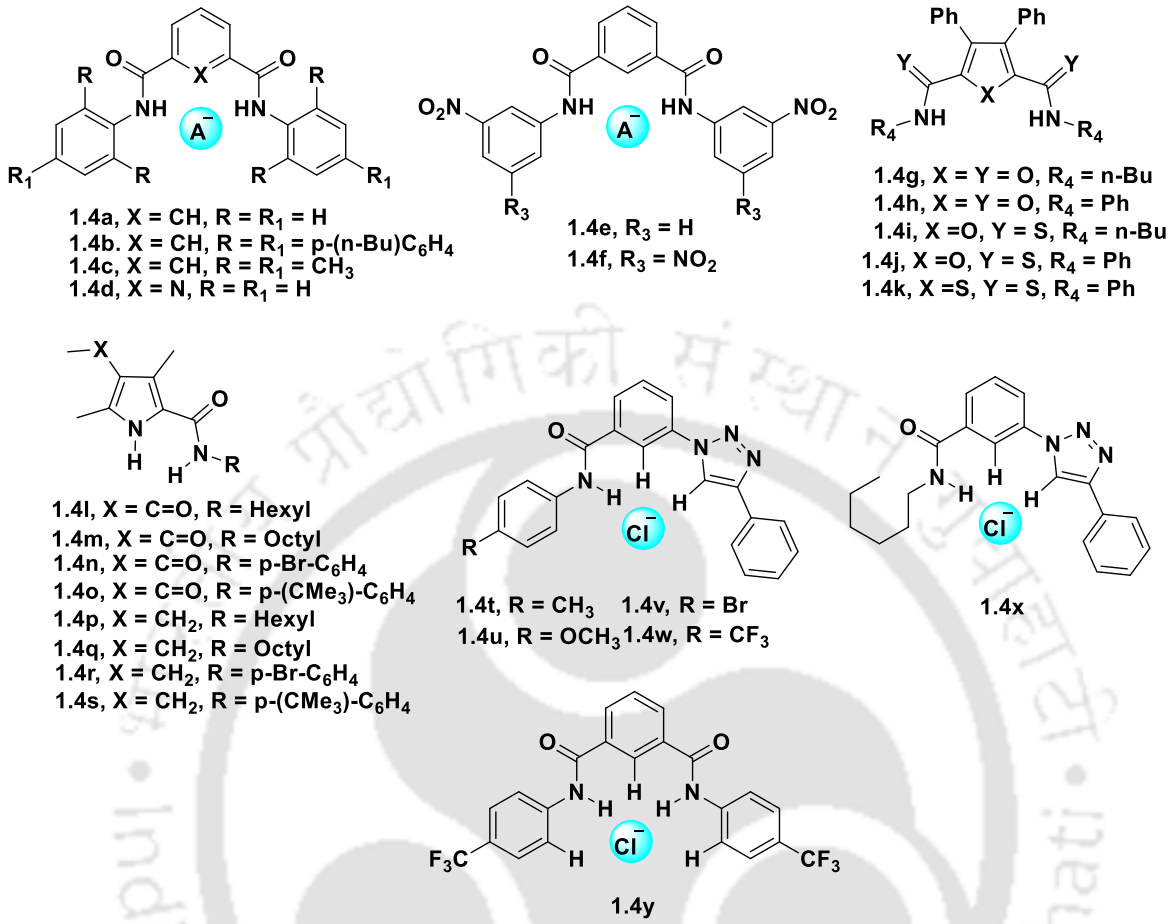

Figure 1.8. Amide functionalised receptors.

Talukdar and coworkers have developed synthetic anion receptors (**1.5a-g**) using 1H-indole-2-carboxyamide (Figure 1.9). These receptors were created by attaching a sulfonamide group with different aryl groups. This category of compounds was developed to attach to anions, thereby facilitating the transportation of the anion and a proton by removing a proton from its sulfonamide group. The co-crystallization of **1.5e** with TBACl demonstrated the complexation of two Cl^- ions by two receptor molecules facilitated by several water molecules. The ^{1}H-NMR titration experiments provided more evidence of anion binding. The thorough mechanistic analysis using the most effective transporter revealed the hypothesized method of proton–anion symport. These compounds have the potential to effectively target solid tumors by inducing intracellular acidity.[28] Shin, Gale, Sessler, and coworkers designed a thorough investigation of the cellular processes of squaramide compounds that function via anion transport, (Figure 11). The ability of Squaramide **1.5h** and its bis-squaramide derivatives, ortho-phenylenediamine

1.5i and **1.5j**, in enhancing the transport of Cl^- ions inside a liposomal environment was confirmed.[29] Transport analysis showed that these anionophores enhance the movement of Cl^- ions and, as a consequence, there is an increase in the entry of Na^+ ions via sodium channels. This leads to higher concentrations of Cl^- and Na^+ ions within FRT cells. The viability experiments, which varied in dosage, demonstrated that squaramides (**1.5h-j**) have lethal effects (with IC_{50} values ranging from 2-6 µM) on several cancer cell lines, such as HeLa and A549 cells. Gale and his colleagues conducted a comprehensive examination of the biological properties of squaramide **1.5h**.[29, 30] The researchers noted that squaramide **1.5h** has the ability to raise the pH of lysosomes. This, in turn, decreases the activities of cathepsin B and L, ultimately impacting the normal functioning of lysosomes. As a consequence, autophagy is disrupted and apoptosis is induced. The western blot examination of the HeLa cell demonstrated an increase in the extents of LC3-II and p62 proteins, suggesting that squaramide 8 disrupts autophagy. Multiple investigations on cellular activity have shown that the squaramides (**1.5h-j**) stimulate the liberation of cytochrome c from mitochondria, resulting in caspase-dependent apoptotic cell demise. In general, the abundant experimental evidence confirm that these ion transporters interfere with autophagy and trigger apoptosis by disturbing cellular chloride levels.

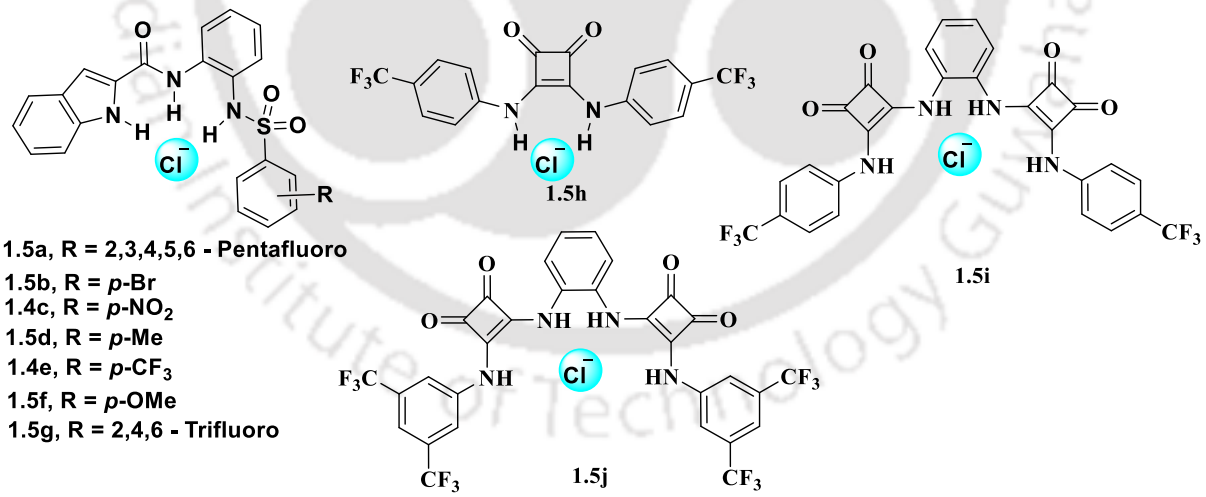

Figure 1.9. Sulfonamide and squaramide based receptors.

1.6.2. Urea and thiourea functionalised synthetic anionophores

In 2010, Gale and his colleagues synthesized simple TREN-based trisureas and thiourea as **1.6a-j** and analyzed their ability to transport anions and promote cellular functions (Figure 1.10).[31] The fluorescence-based anion transport experiments revealed that the TREN-based

were successful in transporting Cl^-/NO_3^- and Cl^-/HCO_3^- ions in antiport mechanism. The incorporation of fluorine or trifluoromethyl groups is seen as a promising strategy for the development of efficient ionophores. Both the fluorine and trifluoromethyl substituents enhance the lipophilicity of the compounds and raise the acidity of the N-H proton in the urea or thiourea moieties. The powerful ionophores exhibited detectable anion transport capabilities at a ratio of 1 transporter to 250,000 lipids. The biological activity investigations shown that the very effective TREN-based ionophores **1.6h** and **1.6j** provoke cytotoxicity in different cancer cell lines. The fluorinated tripodal carriers' ability to carry anions led to changes in the intracellular pH, which triggered death in cancer cells.

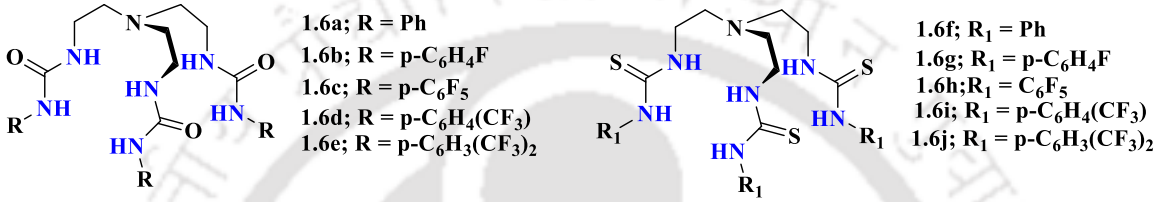

Figure 1.10. TREN based thiourea derivatives receptors.

Manna and coworkers developed a selective Cl^- ion receptors, conformationally regulated 1,2-diphenylethylenediamine-based bis(thiourea) derivatives (**1.7a-h**) (Figure 1.11).[32] The bis(thiourea) derivatives of diamine-based compounds have a significant ability to bind Cl^- ions, with a binding constant (K_d) ranging from 3.87 to 6.66 mM. This strong binding property is closely associated with their ability to transport anions across cell membranes, as seen by their effective concentration (EC_{50}) ranging from 2.09 to 4.15 nM. The transportation of chloride ions via a chloride/nitrate antiport mechanism was verified for the most active molecule. The disruption of Cl^- ion balance caused by this anion carrier leads to cell death by facilitating the caspase-mediated intrinsic route of apoptosis.

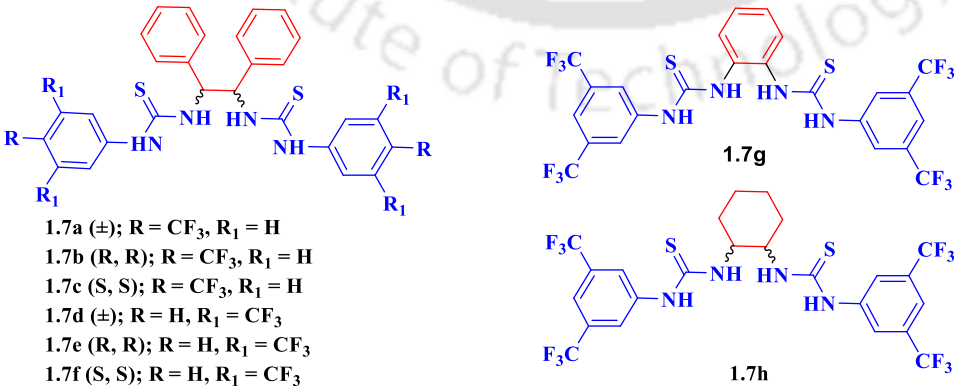

Figure 1.11. Diphenylethylenediamine based thiourea derivatives receptors.

In 2020, Gale and others synthesized a range of ortho-phenylene bisurea variants (Figure 1.12).[33] The study examined the impact of including a fluorinated central aromatic group and a urea motif containing either thiophene or benzothiophene on the activities of anion transport (**1.8a-o**). The chloride ion-selective electrode was used to assess the anion transport activities of these compounds inside the liposomal environment. The compounds with a fluorinated core aromatic component were identified as the most efficient carriers in all biophysical experiments.

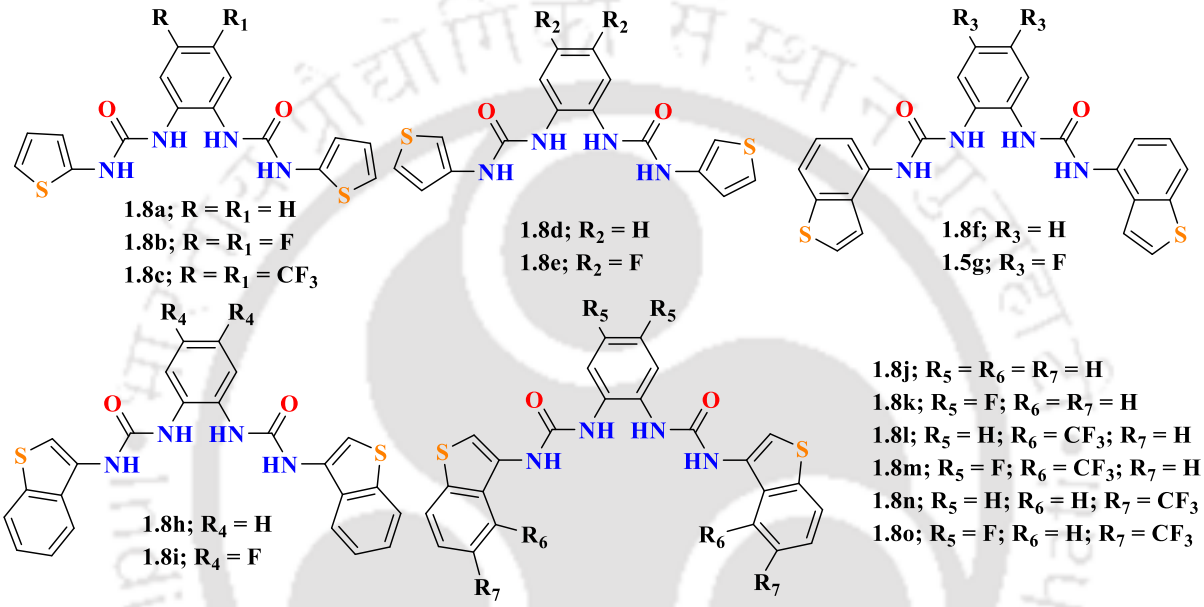

Figure 1.12. *o*-phenylenediamine based urea derivatives receptors.

1.6.3. Stimuli-responsive anionophores

Synthetic anionophores provide significant therapeutic promise, although they also exhibit certain limits. Due to their lipophilic nature, the delivery of anionophores into the cell is difficult. The lack of specificity among healthy cells and tumor cells is a significant limitation of the traditional anionophore. Normally, cancer cells have a lower pH value, for the oxidative stress overexpression of glutathione, ROS and other, and increased enzyme activity. Thus, pH, glutathione, ROS, enzymes, and other factors have the potential to function as endogenous triggers. While near-infrared light, ultrasound, and other stimuli have the potential to operate as exogenous stimuli. The design and development of stimuli-responsive anionophores are considered a very needed approach for selectively targeting cancer cells and minimizing negative effects. Scientific frat has developed proanionophores, in which the anionophore itself is concealed by stimuli-

responsive linkers. These linkers release the active anionophore based on the specific stimuli inside the cell. The abnormal metabolism enables cancer cells to modify the pH of both the intracellular and external surroundings, increase the concentration of glutathione (GSH), ROS and enzymes, among other effects. These triggers enable cancer cells to develop aggressive characteristics, such as invasiveness, the capacity to spread to other parts of the body, increased movement, resistance to drugs, and other traits. Compounds that exhibit enhanced anion transport activities under acidic conditions or in the presence of GSH are regarded as promising approaches for ion transport-mediated anticancer effects. Thus, ion transporters that have the ability to enhance their ion transport characteristics under acidic conditions are regarded as promising targets for specific anticancer effects.

1.6.3.1. pH responsive synthetic ionophores

In 2016, Gale and co-workers executed an investigation on the transport of chloride ions across cell membranes using synthetic phenylthiosemicarbazones derivatives (**1.9a-c**) (Figure 1.13).[34] These compounds were designed to replicate the action of acid-sensing ion channels, which are gated by protons. These anionophores have notable pH-dependent transport features, with a transport effectiveness that may rise up to 640 times when transitioning from pH 7.2 to 4.0. The initiation of this "gated" process occurs when the imino nitrogen is protonated and simultaneously causes a conformational shift in the anion-binding thiourea group, transitioning it from an anti to a syn configuration. Through the use of two cationophore-coupled transport experiments, using either monensin or valinomycin, we have successfully determined the underlying transport mechanism of phenylthiosemicarbazones. The analysis showed that the transport process is non-electrogenic and involves the simultaneous movement of H^+ and Cl^- ions. This work presents the first instances of pH-responsive non-electrogenic anion transporters.[34]

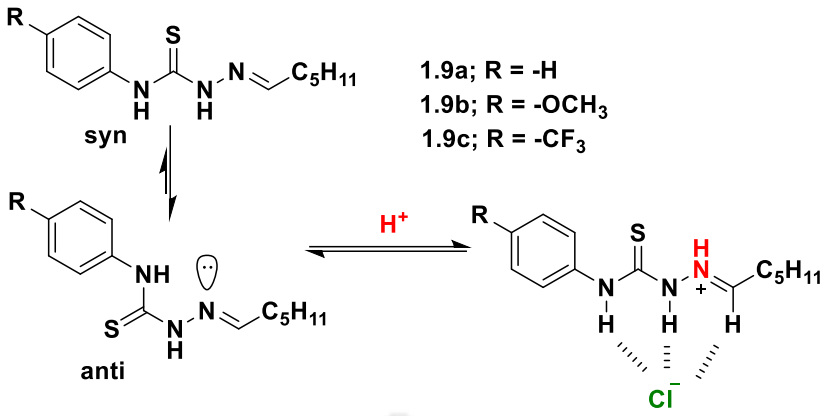

Figure 1.13. Phenylthiosemicarbazones based anionophores.

In 2019, Manna and co-workers developed a pH responsive chloride transporter, which are 1,2-bis(benzimidazol-2-yl)benzene derivatives (**1.10a-d**), and investigated their biological activity related to ion transport (Figure 1.14).[35] The ion transport activity investigated using ISE (Ion-Selective Electrode) shown that compound **1.10d**, which is based on iminourea, has transmembrane anion transport capabilities that are dependent on pH. The transporter **1.10d** has a pKa value of 6.2, indicating its high propensity to undergo protonation in a mildly acidic environment. There is enough evidence to support the fact that normal, healthy cells often have a slightly lower internal pH (pH_{in} = 7.2) compared to the pH of their surrounding environment ($pH_{ex} \approx 7.4$). However, the pH level in cancer cells is often between 6.2 - 6.9. The pH gradient reversal increases the ability of cancer cells to avoid apoptosis. Multiple biophysical experiments have shown that compound **1.10d** is capable of facilitating the transport of the H^+/Cl^- ion pair across the lipid bilayers. Cell viability experiments conducted in several acidic media demonstrated that the compound exhibits more cytotoxicity at pH 6.5 in MCF7 cells as compared to pH 7.4. The compound showed cytotoxicity towards cancer cell by Cl^- ion transport. The compound exhibited cytotoxicity that was more than twice as high in cancer cells compared to normal cells.[35]

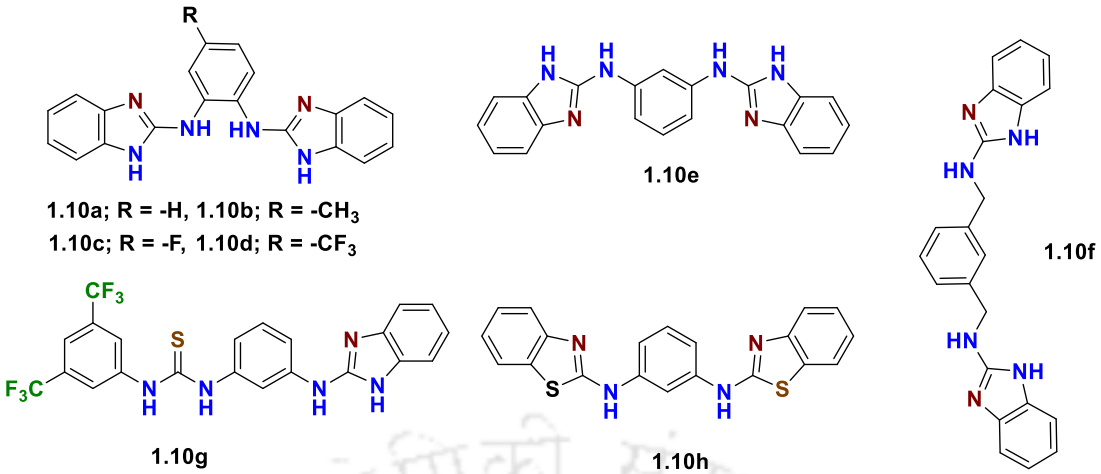

Figure 1.14. Anionophores of 1,2-bis(benzimidazol-2-yl)benzene and others controlled derivatives.

In 2020, Manna and co-workers developed squaramide and thiourea analogues of quinine derivatives (**1.11a-h**) and biophysical assays for ion transport activity and cellular activity were analysed (Figure 1.15).[36] The presence of a quinuclidine group facilitates the synergistic interaction involving Cl^- and H^+ ions and the thiourea or squaramide group, leading to an efficient transport of these ions across membranes. The disruption of ionic equilibrium caused by the strong Cl^- ion carrier specifically triggered the demise of cancer cells by promoting caspase-mediated apoptosis. The in *in-vivo* study of the potent ionophore **1.11c** revealed a significant decrease in growth of tumors while causing minimal immunotoxicity to adjacent organs.[36]

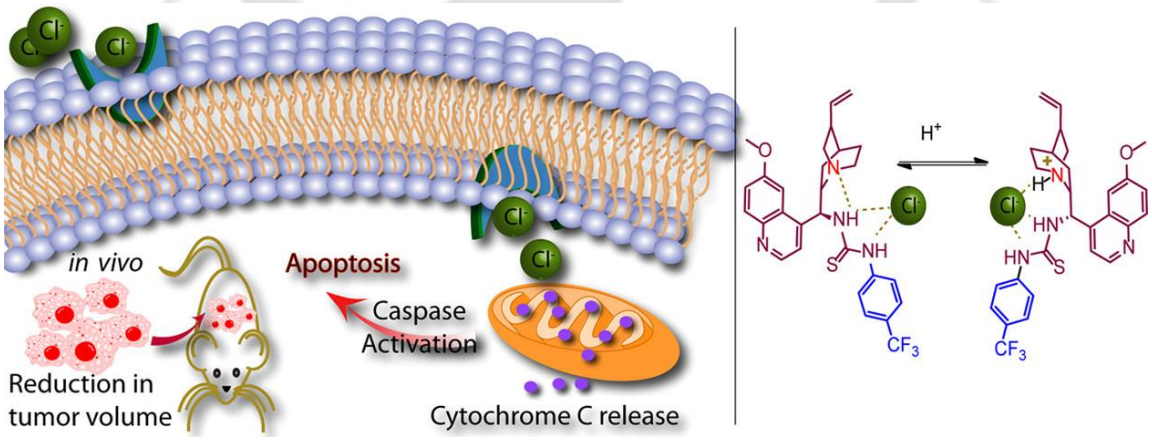

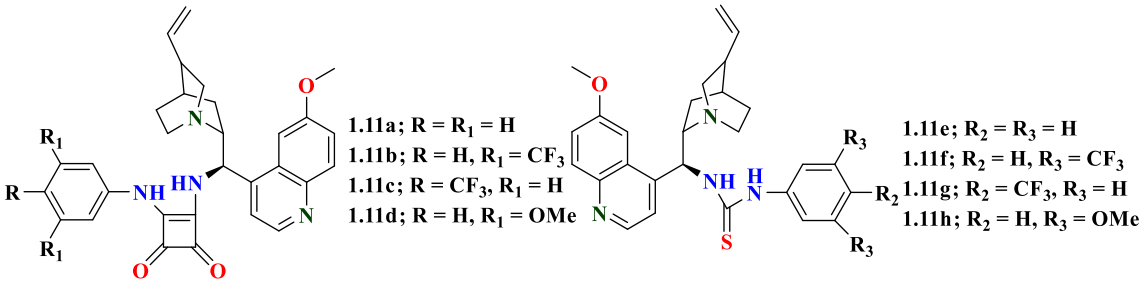

Figure 1.15. Squaramide and thiourea derivatives of quinine.

1.6.3.2. Glutathione responsive synthetic ionophores

In 2020, Manna and colleagues developed thiourea-based tripodal compound which selectively transport the Cl^- ions across the lipid bilayers. This receptor has the ability to form molecular capsules inside lipid bilayers for transportation of Cl^- ions. In addition they have introduced a sulfonium group to each arm of the ionophore **1.12** which facilitated the increment of water-solubility of proanionophore, which is sensitive to glutathione as stimuli (Figure 1.16**)**.[37] The application of GSH resulted in the effective regeneration of the hydrophobic active anionophore and facilitated the transfer of Cl^- ions in a regulated manner. The active anionophore restoration in biological conditions has been proven by many physiological investigations. The microscope assessment showed a greater cellular intake of the sulfonium-based proanionophore, indicating its enhanced viability. The reduced toxicity of the powerful drug indicates that the GSH-responsive anion transport approach has promise for treating disorders associated with ion transport, such as cystic fibrosis.[37]

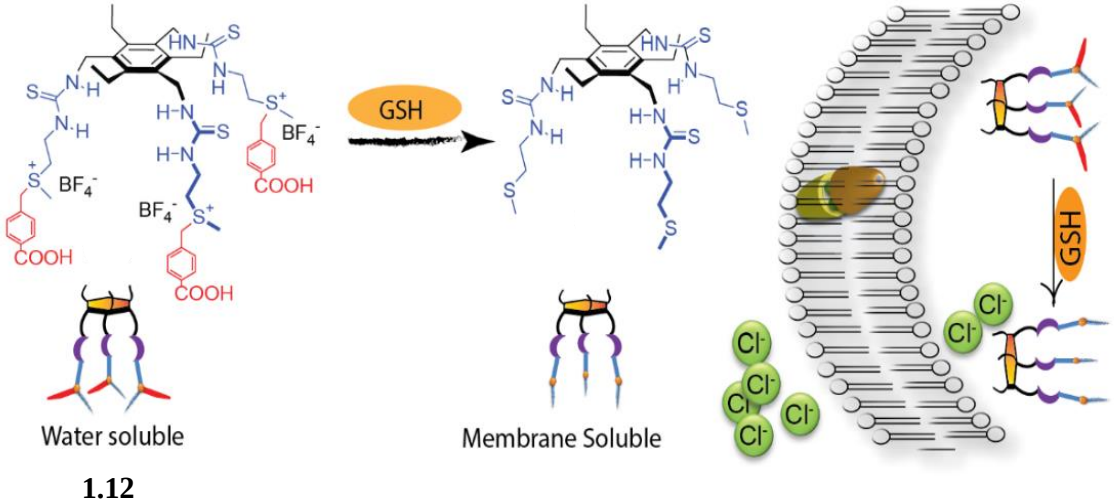

1.12

Figure 1.16. Sulfonium based GSH responsive proanionophore.

In 2023, Manna and co-workers synthesized a GSH responsive synthetic proanionophore using thiourea binding cavity (Figure 1.17).[38] This anionophore **1.13a** is capable of transporting H^+ and Cl^- ions across the lipid bilayer via a symport mechanism. The proionophore **1.13b**, which has been modified with RGD, effectively stimulates the transport of ions across the cell membrane by releasing its traceless tag in response to glutathione (GSH). The cell viability assays revealed that the active ionophore effectively inhibited the growth of A375 melanoma skin cancer cells, perhaps via facilitating the transportation of H^+/Cl^- ions across the cell membrane. Moreover, the proionophore attached with RGD-peptide exhibited greater cytotoxicity against A375 cells in comparison to HEK293T cells, may be because of its selective uptake via the integrin-mediated route.

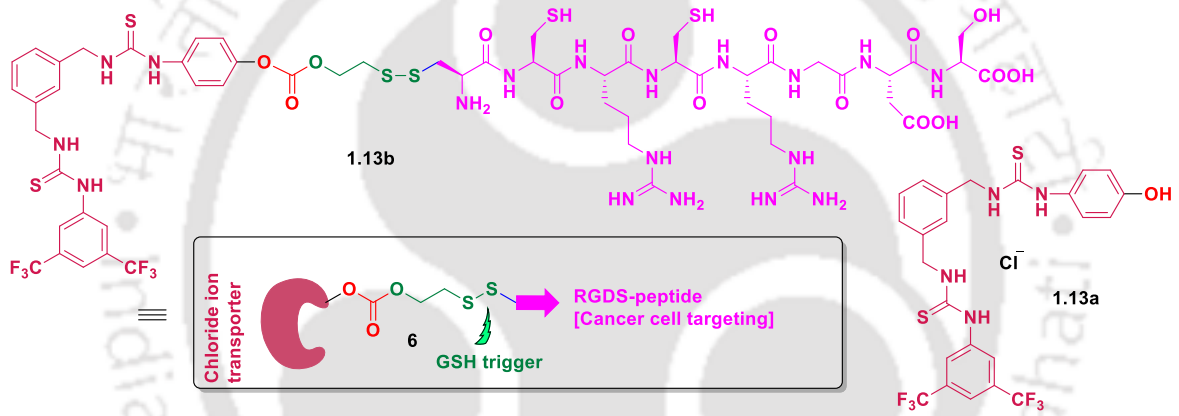

Figure 1.17. RGD-linked GSH responsive proanionophore

1.6.3.3. Enzyme responsive synthetic ionophores

In 2023, Talukdar and co-workers developed the initial use of NQO1 to selectively activate 'protransporter' receptors in cancer cells, resulting in the initiation of apoptosis. They successfully synthesized salicylamides, a class of small compounds that may efficiently facilitate the transport of H^+/Cl^- ions across lipid membranes.[39] The ability of salicylamides to transport ions was significantly reduced by enclosing the hydroxyl group with NQO1 activatable quinones using either an ether or ester bond (**1.14a-g**) (Figure 1.18). The verification of the release of active transporters was conducted after the decrease of quinone-caged 'protransporters' by NQO1. Both the transporters and protransporters had notable harmful effects on the MCF-7 breast cancer line, primarily by triggering oxidative stress, mitochondrial membrane depolarization, and lysosomal

deacidification. The verification of cell death induction via the intrinsic apoptotic route was conducted by monitoring the cleavage of PARP1.[39]

Jeong and co-workers synthesized an enzyme responsive proanionophore. The procarriers **1.15a-d** were synthesized with hydrophilic parts such as polysaccharides or carboxylate moieties.[40] These parts are sensitive to certain enzymes such as lipases, esterases, or glycosylase (Figure 1.19). The biophysical and cellular analyses revealed the regeneration of the active anionophore **1.15a** from its water-soluble counterparts. The investigation of transport in YFP-expressing FRT cells revealed that the entry of Cl^- ions was enhanced when polysaccharides were attached to the procarrier molecule, particularly in the presence of β-galactosidase enzyme derived from Aspergillus oryzae, and under mildly acidic circumstances (pH = 5.5–6). Therefore, the conjugation of polysaccharides might improve the transportability of the active anionophore in cancer cells, ultimately leading to the manifestation of its anticancer properties.[40]

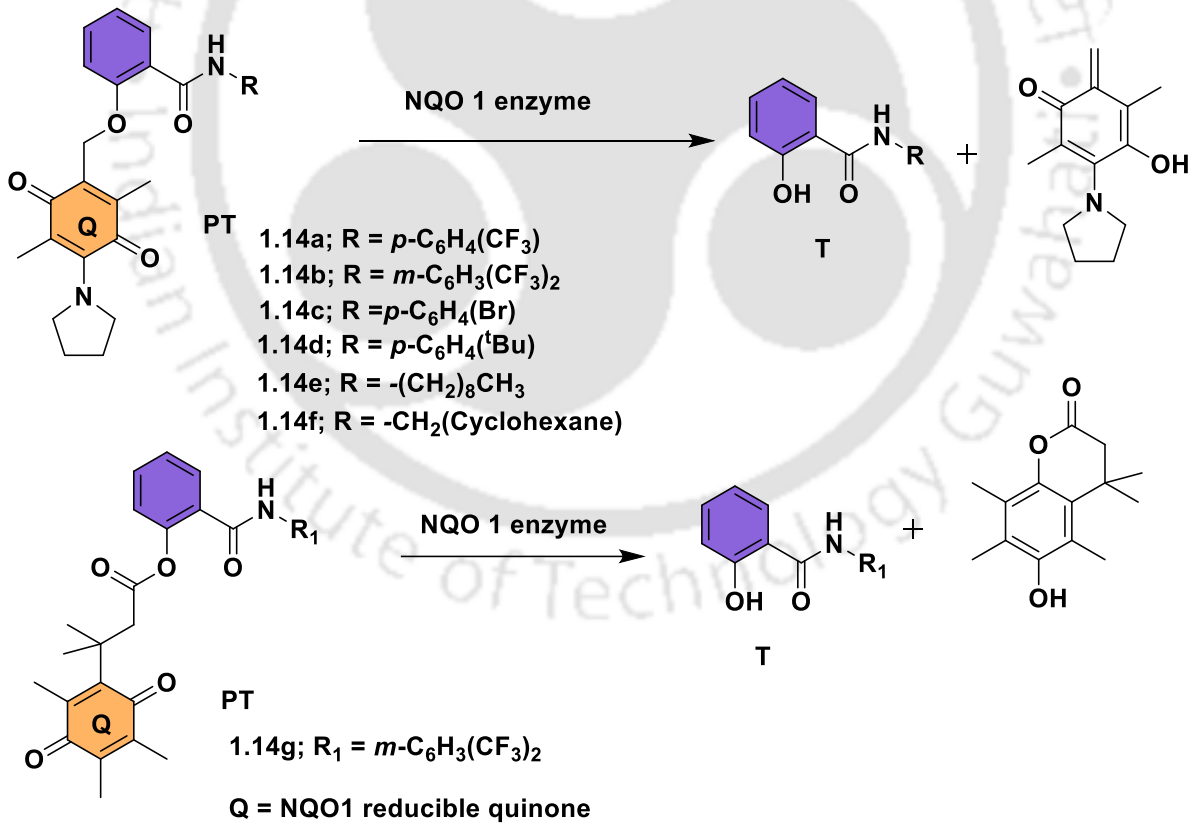

Figure 1.18. NQO1 responsive proanionophores.

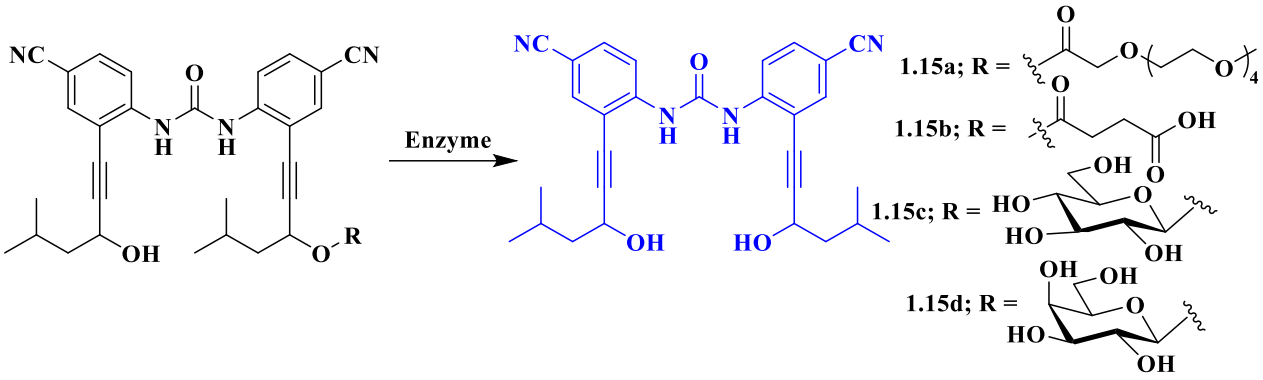

Figure 1.19. Enzyme responsive anionophores.

1.6.3.4. Light responsive ionophores

Talukdar and colleagues developed a proionophore which opens up to light and can be triggered by UV-light to restore the active anionophore (Figure 1.20). They successfully synthesized indole-2-carboximide analogue **1.16a2**.[41] In this receptor, the amide group was protected by the photo-cleavable ortho-nitrobenzyl group. The ^{1}H NMR analysis demonstrated the formation of an active ionophore from the proanionophore when exposed to 365 nm light. The fluorescent assay using HPTS demonstrated that the active ionophore **1.16a2** transports anions via the OH^-/Cl^- antiport mechanism when base-pulse is present. The cell viability assays demonstrated that the photo-release of the active ionophore resulted in a modest level of cell death in MCF7 cells. While the utilization of 365 nm light for photo-activation may not be optimal for future biological investigations, a photo-responsive proionophore like this has promise for use in photodynamic treatment. Talukdar and co-workers have shown that acylhydrazones exhibit photoresponsive anionophoric properties **1.16b1** (Figure 1.20).[42] The *E*-form of the system's chloride binding was verified using single crystal X-ray diffraction and ^{1}H NMR spectroscopic investigations. The transporter exhibited a high level of activity, with an EC_{50} value of 0.62 μM and a Hill coefficient of around 2, suggesting that two molecules are involved in the production of the active transporter. The mechanistic investigations have verified that the fundamental transport pathway is a carrier-mediated anion antiport. The reversible *E-Z* isomerization created the gated ion transport via the potent compound. Talukdar and co-workers synthesized a photoregulatory anionophoric system based on trans-azobenzene (**1.16c-g**) (Figure 1.20).[43] This system effectively transports chloride ions by creating a dimeric complex in the shape of a sandwich structure. In addition, studies validated the existence of a transport-mediated process

involving the exchange of chloride anions, and theoretical investigations revealed the supramolecular interactions responsible for chloride recognition inside the sandwich complex. The azobenzene underwent reversible trans-cis photoisomerization at room temperature, with no major involvement of heat cis-trans isomerization. Photoregulatory transport activity across the lipid bilayer membrane deduced an excellent off-on behaviour of the azobenzene photoswitch.

In 2021, Gale and coworkers developed a series of bis(thio)ureas based on photoswitchable stiff-stilbene derivatives (**1.17a-c** and **1.18a-c**) (Figure 1.21).[44] UV–vis and ^{1}H NMR spectroscopy are used to investigate the *E*–*Z* photoisomerization of these bis(thio)ureas. Additionally, ^{1}H NMR titrations demonstrate that chloride binds more strongly to the (*Z*)-form than to the (*E*)-form. Single crystal X-ray diffraction study and DFT geometry optimization offer further understanding of the interaction features. Significantly, the (*Z*)-isomers exhibit significantly greater efficacy in transport across membranes compared to their corresponding (*E*)-isomers, confirmed by various assays.

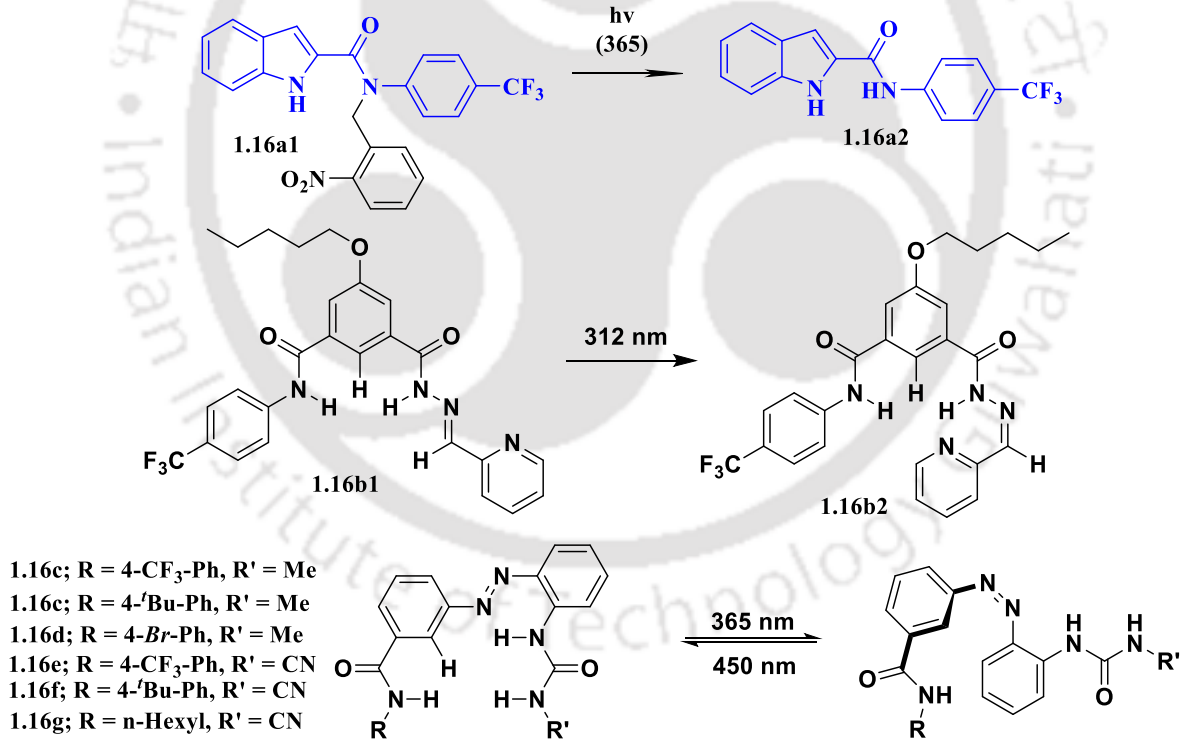

Figure 1.20. Photoswitchable synthetic anionophore.

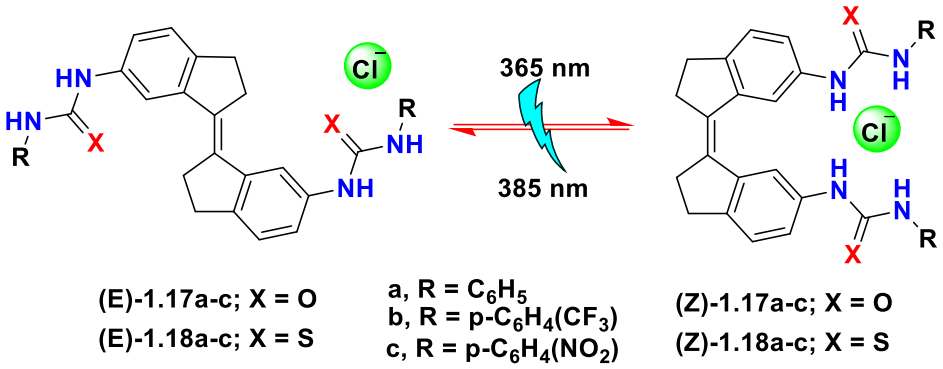

Figure 1.21. Light responsive stiff-stilbene derivatives

1.6.4. Non-toxic synthetic anion carriers

The importance of CFTR in controlling the movement of water and salt within epithelial cells indicates its essential role in the pathogenesis of cystic fibrosis. Although there are a few CF drugs available that target the faulty CFTR, the large number of CFTR gene variants is a substantial obstacle. Artificial anionophores, which have been designed specifically to engage with membranes instead of targeting particular proteins or genes, are being considered as a potential approach for addressing the complex challenges associated with CF. Anionophores provide a distinct treatment approach to overcome the difficulties caused by CFTR mutations. These synthetic anionophores provide a possible alternative by regulating ion transport across the cell membrane, eliminating the need for gene-specific targeting. Anionophores have the potential to mitigate the conflicts that arise from CFTR mutations or the overexpression of related genes and proteins. An essential factor for the effectiveness of anionophores in treating cystic fibrosis is their capacity to exhibit non-toxic behavior. It is very desired to have anionophores that promote the preference of Cl^- over H^+/OH^-, especially given the claimed toxicity attributed to the participation of protons in transport mechanisms. However, the unique toxicity of molecules presents a difficulty in accurately adjusting anionophores to fulfil therapeutic goals. The Davis group conducted extensive studies to find an appropriate anionophore for cystic fibrosis therapy.[45] They examined compounds with trans-decalins, substituted cyclohexanes, and steroid scaffolds. The team tested each compound using standard assays, focusing on fluorescence assays using YFP-expressed FRT cells. The steroidal framework's naturalness may have contributed to the inactivity of all steroidal cholapods. Compound **1.19a** showed significant activity in YFP-FRT cells, particularly in LUVs. The non-steroid compound **1.19b** was the best candidate in the LUV deliverability test. The team also found that

cells could be easily supplied with bisureiododecalin **1.19b** without the need for special adjuvants. In 2019, the team screened several classes of compounds to find compounds with greater or comparable potency.[46] They used the CF bronchial epithelial cell line (CFBE41o−) because it can express the Ca^{2+}-activated Cl^- channel (CaCC), unlike YFP-FRT cells. The analysis showed that anion transport by anionophores in YFP-CFBE cells occurs independently of CaCC activation and is additive in the case of compound **1.19f**. The team investigated the overall toxicity and activation of apoptosis in YFP-FRT cells using live-cell analysis. Anionophores **1.10c**, **1.10d**, and **1.10f** had some cytotoxic effects on YFP-CFBE cells, but **1.19a** exhibited no cytotoxicity and resulted in a negative apoptotic response (Figure 1.22).

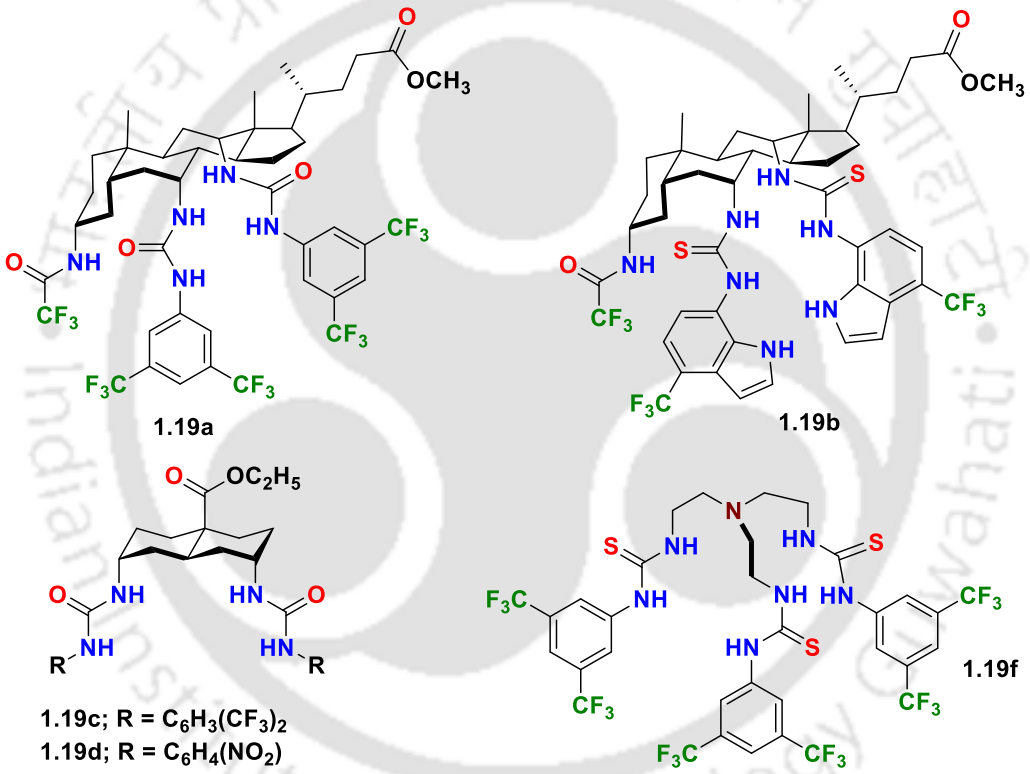

Figure 1.22. Anion receptors with steroids, trans-decalins and TREN-based trisureas derivatives

1.6.5. Synthetic ionophores with antibacterial properties

Drug resistance is a prominent global issue that poses a threat to the effectiveness of antibiotics. The Centers for Disease Control and Prevention (CDC), USA have previously categorized many microorganisms as posing significant risks to human health. Initially, the study on the anion transport mostly concentrated on developing of ionophores for the purpose of treating cystic fibrosis and cancer. Recent investigations have shown that synthetic ion transporters may produce antibacterial activity by facilitating the transmembrane transfer of Cl^-, either fully or

partially. These artificial ion transporters are very valuable in addressing drug-resistant bacterial strains, since more than 80% of infections acquired in hospitals are growing more resistant to medicines that are currently available on the market. Therefore, it is essential to find novel strategies or molecules to address the issue of infections produced by ESKAPE viruses. In 2015, Schmitzer and co-workers synthesized a class of anionophores (**1.20a-h**) using benzimidazolium salts had the ability to kill both gram-positive (*B. thuringiensis strain*) and gram-negative bacteria (*E. coli*) (Figure 1.23).[5] The benzimidazolium salts-based anionophores facilitate the transportation of anions by both channel and carrier routes, depending on the kinds of counter anions. The powerful substances have little toxicity towards human cells, making it a crucial characteristic for an optimal antibacterial contender. Multiple mechanistic investigations have shown that the membrane depolarization caused by these anionophores is the main factor contributing to their potential antibacterial effect. The presence of the anionophores on the membrane hinders the bacteria's ability to build resistance. Similarly, the anionophores should have efficacy against microorganisms that are resistant to drugs.

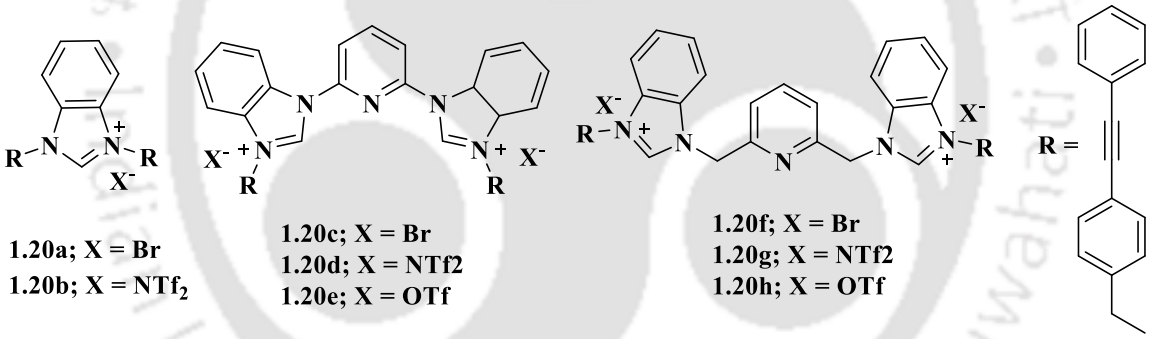

Figure 1.23. Benzimidazolium based anionophores.

Sessler et al. showed both aminopyrrolic and TREN-based molecules **1.21a-c** have antibacterial action towards methicillin-resistant Staphylococcus aureus (MRSA) strains, namely Mu50 and HP1173, via facilitating anion migration (Figure 1.24).[47] The bacterial investigations executed shown that compounds **1.21a-c** exhibit significant inhibitory effects on both gram-positive (S. aureus) and gram-negative (Pseudomonus aeruginosa) bacterial strains. The thiourea-based anionophores have significant activity, with minimum inhibitory concentration (MIC) values ranging from 0.93-1.78 μg/mL for Mu50 and S. aureus, respectively. While these anionophores demonstrated antibacterial effects, there is no discernible relationship between anion transport and the antibacterial activity. Furthermore, a

meticulous evaluation has shown that ion transport alone is not the only determinant of the antibiotic effectiveness exhibited by these aminopyrrolic and TREN-based drugs.

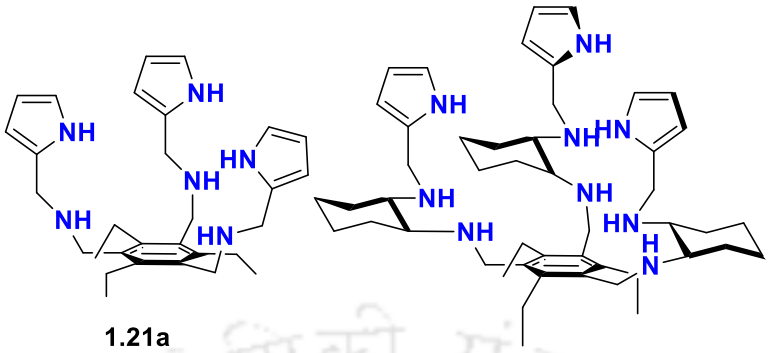

Figure 1.24. TREN-based anionophores.

Quesada's group explored the correlation among anionophores and antibacterial properties by examining indolyl adorned tambjamine analogues (**1.22a-f**) with various modifications on the pyrrole ring connected to the imine component (Figure 1.25).[48] The compounds' ability to transport anions was examined inside a liposomal environment. The HPTS fluorescence-based investigations demonstrated that the powerful compounds efficiently transport anions (with an EC_{50} of 16 nM) via an anion/Cl^- exchange route. The powerful compounds shown efficacy against both gram-positive bacteria, such as *E. faecium* and *S. aureus*, and gram-negative bacteria, such as *A. baumannii* and *K. pneumonia*, which are often seen in hospital-acquired illnesses. The molecules additionally demonstrated satisfactory hemocompatibility.

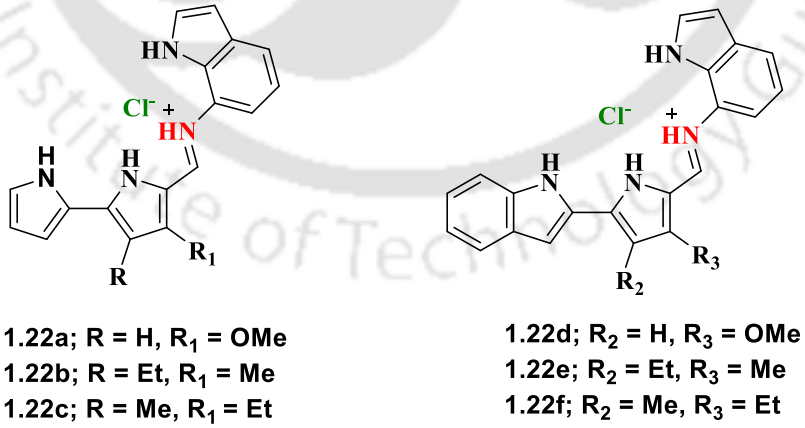

Figure 1.25. Indolyl adorned tambjamine analogues.

In 2024, Talukdar and co-workers have discovered that pyridyl-linked hetero hydrazones (**1.23a-h**) are very effective in transporting HCl across cell membranes (Figure 1.26).[49] These

compounds provide a suitable location for interaction with HCl via a cooperative process of protonation, followed by the identification of chloride ions. The transport of HCl by these chemicals effectively limits the development of several gram-negative bacterial strains by disrupting the balance of the cell membrane.

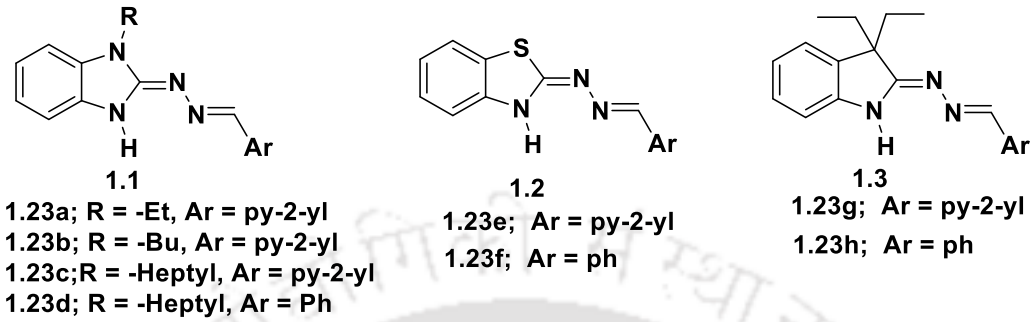

Figure 1.26. pyridyl-linked hetero hydrazones derivatives.

1.7. Methods for quantifying anion transport across lipid bilayers

Ion transporter have a crucial function in regulating the concentrations of solutes across cell membranes, which requires the precise and precise detection of their transport processes.[1, 50] Two primary methods used for this aim consist of the determination of conductance through planar bilayer membranes, also referred to as the black lipid membrane (BLM) test, and experiments using liposomes. The BLM test provides a direct measurement of voltage, allowing for the differentiation of ion channel processes from carrier mechanisms. Conversely, liposome-based assays are used to investigate ion carriers. Unilamellar phospholipid vesicles, which are used to create liposomes, are dependable models that enable the replication and examination of ion transport via biological membranes. Liposomes' adaptability allows for careful manipulation of liquids inside and outside the vesicles. Concentration gradients across vesicular membranes are established by substituting ions outside the vesicles, either using size exclusion chromatography or dialysis procedures. The ion transport promoted by the injection of a transporter molecule may be measured using many methods, including as fluorescence, ion-selective electrodes, nuclear magnetic resonance (NMR), and others. These approaches allow scientists to thoroughly investigate and comprehend the complex processes involved in ion transport, revealing the mechanisms that govern cell homeostasis and offering important information for therapeutic advancements.

1.7.1. Fluorescence-based assay

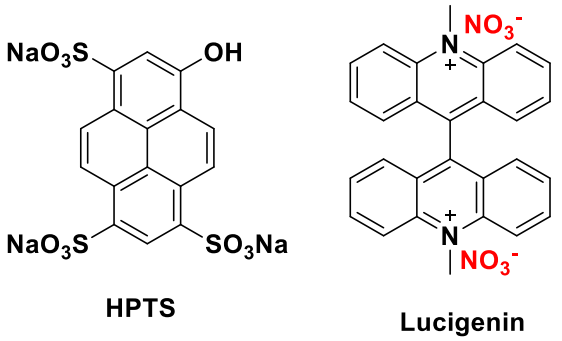

Figure 1.27. Fluorescent dyes for the ion transport assays.

Fluorescent-based studies quantify mobility by detecting the fluctuations like fluorescence emission from a specific enclosed dye that is responsive to variations in pH, anion concentration, or electric potential during a certain time frame. Fluorescent dyes often used for measuring the transport of ions in liposomal tests include 8-Hydroxypyrene-1,3,6-trisulfonic acid trisodium salt (HPTS), *N, N′*-dimethyl-9,9′-biacridinium dinitrate (Lucigenin) (Figure 1.27). HPTS is a pH responsive dye that is not able to pass across membranes and dissolves easily in water. It has a pKa value of around 7.3 in water-based solutions. The HPTS molecule exists in two states: protonated and deprotonated. Both of these forms have distinct excitation wavelengths, specifically 403 nm to reflect the protonated one and 460 nm with the deprotonated one. Yet, activation at both wavelengths results in emission at a single wavelength, namely 510 nm. In assays that are based on pH gradient, a difference in pH is established along vesicles that containing HPTS. The transport process is then studied by measuring the emission intensity of HPTS after adding the transporter molecule. The alteration in intravesicular pH after the introduction of an anion transporter suggests that the transportation takes place by either H^+/Cl^- efflux, which is a symport process, or OH^-/Cl^- exchange mechanism (Figure 1.28). This test enables the quantification of intravesicular pH by assessing the proportion of dye that is protonated vs deprotonated.[51]

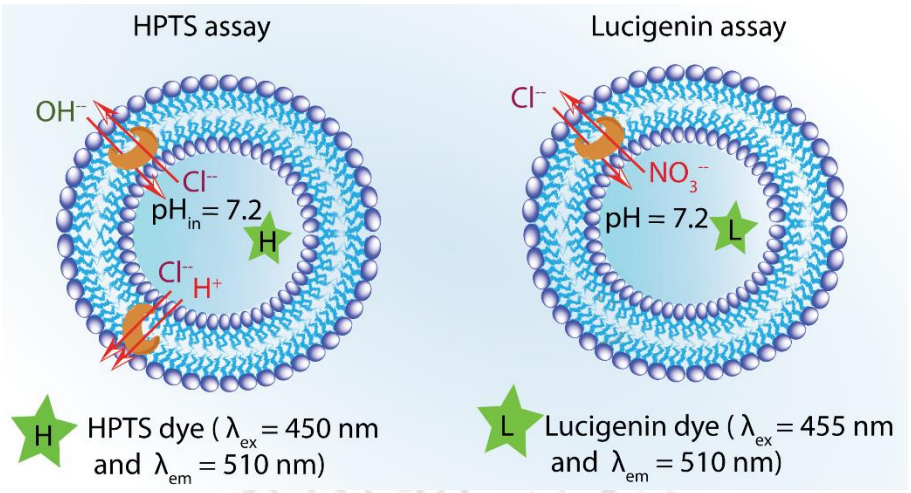

Figure 1.28. Representation of fluorescence based HPTS and Lucigenin assay.

Lucigenin assays are used to directly evaluate anion transport. The presence of halide anions preferentially reduces the fluorescence of Lucigenin, but oxoanions such as nitrate or sulphate do not have an effect on its fluorescence. The conventional procedure entails the inclusion of vesicles containing NO_3^-, together with lucigenin dye, and the establishment of a chloride gradient by introducing Cl^- into the extravesicular matrix. The transport mechanism is distinguished by the observation of fluorescence quenching after the introduction of transporter molecules. The transport process involves the exchange of NO_3^- ions with Cl^- ions (Figure 1.28).[52]

1.7.2. Ion selective electrode-based assay

The measurement of ion release from vesicles may be accomplished using ion-selective electrodes, which provide a direct and simplest approach, similar to lucigenin-based assays. In further detail, the measurement of ion efflux entails the assessment of the conductivity of the fluid outside the vesicles by use of ion-selective electrodes. In a typical chloride efflux experiment, liposomes carrying a reasonably high concentration of MCl are added to an isoosmolar solution of MNO_3 or M_2SO_4, where M denotes monovalent alkali cations. The subsequent measurement of Cl^- ion efflux involves measuring the conductivity of the extravesicular solution, both with and without the transporter. The measurement is conducted using a chloride-selective electrode, (Figure 1.29). This method provides a straightforward way to evaluate anion transport, showcasing its simplicity and efficacy in revealing the kinetics of ion transfer across vesicular membranes.[52]

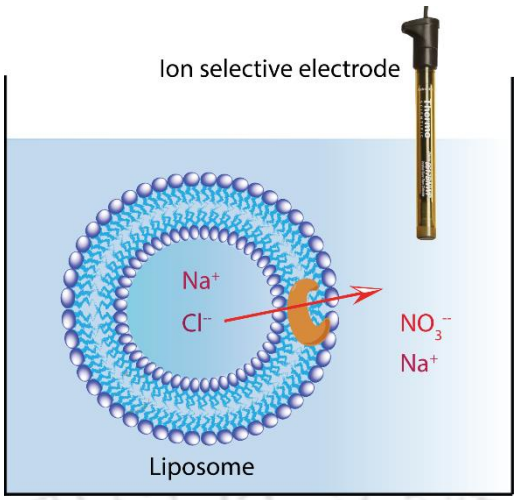

Figure 1.29. Schematic representation of ISE based ion transport assay.

1.7.3. NMR based assay

The species that it transports requires intrinsic nuclear magnetic resonance (NMR) activity, as shown through isotopes such as $^{35}Cl^-$, $H^{13}CO_3^-$, or $^{33}SO_4^{2-}$. Unilamellar vesicles are carefully prepared in a typical experimental arrangement using N_aA, where A^- may be either $^{35}Cl^-$, $H^{13}CO_3^-$, or $^{33}SO_4^{2-}$. NaA is used as an anion that does not produce any NMR signals. Extravesicular buffer is supplemented with paramagnetic shift reagents, such as Co^{2+} and Mn^{2+}.[53]

The inclusion of these paramagnetic shift reagents causes a noticeable difference in either the NMR chemical shift or the widening of peaks that correspond to anions within and outside of vesicles (Figure 1.30). Therefore, when an ion-transporting agent is present, changes in the width or position of peaks associated with NMR-active anions outside of the vesicles may be consistently seen. This analytical method provides a detailed way to evaluate and confirm the effectiveness of anion transport across the membrane, offering essential insights into the kinetics of molecular movement in the experimental environment.

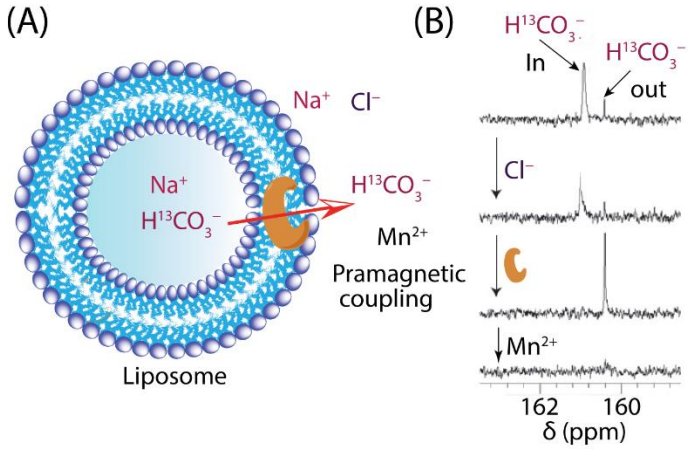

Figure 1.30. Schematic representation of transport experiment using ^{13}C NMR method.

1.8. Design criteria for synthetic anionophores

This integrated method to designing synthetic Cl^- carriers incorporates considerations of structure, solubility, binding, and interactions, offering a clear plan for developing efficient molecular systems for anion transport. A few essential considerations that must be taken into account while designing synthetic carriers are described below:

- **Structural Simplicity and Avoidance of Special Folding Patterns:** Synthetic Cl^- carriers should possess a structurally uncomplicated design, eschewing any intricate folding patterns. This ensures simplicity in molecular architecture.
- **Water Solubility and Lipid Bilayer Partitioning:** Compounds must exhibit adequate water solubility for effective delivery to target membranes. Simultaneously, they should be membrane-soluble, facilitating partitioning into the lipid bilayer.
- **Moderate to Strong Cl^- Binding with Reversibility:** The synthetic Cl^- carrier must demonstrate moderate to strong binding affinity for Cl^- to enable efficient extraction from aqueous solutions. This binding should be reversible, allowing for the release of Cl^- on the opposite side of the membrane.
- **Hydrogen Bond Donors:** The Cl^- carrier should possess a sufficient number of hydrogen bond donors capable of replacing solvated water molecules surrounding Cl^-. This feature is crucial for effective anion binding.
- **Desolvation Penalty Compensation:** Binding of Cl^- involves desolvation of the anionic guest, necessitating compensation for the resulting desolvation penalty. The synthetic carrier must establish favorable interactions with the anionic guest to offset this penalty.

- **Noncovalent Interaction Strength:** The binding affinity of the anionic guest depends on the strength of various noncovalent interactions, including hydrogen bonds, dipole-dipole interactions, dipole–induced dipole interactions, and others. Among these, the highly directional nature of hydrogen bonds makes the spatial arrangement critical for Cl^- selectivity. The molecular design should consider optimizing these interactions to enhance Cl^- binding specificity.
- **Compounds with N-H bonds that have an acidic nature:** Several types of chemical groups with acidic N-H bonds, including indole, pyrrole, caracole, (thio)amide, (thio)urea, guanidine, and amine, have been shown to effectively bind with Cl^-. These structures enhance the ability to recognize anions effectively.
- **Extra hydrogen bond donors:** Additional functional groups, including as OH, CH, and halogen bonds, have been shown as efficient hydrogen bond donors for Cl^- binding. The presence of various groups enhances the flexibility of synthetic Cl^- carriers.

1.9. Summary

Over the last twenty years, there has been a noticeable spike in scientific investigation of anion transport, which includes a pragmatic focus on various physiological system problems. Significant developments recently took place in the field of cancer therapy, where very specific approaches have been developed, including stimuli-responsive proanionophores. Within the physiological environment, these novel proanionophores provide fine control over their spatial functioning. It has been possible to develop and synthesize non-toxic anionophores that show positive results in epithelial cells when it comes to channelopathies, such as cystic fibrosis. These anionophores have the potential to be therapeutic agents since, in epithelial cells, they notably display negative toxicity profiles. Despite impressive improvements, obstacles still exist, requiring concentrated work to better understand anionophores' influence on regular cellular operations and reduce unwanted effects. In the growing field of antibacterial agents, anionophores have garnered acclaim for their utility. Worldwide scientific endeavors have succeeded in augmenting the selectivity gap between cancer cells and normal cells, although complete mitigation of impact on normal cells remains an elusive goal. There is an imperative need to concentrate on overcoming existing challenges to optimize anionophore deliverability and enhance cellular absorption for more efficacious therapeutic outcomes. Anion transport research has a lot of potential to help understand the complexities of angiogenesis in diabetic

patients, even in non-traditional fields. Investigating anion transport routes in relation to angiogenesis opens up a new field of study that may have bearings on our ability to comprehend and treat diabetic vascular problems. Anion transport is a fascinating field with a wealth of opportunities as we approach new developments. Research is expected to continue in this direction, which will lead to the discovery of new avenues for investigation and breakthroughs in the fields of biology and medicine. The scientific community eagerly anticipates how these exciting new possibilities will pan out in the near future.

1.10. References

1. Davis, J. T.; Gale, P. A.; Quesada, R., Advances in anion transport and supramolecular medicinal chemistry. *Chem. Soc. Rev.* **2020,** *49* (16), 6056-6086.
2. Hladky, S.; Haydon, D., Ion movements in gramicidin channels. In *Current topics in membranes and transport*, Elsevier: 1984; Vol. 21, pp 327-372.
3. Vaughan-Jones, R. D.; Spitzer, K. W.; Swietach, P., Intracellular pH regulation in heart. *J. Mol. Cell. Cardiol.* **2009,** *46* (3), 318-331.
4. Saha, T.; Hossain, M. S.; Saha, D.; Lahiri, M.; Talukdar, P., Chloride-mediated apoptosis-inducing activity of bis (sulfonamide) anionophores. *J. Am. Chem. Soc.* **2016,** *138* (24), 7558-7567.
5. Elie, C. R.; David, G.; Schmitzer, A. R., Strong antibacterial properties of anion transporters: a result of depolarization and weakening of the bacterial membrane. *J. Med. Chem.* **2015,** *58* (5), 2358-2366.
6. Fulda, S., Targeting apoptosis signaling pathways for anticancer therapy. *Front. Oncol.* **2011,** *1*, 23.
7. Lang, F.; Föller, M.; Lang, K.; Lang, P.; Ritter, M.; Gulbins, E.; Vereninov, A.; Huber, S., Ion channels in cell proliferation and apoptotic cell death. *J. Membr. Biol.* **2005,** *205*, 147-157.
8. Berridge, M. J.; Lipp, P.; Bootman, M. D., The versatility and universality of calcium signalling. *Nat. Rev. Mol. Cell Biol.* **2000,** *1* (1), 11-21.
9. Joseph, S. K.; Hajnóczky, G., IP 3 receptors in cell survival and apoptosis: Ca 2+ release and beyond. *Apoptosis* **2007,** *12*, 951-968.
10. Bortner, C. D.; Cidlowski, J. A., Cell shrinkage and monovalent cation fluxes: role in apoptosis. *Arch. Biochem. Biophys.* **2007,** *462* (2), 176-188.
11. Maeno, E.; Ishizaki, Y.; Kanaseki, T.; Hazama, A.; Okada, Y., Normotonic cell shrinkage because of disordered volume regulation is an early prerequisite to apoptosis. *Proc. Natl. Acad. Sci. U.S.A.* **2000,** *97* (17), 9487-9492.
12. Nukui, M.; Shimizu, T.; Okada, Y., Normotonic cell shrinkage induced by Na+ deprivation results in apoptotic cell death in human epithelial HeLa cells. *J Physiol Sci* **2006,** *56* (5), 335-339.
13. Okada, Y.; Numata, T.; Sato-Numata, K.; Sabirov, R. Z.; Liu, H.; Mori, S.-i.; Morishima, S., Roles of volume-regulatory anion channels, VSOR and Maxi-Cl, in apoptosis, cisplatin resistance, necrosis, ischemic cell death, stroke and myocardial infarction. *Curr. Top. Membr.* **2019,** *83*, 205-283.

14. Bortner, C. D.; Cidlowski, J. A., Ion channels and apoptosis in cancer. *Philos. Trans. R. Soc. B* **2014,** *369* (1638), 20130104.
15. (a) Busschaert, N.; Park, S.-H.; Baek, K.-H.; Choi, Y. P.; Park, J.; Howe, E. N.; Hiscock, J. R.; Karagiannidis, L. E.; Marques, I.; Félix, V., A synthetic ion transporter that disrupts autophagy and induces apoptosis by perturbing cellular chloride concentrations. *Nat. Chem.* **2017,** *9* (7), 667-675; (b) Hernando, E.; Soto-Cerrato, V.; Cortés-Arroyo, S.; Pérez-Tomás, R.; Quesada, R., Transmembrane anion transport and cytotoxicity of synthetic tambjamine analogs. *Org. Biomol. Chem.* **2014,** *12* (11), 1771-1778.
16. Cournoyer, S.; Addioui, A.; Belounis, A.; Beaunoyer, M.; Nyalendo, C.; Le Gall, R.; Teira, P.; Haddad, E.; Vassal, G.; Sartelet, H., GX15–070 (Obatoclax), a Bcl-2 family proteins inhibitor engenders apoptosis and pro-survival autophagy and increases Chemosensitivity in neuroblastoma. *BMC Cancer* **2019,** *19*, 1-14.
17. Díaz de Greñu, B.; Hernández, P. I.; Espona, M.; Quiñonero, D.; Light, M. E.; Torroba, T.; Pérez-Tomás, R.; Quesada, R., Synthetic prodiginine obatoclax (GX15-070) and related analogues: Anion binding, transmembrane transport, and cytotoxicity properties. *Chem. Eur. J.* **2011,** *17* (50), 14074-14083.
18. Cavalcanti, B. C.; Júnior, H. V.; Seleghim, M. H.; Berlinck, R. G.; Cunha, G. M.; Moraes, M. O.; Pessoa, C., Cytotoxic and genotoxic effects of tambjamine D, an alkaloid isolated from the nudibranch Tambja eliora, on Chinese hamster lung fibroblasts. *Chem.-Biol. Interact.* **2008,** *174* (3), 155-162.
19. Hernández, P. I.; Moreno, D.; Javier, A. A.; Torroba, T.; Pérez-Tomás, R.; Quesada, R., Tambjamine alkaloids and related synthetic analogs: efficient transmembrane anion transporters. *Chem. Commun.* **2012,** *48* (10), 1556-1558.
20. Rodilla, A. M.; Korrodi-Gregório, L.; Hernando, E.; Manuel-Manresa, P.; Quesada, R.; Pérez-Tomás, R.; Soto-Cerrato, V., Synthetic tambjamine analogues induce mitochondrial swelling and lysosomal dysfunction leading to autophagy blockade and necrotic cell death in lung cancer. *Biochem. Pharmacol* **2017,** *126*, 23-33.
21. Soto-Cerrato, V.; Manuel-Manresa, P.; Hernando, E.; Calabuig-Farinas, S.; Martinez-Romero, A.; Fernandez-Duenas, V.; Sahlholm, K.; Knöpfel, T.; Garcia-Valverde, M.; Rodilla, A. M., Facilitated anion transport induces hyperpolarization of the cell membrane that triggers differentiation and cell death in cancer stem cells. *J. Am. Chem. Soc.* **2015,** *137* (50), 15892-15898.
22. Carreira-Barral, I.; Mielczarek, M.; Alonso-Carrillo, D.; Capurro, V.; Soto-Cerrato, V.; Tomás, R. P.; Caci, E.; García-Valverde, M.; Quesada, R., Click-tambjamines as efficient and tunable bioactive anion transporters. *Chem. Commun.* **2020,** *56* (21), 3218-3221.
23. Van Rossom, W.; Asby, D. J.; Tavassoli, A.; Gale, P. A., Perenosins: a new class of anion transporter with anti-cancer activity. *Org. Biomol. Chem.* **2016,** *14* (9), 2645-2650.
24. Kavallieratos, K.; de Gala, S. R.; Austin, D. J.; Crabtree, R. H., A readily available non-preorganized neutral acyclic halide receptor with an unusual nonplanar binding conformation. *J. Am. Chem. Soc.* **1997,** *119* (9), 2325-2326.
25. Coles, S. J.; Gale, P. A.; Hursthouse, M. B.; Light, M. E.; Warriner, C. N., Crystallographic and solution anion binding studies of bis-amidofurans and thiophenes. *Supramol Chem* . **2004,** *16* (7), 469-486.
26. Roy, N. J.; Pujari, P. L.; Talukdar, P., Bimodal structural tuning of pyrrole-2-carboxamide-based transmembrane ion transport systems. *Org. Biomol. Chem.* **2023,** *21* (16), 3323-3329.
27. Malla, J. A.; Upadhyay, A.; Ghosh, P.; Mondal, D.; Mondal, A.; Sharma, S.; Talukdar, P., Chloride Transport across Liposomes and Cells by Nontoxic 3-(1 H-1, 2, 3-Triazol-1-yl) benzamides. *Org. Lett.* **2022,** *24* (23), 4124-4128.

28. Shinde, S. V.; Talukdar, P., An anion receptor that facilitates transmembrane proton–anion symport by deprotonating its sulfonamide N–H proton. *Chem. Commun.* **2018,** *54* (73), 10351-10354.
29. Busschaert, N.; Park, S.-H.; Baek, K.-H.; Choi, Y. P.; Park, J.; Howe, E. N.; Hiscock, J. R.; Karagiannidis, L. E.; Marques, I.; Félix, V., A synthetic ion transporter that disrupts autophagy and induces apoptosis by perturbing cellular chloride concentrations. *Nat. Chem.* **2017,** *9* (7), 667-675.
30. Zhang, S.; Wang, Y.; Xie, W.; Howe, E. N.; Busschaert, N.; Sauvat, A.; Leduc, M.; Gomes-da-Silva, L. C.; Chen, G.; Martins, I., Squaramide-based synthetic chloride transporters activate TFEB but block autophagic flux. *Cell Death Dis.* **2019,** *10* (3), 242.
31. Busschaert, N.; Wenzel, M.; Light, M. E.; Iglesias-Hernández, P.; Pérez-Tomás, R.; Gale, P. A., Structure–activity relationships in tripodal transmembrane anion transporters: the effect of fluorination. *J. Am. Chem. Soc.* **2011,** *133* (35), 14136-14148.
32. Akhtar, N.; Saha, A.; Kumar, V.; Pradhan, N.; Panda, S.; Morla, S.; Kumar, S.; Manna, D., Diphenylethylenediamine-based potent anionophores: transmembrane chloride ion transport and apoptosis inducing activities. *ACS Appl. Mater. Interfaces* **2018,** *10* (40), 33803-33813.
33. Vieira, P.; Miranda, M. Q.; Marques, I.; Carvalho, S.; Chen, L. J.; Howe, E. N.; Zhen, C.; Leung, C. Y.; Spooner, M. J.; Morgado, B., Development of a Library of Thiophene-Based Drug-Like Lego Molecules: Evaluation of Their Anion Binding, Transport Properties, and Cytotoxicity. *Chem. Eur. J.* **2020,** *26* (4), 888-899.
34. Howe, E. N.; Busschaert, N.; Wu, X.; Berry, S. N.; Ho, J.; Light, M. E.; Czech, D. D.; Klein, H. A.; Kitchen, J. A.; Gale, P. A., pH-regulated nonelectrogenic anion transport by phenylthiosemicarbazones. *J. Am. Chem. Soc.* **2016,** *138* (26), 8301-8308.
35. Saha, A.; Akhtar, N.; Kumar, V.; Kumar, S.; Srivastava, H. K.; Kumar, S.; Manna, D., pH-Regulated anion transport activities of bis (iminourea) derivatives across the cell and vesicle membrane. *Org. Biomol. Chem.* **2019,** *17* (23), 5779-5788.
36. Akhtar, N.; Pradhan, N.; Barik, G. K.; Chatterjee, S.; Ghosh, S.; Saha, A.; Satpati, P.; Bhattacharyya, A.; Santra, M. K.; Manna, D., Quinine-based semisynthetic ion transporters with potential antiproliferative activities. *ACS Appl. Mater. Interfaces* **2020,** *12* (23), 25521-25533.
37. Akhtar, N.; Pradhan, N.; Saha, A.; Kumar, V.; Biswas, O.; Dey, S.; Shah, M.; Kumar, S.; Manna, D., Tuning the solubility of ionophores: glutathione-mediated transport of chloride ions across hydrophobic membranes. *Chem. Commun.* **2019,** *55* (58), 8482-8485.
38. Srimayee, S.; Badajena, S. R.; Akhtar, N.; Kar, M. K.; Dey, S.; Mohapatra, P.; Manna, D., Stimuli-responsive release of active anionophore from RGD-peptide-linked proanionophore. *Chem. Commun.* **2023,** *59* (85), 12759-12762.
39. Roy, N. J.; Save, S. N.; Sharma, V. K.; Abraham, B.; Kuttanamkuzhi, A.; Sharma, S.; Lahiri, M.; Talukdar, P., NAD (P) H: Quinone Acceptor Oxidoreductase 1 (NQO1) Activatable Salicylamide H+/Cl− Transporters. *Chem. Eur. J.* **2023,** *29* (51), e202301412.
40. Choi, Y. R.; Lee, B.; Park, J.; Namkung, W.; Jeong, K.-S., Enzyme-responsive procarriers capable of transporting chloride ions across lipid and cellular membranes. *J. Am. Chem. Soc.* **2016,** *138* (47), 15319-15322.
41. Salunke, S. B.; Malla, J. A.; Talukdar, P., Phototriggered Release of a Transmembrane Chloride Carrier from an o-Nitrobenzyl-Linked Procarrier. *Angew. Chem.* **2019,** *58* (16), 5354-5358.
42. Ahmad, M.; Chattopadhayay, S.; Mondal, D.; Vijayakanth, T.; Talukdar, P., Stimuli-Responsive Anion Transport through Acylhydrazone-Based Synthetic Anionophores. *Org. Lett.* **2021,** *23* (19), 7319-7324.

43. Ahmad, M.; Metya, S.; Das, A.; Talukdar, P., A sandwich azobenzene–diamide dimer for photoregulated chloride transport. *Chem. Eur. J.* **2020,** *26* (40), 8703-8708.
44. Wezenberg, S. J.; Chen, L.-J.; Bos, J. E.; Feringa, B. L.; Howe, E. N.; Wu, X.; Siegler, M. A.; Gale, P. A., Photomodulation of transmembrane transport and potential by stiff-stilbene based bis (thio) ureas. *J. Am. Chem. Soc.* **2021,** *144* (1), 331-338.
45. Li, H.; Valkenier, H.; Judd, L. W.; Brotherhood, P. R.; Hussain, S.; Cooper, J. A.; Jurček, O.; Sparkes, H. A.; Sheppard, D. N.; Davis, A. P., Efficient, non-toxic anion transport by synthetic carriers in cells and epithelia. *Nat. Chem.* **2016,** *8* (1), 24-32.
46. Li, H.; Valkenier, H.; Thorne, A. G.; Dias, C. M.; Cooper, J. A.; Kieffer, M.; Busschaert, N.; Gale, P. A.; Sheppard, D. N.; Davis, A. P., Anion carriers as potential treatments for cystic fibrosis: transport in cystic fibrosis cells, and additivity to channel-targeting drugs. *Chem. Sci.* **2019,** *10* (42), 9663-9672.
47. Share, A. I.; Patel, K.; Nativi, C.; Cho, E. J.; Francesconi, O.; Busschaert, N.; Gale, P. A.; Roelens, S.; Sessler, J. L., Chloride anion transporters inhibit growth of methicillin-resistant Staphylococcus aureus (MRSA) in vitro. *Chem. Commun.* **2016,** *52* (48), 7560-7563.
48. Carreira-Barral, I.; Rumbo, C.; Mielczarek, M.; Alonso-Carrillo, D.; Herran, E.; Pastor, M.; Del Pozo, A.; García-Valverde, M.; Quesada, R., Small molecule anion transporters display in vitro antimicrobial activity against clinically relevant bacterial strains. *Chem. Commun.* **2019,** *55* (68), 10080-10083.
49. Mondal, A.; Siwach, M.; Ahmad, M.; Radhakrishnan, S. K.; Talukdar, P., Pyridyl-Linked Hetero Hydrazones: Transmembrane H^+/Cl^- Symporters with Efficient Antibacterial Activity. *ACS Infect. Dis.* 10.2 (**2024**): 371-376.
50. Akhtar, N.; Biswas, O.; Manna, D., Biological applications of synthetic anion transporters. *Chem. Commun.* **2020,** *56* (91), 14137-14153.
51. Gilchrist, A. M.; Wang, P.; Carreira-Barral, I.; Alonso-Carrillo, D.; Wu, X.; Quesada, R.; Gale, P. A., Supramolecular methods: the 8-hydroxypyrene-1, 3, 6-trisulfonic acid (HPTS) transport assay. *SupraMolChem.* **2021,** *33* (7), 325-344.
52. Jowett, L. A.; Gale, P. A., Supramolecular methods: the chloride/nitrate transmembrane exchange assay. *SupraMolChem.* **2019,** *31* (5), 297-312.
53. Andrews, N. J.; Haynes, C. J.; Light, M. E.; Moore, S. J.; Tong, C. C.; Davis, J. T.; Harrell Jr, W. A.; Gale, P. A., Structurally simple lipid bilayer transport agents for chloride and bicarbonate. *Chem. Sci.* **2011,** *2* (2), 256-260.

भारतीय प्रौद्योगिकी संस्थान गुवाहाटी
Indian Institute of Technology Guwahati

Chapter 2

Development of tryptophan-based ion transporter for efficient chloride ion transport across lipid membranes

भारतीय प्रौद्योगिकी संस्थान गुवाहाटी
Indian Institute of Technology Guwahati

2.1. Background and objectives of the present work

In **chapter 1** provides a concise overview of synthetic anionophores, emphasizing their potential efficacy against various pathological conditions. A comprehensive literature survey establishes that ion transport plays a pivotal role.[1, 2, 3] Chloride, a predominant anion under normal physiological conditions, linked to vital biological processes.[4, 5] Malfunctions in Cl^- ion transport proteins, often attributed to mutations, can lead to pathological conditions. In response to these challenges, scientists worldwide have explored artificial ion transporting molecules as an alternative strategy to address the consequences of defective Cl^- ion transport proteins. Initially designed to tackle cystic fibrosis, this approach has evolved to encompass a broader spectrum of diseases. However, despite the development of various synthetic anionophores, their biological activities beyond the scope of "channel replacement therapy" have only recently begun to be elucidated. Recent investigations indicate that the transport of Cl^- ions is associated with the induction of apoptosis in cancer cells, achieved through disruption of ionic homeostasis or alterations in intracellular pH. Synthetic ion transporters have shown promise in preventing drug resistance in cancer cells by normalizing pH and Cl^- ion concentration in comparison to normal cells. Synthetic Cl^- transporters can also damage bacterial membranes and disrupt their ionic balance, showing potential as antibacterial agents.[6, 7] Various natural and synthetic Cl^- ion transporters, including prodigiosin,[8] tambjamine,[9] calix[4]pyrroles,[10] squaramides,[11] bis-sulfonamides,[12] quinine[13] and diphenylethylenediamine-based [14] derivatives, showed apoptosis-mediated cell death. In light of these findings, the development of synthetic Cl^- ion transporters capable of mimicking the cellular functions of natural Cl^- ion channel systems is anticipated to represent a promising avenue for addressing diseases associated with the malfunctioning of these systems.

Over the last twenty years, several anionophores have been developed to overcome limitations in natural ion transporters. These artificial molecules have shown effectiveness in specifically targeting both cancerous and non-cancerous cells, albeit they do come with related toxicity. Although attempts have been made to developed anionophores that respond to stimuli in order to reduce toxicity, achieving total elimination of negative effects has been difficult. Due to the inherent biocompatibility of amino acids in physiological systems, we have embarked on a unique method. More precisely, three amino acids, namely tryptophan, phenylalanine, and leucine, were selected due to their significant biological influence. By using the natural biocompatibility of these amino acids, we have included anion-binding cavities in order to take

use of their beneficial biological features while simultaneously reducing harm to healthy cells. This novel approach employs the inherent characteristics of amino acids to improve the compatibility of anionophores with living organisms, therefore providing an efficient approach to developing ion transporters that are less toxic and more suited in biological systems.

In this chapter, we developed tryptophan analogues containing thiourea and amide functionalities that selectively recognised and transport the chloride ion. We hypothesize that the tryptophan derivatives could introduce multivalent NH bond interactions within the binding cavity, thereby affording the opportunity to developed a novel class of anion transporters rooted in thiourea-amide-based tryptophan derivatives. This pioneering approach holds the potential to redefine the landscape of Cl^- transporters, offering a unique and unexplored avenue within the realm of synthetic ion transporter design.

2.2. Result and discussion

2.2.1. Design and synthesis of tryptophan-based derivatives

The synthesis of (tert-butoxycarbonyl)tryptophan was done with a reaction of tryptophan and di-tert-butyldicarbonate, in the presence of sodium hydroxide (1N).[15] Then the (tert-butoxycarbonyl)tryptophan was subsequently subjected to further reactions with different substituted arylamines with the help of a coupling reagent, HBTU and trimethylamine as a base, leading to the synthesis of Boc-protected amide-functionalized tryptophan derivatives. Afterward, the deprotection of the Boc-protected amine group was carried out by using trifluoroacetic acid (TFA) (30%). Finally, the amine group was functionalized to a thiourea group by the reaction with various arylisothiocyanates, resulting the formation of tryptophan-based thiourea-amide (**2.3a-2.3i** and **2.4**) derivatives (Scheme 2.1).

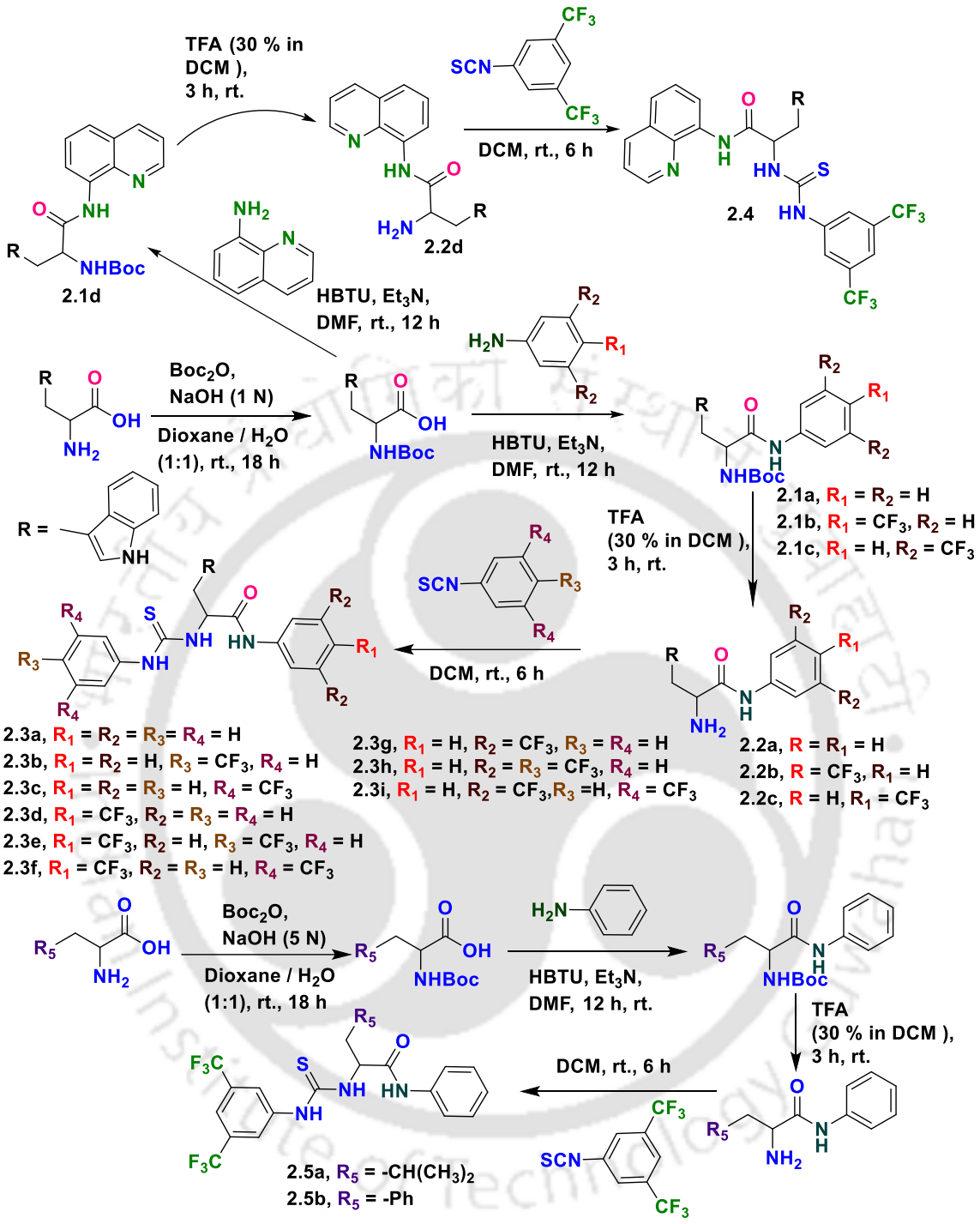

Scheme 2.1. Synthetic steps for tryptophan analogs (2.3a-2.3i and 2.4) and leucine (2.5a) and phenylalanine (2.5b) derivatives.

We believed that incorporating the thiourea and amide motifs into tryptophan better the aptitude of the tryptophan base scaffolds to assist the transmembrane transport of ions. The

phenyl groups were modified with strong electron-withdrawing groups, such as -CF_3, to enhance the lipophilicity (logP) and acidity (pKa) of the N-H proton. These modifications are helpful for enhancing ion binding capability, membrane permeability, and ion transport efficiency. To investigate the function of the tryptophan moiety particularly the N-H and CH proton in the indole unit to the anion interaction, derivatives of leucine and phenylalanine were synthesized (**2.5a** and **2.5b**). The primary binding interactions occur between the two thiourea N-H units and one amide N-H unit with the anion. Furthermore, the involvement of the indole N-H and C-H in tryptophan is crucial in the process of anion recognition.

2.2.2. Anion recognition study

^{1}H nuclear magnetic resonance (NMR) titration of compounds 2.3f and 2.3i in DMSO-d_6 solvent was done with different concentration of TBACl. The purpose was to examine how these compounds interact with each other in the solution phase, (Figure 2.1). The N-H_a, N-H_b, N-H_c, and N-H_d protons of the thiourea groups, amide groups, and indole NH groups of tryptophan units change chemical shift to the downfield shift. This shows that the molecule interacts with Cl^- through hydrogen bonds. The presence of Cl^- may induce polarization in the N-H_a, N-H_b, N-H_c, and N-H_d protons by a through-space action. The interaction between particles is mostly based on electrostatic forces, causing the proton to acquire a partial positive charge. This leads to a deshielding effect, resulting in a shift towards higher magnetic field strengths.[16] The concentration-dependent experiment revealed that the host and guest molecules interacted 1:1 to form a complex. The binding affinity of compound 2.**3i** of 144.8 ± 17 M^{-1} was observed in the solution (Figure 2.8B). Additionally, the binding affinity of the compound 2.**3f** was determined to be 138.37 ± 8.7 M^{-1} (Figure 2.9B), indicating that compound 2.**3i has a** stronger binding affinity than 2.**3f** towards Cl^- ions in the solution phase.

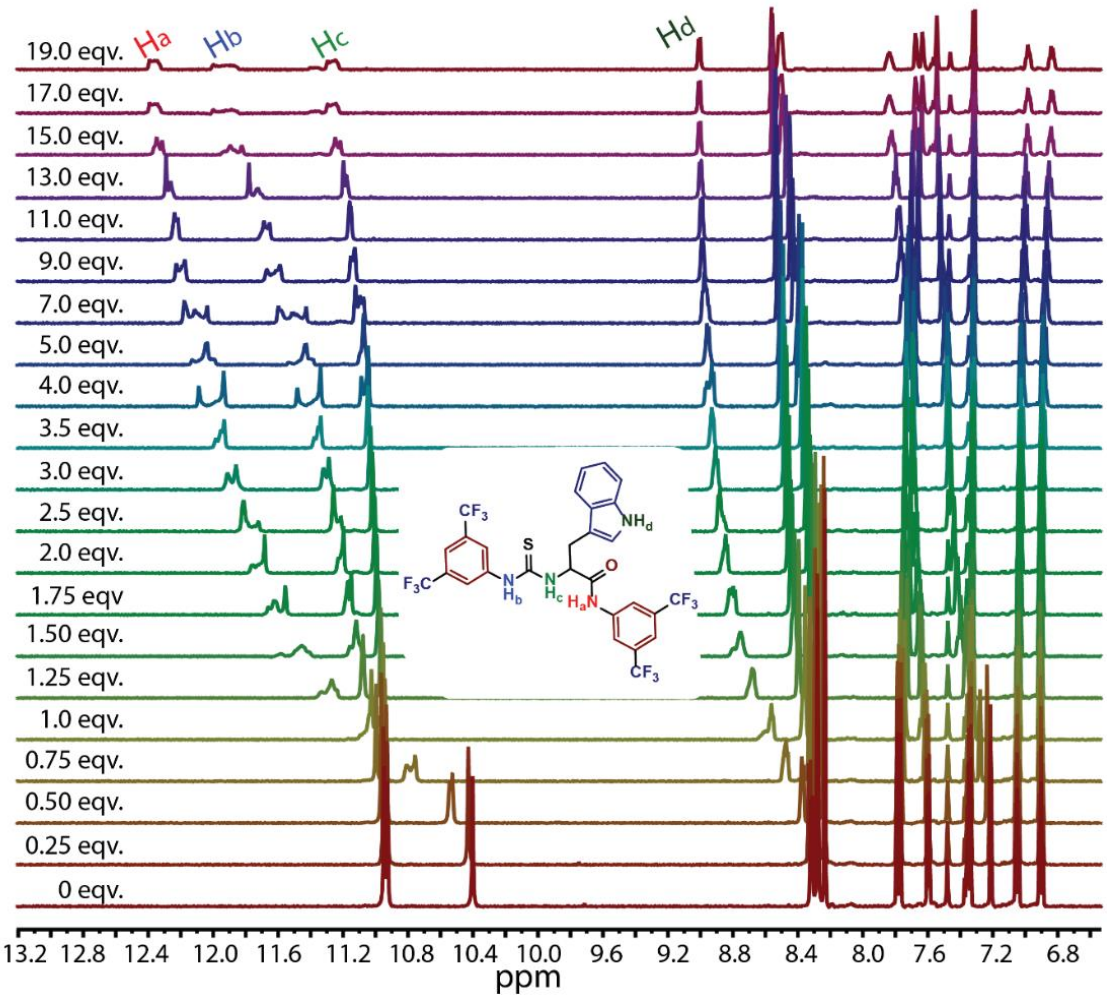

Figure 2.1. The partially stacked plot of ^{1}H NMR titration study of **2.3i** (20 mM) with sequential adding of TBACl in DMSO-d_6 solvent.

2.2.3. Ion transport activity

The investigation explored the transport of ions abilities of the amino acid analogues by using large unilamellar vesicles (LUVs). The vesicles were carefully made from a combination of egg yolk phosphatidylcholine (EYPC) and cholesterol (CHOL) lipids in a molar ratio of 8:2.[17] The vesicles were created by enclosing lucigenin dye in the presence of 100 mM $NaNO_3$ within a 20 mM HEPES buffer at a pH of 7.2. The extravesicular media comprised a solution of NaCl (100 mM) and HEPES (20 mM), which was isotonic. In order to begin the transportation of chloride ions (Cl^-), a compound pulse was provided, and the resulting fluorescence intensity of lucigenin was carefully observed.[18] Initial evaluation at a concentration of 5 μM at pH 7.2 revealed that all amino acid derivatives had a significant increase in the rate of Cl^- inflow,

indicating their ability for transmembrane transport. The assessment showed that compound 2.3i had the best effectiveness in enabling Cl^- transfer compared to the other compounds examined (Figure 2.2). The outcome yields significant understanding regarding the ion transportation capacities of the produced amino acid derivatives in a lipid membrane setting. The effectiveness of these derivatives in increasing the entry of Cl^- ions indicates their potential usefulness in regulating the movement of ions across cell membranes, thereby aiding in the comprehension of their biological and pharmacological uses.

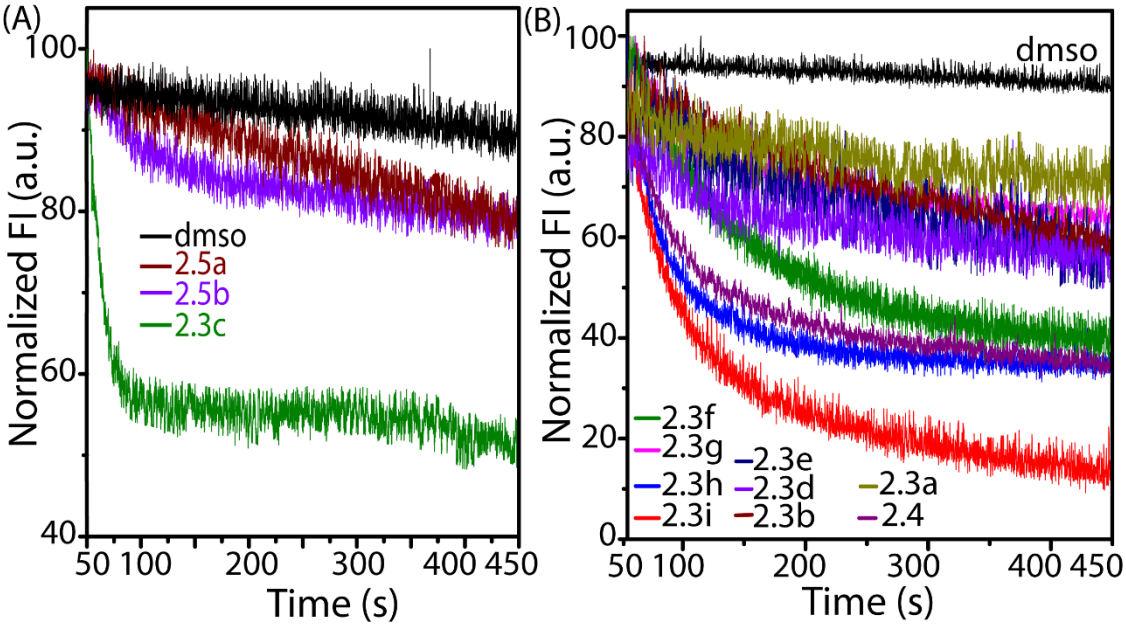

Figure 2.2. Standardized fluorescence curve for Cl^- transport activity of the synthesized compounds (5 µM) using EYPC/CHOL-LUVs⊃lucigenin vesicle (This assay was performed twice, and the result from one of the data set is presented).

The existence of the free N-H group indicates that the tryptophan moiety might have a substantial impact on the ability of the produced compounds to interact with anions. Therefore, concentration dependent lucigenin assay was conducted to find out the EC_{50} at a pH of 7.2 (Figure 2.3A). The results of this experiment demonstrated that **2.3i** has a higher capacity for Cl^- transfer compared to the other derivatives. The potent compound **2.3i** had an EC_{50} value of 1.55 at pH 7.2 (Figure 2.3B).

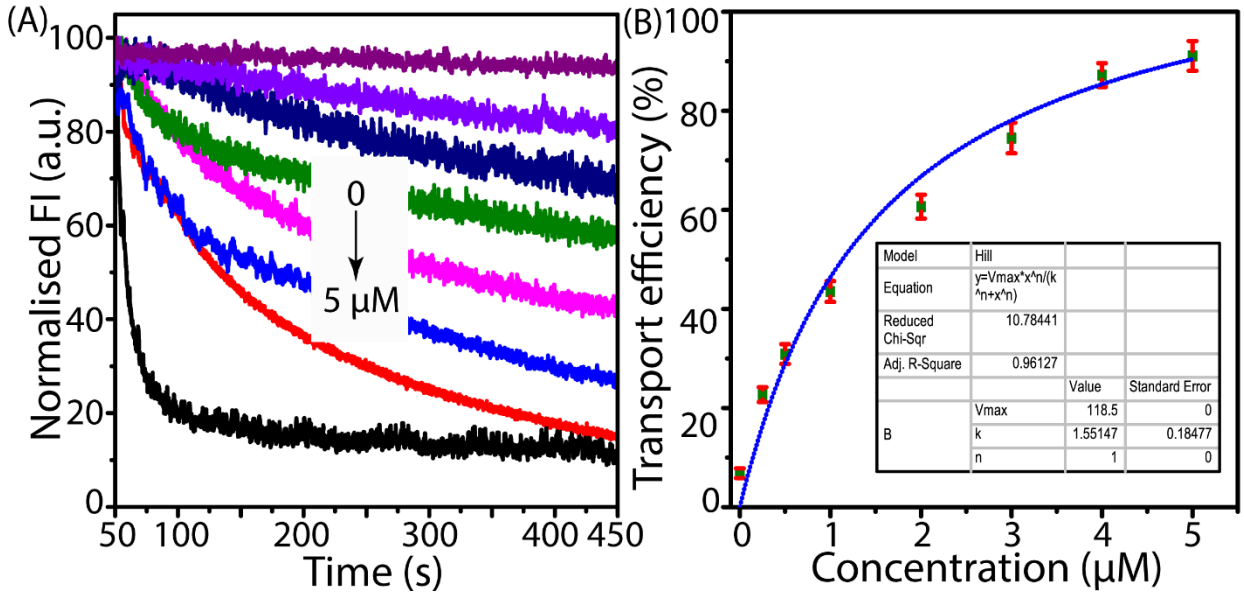

Figure 2.3. Concentration-dependent transmembrane transport of Cl^- ion in the presence of compound **2.3i** across the EYPC/CHOL-LUVs⊃lucigenin. The ion transport efficacy was determined by lucigenin fluorescence experiment at pH 7.2 (A) (this assay was performed twice, and the result from one of the data set is presented). The EC_{50} value was calculated using the Hill equation (B). The compound concentration was varied from 5.0 to 0.25 μM.

2.2.4. Ion selectivity study

The HPTS assay was used to scrutinize the impact of extravesicular anions on the Cl^- transport capabilities of **2.3i**. The intravesicular solution encapsulated HPTS with a buffer containing NaCl pH 7.2, whereas the extravesicular solution consisted of isosmotic buffer solutions containing various NaX salts (X = Cl^-, Br^-, I^-, NO_3^-, ClO_4^-, and SCN^-) (Figure 2.4A).[19] Notably, there were prominent differences in anion transport, with Cl^- demonstrating the highest transport capability compared to the other examined anions. The potent compound **2.3i** exhibited a higher binding affinity towards Cl^- compared to other anions. The capacity of **2.3i** to selectively transport Cl^- ions may be attributed to its similar ability to recognize and release Cl^- ions through the cavity formed by the thiourea and amide structures. In the same manner, the lucigenin assay was employed to examine how extravesicular cations impact the Cl^- transport activities of **2.3i**. The study employed isosmotic buffer solutions containing several monovalent metal chloride salts (Li^+, Na^+, K^+, Rb^+, and Cs^+) in the extravesicular solution.[20] The purpose was to explore how different cations affect the efficiency of Cl^- transport in the

compounds (Figure 2.4B). Therefore, the investigated cations may have a negligible impact on the transmembrane Cl^- transport activities of potent compound **2.3i**.

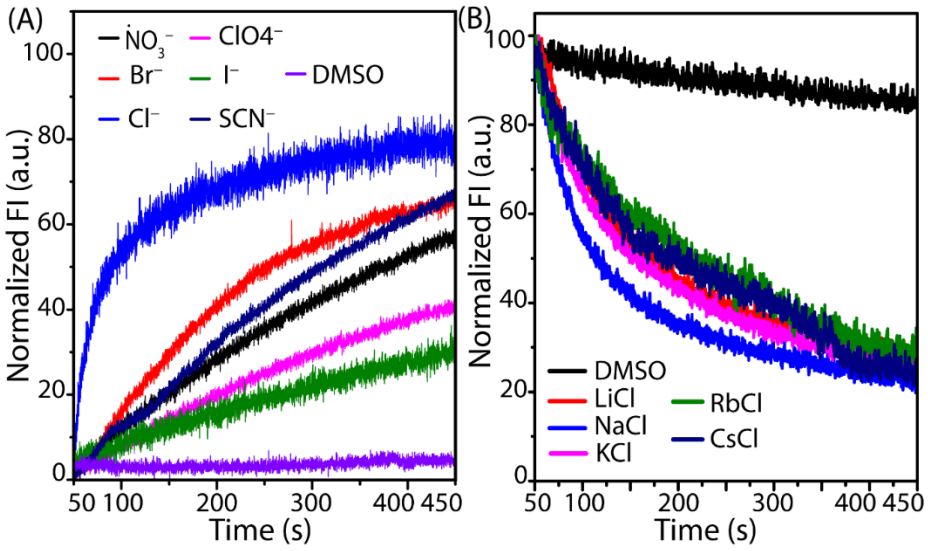

Figure 2.4. The anion transport selectivity of **2.3i** (5 μM) across the EYPC/CHOL-LUVs⊃HPTS (8:2 molar ratio) was measured at pH 7.2 (A), Cation selectivity of **2.3i** (5 μM) determined by changing the external cations (M^+ = Li^+ , Na^+ , K^+ , Rb^+ , Cs^+) across EYPC/CHOL-LUVs⊃lucigenin (B) (these assay were performed twice, and the result from one of the data set is presented).

2.2.5. Evidence for the transport mechanism

The lucigenin experiment was conducted to investigate the Cl^- ion transport mechanism of the potent compound **2.3i**, H^+ / Cl^- symport or OH^- /Cl^- antiport mechanism. This was performed in the absence and presence of 4-(trifluoromethoxy)phenylhydrazone (FCCP), (which is a protonophore). The observed increase of the Cl^- ion transport rate in the presence of FCCP indicates a synergistic interaction between the compound and FCCP, hence ruling out the possible H^+ transport facilitated by the FCCP (Figure 2.5A). After that, additional lucigenin assay was performed in presence and absence of valinomycin (K^+ transporter). The valinomycin-facilitated transport of K^+ influx might cause the efflux of Cl^- ions and/or the influx of OH^- ions in order to tolerate the pH gradient. In presence of valinomycin leads to a significant drop in the transport of Cl^- ions, indicating the involvement of the OH^- / Cl^- antiport mechanism (Figure 2.5B). The synergistic action of potent compound **2.3i** with valinomycin indicates the selective transportation of OH^- ions rather than Cl^- ions.[21]

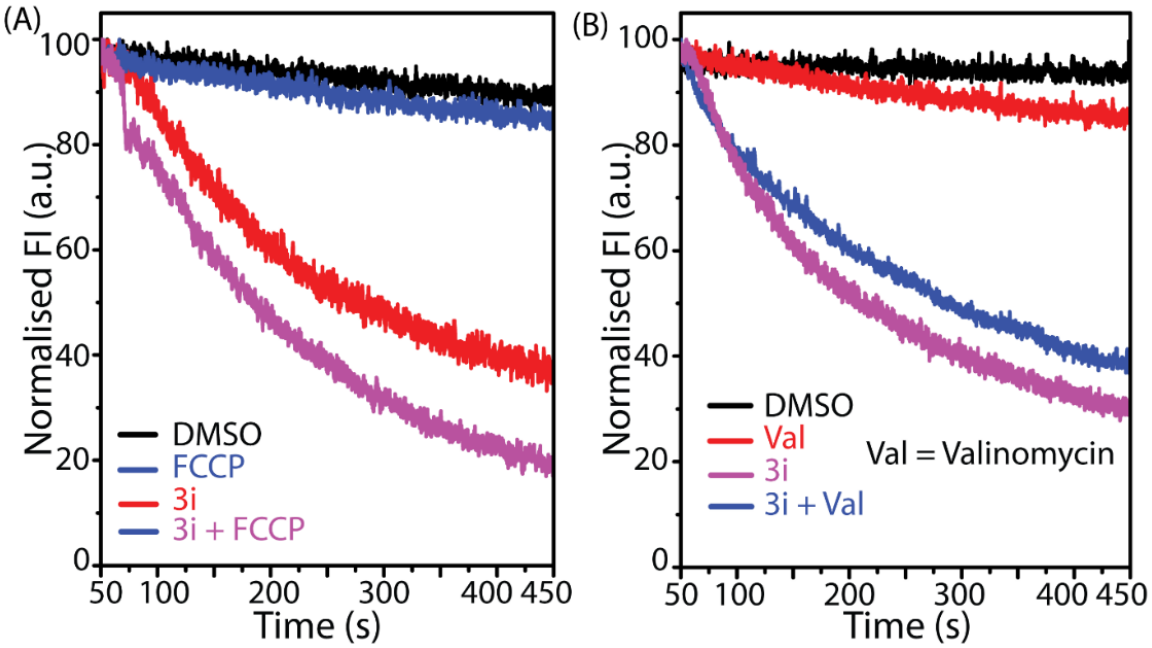

Figure 2.5. The Cl^- transport activity of **2.3i (**2.5 µM**)** in the absence and presence of FCCP (A) and valinomycin (Val) (B) (this assay was performed twice, and the result from one of the data set is presented).

The temperature-dependent Cl^- transport across the model liposome was conducted to find out the transport pathways either a carrier or channel pathways. At 45 °C, there was a significant increase in the Cl^- transport efficiency of **2.3i** compared to 25 °C.[21] This indicates that the Cl^- transport activity of **2.3i** is directly associated to the fluidity of the membrane, (Figure 2.6A). The U-tube experiment also validated the transportation of Cl^- across the organic medium that is chloroform layer (mimic the lipid bilayers). Therefore, **2.3i** facilitates the transportation of Cl^- via carrier pathways (Figure 2.6B). Furthermore, the carboxyfluorescein (CF) assay was performed for the membrane leakage result revealed that the dye does not leak from the vesicles, both with and without the compound, which indicates that the vesicles remain intact during the measurements (Figure 2.13).

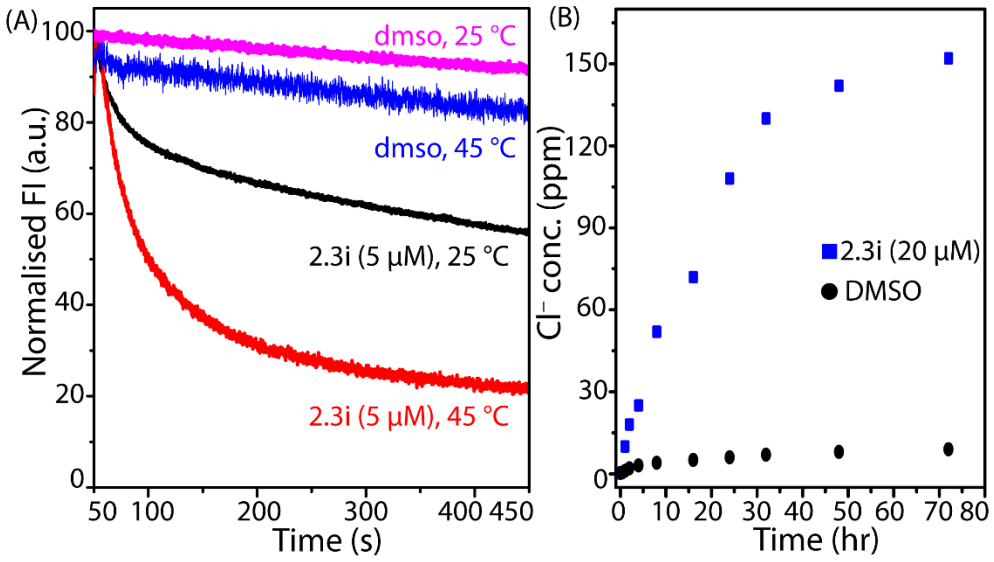

Figure 2.6. Temperature-dependent Cl^- transport by **2.3i** (5 μM) using DPPC-LUV⊃lucigenin (A), The Cl^- ion transport activity of compound **2.3i** (20 μM) was recorded across a U-tube by using the Cl^- ion gradient, using a chloride ion-selective electrode (B) (these assay were performed twice, and the results from one of the data set are presented).

2.2.6. Theoretical analysis (DFT)

The ^1H NMR titration and fluorescence-based investigations have demonstrated tryptophan analogues consisting of thiourea N-H and amide N-H groups had an aptitude to recognize Cl^- ions. Furthermore, these derivatives exhibited Cl^- ion transport activity across the vesicles. Therefore, in order to investigate possible ways of how the Cl^- ion engages, density functional theory (DFT) calculations were performed in the gas phase for the neutral form of compound **2.3i**. The optimized structure of compound **2.3i** reveals that the interactions with the Cl^- ion are predominantly attributed to the two thiourea N–H, amide N-H, and indole C-H protons (Figure 2.7). The DFT analysis also revealed that the distances between compound **2.3i** and a Cl^- ion for their interactions fall within the range of hydrogen-bond distance (2.16 – 2.51 Å). The total energy with Cl^- ion's -3428.674 Hartree and the total energy of **2.3f** is -3091.75287693 Hartree. Theoretical results validate the experimental findings that the Cl^- ion exhibits significant interactions with the molecules. It should be noted that the intensity of interaction shown in DFT investigations is not directly correlated with experimental data. The transport efficiency of the compounds may be controlled by factors such as lipophilicity, pKa values, and surroundings including the intensity of contact with the membrane head groups.

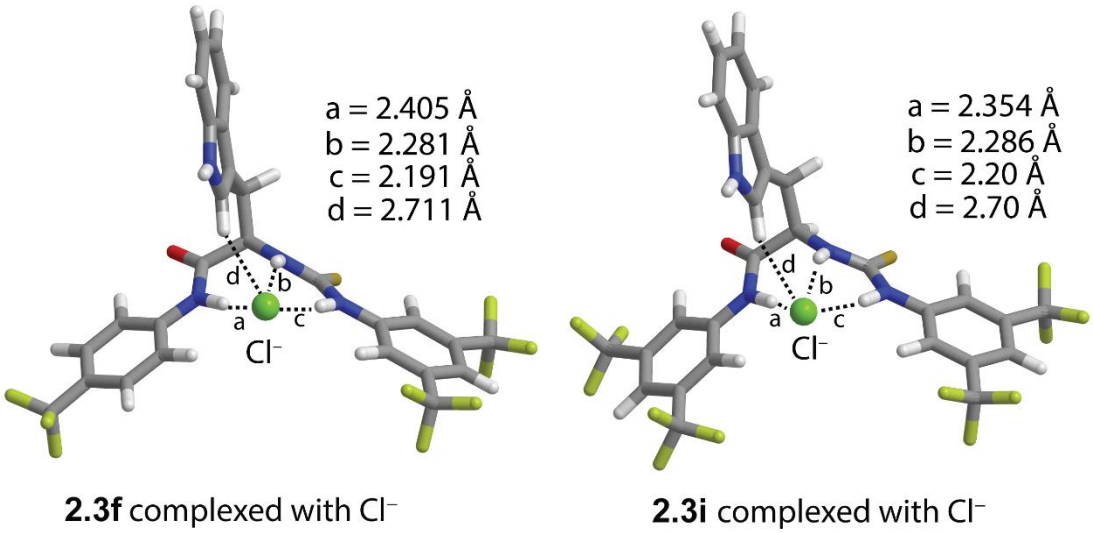

Figure 2.7. DFT optimized structure of the compound **2.3f** and **2.3i** in complexation with a Cl^- ion.

2.3. Conclusions

We developed a new class of tryptophan-based derivatives that transport Cl^- ions across the lipid bilayer. ^1H NMR and fluorescence-based assays revealed the potent compound selectively recognized the Cl^- ions and transported across the model lipid bilayers. The transport mechanism investigations suggest that OH^- / Cl^- antiport mechanism with a mobile carrier pathway. DFT analysis supported the interaction of Cl^- ions with the potent compound **2.3i**. Therefore, tryptophan-based transporters have valuable insights into the development of novel therapeutic agents, especially in addressing ion transport-related challenges. We propose that these tryptophan-based transporters hold significant promise for designing innovative solutions to ion transport-related disorders.

2.4. Experimental sections

2.4.1. General information

The experiment used chemicals and solvents procured from commercial suppliers, including Sigma-Aldrich and TCI. These were used without undergoing further purification unless clearly specified. The reactions were monitored using thin-layer chromatography (TLC) on silica gel 60 F254 (0.25 mm). A 120-200 mesh size silica gel was used for performing column chromatography. The ^1H NMR and ^{13}C NMR were recorded using the Bruker spectrometer operating at frequencies of 600 MHz and 151 MHz, respectively. The chemical shifts were calculated using internal solvents DMSO-d_6 and $CDCl_3$ and were expressed in parts per million

(ppm). The coupling constant (J) values were denoted in hertz, and the associated abbreviations were as follows: s (for singlet), d (for doublet), t (for triplet), q (for quartet), m (for multiple), and br (for broadened). The acquisition of high-resolution mass spectra (HRMS) was performed using an Agilent Q-TOF mass spectrometer that was fitted with a Z-spray source. The acquired mass data were evaluated using the software incorporated within the device. The chemical molecules used in the investigation, namely dipalmitoylphosphatidylcholine (DPPC) and egg-yolk phosphatidylcholine (EYPC), were obtained from Sigma Aldrich. The reagents used in this investigation, such as HEPES buffer, 8-hydroxylysine-1, 3, 6-trisulfonic acid (HPTS), bis-*N*-methylacridinium nitrate (Lucigenin), calcein, Triton X-100, and other inorganic salts, together with their respective hydroxide bases, were obtained from Sigma Aldrich. The buffers were made using ultrapure water obtained from the Milli-Q system produced by Millipore, based in Billerica, MA. The stock solutions of the chemicals were produced using gas chromatographic grade DMSO, obtained from Sigma.

2.4.2. Synthesis of the Ion Transporters:

2.4.2.1. Synthesis of (tert-butoxycarbonyl)tryptophan ─ Tryptophan (500 mg, 2.45 mmol) was dissolved in 20 ml of 1,4-dioxane: water (2:1) while stirring 1 (N) NaOH (4.42 mL) was then added and activated for 15 minutes. To the reaction mixture di-tert-butyl dicarbonate (965 mg, 2.45 mmol, 1 equiv.) was added and stirred for 18 hours at room temperature. After the reaction was completed, the organic solvent was removed under reduced pressure, ice water was added, and the pH was adjusted to 2-3 by adding 1 (N) HCl solution. Immediately, a white precipitate formed, which was then filtered out and repeatedly washed with water before being dried under reduced pressure. The compound was characterized by ^{1}H NMR, ^{13}C NMR, and HRMS (ESI) analysis. **^{1}H NMR (600 MHz, Chloroform-*d*) δ:** 10.52 (s, 1H), 8.42 (s, 1H), 8.37 (s, 1H), 7.61 (d, J = 7.9 Hz, 1H), 7.27 (d, J = 8.0 Hz, 1H), 7.19-7.14 (m, 1H), 7.12 − 7.10 (m, 1H), 6.89 (s, 1H), 5.28 − 5.27, 4.62 − 4.61(bs, 1H), 3.38 – 3.21 (m, 2H), 1.40 (s, 9H). **^{13}C NMR (151 MHz, $CDCl_3$) δ:** 176.57, 155.66, 136.09, 127.76, 123.08, 122.21, 119.72, 118.80, 111.24, 109.90, 80.32, 54.23, 28.34, 27.54. **HRMS (ESI) m/z:** calculated for $C_{16}H_{20}N_2O_4$ $(M + H)^+$: 305.1496, found:.305.1496.

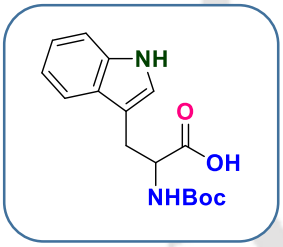

2.4.2.2. Synthesis of compound 2.1a-2.1d (general procedure) ─ To a solution of (tert-butoxycarbonyl)tryptophan (200 mg, 0.66 mmol, 1 equiv.) in N,N-dimethylformamide (4 mL)

were added *N,N,N′,N′*-tetramethyl-O-(1H-benzotriazol-1-yl)uroniumhexafluorophosphate (HBTU) (300 mg, 0.8 mmol, 1.2 equiv.) and triethylamine (280 µL, 2 mmol, 3 equiv.), the mixture was stirred at room temperature for 20 minutes, and the corresponding phenylaniline derivative and 8-aminoquinoline (0.66 mmol, 1 equiv.) was added. The mixture was agitated for 12 hours and then poured into water. The organic layers were combined and rinsed successively with cold water and brine, dried using anhydrous sodium sulphate, and reduced in a vacuum after being extracted five times with ethyl acetate. The resulting residue was purified by silica gel chromatography with hexane / ethylacetate (4:1 ratio) with a resulting yield of 70–80%.

2.4.2.3. Synthesis of compound 2.2a-2.2d (general procedure) ─ Compounds **2.1a-2.1d** (0.5 mmol, 1 equiv.) was dissolved in dichloromethane (4 mL), and trifluoroacetic acid (TFA) (5 mmol, 10 equiv.) was added. The reaction mixture was stirred at room temperature for 3 hours and concentrated in a vacuum. The residue was neutralised by adding saturated sodium bicarbonate solution, extracted using ethylacetate, and dried using anhydrous sodium sulphate. The solvent was removed under reduced pressure. The product was used without purification.

2.4.2.4. Synthesis of compound 2.3a-2.3i and 2.4 (general procedure) ─ To the stirring solutions of compounds **2.3a-2.3i** (0.2 mmol, 1 equiv.) in dichloromethane, a solution of respective phenyl isothiocyanate derivatives (0.2 mmol, 1 equiv.) in dichloromethane was added (dropwise) to the solution under an inert atmosphere at room temperature. Then the reaction mixture was allowed to stir for 6 hours at room temperature. After the completion of the reaction, the crude was purified by silica gel chromatography with hexane / ethylacetate (4:1 ratio) with a resulting yield of 90–95%.

2.4.3. Characterization of the Synthesized Compounds:

2.4.3.1. Tert-butyl (3-(1H-indol-3-yl)-1-oxo-1-(phenylamino)propan-2-yl)carbamate (2.1a) ─ Following the general procedure as point out in section 2.4.2.2, provided the light yellowish solid compound **2.1a** as 80% yield. The compound was characterized by ^{1}H NMR, ^{13}C NMR, and HRMS (ESI) analysis. **^{1}H NMR (600 MHz, Chloroform-*d*) δ:** 8.19 (s, 1H),

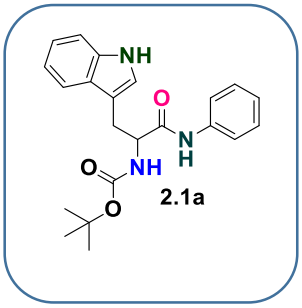

7.77 – 7.69 (bs, 2H), 7.39 (d, *J* = 7.9 Hz, 1H), 7.30 (m, 2H), 7.27 (d, *J* = 8.4 Hz, 2H), 7.25 – 7.21 (m, 1H), 7.15 (t, *J* = 7.0 Hz, 1H), 7.09 (t, J = 7.0 Hz, 1H), 7.06 (bs, 1H), 5.32, 4.64 (s, 1H), 3.34 (m, 2H), 1.46 (s, 9H). **^{13}C NMR (151 MHz, CDCl$_3$) δ:** 170.05, 137.30, 136.26, 128.89, 127.30, 124.44, 123.32, 122.43, 120.04, 118.86, 111.31, 55.84, 29.72, 28.31. **HRMS (ESI) m/z:** calculated for $C_{22}H_{25}N_3O_3$ (M - H)$^-$: 378.1823, found:.378.1813.

2.4.3.2. Tert-butyl(3-(1H-indol-3-yl)-1-oxo-1-((4-(trifluoromethyl)phenyl)amino)propan-2-yl)carbamate (2.1b) ─ Following the general procedure as point out in section 2.4.2.2, provided the light yellowish solid compound **2.1b** as 75% yield. The compound was characterized by ^{1}H NMR, ^{13}C NMR, and HRMS (ESI) analysis. **^{1}H NMR (600 MHz, Chloroform-*d*) δ:** 8.17 (bs, 1H), 7.66 (d, J = 7.6 Hz, 1H), 7.55 (d, J = 7.7 Hz, 1H), 7.49 – 7.46 (m, 2H), 7.39 -7.38(bs, 1H), 7.35 (t, J = 8.0 Hz, 1H), 7.21-7.17 (m, 1H), 7.12 – 7.09 (m, 1H), 7.04 (s, 1H), 6.99 (s, 1H), 5.29, 4.64- 4.63(bs, 1H), 3.34 – 3.27 (m, 2H), 1.43 (s, 9H). **^{13}C NMR (151 MHz, CDCl$_3$) δ:** 172.81, 170.52, 140.45, 136.27, 127.21, 126.07, 123.28, 122.53, 122.23, 120.02, 119.64, 119.52, 119.47, 118.72, 111.36, 60.43, 52.25, 28.34, 28.29. **HRMS (ESI) m/z:** calculated for $C_{23}H_{24}F_3N_3O_3$ (M - H)$^-$: 446.1693, found:.446.1684.

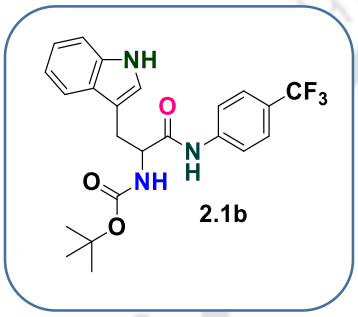

2.4.3.3. Tert-butyl(1-((3,5-bis(trifluoromethyl)phenyl)amino)-3-(1H-indol-3-yl)-1 oxopropan-2-yl)carbamate (2.1c) ─ Following the general procedure as point out in section 2.4.2.2, provided the light yellowish solid compound **2.1c** as 70 % yield. The compound was characterized by ^{1}H NMR, ^{13}C NMR, and HRMS (ESI) analysis. ^{1}H NMR (600 MHz, Chloroform-*d*) δ 8.47 – 8.30 (m, 1H), 8.16 – 8.05 (m, 1H), 7.97 (s, 1H), 7.74 (d, *J* = 10.6 Hz, 1H), 7.64 (t, *J* = 7.9 Hz, 1H), 7.56 (d, *J* = 9.6 Hz, 1H), 7.38 (d, *J* = 8.0 Hz, 1H), 7.21 (t, *J* = 7.5 Hz, 1H), 7.14 – 7.08 (m, 2H), 7.04 (d, *J* = 9.9 Hz, 1H), 5.30 (d, *J* = 14.6 Hz, 1H), 4.64 (d, *J* = 4.4 Hz, 1H), 3.38 (dd, *J* = 14.5, 6.3 Hz, 1H), 3.29 (dd, *J* = 14.4, 7.3 Hz, 1H), 1.46 (s, 9H). **^{13}C NMR (151 MHz, CDCl$_3$) δ:** 171.21, 170.74, 138.84, 136.25, 132.22, 132.00,

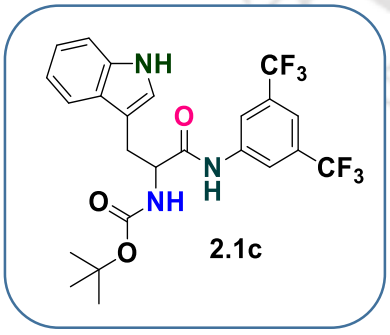

127.08, 125.99, 123.92, 123.27, 122.68, 122.11, 120.12, 119.52, 118.57, 117.53, 111.39, 60.42, 28.28, 21.06, 14.20. **HRMS (ESI) m/z:** calculated for $C_{24}H_{23}F_6N_3O_3$ $(M - H)^-$: 514.1571, found: 514.15.

2.4.3.4. Tert-butyl (3-(1H-indol-3-yl)-1-oxo-1-(quinolin-8-ylamino)propan-2-yl)carbamate (2.1d) — Following the general procedure as point out in section 2.4.2.2, provided the light yellowish solid compound **2.1d** as 78 % yield. The compound was characterized by ^{1}H NMR, ^{13}C NMR, and HRMS (ESI) analysis. **^{1}H NMR (600 MHz, Chloroform-*d*) δ:** 10.47 (s, 1H), 8.34 (d, *J* = 33.6 Hz, 1H), 7.56 (d, *J* = 7.9 Hz, 2H), 7.22 (d, *J* = 8.0 Hz, 2H), 7.12 (m, 2H), 7.06 (t, *J* = 7.0 Hz, 2H), 6.84 (s, 1H), 6.72 (s, 1H), 6.14 (s, 1H), 5.23 (d, *J* = 6.9 Hz, 1H), 4.59 – 4.49 (m, 1H), 3.30 – 3.25 (m, 1H), 3.22 – 3.17 (m, 2H), 1.35 (s, 9H). **^{13}C NMR (151 MHz, $CDCl_3$) δ:** 171.20, 170.39, 155.54, 148.09, 138.52, 136.33, 136.07, 134.02, 127.82, 127.23, 123.16, 122.17, 121.77, 121.53, 119.70, 118.92, 116.46, 111.10, 110.50, 56.18, 28.53, 28.38. **HRMS (ESI) m/z:** calculated for $C_{25}H_{26}N_4O_3$ $(M + H)^+$: 431.2078, found: 431.2078.

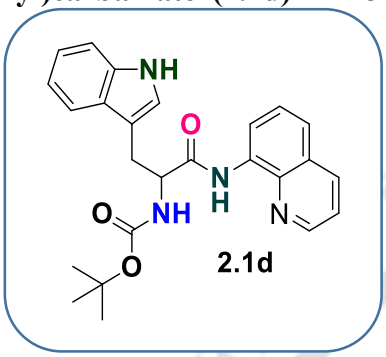

2.4.3.5. 2-amino-3-(1H-indol-3-yl)-N-phenylpropanamide (2.2a) — Following the general procedure as point out in section 2.4.2.3, provided the yellowish white solid compound **2.2a**. The compound was characterized by ^{1}H NMR, ^{13}C NMR, and HRMS (ESI) analysis. **^{1}H NMR (600 MHz, Chloroform-*d*) δ:** 10.33 (d, *J* = 76.3 Hz, 2H), 8.29 (s, 2H), 7.60 (m, 1H), 7.51 (m, 2H), 7.31 (m, 1H), 7.25 – 7.15 (m, 3H), 7.07 – 6.98 (m, 2H), 6.96 – 6.90 (m, 1H), 4.36 (s, 1H), 3.38 (m, 1H). **^{13}C NMR (151 MHz, $CDCl_3$) δ:** 167.26, 137.88, 136.42, 128.60, 127.06, 124.89, 124.11, 121.48, 120.05, 118.92, 118.50, 111.51, 106.93, 54.03, 27.45. **HRMS (ESI) m/z:** calculated for $C_{17}H_{17}N_3O$ $(M + H)^+$: 280.1444, found:. 280.1444.

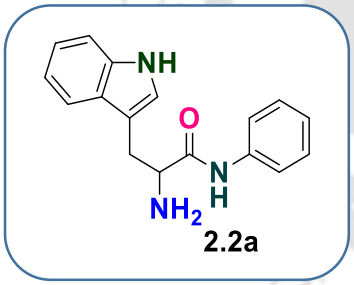

2.4.3.6. 2-amino-3-(1H-indol-3-yl)-N-(4-(trifluoromethyl)phenyl)propanamide (2.2b) — Following the general procedure as point out in section 2.4.2.3, provided the yellowish white solid compound **2.2b**. The compound was characterized by ^{1}H NMR, ^{13}C NMR, and HRMS (ESI) analysis. **^{1}H NMR (600 MHz, Chloroform-*d* + DMSO-*d*$_6$) δ**: 10.98 (s, 1H), 10.54 (s, 1H), 8.32 (broad, 2H), 7.81-7.75 (m, 2H), 7.69-7.64 (m, 1H), 7.58 – 7.51 (m, 2H), 7.41-7.35 (m, 1H), 7.26 – 7.20 (m, 1H), 7.14 – 7.08 (m, 1H), 7.00 – 6.95 (m, 1H), 4.37 (m, 1H), 3.57 – 3.37 (m, 1H), 3.39 – 3.33 (m, 1H). **^{13}C NMR (151 MHz, CDCl$_3$ + DMSO-*d*$_6$) δ:** 168.01, 141.28, 136.32, 126.96, 125.61, 125.59, 124.72, 121.29, 119.54, 118.74, 118.71, 118.32, 111.38, 106.72, 54.02, 27.40. **(ESI) m/z:** calculated for $C_{18}H_{16}F_3N_3O$ $(M + Na)^+$: 370.1138, found:. 370.2949.

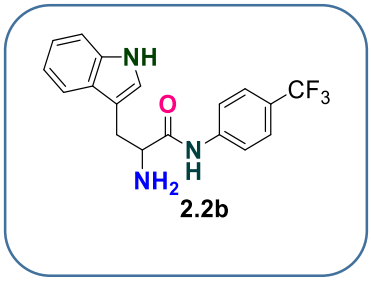

2.2b

2.4.3.7. 2-amino-N-(3,5-bis(trifluoromethyl)phenyl)-3-(1H-indol-3-yl)propanamide (2.2c) — Following the general procedure as point out in section 2.4.2.3, provided the yellowish white solid compound **2.2c**. The compound was characterized by ^{1}H NMR, ^{13}C NMR, and HRMS (ESI) analysis. **^{1}H NMR (600 MHz, Chloroform-*d*):** δ 9.90 (s, 1H), 8.24 (broad, 2H), 8.11 (s, 2H), 7.69 (d, *J* = 7.8 Hz, 1H), 7.61 (s, 1H), 7.40 (d, *J* = 8.0 Hz, 1H), 7.24 (t, *J* = 7.4 Hz, 1H), 7.15 (t, *J* = 7.4 Hz, 1H), 7.12 (s, 1H), 3.92 (dd, *J* = 8.1, 3.8 Hz, 1H), 3.52 – 3.46 (m, 1H), 3.10 (dd, *J* = 14.5, 8.7 Hz, 1H). **^{13}C NMR (151 MHz, CDCl$_3$) δ:** 173.59, 139.17, 136.45, 132.39, 132.16, 127.33, 124.06, 123.24, 122.56, 122.26, 119.91, 119.16, 118.74, 117.28, 111.41, 110.94, 55.79, 30.29. **HRMS (ESI) m/z:** calculated for $C_{19}H_{15}F_6N_3O$ $(M - H)^-$: 414.1047, found: 414.1570.

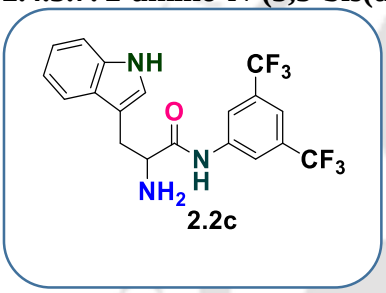

2.2c

2.4.3.8. 2-amino-3-(1H-indol-3-yl)-N-(quinolin-8-yl)propanamide (2.2d) — Following the general procedure as point out in section 2.4.2.3, provided the yellowish white solid compound **2.2d**. The compound was characterized by ^{1}H NMR, ^{13}C NMR, and HRMS (ESI) analysis. **^{1}H NMR (600 MHz, Chloroform-*d*) δ:** 11.44 (s, 1H), 8.91 (d, *J* = 7.5 Hz, 1H), 8.85 (d, *J* = 2.9 Hz, 1H), 8.25 (s, 1H), 8.17 (d, *J* = 8.1 Hz, 1H), 7.77 (d, *J* = 7.9 Hz, 1H), 7.60 – 7.52 (m, 2H), 7.45 (dd, *J* = 8.2, 4.1 Hz, 1H), 7.39 (d, *J* = 8.1 Hz, 1H), 7.22 (t, *J* = 7.5 Hz,

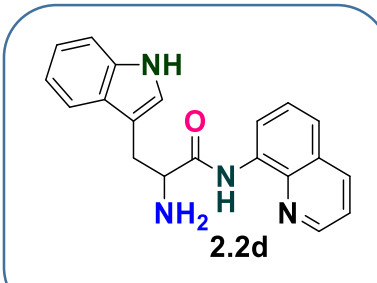

2.2d

1H), 7.16 (t, *J* = 7.5 Hz, 2H), 4.06 (dd, *J* = 9.1, 3.8 Hz, 1H), 3.60 (dd, *J* = 14.6, 3.7 Hz, 1H), 3.13 (dd, *J* = 14.5, 9.3 Hz, 1H), 2.22 (broad, 2H). **^{13}C NMR (151 MHz, $CDCl_3$) δ**: 173.45, 148.57, 139.06, 136.48, 136.26, 134.38, 128.10, 127.46, 127.34, 123.30, 122.33, 121.81, 121.52, 119.69, 118.99, 116.60, 111.64, 111.29, 56.74, 30.85. **HRMS (ESI) m/z:** calculated for $C_{20}H_{18}F_6N_4O$ (M - H)$^-$: 331.1553, found: 331.1553.

2.4.3.9. 3-(1H-indol-3-yl)-N-phenyl-2-(3-phenylthioureido)propanamide (2.3a) — Following the general procedure as mentioned in section 2.4.2.4, using compound **2.2a** (50 mg, 0.18 mmol) and phenylisothiocyanate (24 mg, 0.18 mmol) provided the yellowish solid compound **2.3a** as 95% yield. The compound was characterized by ^{1}H NMR, ^{13}C NMR, and HRMS (ESI) analysis. **^{1}H NMR (600 MHz, Chloroform-*d*):** δ 8.18 (s, 1H), 8.08 (s, 1H), 8.01 (s, 1H), 7.81 (d, *J* = 7.9 Hz, 1H), 7.38 (d, *J* = 8.2 Hz, 1H), 7.28 – 7.21 (m, 8H), 7.15 (t, *J* = 7.5 Hz, 1H), 7.08 (t, *J* = 6.0 Hz, 1H), 7.05 (d, *J* = 2.0 Hz, 1H), 7.01 (d, *J* = 7.5 Hz, 2H), 6.98 (d, *J* = 7.5 Hz, 1H), 4.15 (q, *J* = 7.1 Hz, 1H), 3.57 (dd, *J* = 14.6, 5.9 Hz, 1H), 3.28 (dd, *J* = 14.7, 8.3 Hz, 1H).**^{13}C NMR (151 MHz, $CDCl_3$):** δ 179.89, 169.30, 137.11, 136.18, 135.69, 130.04, 128.91, 127.28, 124.82, 124.63, 123.31, 122.51, 120.22, 120.09, 119.12, 111.31, 110.32, 59.44, 27.86. **HRMS (ESI) m/z:** calculated for $C_{24}H_{22}N_4OS$ (M - H)$^-$: 413.1442, found: 413.1437.

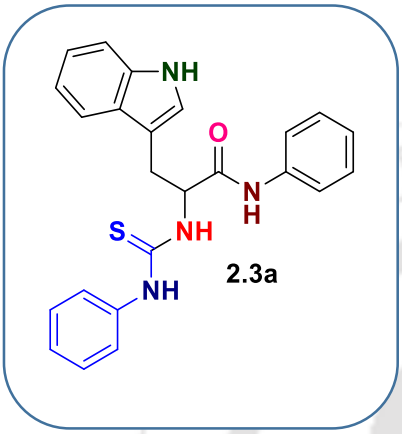

2.4.3.10. 3-(1H-indol-3-yl)-N-phenyl-2-(3-(4-(trifluoromethyl)phenyl)thioureido)propanamide (2.3b) — Following the general procedure as mentioned in section 2.4.2.4, using compound **2.2a** (50 mg, 0.18 mmol) and 1-isothiocyanato-4-(trifluoromethyl)benzene (0.18 mmol, 1 equiv.) provided the yellowish solid compound **2.3b** as 95% yield. The compound was characterized by ^{1}H NMR, ^{13}C NMR, and HRMS (ESI) analysis. **^{1}H NMR (600 MHz, Chloroform-*d*):** δ 8.37 (s, 1H), 8.15 (s, 1H), 7.82 (d, *J* = 8.0 Hz, 1H), 7.80 (s, 1H), 7.54 (d, *J* = 7.2 Hz, 1H), 7.44 (d, *J* = 8.4 Hz, 2H), 7.40 (d, *J* = 8.2 Hz, 1H), 7.25 (t, *J* = 7.5 Hz, 1H), 7.22 – 7.17 (m, 4H), 7.16 – 7.12 (m, 3H), 7.11 – 7.06 (m, 2H), 4.15 (q, *J* = 7.1 Hz, 1H), 3.63 (dd, *J* = 14.5, 5.3 Hz, 1H), 3.32 (dd, *J*

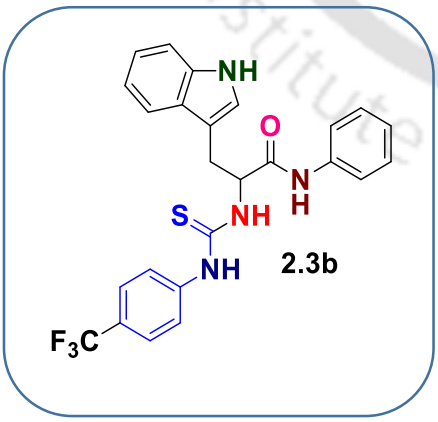

= 14.5, 8.7 Hz, 1H). **^{13}C NMR (151 MHz, $CDCl_3$):** δ 179.91, 169.90, 139.97, 136.49, 136.20, 129.00, 127.19, 126.62, 125.16, 123.57, 123.40, 122.72, 120.69, 120.24, 119.01, 111.43, 110.18, 59.46, 28.27. **HRMS (ESI) m/z:** calculated for $C_{25}H_{21}F_3N_4OS$ (M - H)$^-$: 481.1315, found: 481.1308.

2.4.3.11. 2-(3-(3,5-bis(trifluoromethyl)phenyl)thioureido)-3-(1H-indol-3-yl)-N-phenylpropanamide (2.3c) — Following the general procedure as mentioned in section 2.4.2.4, using compound **2.2a** (50 mg, 0.18 mmol) and 1-isothiocyanato-3,5-bis(trifluoromethyl)benzene (0.18 mmol, 1 equiv.) provided the yellowish solid compound **2.3c** as 98% yield. The compound was characterized by ^{1}H NMR, ^{13}C NMR, and HRMS (ESI) analysis. **^{1}H NMR (600 MHz, Chloroform-*d*):** δ 8.85 (s, 1H), 8.29 (d, *J* = 7.0 Hz, 1H), 8.16 (s, 1H), 7.84 (d, *J* = 7.8 Hz, 2H), 7.75 (s, 2H), 7.57 (s, 1H), 7.40 (d, *J* = 8.1 Hz, 1H), 7.25 (t, *J* = 7.6 Hz, 1H), 7.15 (t, *J* = 7.5 Hz, 1H), 7.13 – 7.12 (m, 1H), 7.09 (t, *J* = 7.7 Hz, 2H), 7.05 (d, *J* = 7.7 Hz, 2H), 6.97 (t, *J* = 7.2 Hz, 1H), 5.56 (q, *J* = 7.5 Hz, 1H), 3.61 (dd, *J* = 14.3, 5.4 Hz, 1H), 3.37 (dd, *J* = 14.3, 8.9 Hz, 1H). **^{13}C NMR (151 MHz, $CDCl_3$):** δ 181.03, 171.35, 139.86, 136.27, 135.66, 131.72, 131.50, 129.01, 127.12, 125.74, 124.12, 123.90, 123.25, 122.73, 122.09, 121.31, 120.18, 118.95, 118.52, 111.50, 110.23, 59.44, 28.91. **HRMS (ESI) m/z:** calculated for $C_{26}H_{20}F_6N_4OS$ (M - H)$^-$: 549.1189, found: 549.1175.

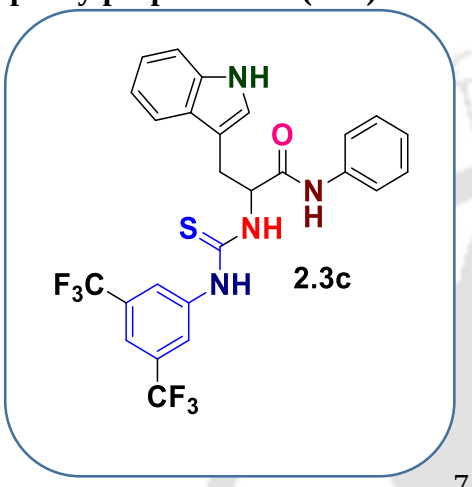

2.4.3.12. 3-(1H-indol-3-yl)-2-(3-phenylthioureido)-N-(4-(trifluoromethyl)phenyl)propanamide(2.3d) — Following the general procedure as mentioned in section 2.4.2.4, using compound **2.2b** (50 mg, 0.14 mmol) and phenylisothiocyanate (0.14 mmol, 1 equiv.) provided the yellowish solid compound **2.3d** as 95% yield. The compound was characterized by ^{1}H NMR, ^{13}C NMR, and HRMS (ESI) analysis. **^{1}H NMR (600 MHz, Chloroform-*d*):** δ 8.42 (s, 1H), 8.12 (s, 1H), 7.78 (d, *J* = 7.9 Hz, 1H), 7.73 (s, 1H), 7.52 (d, *J* = 8.5 Hz, 3H), 7.42 (dd, *J* = 8.1, 3.5 Hz, 3H), 7.26 (d, *J* = 6.2 Hz, 4H), 7.18 (t, *J* = 7.4 Hz, 1H), 7.11 (s, 1H), 6.98 (d, *J* = 6.6 Hz, 1H), 6.73

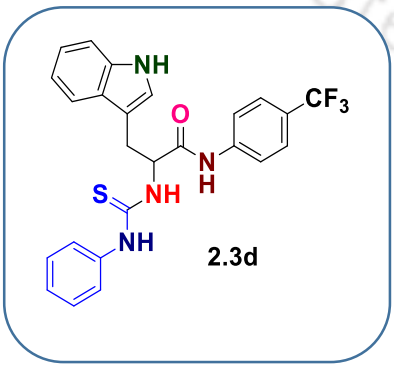

(d, *J* = 7.9 Hz, 1H), 5.56 (q, *J* = 7.8 Hz, 1H), 3.58 (dd, *J* = 14.6, 6.3 Hz, 2H), 3.26 (dd, *J* = 14.8, 8.2 Hz, 1H).**^{13}C NMR (151 MHz, CDCl$_3$):** δ 181.49, 170.54, 148.99, 136.19, 130.24, 126.17, 124.95, 123.24, 122.71, 120.28, 119.55, 118.97, 117.07, 112.99, 111.34, 110.23, 104.23, 58.50, 27.63. **HRMS (ESI) m/z:** calculated for $C_{25}H_{21}F_3N_4OS$ (M - H)$^-$: 481.1315, found: 549.1315.

2.4.3.13. 3-(1H-indol-3-yl)-N-(4-(trifluoromethyl)phenyl)-2-(3-(4-(trifluoromethyl)phenyl)thioureido)propanamide (3e) ─ Following the general procedure as mentioned in section 2.4.2.4, using compound **2.2b** (50 mg, 0.14 mmol) and 1-isothiocyanato-4-(trifluoromethyl)benzene (0.14 mmol, 1 equiv.) provided the yellowish solid compound **2.3e** as 95% yield. The compound was characterized by ^{1}H NMR, ^{13}C NMR, and HRMS (ESI) analysis. **^{1}H NMR (600 MHz, Chloroform-*d* + DMSO-*d*$_6$) δ:** 10.16 (s, 1H), 10.05 (s, 1H), 9.90 (s, 1H), 7.90 (q, *J* = 7.8, 7.2 Hz, 1H), 7.76 – 7.61 (m, 5H), 7.55 – 7.49 (m, 4H), 7.38 – 7.29 (m, 1H), 7.14 – 7.07 (m, 1H), 7.03 – 6.94 (m, 2H), 5.66 – 5.11 (m, 1H), 3.74 – 3.52 (m, 1H), 3.52 – 3.23 (m, 1H). **^{13}C NMR (151 MHz, CDCl$_3$ + DMSO-*d*$_6$) δ:** 179.86, 170.39, 142.60, 141.72, 136.17, 136.15, 127.78, 125.69, 125.48, 124.99, 123.50, 123.20, 122.16, 122.10, 121.29, 119.40, 118.81, 118.78, 111.20, 109.26, 58.62, 28.12. **HRMS (ESI) m/z:** calculated for $C_{26}H_{20}F_6N_4OS$ (M - H)$^-$: 549.1189, found: 549.1184.

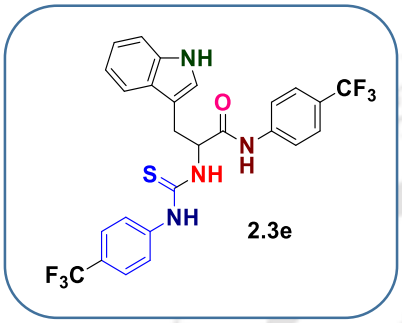

2.4.3.14. 2-(3-(3,5-bis(trifluoromethyl)phenyl)thioureido)-3-(1H-indol-3-yl)-N-(4-(trifluoromethyl)phenyl)propanamide (2.3f) ─ Following the general procedure as mentioned in section 2.4.2.4, using compound **2.2b** (50 mg, 0.14 mmol) and 1-isothiocyanato-3,5-bis(trifluoromethyl)benzene (0.14 mmol, 1 equiv.) provided the yellowish solid compound **2.3f** as 96% yield. The compound was characterized by ^{1}H NMR, ^{13}C NMR, and HRMS (ESI) analysis. **^{1}H NMR (600 MHz, DMSO-*d*$_6$) δ:** 10.91 (s, 1H), 10.75 (s, 1H), 10.42 (s, 1H), 8.29 (s, 2H), 8.28 (s, 1H), 7.81 (d, *J* = 8.2 Hz, 2H), 7.77 (s, 1H), 7.70 (d, *J* = 8.3 Hz, 2H), 7.60 (d, *J* = 7.8 Hz, 1H), 7.33 (d, *J* = 8.0 Hz, 1H), 7.15 (s, 1H), 7.05 (t, *J* = 7.4 Hz, 1H), 6.92 (t, *J* = 7.4 Hz, 1H), 5.32 (q, *J* = 6.4 Hz, 1H), 3.45 – 3.41 (m, 1H), 3.30 (m, 1H). **^{13}C NMR (151 MHz, CDCl$_3$):**

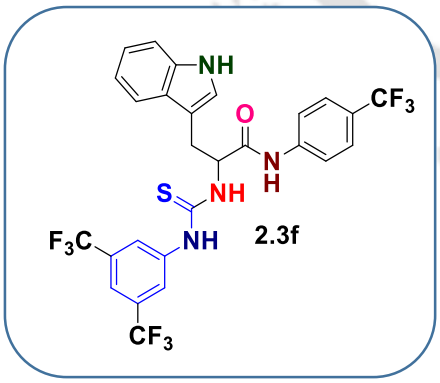

δ 180.69, 171.04, 139.38, 139.17, 136.26, 132.31, 132.08, 126.93, 126.24, 123.66, 123.35, 122.90, 121.92, 120.36, 120.10, 119.03, 118.74, 114.19, 111.60, 109.89, 59.54, 28.47. **HRMS (ESI) m/z:** calculated for $C_{27}H_{19}F_9N_4OS$ (M - H)$^-$: 617.1063, found: 617.1056.

2.4.3.15. N-(3,5-bis(trifluoromethyl)phenyl)-3-(1H-indol-3-yl)-2-(3-phenylthioureido)propanamide (2.3g) ─ Following the general procedure as mentioned in section 2.4.2.4, using compound **2.2c** (50 mg, 0.12 mmol) and phenylisothiocyanate (0.12 mmol, 1 equiv.) provided the yellowish solid compound **2.3g** as 95% yield. The compound was characterized by ^{1}H NMR, ^{13}C NMR, and HRMS (ESI) analysis. **^{1}H NMR (600 MHz, Chloroform-*d*):** δ 8.82 (s, 1H), 8.16 (s, 1H), 7.94 (s, 1H), 7.77 (s, 2H), 7.68 (d, *J* = 7.9 Hz, 1H), 7.57 (s, 1H), 7.42 (d, *J* = 8.2 Hz, 1H), 7.28 (s, 1H), 7.29 – 7.25 (m, 1H), 7.28 – 7.25 (m, 2H), 7.14 (t, *J* = 7.5 Hz, 1H), 7.12 (d, *J* = 2.3 Hz, 1H), 7.00 – 6.94 (m, 1H), 6.72 (d, *J* = 7.5 Hz, 1H), 5.57 (q, *J* = 7.5 Hz, 1H), 3.55 (dd, *J* = 14.8, 6.4 Hz, 1H), 3.28 (dd, *J* = 14.8, 8.1 Hz, 1H). **^{13}C NMR (151 MHz, CDCl$_3$):** δ 180.21, 169.80, 138.83, 136.16, 135.12, 132.30, 132.07, 130.23, 127.77, 127.17, 124.96, 123.92, 123.28, 122.79, 122.11, 120.32, 119.60, 118.71, 117.60, 111.42, 109.95, 59.38, 26.99. **HRMS (ESI) m/z:** calculated for $C_{26}H_{20}F_6N_4OS$ (M - H)$^-$: 549.1189, found: 549.1178.

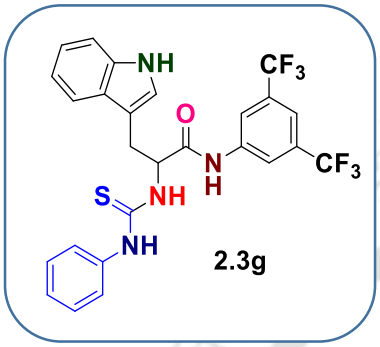

2.4.3.16. N-(3,5-bis(trifluoromethyl)phenyl)-3-(1H-indol-3-yl)-2-(3-(4-(trifluoromethyl)phenyl)thioureido)propanamide (2.3h) ─ Following the general procedure as mentioned in section 2.4.2.4, using compound **2.2c** (50 mg, 0.12 mmol) and 1-isothiocyanato-4-(trifluoromethyl)benzene (0.12 mmol, 1 equiv.) provided the yellowish solid compound **2.3h** as 94% yield. The compound was characterized by ^{1}H NMR, ^{13}C NMR, and HRMS (ESI) analysis. **^{1}H NMR (600 MHz, Chloroform-*d*):** δ 8.58 (s, 1H), 8.23 (d, *J* = 23.0 Hz, 2H), 7.72 (s, 2H), 7.68 (d, *J* = 7.5 Hz, 1H), 7.58 (s, 1H), 7.46 (d, *J* = 8.0 Hz, 1H), 7.43 (d, *J* = 8.1 Hz, 1H), 7.30 – 7.24 (m, 2H), 7.16 (s, 1H), 7.12 (t, *J* = 8.4 Hz, 2H), 7.03 (s, 1H), 5.55 (q, *J* = 7.1 Hz, 1H), 3.65 – 3.59 (m, 1H), 3.30 (dd, *J* = 14.5, 8.3 Hz, 1H). **^{13}C NMR (151 MHz, CDCl$_3$):** δ 179.98, 169.87, 138.82, 138.59, 136.16,

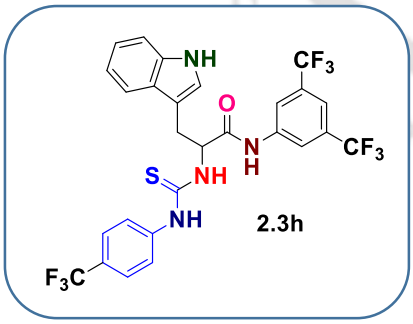

132.37, 132.15, 127.20, 127.18, 127.09, 123.90, 123.52, 122.99, 122.05, 120.47, 119.61, 118.55, 117.82, 111.60, 109.64, 59.54, 27.16. **HRMS (ESI) m/z:** calculated for $C_{27}H_{19}F_9N_4OS$ $(M - H)^-$: 617.1063, found: 617.1055.

2.4.3.17. N-(3,5-bis(trifluoromethyl)phenyl)-2-(3-(3,5bis(trifluoromethyl)phenyl)thioureido)-3-(1H-indol-3-yl)propanamide (2.3i) — Following the general procedure as mentioned in section 2.4.2.4, using compound **2.2c** (50 mg, 0.12 mmol) and 1-isothiocyanato-3,5-bis(trifluoromethyl)benzene (0.12 mmol, 1 equiv.) provided the yellowish solid compound **2.3i** as 98% yield. The compound was characterized by ^{1}H NMR, ^{13}C NMR, and HRMS (ESI) analysis. **^{1}H NMR (600 MHz, DMSO-*d*$_6$):** δ 10.95 (s, 1H), 10.93 (s, 1H), 10.40 (s, 1H), 8.32 (d, *J* = 7.1 Hz, 1H), 8.28 (s, 2H), 8.23 (s, 2H), 7.78 (d, *J* = 12.7 Hz, 2H), 7.60 (d, *J* = 7.9 Hz, 1H), 7.48 (s, 1H), 7.34 (d, *J* = 8.1 Hz, 1H), 7.21 (d, *J* = 2.0 Hz, 1H), 7.05 (t, *J* = 7.4 Hz, 1H), 6.90 (t, *J* = 7.4 Hz, 1H), 5.27 (q, *J* = 6.9 Hz, 1H), 3.42 (dd, *J* = 15.0, 5.4 Hz, 1H), 3.31 (dd, *J* = 13.9, 8.9 Hz, 1H). **^{13}C NMR (151 MHz, CDCl$_3$):** δ 180.61, 170.62, 138.55, 138.13, 136.22, 133.16, 132.80, 132.45, 132.23, 127.56, 126.83, 126.75, 123.94, 123.92, 123.52, 123.05, 120.51, 119.79, 118.51, 111.69, 109.66, 59.65, 27.99. **HRMS (ESI) m/z:** calculated for $C_{28}H_{18}F_{12}N_4OS$ $(M - H)^-$: 685.0937, found: 685.0937.

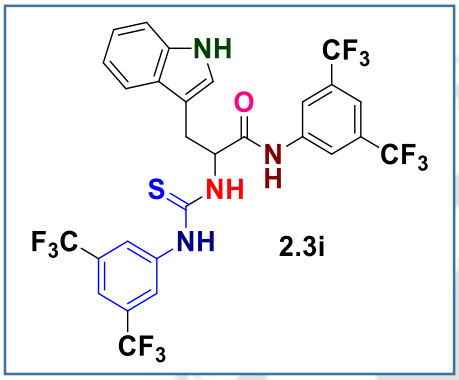

2.4.3.18. 2-(3-(3,5-bis(trifluoromethyl)phenyl)thioureido)-3-(1H-indol-3-yl)-N-(quinolin-8-yl)propanamide (2.4) — Following the general procedure as mentioned in section 2.4.2.4, using compound **2.2d** (50 mg, 0.15 mmol) and 1-isothiocyanato-3,5-bis(trifluoromethyl)benzene (0.15 mmol, 1 equiv.) provided the yellowish solid compound **2.4** as 97% yield. The compound was characterized by ^{1}H NMR, ^{13}C NMR, and HRMS (ESI) analysis. **^{1}H NMR (600 MHz, Chloroform-*d*) δ:** 10.11 (s, 1H), 8.66 (d, *J* = 4.1, 1.3 Hz, 1H), 8.55 (d, *J* = 7.6 Hz, 1H), 8.51 (d, *J* = 6.3 Hz, 1H), 8.16 (d, *J* = 8.2, 1.3 Hz, 1H), 7.97 (s, 1H), 7.83 (s, 3H), 7.74 (d, *J* = 7.9 Hz, 1H), 7.56 (s, 1H), 7.54 (d, *J* = 8.3 Hz, 1H), 7.46 (d, *J* = 8.2, 4.2 Hz, 1H), 7.43 (t, *J* = 8.0 Hz, 1H), 7.30 (s,

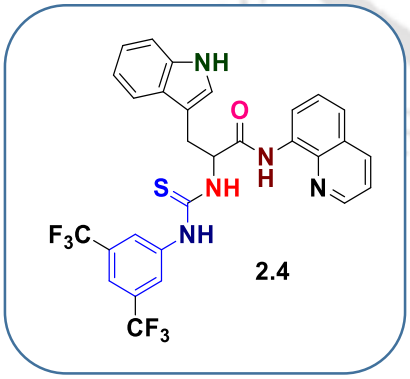

1H), 7.15 (t, *J* = 7.5 Hz, 1H), 7.07 – 7.01 (m, 2H), 5.76 – 5.72 (m, 1H), 3.63 (dd, *J* = 14.7, 5.2 Hz, 1H), 3.56 (dd, *J* = 14.7, 7.2 Hz, 1H). **^{13}C NMR (151 MHz, $CDCl_3$) δ:** 182.22, 172.34, 148.37, 147.45, 143.91, 136.22, 136.04, 133.80, 132.45, 132.23, 128.71, 127.91, 127.39, 127.06, 126.45, 123.67, 123.05, 121.35, 120.44, 118.51, 116.11, 111.54, 111.22, 110.12, 107.95, 60.41, 28.14. **HRMS (ESI) m/z:** calculated for $C_{29}H_{21}F_6N_5OS$ $(M + H)^+$: 602.1444, found: 602.1444.

2.4.3.19. 2-(3-(3,5-bis(trifluoromethyl)phenyl)thioureido)-4-methyl-N-phenylpentanamide (2.5a) ─ Following the general procedure as mentioned in section 2.4.2.4, using compound 2-amino-4-methyl-N-phenylpentanamide (20 mg, 0.09 mmol) and 1-isothiocyanato-3,5-bis(trifluoromethyl)benzene (27 mg, 0.09 mmol, 1 equiv.) provided the yellowish solid compound **2.5a** as 98% yield. The compound was characterized by ^{1}H NMR, ^{13}C NMR, and HRMS (ESI) analysis. **^{1}H NMR (600 MHz, Chloroform-*d*) δ:** 9.32 (s, 1H), 9.27 (s, 1H), 8.88 (s, 1H), 8.31 – 8.25 (m, 1H), 8.07 (d, *J* = 14.0 Hz, 1H), 7.98 (d, *J* = 17.2 Hz, 2H), 7.89 (s, 1H), 7.56 (s, 1H), 7.53 (d, *J* = 7.6 Hz, 2H), 4.38 (dd, *J* = 9.2, 3.9 Hz, 1H), 3.14 (q, *J* = 7.3 Hz, 2H), 1.93 – 1.84 (m, 1H), 1.04 (s, 6H). **^{13}C NMR (151 MHz, $CDCl_3$) δ:** 182.02, 173.10, 140.93, 140.20, 137.00, 133.99, 132.58, 132.35, 129.19, 129.05, 128.76, 125.48, 125.21, 120.69, 58.52, 40.52, 25.15, 8.55. **HRMS (ESI) m/z:** calculated for $C_{21}H_{21}F_6N_3OS$ $(M + H)^+$: 478.1382, found: 478.1366.

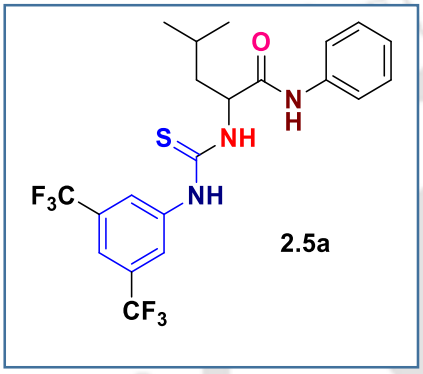

2.4.3.20. 2-(3-(3,5-bis(trifluoromethyl)phenyl)thioureido)-N,3-diphenylpropanamide (2.5b) ─ Following the general procedure as mentioned in section 2.4.2.4, using compound 2-amino-N,3-diphenylpropanamide (20 mg, 0.08 mmol) and 1-isothiocyanato-3,5-bis(trifluoromethyl)benzene (23 mg, 0.08 mmol, 1 equiv.) provided the light yellowish solid compound **2.5b** as 98% yield. The compound was characterized by ^{1}H NMR, ^{13}C NMR, and HRMS (ESI) analysis. **^{1}H NMR (600 MHz, Chloroform-*d*) δ:** 8.70 (s, 1H), 8.05 (d, *J* = 7.2 Hz, 1H), 7.91 (s, 1H), 7.75 (s, 2H), 7.62 (d, *J* = 12.0 Hz, 2H), 7.38

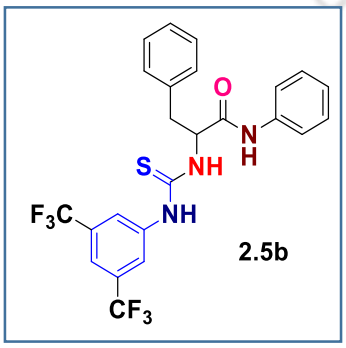

– 7.32 (m, 4H), 7.20 – 7.13 (m, 4H), 7.04 (t, *J* = 7.0 Hz, 1H), 5.46 (q, *J* = 7.9 Hz, 1H), 3.50 (dd, *J* = 13.5, 5.8 Hz, 1H), 3.17 (dd, *J* = 13.5, 9.1 Hz, 1H). **^{13}C NMR (151 MHz, $CDCl_3$) δ:** 180.76, 170.65, 139.49, 135.87, 135.44, 132.08, 129.23, 129.17, 129.14, 127.67, 126.03, 123.88, 122.01, 121.38, 118.80, 60.32, 38.97. **HRMS (ESI) m/z:** calculated for $C_{24}H_{19}F_6N_3OS$ $(M + H)^+$: 512.1226, found: 512.1221.

2.4.4. Chloride ion binding analysis by ^{1}H-NMR experiment

The ^{1}H NMR titration was performed for the compound **2.3f** and **2.3i** in DMSO-d_6. The stock solutions of the ionophore (20 mM) and TBACl (1.5 M) were prepared in DMSO-d_6. The TBACl was used as the source of Cl^- ion. The ^{1}H NMR experiment of ionophore in DMSO-d_6 were achieved by the following addition of TBACl (0-17 equiv.). The variations in chemical shift (Δδ) values of the N-H protons of the compound were examined. MestReNova software was used for the stacking of all the titration spectra. The BindFit v0.5 software fitted the variations in a chemical shift against the Cl^- ion concentration. The association constant (K_a) values were calculated using the BindFit v0.5 software (1:1 binding model).[13]

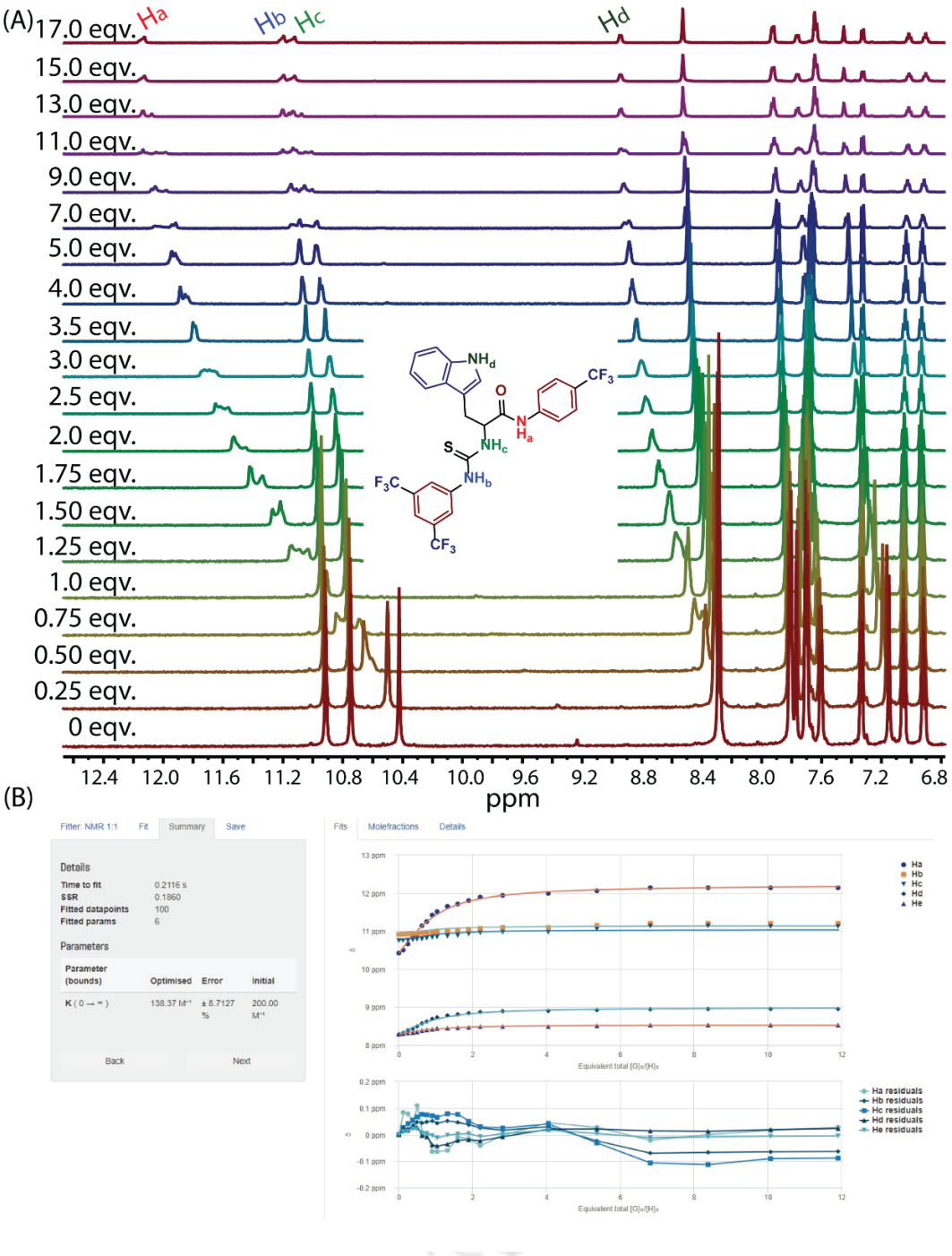

Figure 2.8. ^{1}H-NMR titration spectra for **2.3f** (20 mM) with the successive addition of TBACl in DMSO-d_6 solvent. The amounts of added TBACl are presented on the spectra (**A**). The plot of chemical shift (δ) of N-H_a, N-H_b, N-H_c, N-H_d and N-H_e protons vs. equivalent total ($[G]_0/[H]_0$) added, fitted to 1:1 binding model of BindFit v0.5 program (**B**). H = host = **2.3f** and G = guest = TBACl.

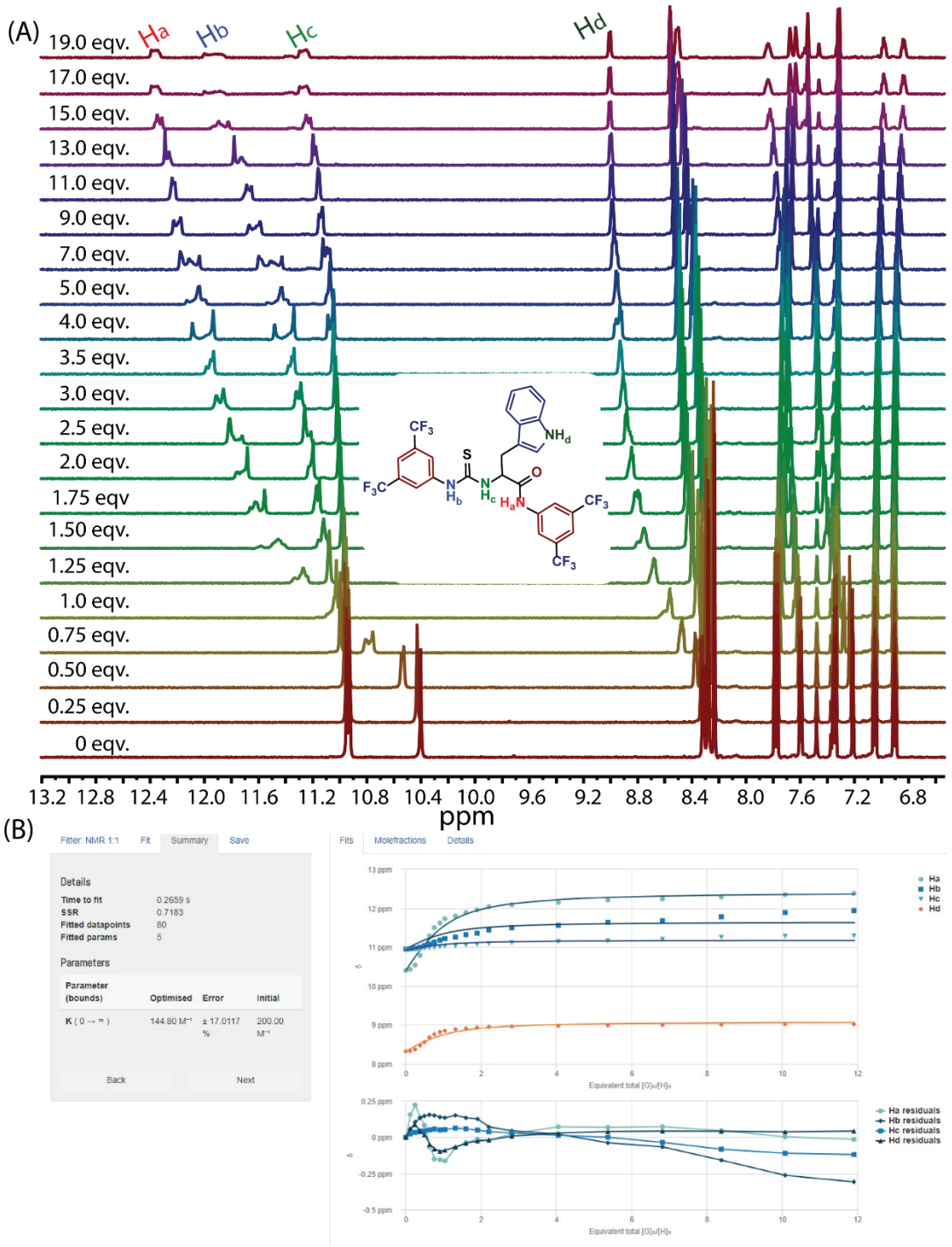

Figure 2.9. ^{1}H-NMR titration spectra for **2.3i** (20 mM) with the successive addition of TBACl in DMSO-d_6 solvent. The amounts of added TBACl are presented on the spectra (**A**). The plot of chemical shift (δ) of N-H_a, N-H_b, N-H_c, and N-H_d protons vs. equivalent total ($[G]_0/[H]_0$) added, fitted to 1:1 binding model of BindFit v0.5 program (**B**). H = host = **2.3i** and G = guest = TBACl.

2.4.5. Ion transport activity studies

2.4.5.1. Preparation of EYPC/CHOL-LUVs⊃lucigenin — To conduct lucigenin-based transport of ions studies, a clean sample vial was used to combine EYPC (50 mg/mL in deacidified $CHCl_3$) and CHOL (25 mg/mL in deacidified $CHCl_3$) in a molar ratio of 8:2. A lipid layer with a little thickness was created when the fluid underwent continuous rotation for a duration of 6 hours as the pressure gradually decreased. The thin lipid layer was moistened by adding 800 µL of a 20 mM HEPES buffer solution containing 1 mM lucigenin and 100 mM $NaNO_3$ (pH 7.2). The solution obtained then agitated using a vortex mixer for 6-7 cycles lasting 1 hour. It was then treated to 13-15 cycles of freezing and thawing. Finally, the solution was vortexed for 15 minutes to incorporate lucigenin into the lipid bilayer. The lipid solution was passed through a polycarbonate membrane with a 200 nm pore size using a mini-extruder. This process was repeated 19-21 times, ensuring an odd number of repetitions. In order to get a lipid content of 25 mM (assuming complete lipid regeneration), the lucigenin dye that was not encapsulated was eliminated using size exclusion column chromatography using Sephadex G-50. The eluting solution used was a 20 mM HEPES buffer containing 100 mM $NaNO_3$, with a pH of 7.2.

2.4.5.2. Preparation of EYPC/CHOL-LUVs⊃HPTS — To prepare HPTS encapsulated LUVs, precise quantities of EYPC and CHOL were mixed in a clean glass vessel in a molar concentration of 8:2 ratios. A lipid film with a small thickness was generated as a result of the constant motion of the solution for a duration of 6 hours while the pressure was gradually reduced. The thin lipid layer was moisturized by introducing 800 µL of a solution containing 20 mM HEPES, pH 7.2, 100 mM NaCl, and 1 mM HPTS. The solution obtained was agitated using a vortex mixer for 6-7 repetitions over a period of 1 hour and then exposed to 10-12 cycles of freezing and thawing. Lastly, the mixture was vigorously agitated for 15 minutes to incorporate HPTS into the lipid bilayer. The lipid solution was passed through a polycarbonate membrane with a pore size of 200 nm using a mini-extruder. This process was repeated 19-21 times, with an odd number of repetitions. In order to get a lipid content of 25 mM (assuming complete regeneration of lipids), the HPTS dye that was not encapsulated was eliminated using size exclusion column chromatography (using Sephadex G-50). The eluting solution used was a 20 mM HEPES buffer containing 100 mM NaCl, with a pH of 7.2.

2.4.5.3. Measuring transport activity (Lucigenin assay) — The fluorescence intensity measurements (Y-axis) for the lucigenin dye have been standardized. The intensities observed at t = 50 and t = 500 s were assigned as 0 and 100 units, respectively. The standardized fluorescent intensities (FI) at t = 450 s (prior to the introduction of Triton X-100) were utilized to assess the transportation capacity of each compound.

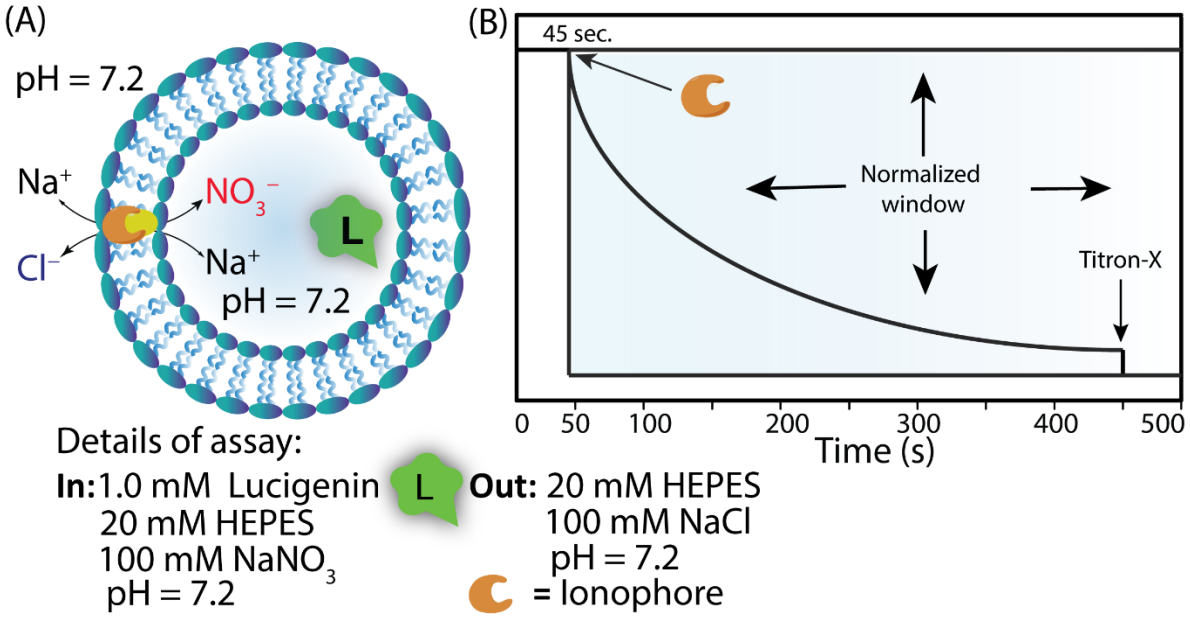

Figure 2.10. Schematic representation of lucigenin entrapped vesicles (A), and representation of transport of ions kinetics utilizing EYPC/CHOL-LUVs⊃lucigenin fluorescence (B).

The percent of transport efficacy,

$$T_{Lucigenin} = \frac{F_t - F_0}{(F_\infty - F_0)} \times 100\ \% \ldots . Eq.2.1$$

The variables F_0 = the fluorescence intensity before the substance is added, measured at 45 seconds. F_∞ = the fluorescence intensity after the addition of Triton X-100, measured at saturation, which occurs at 500 seconds. F_t represents the fluorescence intensity at 450 seconds, just before the addition of Triton X-100.

2.4.5.4. Quantitative analysis of transport activity from HPTS assay — The fluorescence intensity measurements (Y-axis) for the lucigenin dye have been standardized. The intensities observed at t = 50 and t = 500 s were assigned as 0 and 100 units, respectively. The standardized

fluorescent intensities (FI) at t = 450 s (prior to the introduction of Triton X-100) were utilized to assess the transportation capacity of each compound.

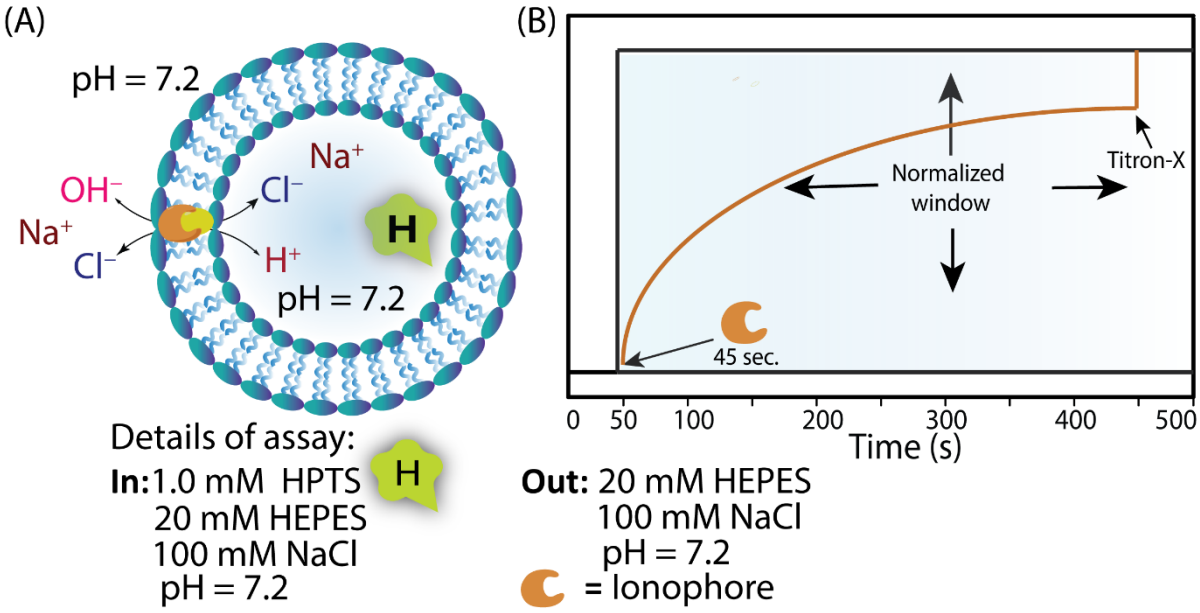

Figure 2.11. Schematic representation of HPTS entrapped vesicles (A), representation of HPTS-based ion transport kinetics (B).

The fluorescence intensity was standardized according to Equation 2.2:

$$T_{HPTS} = \frac{F_t - F_0}{(F_\infty - F_0)} \times 100\ \% \ldots . Eq.\ 2.2$$

In the above equation S2, F_0 = Fluorescence intensity just previously the compound addition (at t = 50 s). F_∞ = fluorescence intensity at saturation after complete release (at t = 450 s). F_t = fluorescence intensity at time t.

2.4.5.5. Chloride transport efficacy (lucigenin assay) ─ In order to conduct the lucigenin experiment, a 3 mL fluorescence cuvette was filled with 1950 µL of 20 mM HEPES buffer, pH 7.2, which included 100 mM NaCl. Additionally, 40 µL of the EYPC/CHOL-LUVs lucigenin was added. Next, the cuvette was inserted into the fluorescence spectrophotometer while being stirred slowly for a duration of 3-5 minutes to guarantee a uniform solution. The kinetic investigation started at time t = 0 s, using an excitation wavelength of 455 nm for lucigenin, while monitoring the reaction at 510 nm. Subsequently, the cuvette was placed in an atmosphere with continuous stirring, while the temperature of the chamber was adjusted to room temperature. Compounds, with a final concentration of 5 µM, were added to initiate the

kinetics of Cl^- influx after 45 seconds. Subsequently, the vesicles were disrupted to terminate the kinetic experiment at a time of 450 seconds, the vesicles were completely broken down to conclude the kinetic experiment. This was achieved by introducing 20% Triton X-100 (20 µL) into the cuvette. Subsequently, fluorescence measurements were carried out for an extra 50 seconds, reaching a total time of 500 seconds.

2.4.5.6. Measurement of EC_{50} of the potent compound (lucigenin assay) ─ The EYPC/CHOL-LUVs⊃lucigenin (pH 7.2) was prepared using the same method as described before. The fluorescence readings (Y-axis) of the lucigenin dye were normalized to a range of 0 to 100 units, with time intervals ranging from t = 50 to t = 500 s (X-axis). The transport efficiency of 1f was assessed by measuring the standardised fluorescence intensity (FI) values at t = 450 s, prior to the injection of Triton X-100. The transport activity (T) of compound **2.3i** was estimated using the previously mentioned equation, Eq.-2.1, at a given concentration. The transport activity data were graphed on the Y-axis against concentration on the X-axis and then analysed using the Hill equation to get the effective concentration (EC_{50}).

2.4.5.7. Ion transport efficacy (HPTS assay) ─ In order for preparing the sample for the HPTS test, a total of 1950 µL of a 20 mM HEPES buffer with a pH of 7.2 and containing 100 mM NaCl, together with 40 µL of the EYPC/CHOL-LUVs⊃HPTS, were put in a 3 mL fluorescence cuvette. Subsequently, the cuvette was introduced into the fluorescence spectrophotometer while being subjected to gentle agitation for a duration of 3 to 5 minutes, in order to guarantee the formation of a uniform solution. The fluorescence emission of HPTS was quantified at a wavelength of 506 nm, with excitation occurring at 455 nm, at the start of the kinetic experiment (t = 0 s). Subsequently, the cuvette was kept in a condition of agitation while the chamber temperature was adjusted to 25 ºC. The chemical, consisting of 10 µL of a 10 µM DMSO stock solution, was added after 45 seconds to initiate the kinetics of Cl^- influx. The vesicles were disrupted by introducing 20% Triton X-100 (20 µL) into the cuvette at t = 450 s, so concluding the kinetic experiment. Fluorescence experiments were then performed for an additional 50 s (t = 500 s).

2.4.5.8. Anion and cation selectivity experiments ─ The same process described before was applied for making the vesicles. The experiment used a 100 mM solution of NaX salt (where

X represents Cl^-, Br^-, I^-, NO_3^-, ClO_4^-, and SCN^-) as an external buffer. At the initial time of t = 0 seconds, the suspension was kept in a condition of gentle stirring using a magnetic stirrer in a fluorescence system. Fluorescence intensity of lucigenin was seen to decrease in time at a wavelength of 510 nm (excitation wavelength of 450 nm), indicating quenching. The incorporation of transporter 1f at time t = 45 seconds. In order to completely eliminate the Cl− gradient that was established, the vesicles were disrupted by adding 20% Triton X-100 (20 µL) at t = 450 s. The time-dependent measurements were turned into a percentage change in fluorescence intensity using equation 2.2.

For the cation selectivity the vesicles formed using the same procedure as described before. A fresh and dry fluorescence cuvette was used to hold a solution consisting of 20 mM HEPES buffer and 100 mM MCl (where M may be Li^+, Na^+, K^+, Rb^+, and Cs^+) in a volume of 1950 µL. Additionally, 40 µL of EYPC/CHOL-LUVs⊃lucigenin was added to the solution.

2.4.5.9. Supporting evidence for the Cl^- Transport pathways:

2.4.5.9.1. Ion transport efficacy in the presence of FCCP ─ The ion transport capability was assessed both with and without FCCP, a selective transporter for H^+ ions. A total of 1950 µL of 20 mM HEPES buffer, pH 7.2, containing 100 mM NaCl, together with 40 µL of the EYPC/CHOL-LUV⊃HPTS, were added to a 3 mL fluorescent cuvette. Subsequently, the cuvette was inserted into the fluorescence apparatus and agitated for a duration of 3 minutes. At time t = 45 s, the solution was supplemented with 8 µL of compound **2.3i** from the stock solution in DMSO, as well as 2 µL of FCCP solution in DMSO at a concentration of 2.5 µM. After a duration of 45 seconds, compound **2.3i** (at its final concentration) was added to the cuvette in order to initiate the kinetics of Cl^- transfer. The kinetic experiment was terminated at 450 seconds by introducing 20 µL of a 20% Triton-X100 solution into the cuvette to disrupt the vesicular structures. Subsequently, fluorescence measurements were conducted for an additional 45 seconds, reaching a total time of 500 seconds (t = 500 s). The control experiment was also done without FCCP.

2.4.5.9.2. Ion transport efficacy in the presence of Valinomycin ─ The vesicles were prepared using the exact same procedure outlined in the previous section. The ion transport activity was assessed both in the absence and presence of valinomycin. 1950 µL of 20 mM HEPES buffer, pH 7.2, including 100 mM KCl, and 40 µL of the EYPC/CHOL-LUVs⊃HPTS

were added to a 3 mL fluorescent cuvette. Subsequently, the cuvette was inserted into the fluorescence apparatus and agitated for a duration of 3 minutes. The fluorescence intensity of HPTS was then quantified at 510 nm (λ_{ex} = 450 nm) at time t = 0 s. The compound, consisting of 8 µL of the stock solution in DMSO, and 2 µL of valinomycin solution in DMSO at a concentration of 10 nM, were given to the mixture at t = 45 s to initiate the Cl^- transport kinetics. The kinetic experiment was halted after 450 seconds by introducing 20 µL of a 20% Triton-X100 solution into the cuvette to disrupt the vesicular configurations. Subsequently, fluorescence experiments went on for an additional 50 seconds (t = 500 s). The control study was also conducted without the presence of valinomycin.

2.4.5.10. Evidence for carrier mechanism:

2.4.5.10.1. Transport activity measured using the DPPC-lucigenin assay─ The transport activity was assessed using a fluorescence assay in the DPPC-LUV ⊃lucigenin experiment. A total of 1950 microliters of HEPES buffer with a concentration of 20 mM and a pH of 7.2, including 100 mM of NaCl, along with 40 µL of DPPC-LUV⊃lucigenin, were added to a 3 mL fluorescence cuvette for this experiment. The kinetic experiment started at time t = 0 s, and the emission of lucigenin fluorescence was quantified at a wavelength of 506 nm, with excitation occurring at 455 nm. Subsequently, the cuvette was constant stirred at room temperature. After 45 seconds, the drug (10 mL of DMSO stock solution) was added to initiate the kinetics of chloride ion influx. At t = 450 s, the vesicles were ruptured by introducing 20 µL of 20% Triton X-100 into the cuvette. Fluorescence measurements were then carried out for a further 50 s, starting at t = 500 s. Similar experiment was conducted to test the efficiency of transportation at a temperature of 45 ºC. To determine the half-life and initial rate at various temperatures, the time-dependent lucigenin fluorescence plot was analysed using a first-order exponential decay equation.

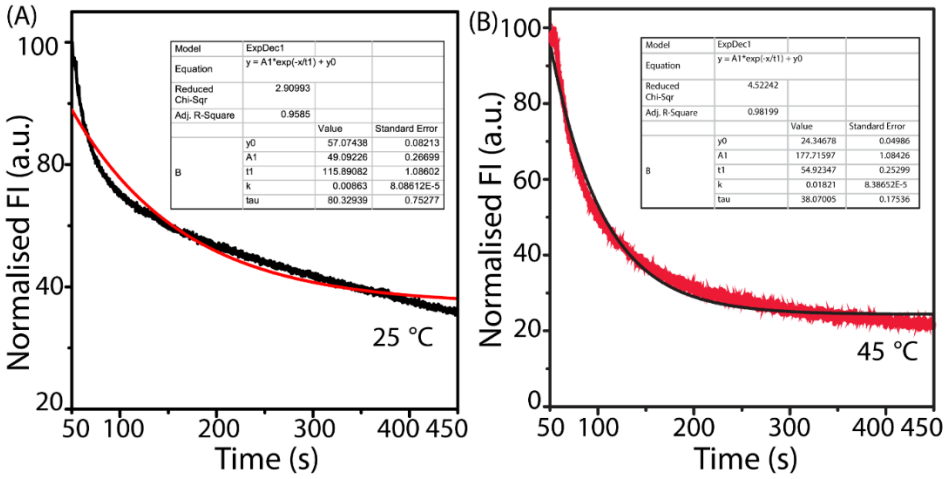

Figure 2.12. Standardized fluorescence quenching curves (F/F_0) were fitted to an exponential decay 1 equation.

2.4.5.10.2. U-tube assay ─ To verify the specific mechanism by which Cl^- ions are transported by **2.3i**, the conventional U-tube experiment was conducted. The experiment included using a 20 mL $CHCl_3$ solution in a U-tube to simulate a lipid bilayer. The solution contained 20 µM of **2.3i** and 2 mM tetrabutylammoniumhexafluorophosphate. The left side of the source end was filled with 10 mL of a NaCl solution with a concentration of 300 mM, which was buffered to pH 7.2 using 5 mM sodium phosphate salts. The right side of the receiver end was filled with 10 mL of a $NaNO_3$ solution with a concentration of 300 mM, also buffered to pH 7.2 using 5 mM sodium phosphate salts. The organic phase was agitated gently using a magnetic stirrer, while the concentration of Cl^- ions was periodically measured over a span of 72 hours using a chloride ion-selective electrode.

2.4.5.11. Carboxyfluorescein (CF) leakage test — In a fresh and dry fluorescence cuvette, 40 µL of the above-mentioned lipid solution and 1950 µL of 20 mM HEPES buffer (100 mM NaCl, pH 7.2) were mixed slowly by a magnetic stirrer fitted through the fluorescence apparatus (at t = 0 s). The temporal path of CF fluorescence emission intensity, F_t, was recorded at λ_{em} = 517 nm (λ_{ex} = 492). The transporter was given at t = 50 s, and lastly, at t = 450 s, 20 µL of 20% Triton X-100 was added to lyse those vesicles for 100% Cl^- influx. Fluorescence intensities (F_t) were standardized to fractional emission intensity (IF) using Eq. 2.2. This investigation demonstrated that neither the bilayer membranes damaged nor large transmembrane pores were generated by **2.3i.**

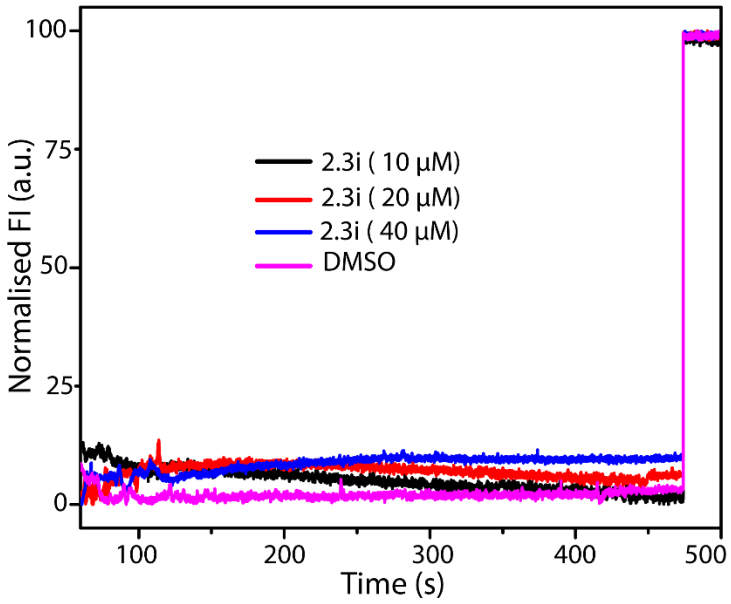

Figure 2.13. The carboxyfluorescein leakage assay of **2.3i** across EYPC/CHOL-LUVs⊃CF

2.4.6. NMR spectra of synthesized compounds:

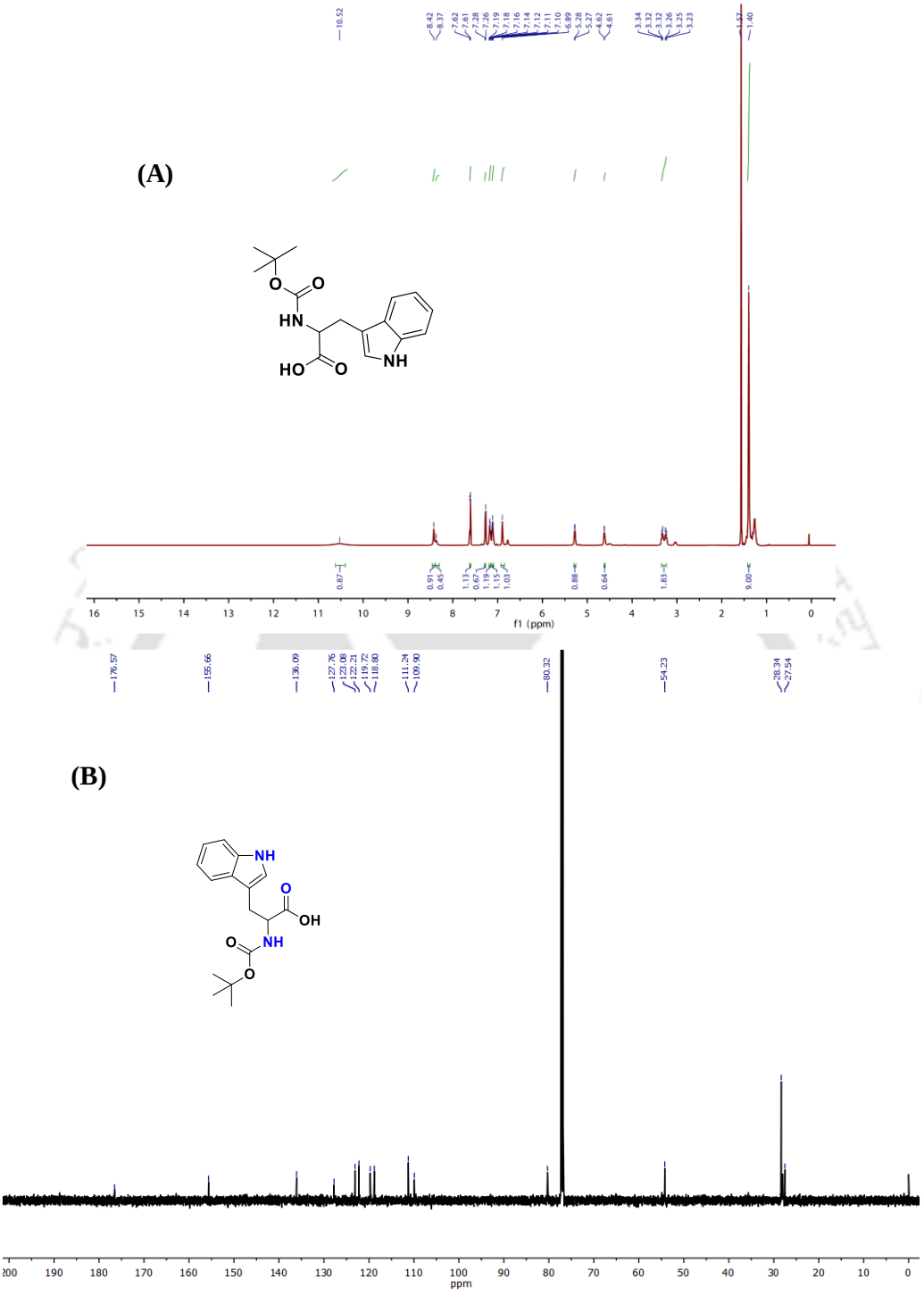

Figure 2.14. ^{1}H NMR (A) and ^{13}C NMR (B) spectra of compound (tert-butoxycarbonyl) tryptophan in $CDCl_3$ solvent.

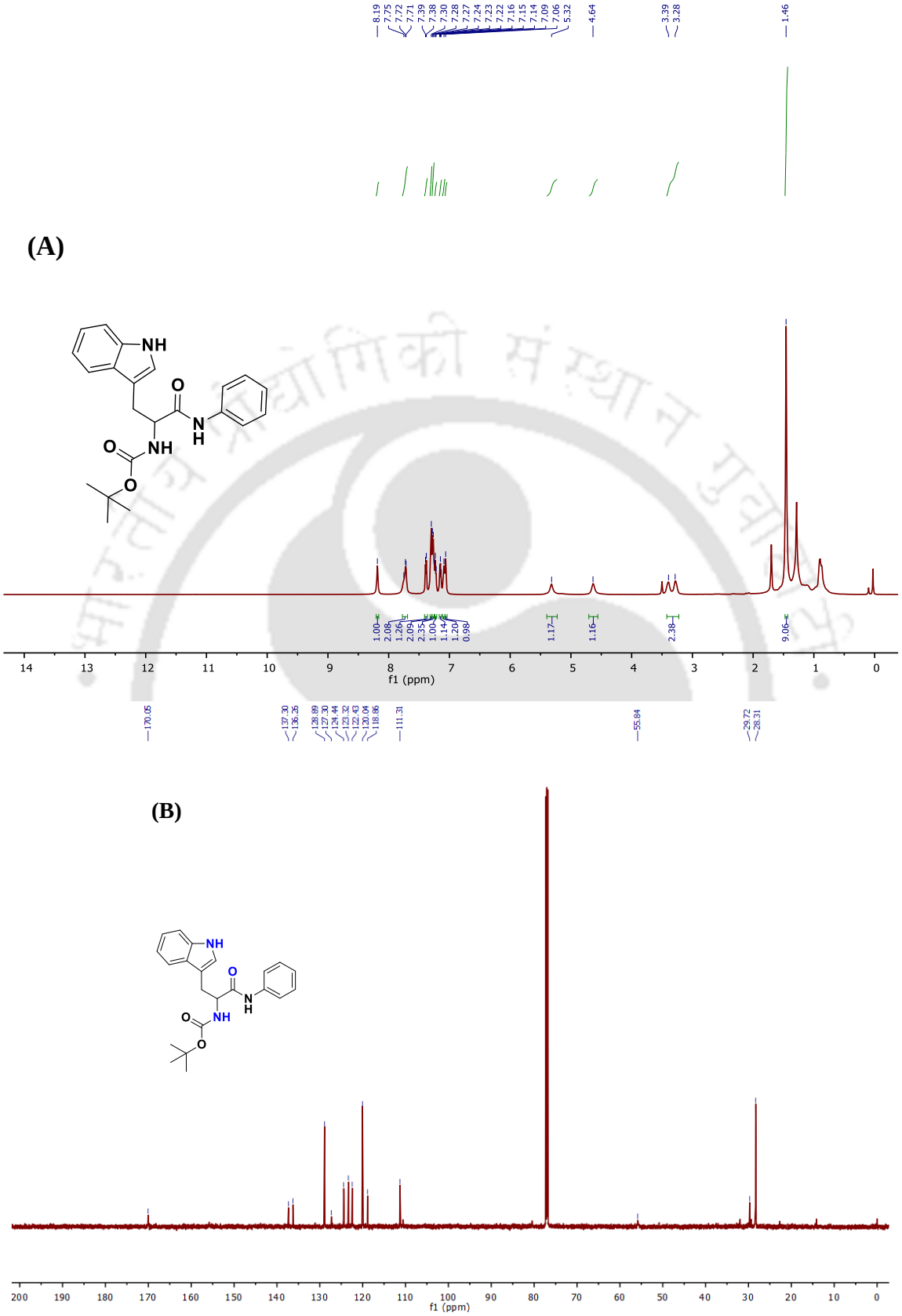

Figure 2.15. ^{1}H NMR (A) and ^{13}C NMR (B) spectra of compound **2.1a** in $CDCl_3$ solvent.

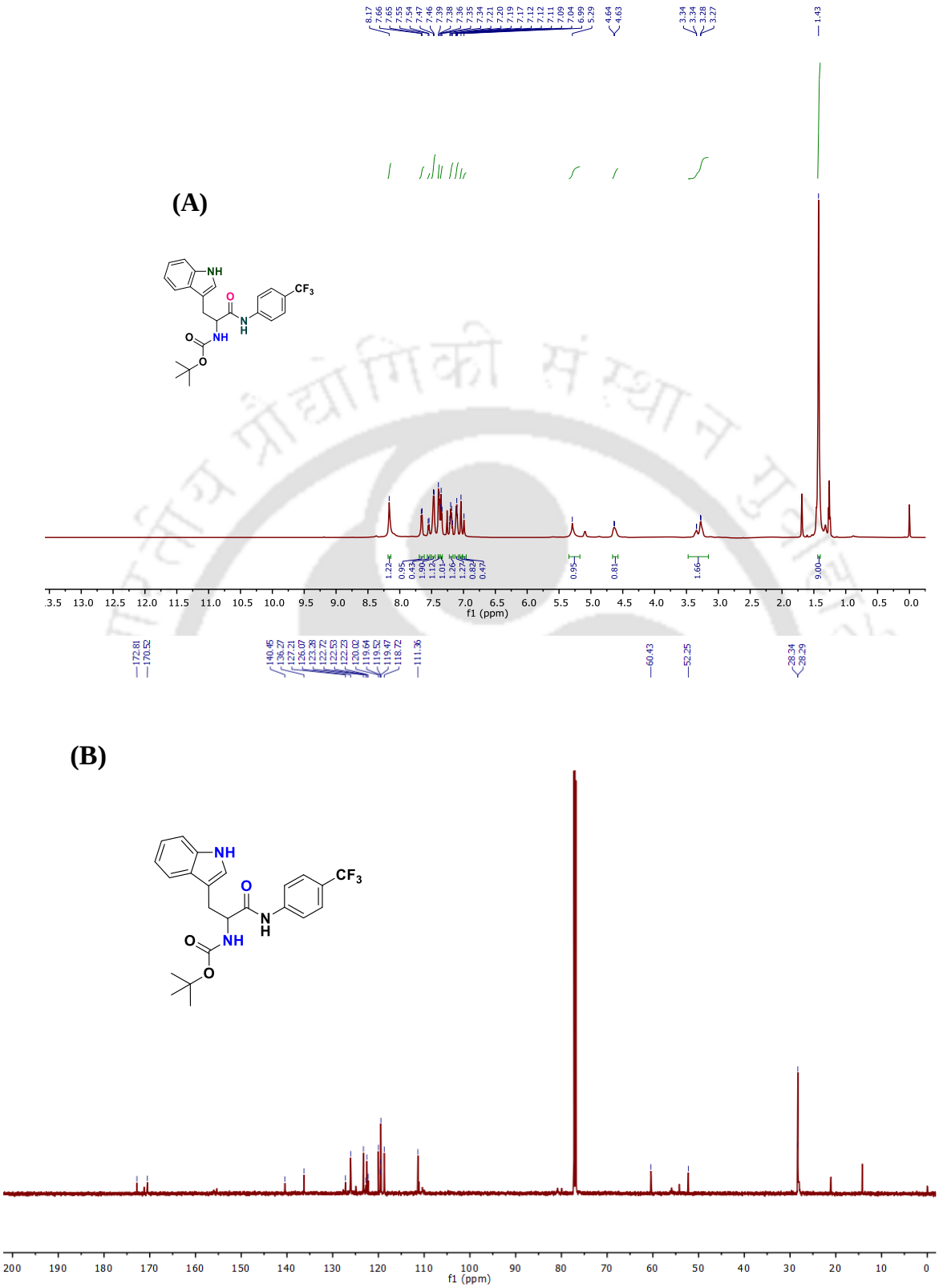

Figure 2.16. ^{1}H NMR (A) and ^{13}C NMR (B) spectra of compound **2.1b** in $CDCl_3$ solvent.

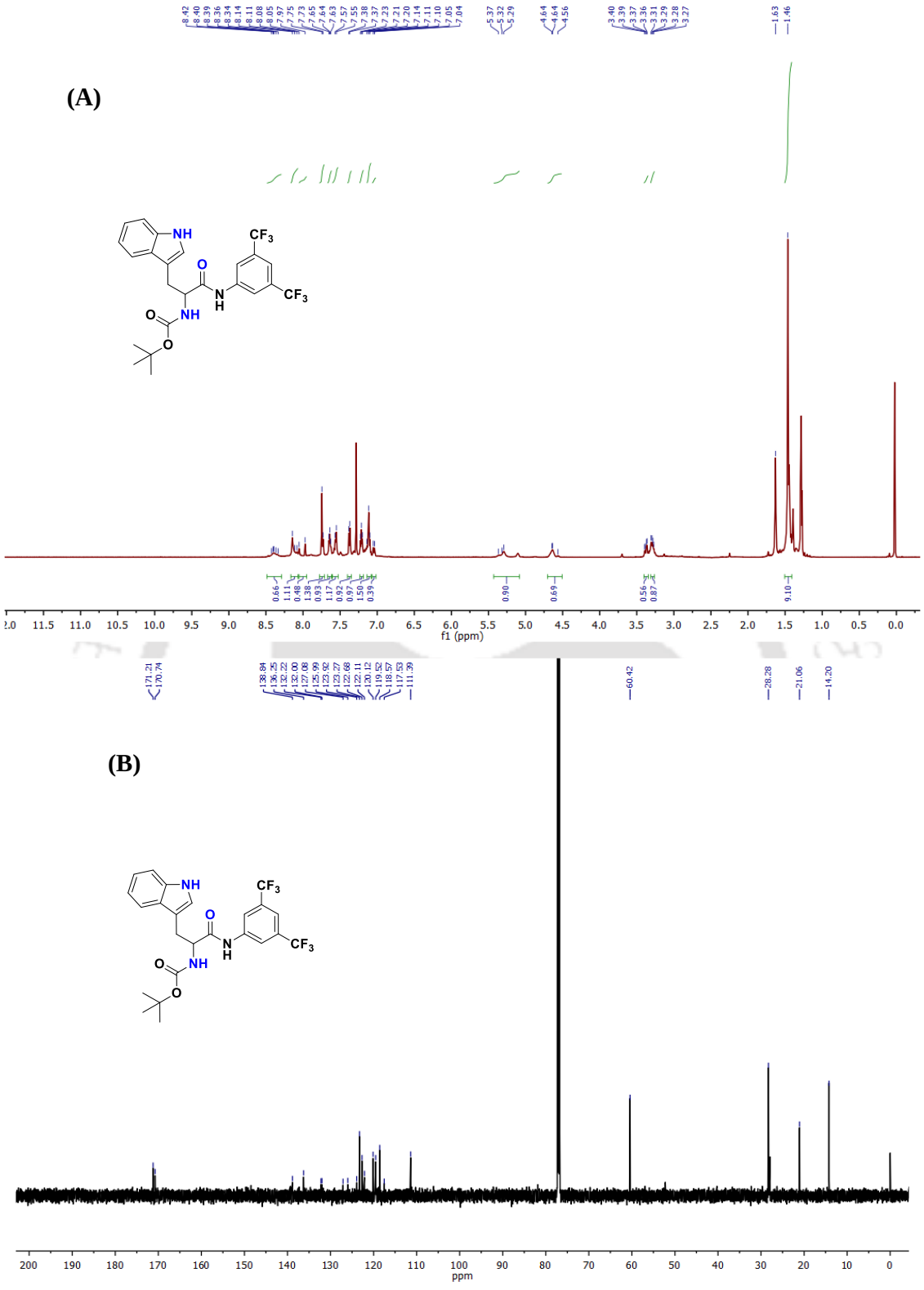

Figure 2.17. ^{1}H NMR (A) and ^{13}C NMR (B) spectra of compound **2.1c** in $CDCl_3$ solvent.

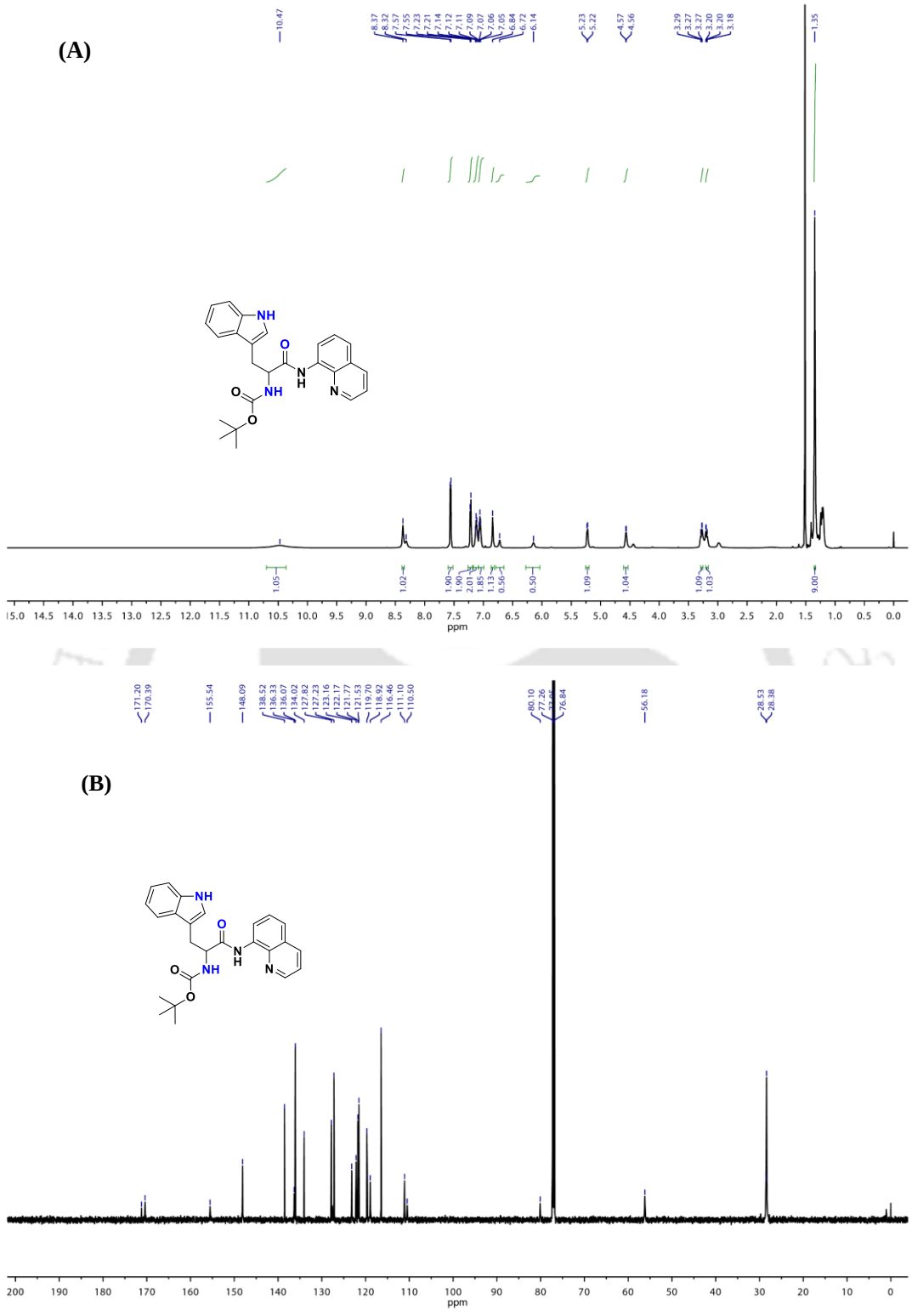

Figure 2.18. ^{1}H NMR (A) and ^{13}C NMR (B) spectra of compound **2.1d** in $CDCl_3$ solvent.

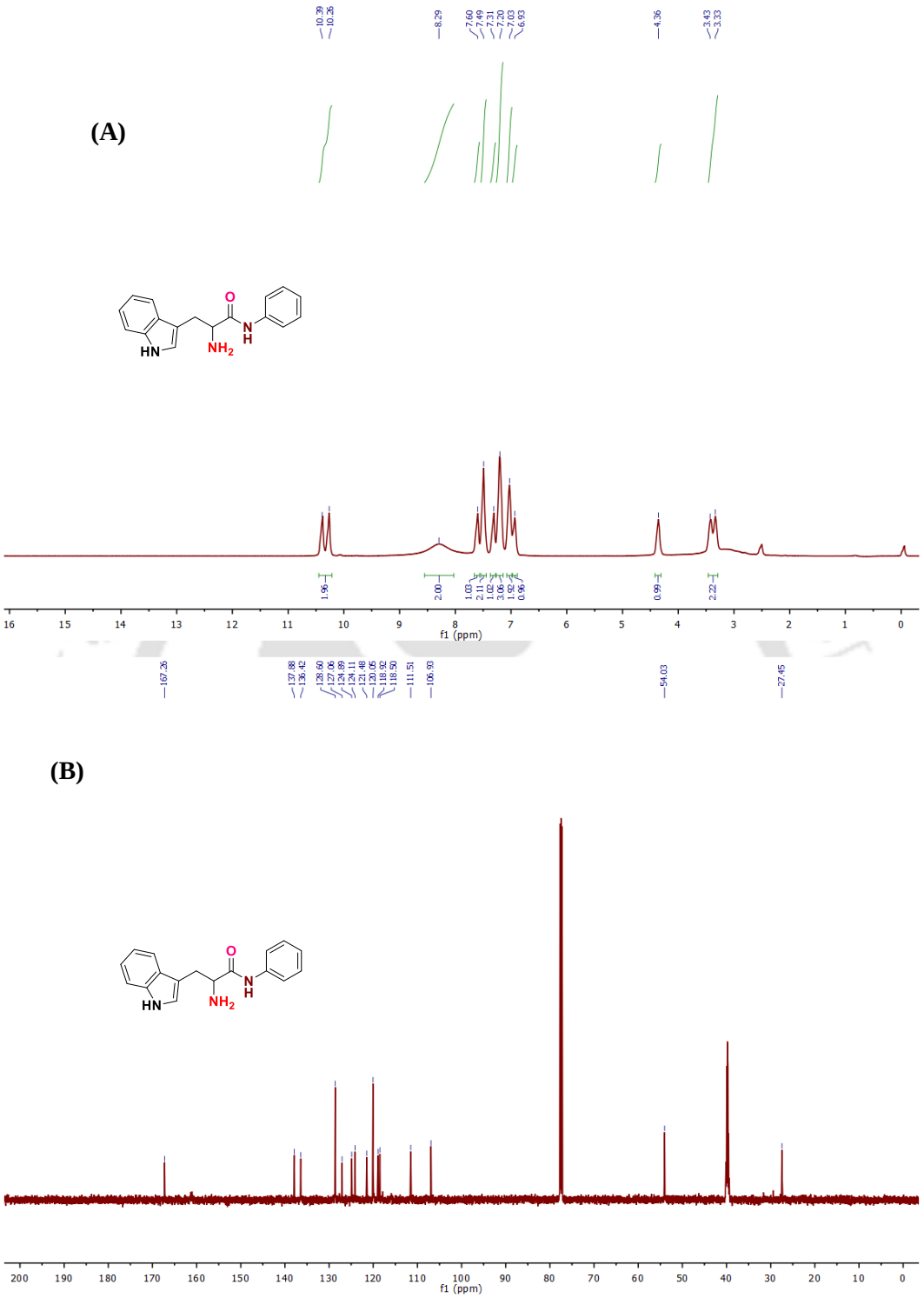

Figure 2.19. ^{1}H NMR (A) and ^{13}C NMR (B) spectra of compound **2.2a** in $CDCl_3$ + DMSO-d_6 solvent mixture.

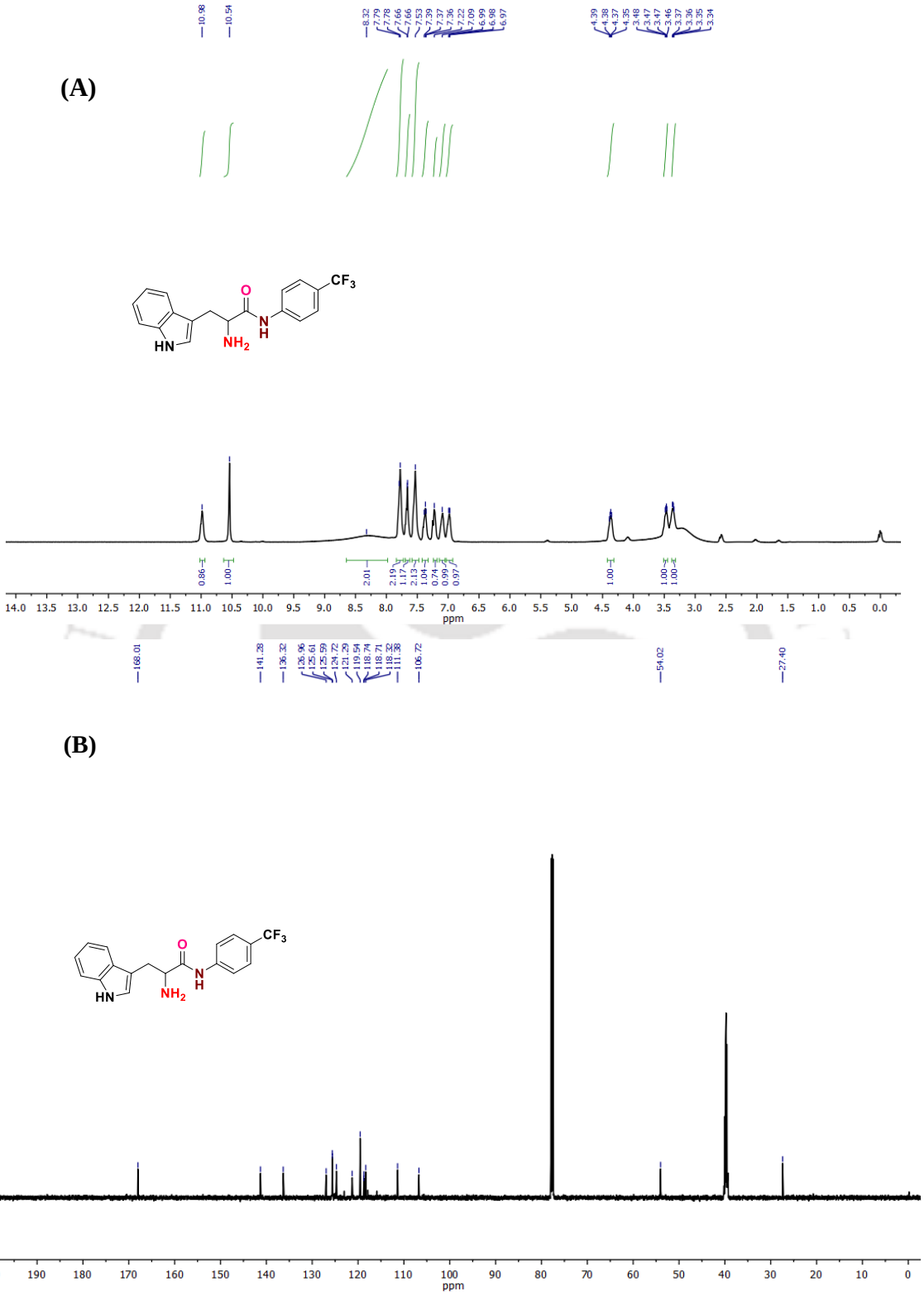

Figure 2.20. ^{1}H NMR (A) and ^{13}C NMR (B) spectra of compound **2.2b** in $CDCl_3$ + DMSO-d_6 solvent mixture.

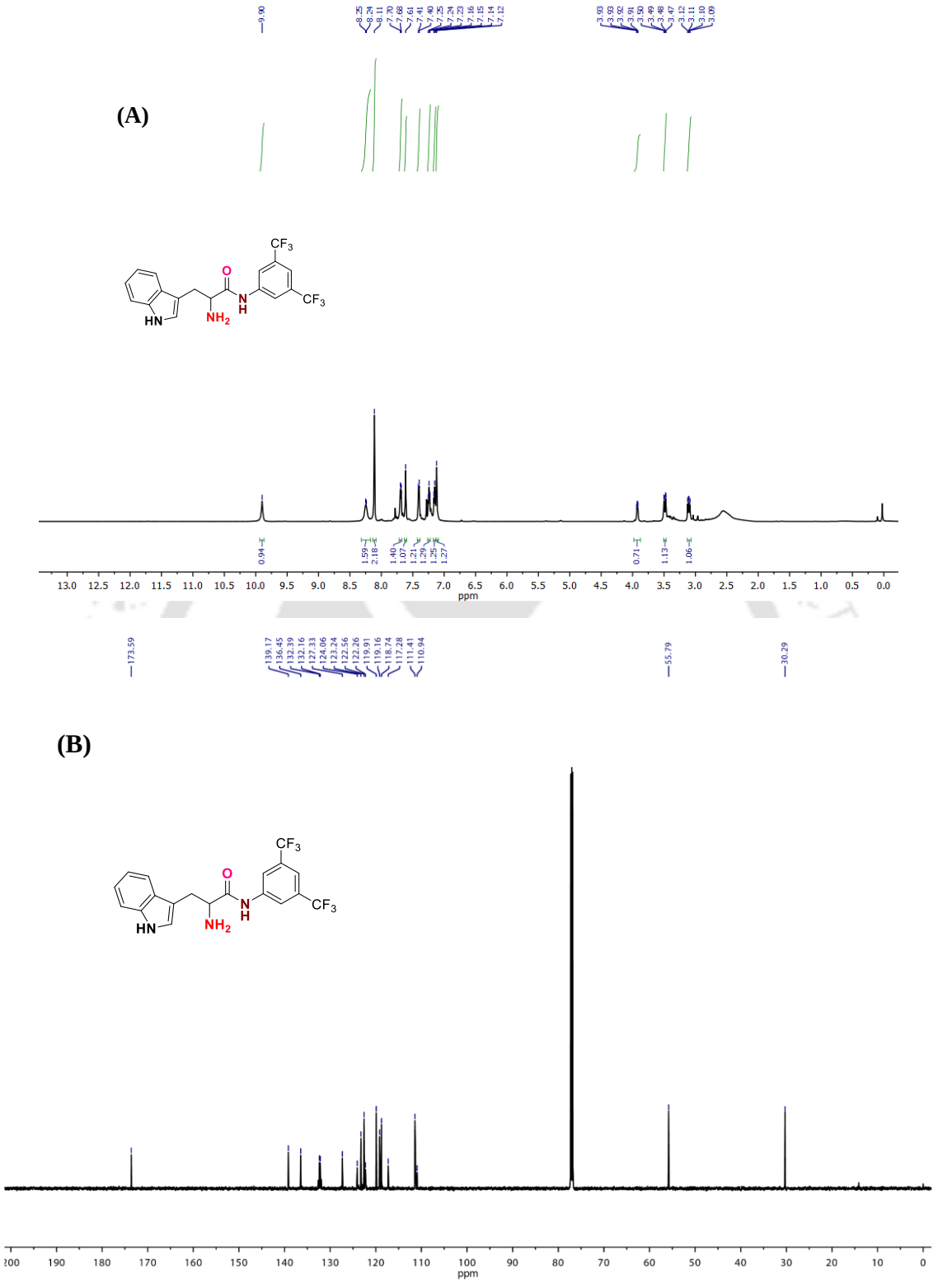

Figure 2.21. ^{1}H NMR (A) and ^{13}C NMR (B) spectra of compound **2.2c** in $CDCl_3$ solvent.

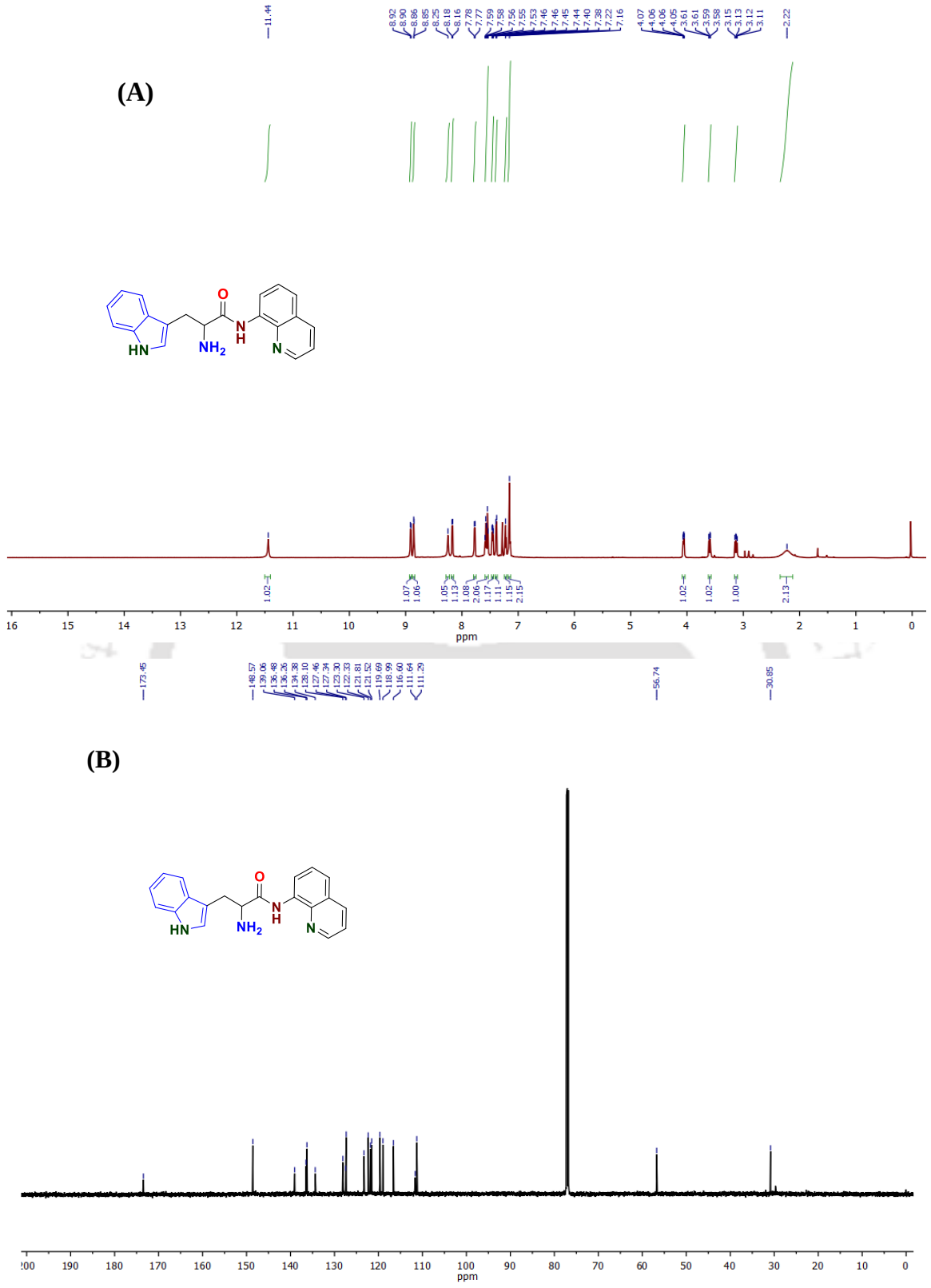

Figure 2.22. ^{1}H NMR (A) and ^{13}C NMR (B) spectra of compound **2.2d** in $CDCl_3$ solvent.

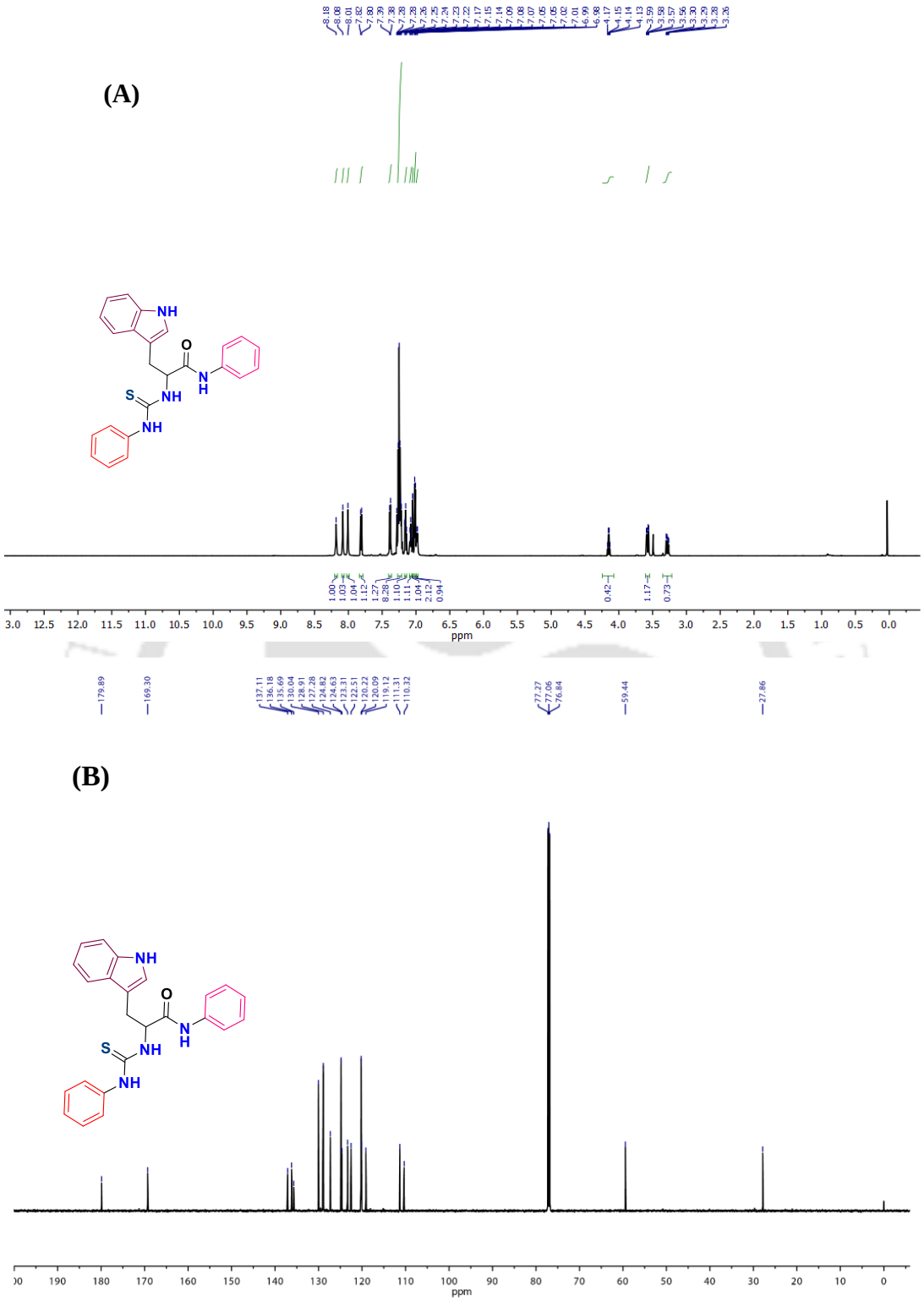

Figure 2.23. ^{1}H NMR (A) and ^{13}C NMR (B) spectra of compound **2.3a** in $CDCl_3$ solvent.

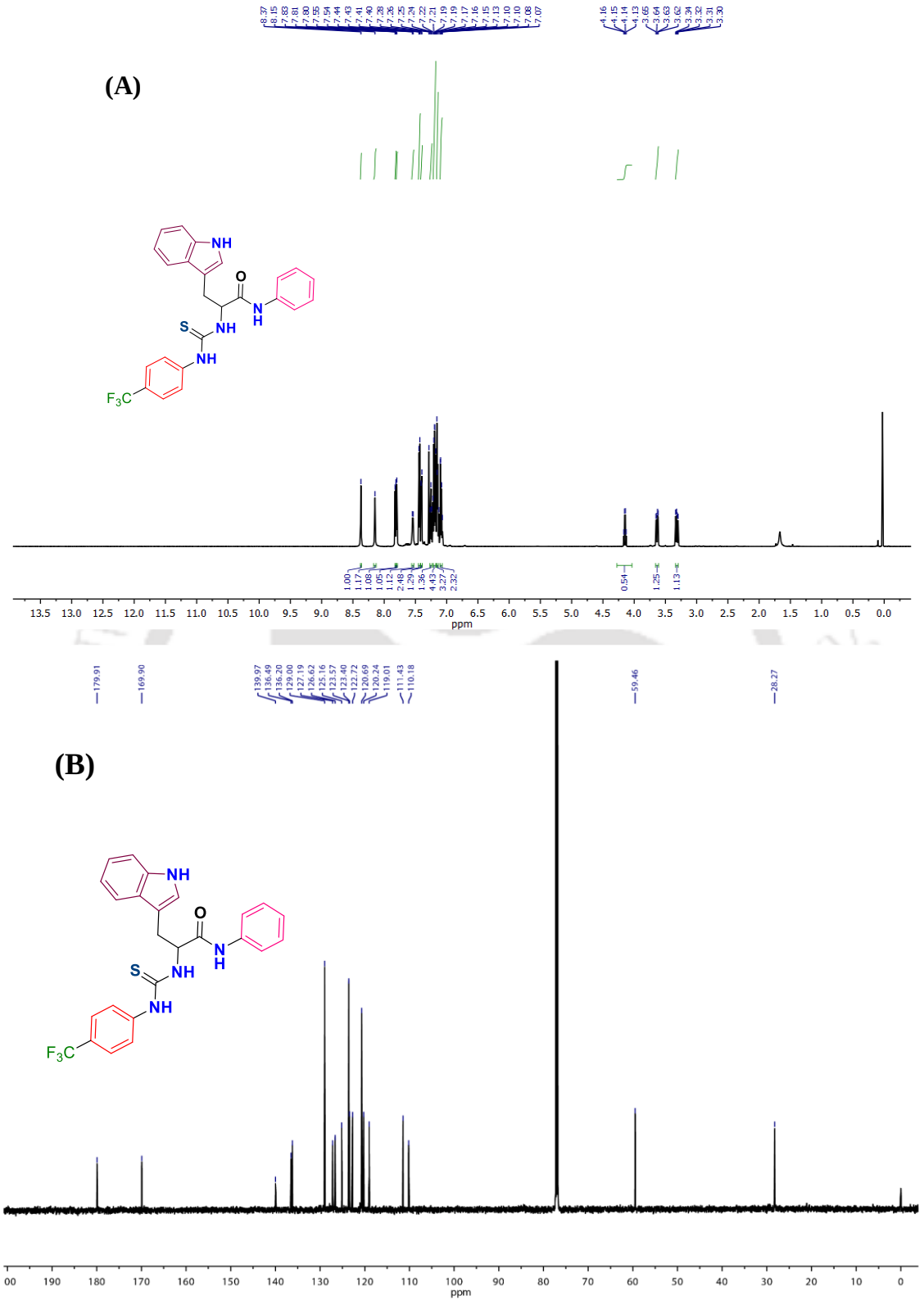

Figure 2.24. ^{1}H NMR (A) and ^{13}C NMR (B) spectra of compound **2.3b** in $CDCl_3$ solvent.

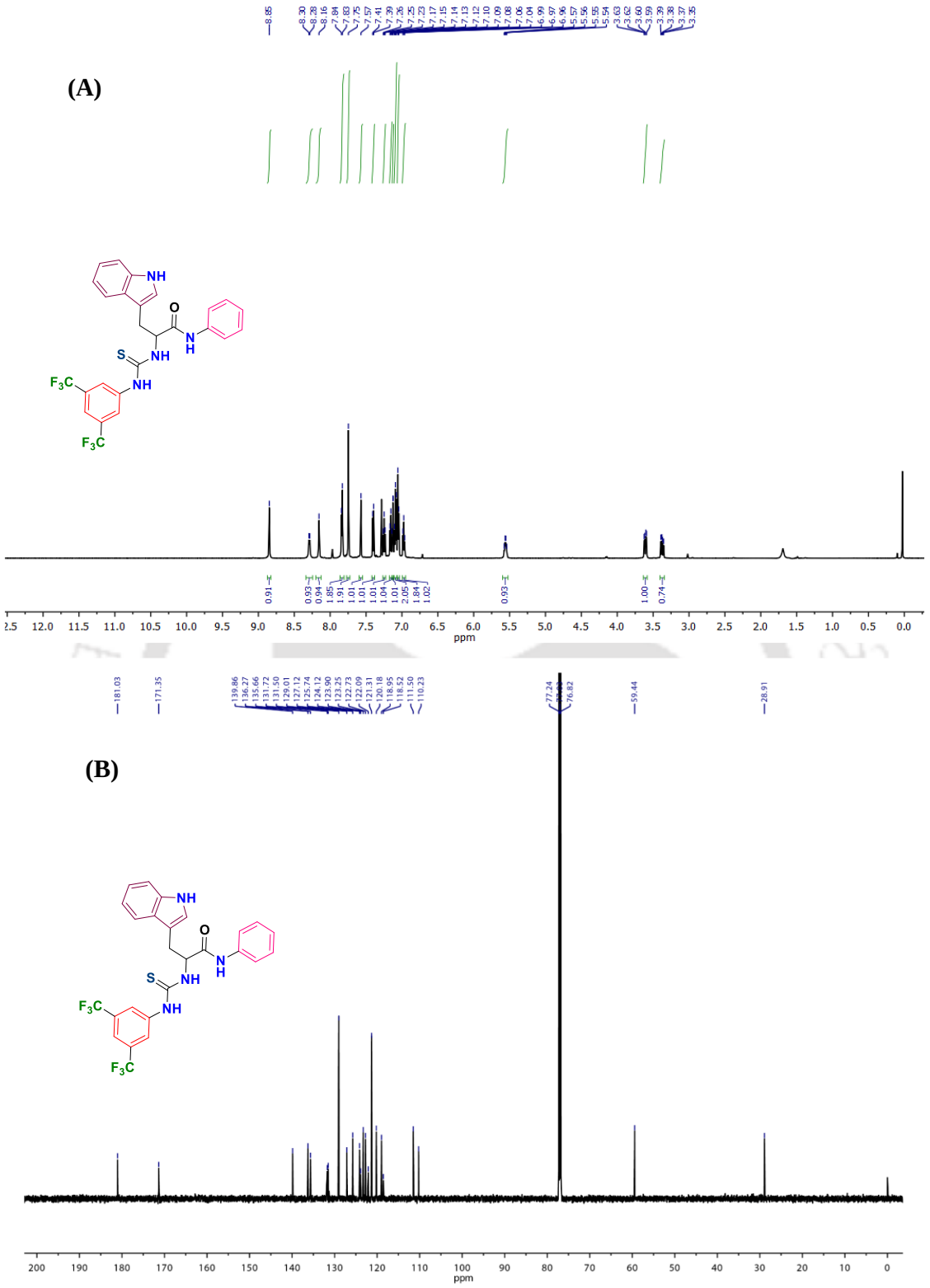

Figure 2.25. ^{1}H NMR (A) and ^{13}C NMR (B) spectra of compound **2.3c** in $CDCl_3$ solvent.

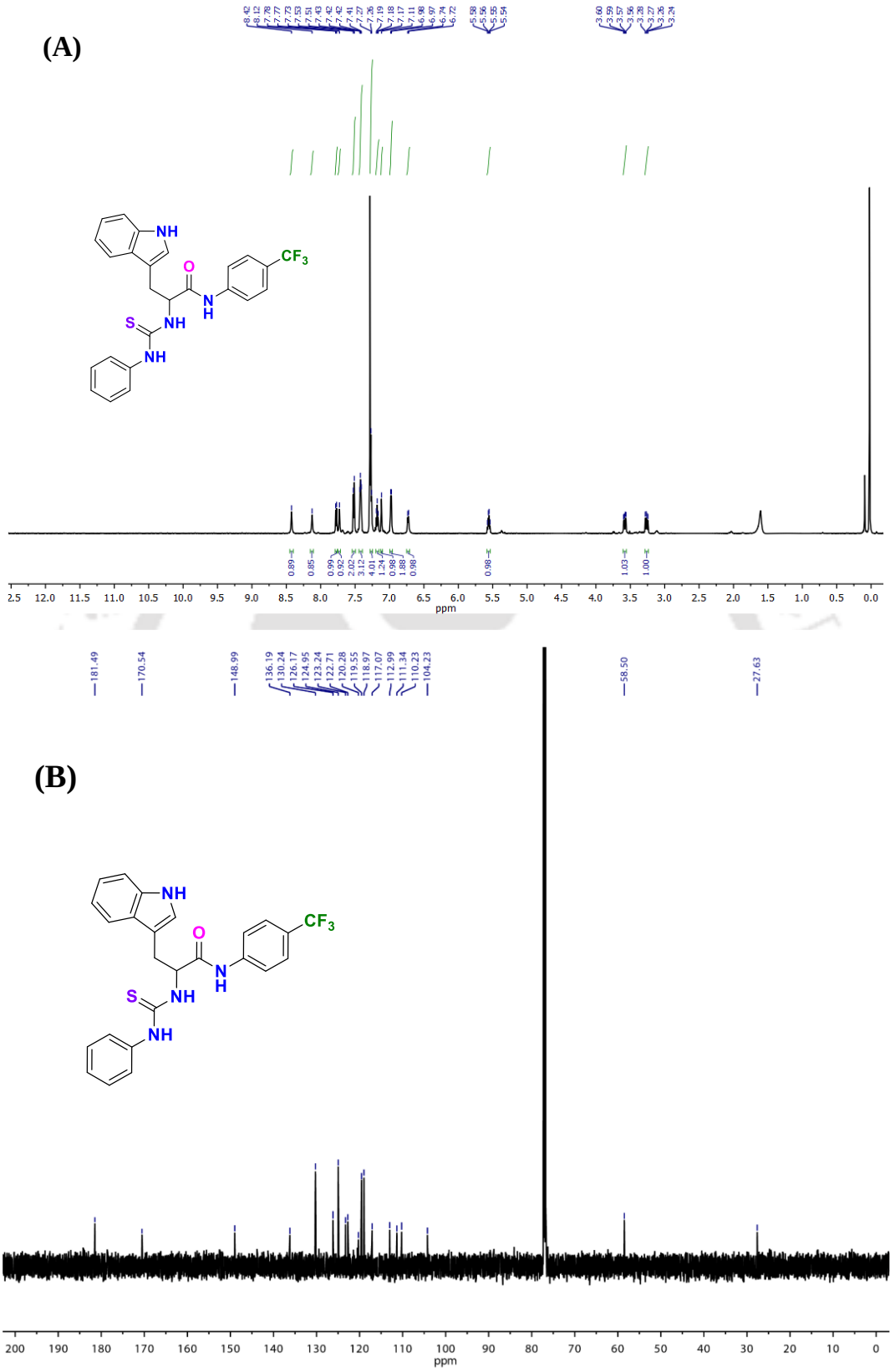

Figure 2.26. ^{1}H NMR (A) and ^{13}C NMR (B) spectra of compound **2.3d** in $CDCl_3$ solvent.

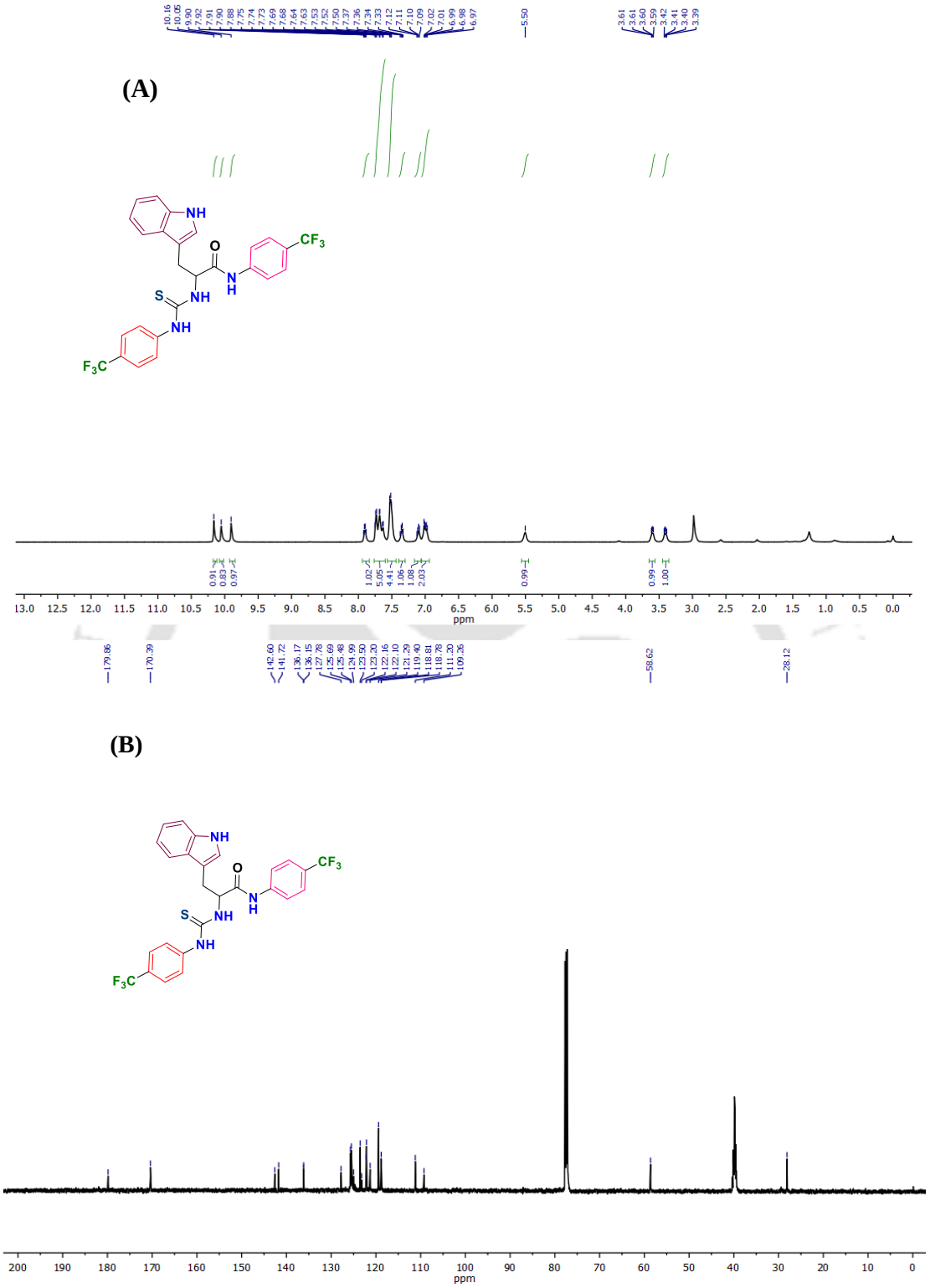

Figure 2.27. ^{1}H NMR (A) and ^{13}C NMR (B) spectra of compound **2.3e** in $CDCl_3$ + DMSO-d_6 solvent.

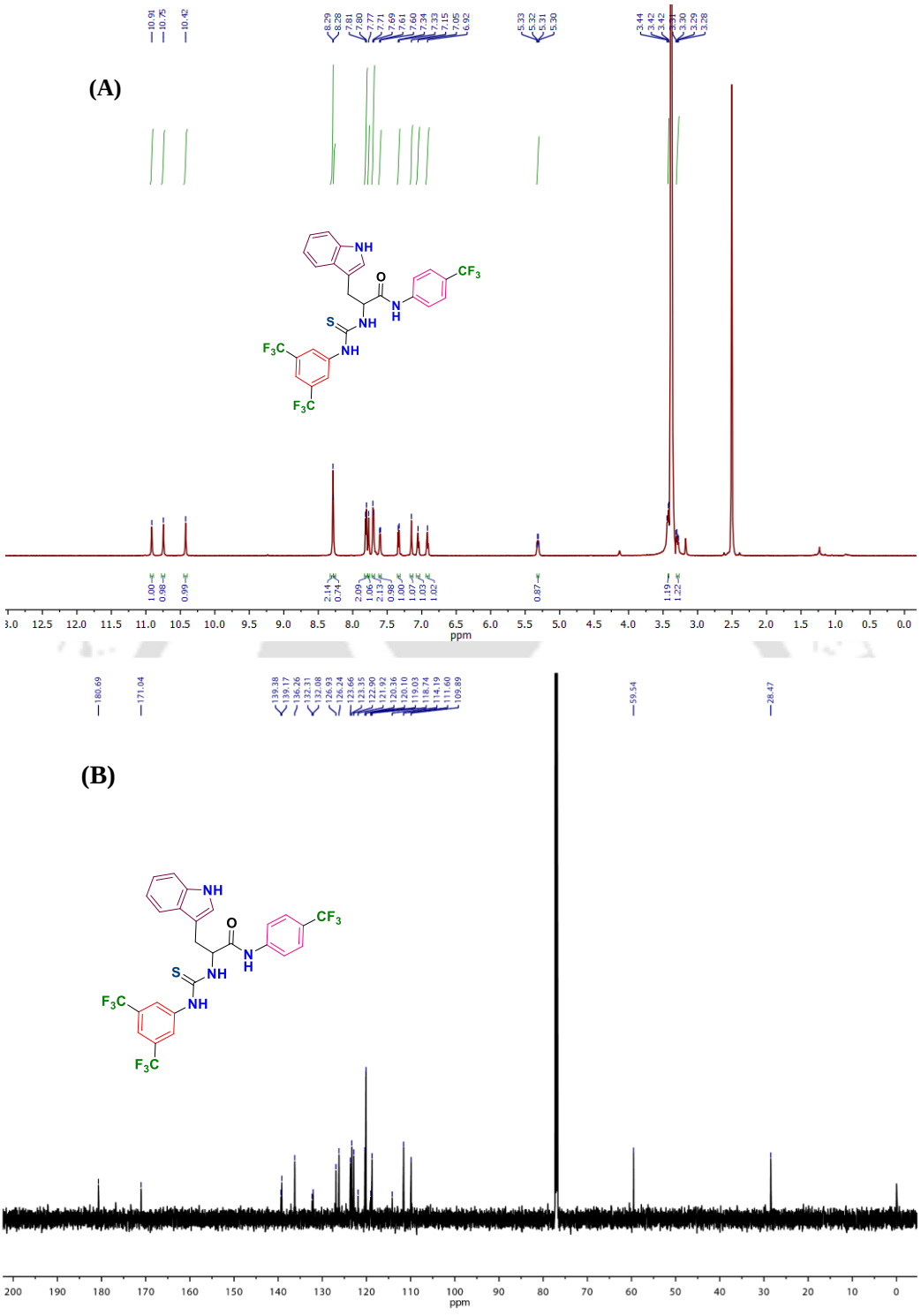

Figure 2.28. ^{1}H NMR in DMSO-d_6 solvent (A), and ^{13}C NMR spectra of compound **2.3f** in $CDCl_3$ solvent (B).

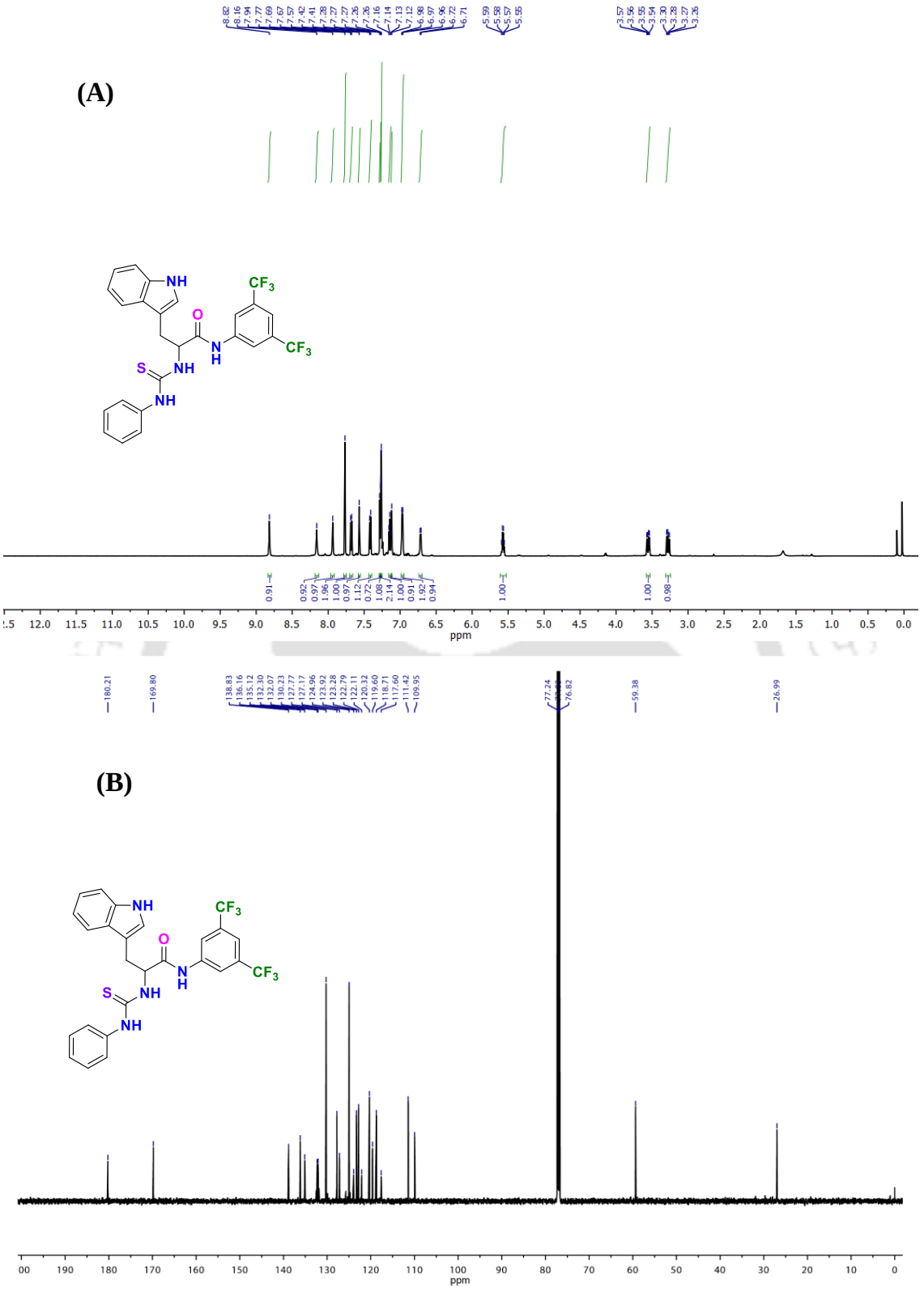

Figure 2.29. ^{1}H NMR (A) and ^{13}C NMR (B) spectra of compound **2.3g** in $CDCl_3$ solvent.

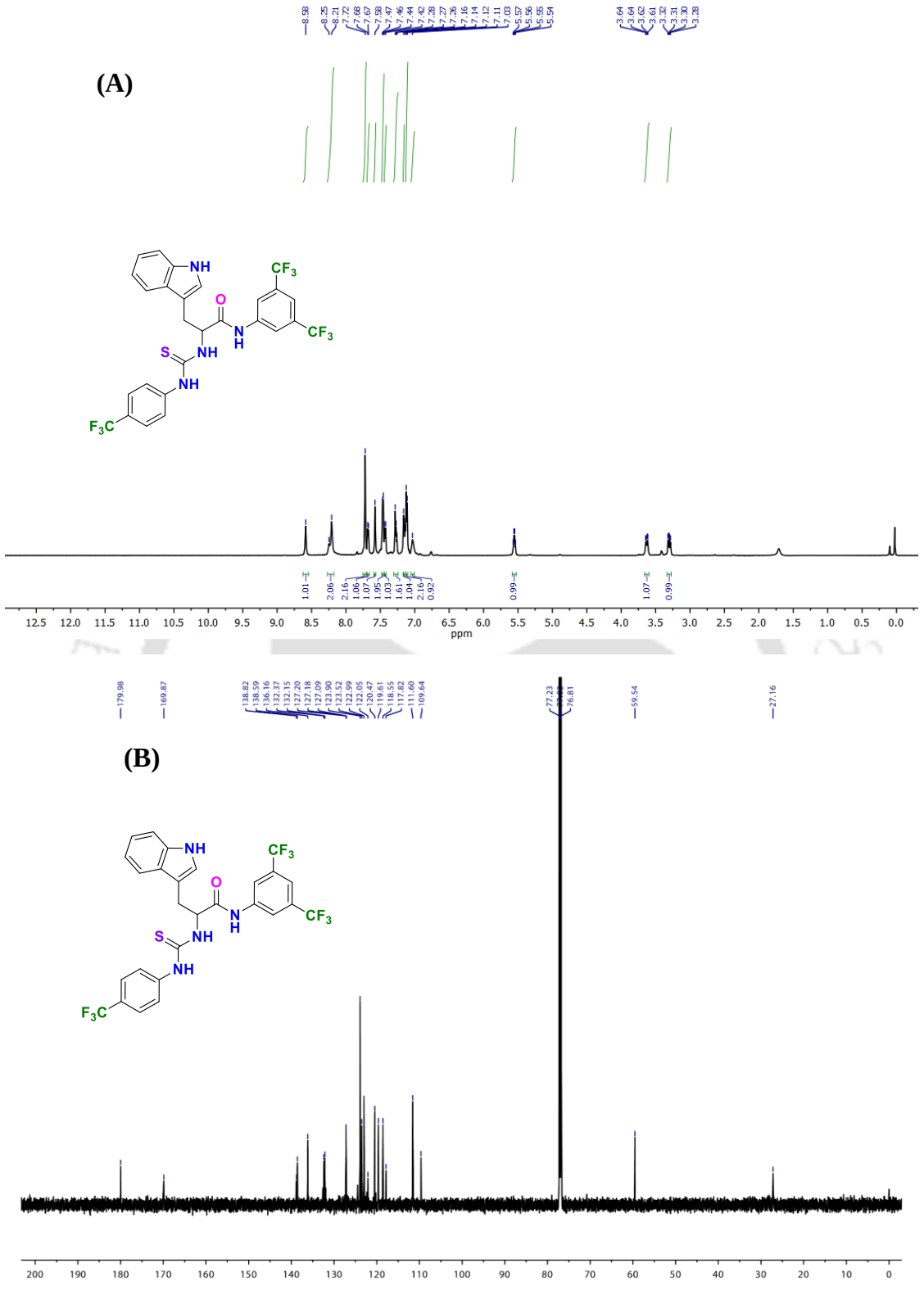

Figure 2.30. ^{1}H NMR (A) and ^{13}C NMR (B) spectra of compound **2.3h** in $CDCl_3$ solvent.

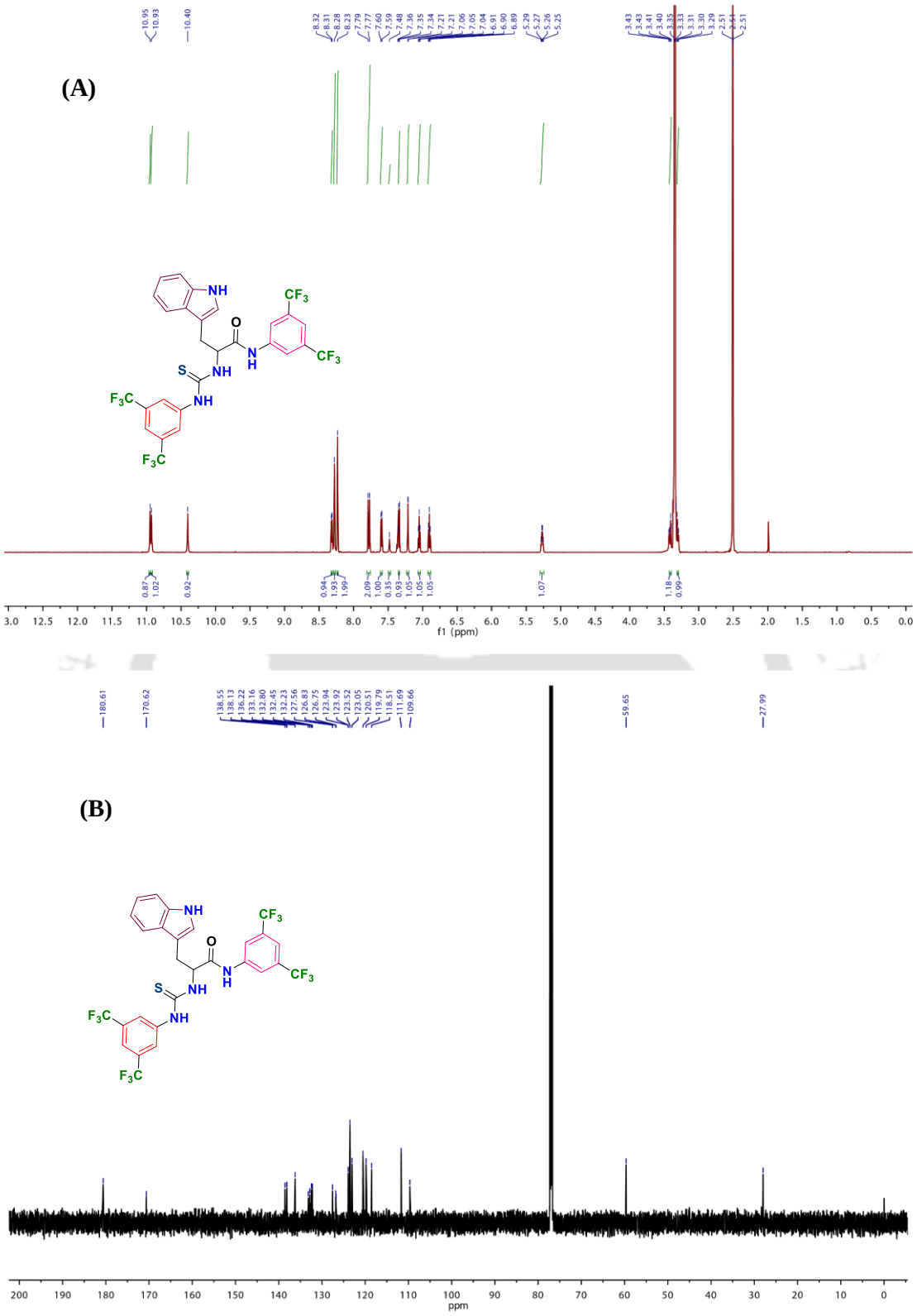

Figure 2.31. ^{1}H NMR (A) and ^{13}C NMR (B) spectra of compound **2.3i** in $CDCl_3$ solvent.

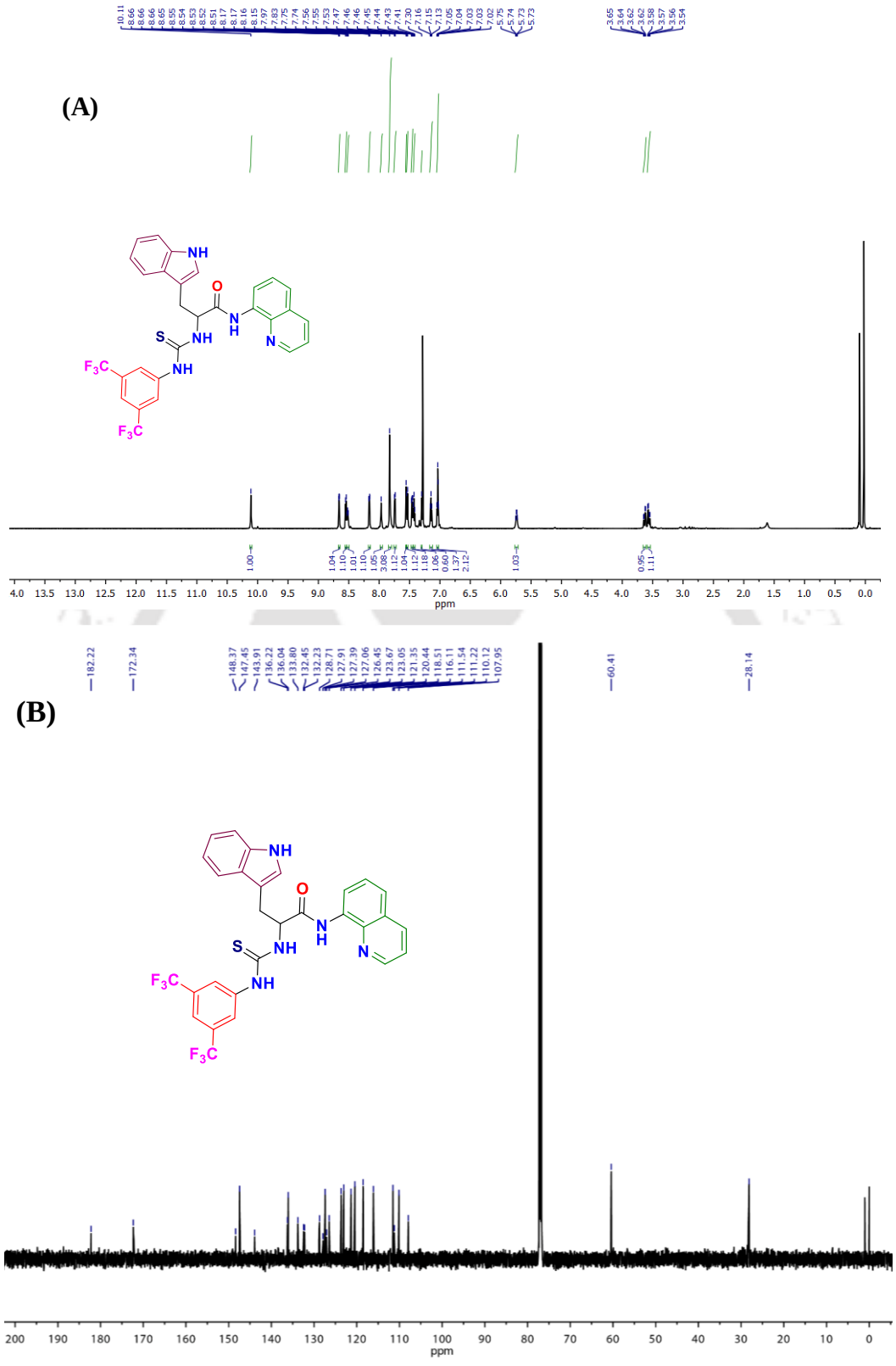

Figure 2.32. ^{1}H NMR (A) and ^{13}C NMR (B) spectra of compound **2.4** in $CDCl_3$ solvent.

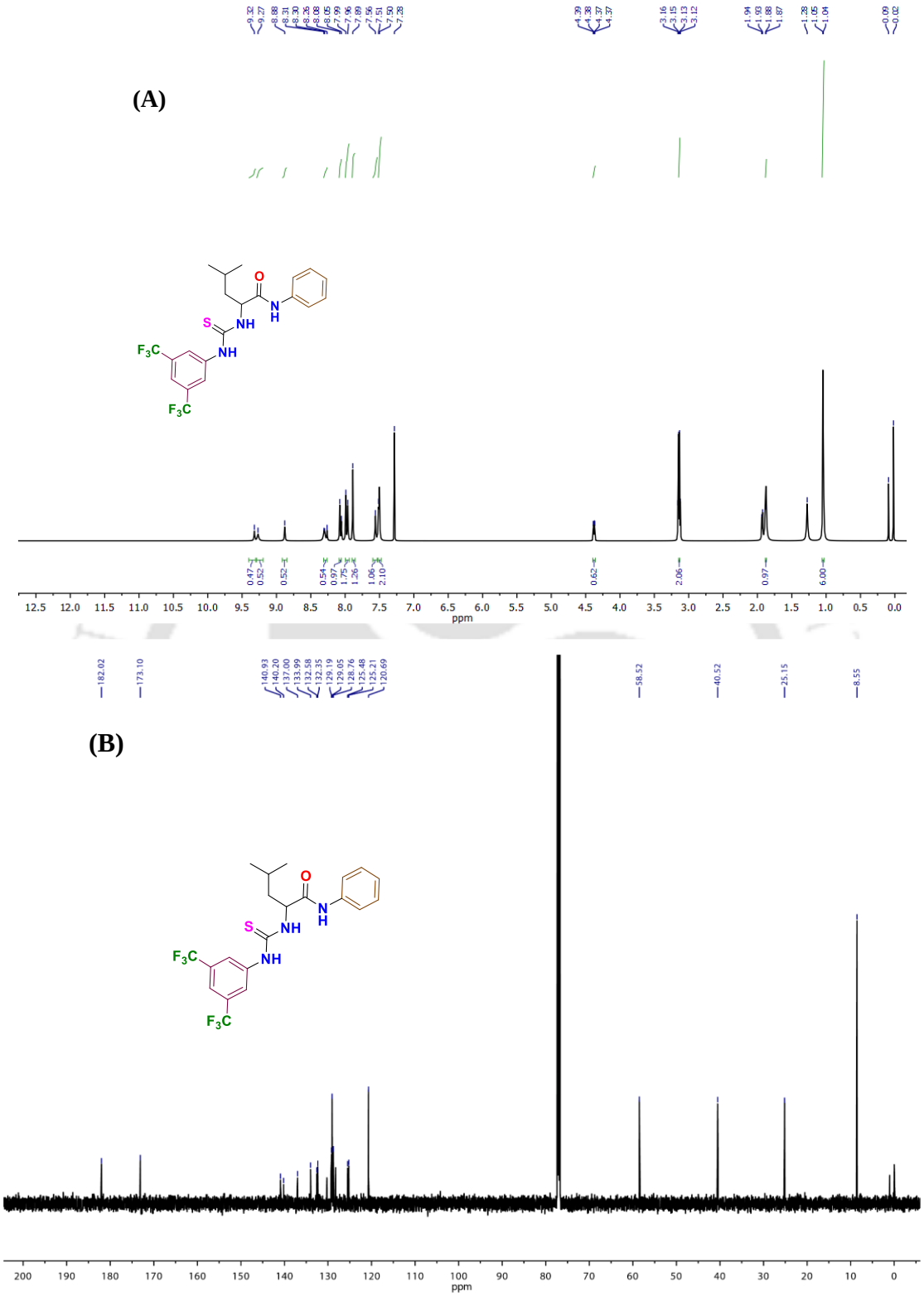

Figure 2.33. ^{1}H NMR (A) and ^{13}C NMR (B) spectra of compound **2.5a** in $CDCl_3$ solvent.

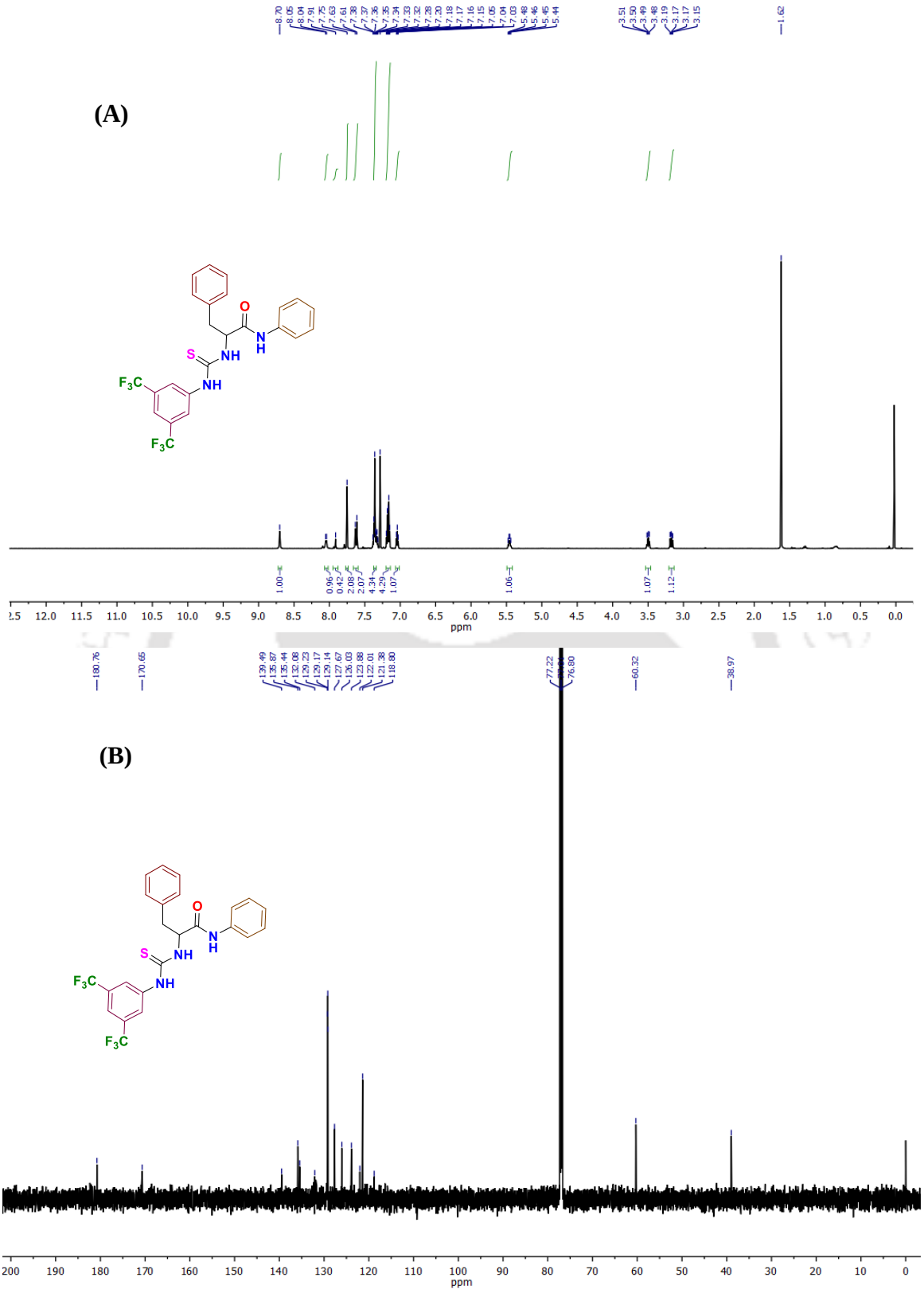

Figure 2.34. ^{1}H NMR (A) and ^{13}C NMR (B) spectra of compound **2.5b** in $CDCl_3$ solvent.

2.5. References

1. Gamper, N.; Shapiro, M. S., Regulation of ion transport proteins by membrane phosphoinositides. *Nat. Rev. Neurosci.* **2007,** *8* (12), 921-934.
2. Diamond, J. M.; Wright, E. M., Biological membranes: the physical basis of ion and nonelectrolyte selectivity. *Annu. Rev. Physiol.* **1969,** *31* (1), 581-646.
3. Song, L.; Hobaugh, M. R.; Shustak, C.; Cheley, S.; Bayley, H.; Gouaux, J. E., Structure of staphylococcal α-hemolysin, a heptameric transmembrane pore. *sci.* **1996,** *274* (5294), 1859-1865.
4. Davis, A. P.; Sheppard, D. N.; Smith, B. D., Development of synthetic membrane transporters for anions. *Chem. Soc. Rev.* **2007,** *36* (2), 348-357.
5. Choi, J. Y.; Muallem, D.; Kiselyov, K.; Lee, M. G.; Thomas, P. J.; Muallem, S., Aberrant CFTR-dependent HCO-3 transport in mutations associated with cystic fibrosis. *Nature* **2001,** *410* (6824), 94-97.
6. Elie, C. R.; David, G.; Schmitzer, A. R., Strong antibacterial properties of anion transporters: a result of depolarization and weakening of the bacterial membrane. *J. Med. Chem.* **2015,** *58* (5), 2358-2366.
7. Yang, J.; Yu, G.; Sessler, J. L.; Shin, I.; Gale, P. A.; Huang, F., Artificial transmembrane ion transporters as potential therapeutics. *chem.* **2021,** *7* (12), 3256-3291.
8. Pérez-Tomás, R.; Montaner, B.; Llagostera, E.; Soto-Cerrato, V., The prodigiosins, proapoptotic drugs with anticancer properties. *Biochem. Pharmacol* **2003,** *66* (8), 1447-1452.
9. Manuel-Manresa, P.; Korrodi-Gregório, L.; Hernando, E.; Villanueva, A.; Martínez-García, D.; Rodilla, A. M.; Ramos, R.; Fardilha, M.; Moya, J.; Quesada, R., Novel indole-based tambjamine-analogues induce apoptotic lung cancer cell death through p38 mitogen-activated protein kinase activation. *Mol. Cancer Ther.* **2017,** *16* (7), 1224-1235.
10. Ko, S.-K.; Kim, S. K.; Share, A.; Lynch, V. M.; Park, J.; Namkung, W.; Van Rossom, W.; Busschaert, N.; Gale, P. A.; Sessler, J. L., Synthetic ion transporters can induce apoptosis by facilitating chloride anion transport into cells. *Nat. Chem.* **2014,** *6* (10), 885-892.
11. Busschaert, N.; Park, S.-H.; Baek, K.-H.; Choi, Y. P.; Park, J.; Howe, E. N.; Hiscock, J. R.; Karagiannidis, L. E.; Marques, I.; Félix, V., A synthetic ion transporter that disrupts autophagy and induces apoptosis by perturbing cellular chloride concentrations. *Nat. Chem.* **2017,** *9* (7), 667-675.
12. Saha, T.; Hossain, M. S.; Saha, D.; Lahiri, M.; Talukdar, P., Chloride-mediated apoptosis-inducing activity of bis (sulfonamide) anionophores. *J. Am. Chem. Soc.* **2016,** *138* (24), 7558-7567.
13. Akhtar, N.; Pradhan, N.; Barik, G. K.; Chatterjee, S.; Ghosh, S.; Saha, A.; Satpati, P.; Bhattacharyya, A.; Santra, M. K.; Manna, D., Quinine-based semisynthetic ion transporters with potential antiproliferative activities. *ACS Appl. Mater. Interfaces* **2020,** *12* (23), 25521-25533.
14. Akhtar, N.; Saha, A.; Kumar, V.; Pradhan, N.; Panda, S.; Morla, S.; Kumar, S.; Manna, D., Diphenylethylenediamine-based potent anionophores: transmembrane chloride ion transport and apoptosis inducing activities. *ACS Appl. Mater. Interfaces* **2018,** *10* (40), 33803-33813.
15. Dola, V. R.; Soni, A.; Agarwal, P.; Ahmad, H.; Raju, K. S. R.; Rashid, M.; Wahajuddin, M.; Srivastava, K.; Haq, W.; Dwivedi, A., Synthesis and evaluation of chirally defined side chain variants of 7-chloro-4-aminoquinoline to overcome drug resistance in malaria chemotherapy. *Antimicrob. Agents Chemother.* **2017,** *61* (3), 10.1128/aac. 01152-16.
16. Mondal, D.; Ahmad, M.; Panwaria, P.; Upadhyay, A.; Talukdar, P., Anion Recognition through Multivalent C–H Hydrogen Bonds: Anion-Induced Foldamer Formation and Transport across Phospholipid Membranes. *J. Org. Chem.* **2021,** *87* (1), 10-17.

17. Das, S.; Biswas, O.; Akhtar, N.; Patel, A.; Manna, D., Multi-stimuli controlled release of a transmembrane chloride ion carrier from a sulfonium-linked procarrier. *Org. Biomol. Chem.* **2020,** *18* (45), 9246-9252.
18. Das, S.; Karn, R.; Kumar, M.; Srimayee, S.; Manna, D., A chloride-responsive molecular switch: driving ion transport and empowering antibacterial properties. *Org. Biomol. Chem.* **2024,** *22* (1), 114-119.
19. Saha, A.; Akhtar, N.; Kumar, V.; Kumar, S.; Srivastava, H. K.; Kumar, S.; Manna, D., pH-Regulated anion transport activities of bis (iminourea) derivatives across the cell and vesicle membrane. *Org. Biomol. Chem.* **2019,** *17* (23), 5779-5788.
20. Mondal, A.; Save, S. N.; Sarkar, S.; Mondal, D.; Mondal, J.; Sharma, S.; Talukdar, P., A Benzohydrazide-Based Artificial Ion Channel that Modulates Chloride Ion Concentration in Cancer Cells and Induces Apoptosis by Disruption of Autophagy. *J. Am. Chem. Soc.* **2023,** *145* (17), 9737-9745.
21. Srimayee, S.; Badajena, S. R.; Akhtar, N.; Kar, M. K.; Dey, S.; Mohapatra, P.; Manna, D., Stimuli-responsive release of active anionophore from RGD-peptide-linked proanionophore. *Chem. Commun.* **2023,** *59* (85), 12759-12762.

Chapter 3

Development of chloride-responsive molecular switch: Driving ion transport and empowering antibacterial activities

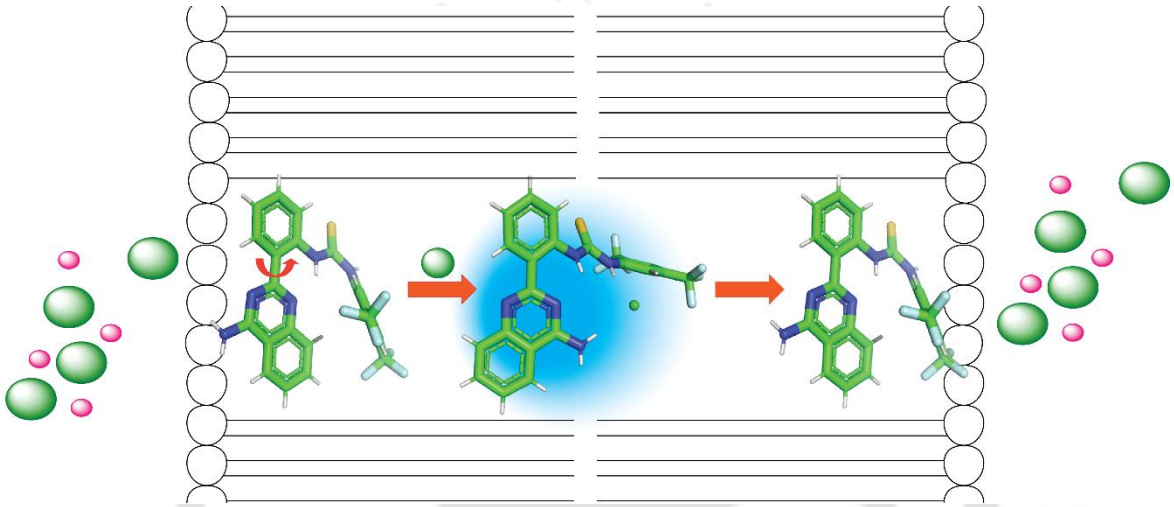

3.1. Background and objectives of the present work

Recent studies validated that the transmembrane transport of Cl^- by synthetic ion transporters in whole or in part could also induce antibacterial activities.[1] Such synthetic ion transporters are of great interest in combating drug-resistant bacterial strains, knowing that over 80% of hospital-acquired infections are becoming increasingly resistant to commercially available antibiotics. Hence, the development of new approaches or chemical entities to combat infections caused by ESKAPE pathogens is the need of the hour.[2-4]

Membrane-directing molecules with ion transport properties are considered a novel class of antibacterial agents. These membrane-directing lipophilic molecules provide the additional advantage of minimizing drug resistance against the majority of bacterial strains. Furthermore, these synthetic ion carriers are structurally much simpler than protein-based natural ion carriers; hence their transport behavior can easily be scrutinized. Lately, a wide range of synthetic ion transporters have been developed. However, developing stimuli-responsive synthetic ion transporters with properties like natural ones remains quite challenging. In this regard, several stimuli (such as pH, enzyme, light)-responsive synthetic ion transporters have been developed to have regulated ion transport properties.[5-7] However, little effort has been made in utilizing biologically active moiety for stimuli-responsive ion transport properties. This approach would provide stimuli-responsive antibacterial, anticancer, or other therapeutic activities to the compounds due to the presence of biologically active moiety and additional ion recognition and transport moiety.

So far, few ion transporters, such as gramicidin and monensin, have been demonstrated with antibacterial activities owing to their cation-selective membrane permeability.[3] However, the antibacterial activities of transmembrane anion transporter continue to be less explored.[3, 8, 9] Previously, Cl^- transport and antibacterial activities were reported for TREN-based tris(thiourea)[8] and benzimidazolium-based[9] compounds. Recently, imine-based indolyl analogs demonstrated Cl^- transport and antibacterial activities. However, the stability of these imine-based compounds could be an issue with their Cl^- transport activities.[3] Continuing our effort in designing and exploring the biological activities of synthetic ion transporter, we describe the transmembrane H^+/Cl^- cotransport and antimicrobial activity of 4-aminoquinazoline-based compounds against Gram-positive and Gram-negative bacterial strains. Recently, several thiourea-based Cl^- transporters were reported.[5, 10, 11] However, the anion recognition and transport efficacy of 4-aminoquinazoline along with the thiourea moiety has never been

explored. The 4-aminoquinazoline moiety could provide multivalent NH bond interactions within the binding cavity to design a new class of thiourea-based anion carrier and pH-responsivity. The quinazole derivatives have been used as antibacterial, anticancer, antituberculosis, and other activities.[12] We hypothesize that the potent molecule would embrace an open or closed conformation in the absence and presence of an anion, respectively, leading to the formation of an anion-induced molecular switch that could recognizes and transport anion across the membrane.[4, 13] Therefore anion itself would act as the stimulus, minimizing need of additional stimulus to regulate anion transport, and the presence of a free amine group would offer additional pH-responsive anion transport properties under an acidic environment. Presumably, the anion-recognition and transport properties of 4-aminoquinazoline analogues have never been explored as pH-responsive Cl^- transporter. Hence, we present a dynamic and adaptable system for anion recognition and transmembrane transport.

3.2. Results and discussions

3.2.1. Design and synthesis

The reaction of anthranilonitrile with sodium hydride provided 2-(2-aminophenyl)quinazolin-4-amine, which upon condensation, various arylisothiocyanate provided the targeted 4-aminoquinazoline thiourea derivatives (3.**1a-f** and **3.3a-b**).[14] We hypothesized that the introduction of the thiourea motif into 2-(2-aminophenyl)quinazoline-4-amine helped the quinazoline base scaffold assist in the transmembrane transport of ions. The strong electron-withdrawing groups, such as $-CF_3$, at the phenyl groups were varied to increase the lipophilicity (logP) and acidity (pK_a) of N–H proton, which are beneficial for improved ion binding aptitude, membrane permeability, and ion transport efficiency. For the same reason, the benzoyl and tosyl moieties were also installed to 2-(2-aminophenyl)quinazolin-4-amine (3.**2a** and 3.**2b**). The protonation of the nitrogen atom of quinazoline could additionally play a pivotal role in enhanced ion recognition, and the pH of the surrounding medium can modulate their binding affinity. Compounds 3.**3a** and 3.**3b** were also prepared to examine the significance of the bis(iminourea) moiety. Additional control compounds 3.4 and 3.5 were synthesized to investigate the role of 4-aminoquinazoline moiety in ion transport efficacy (Scheme 3.1).

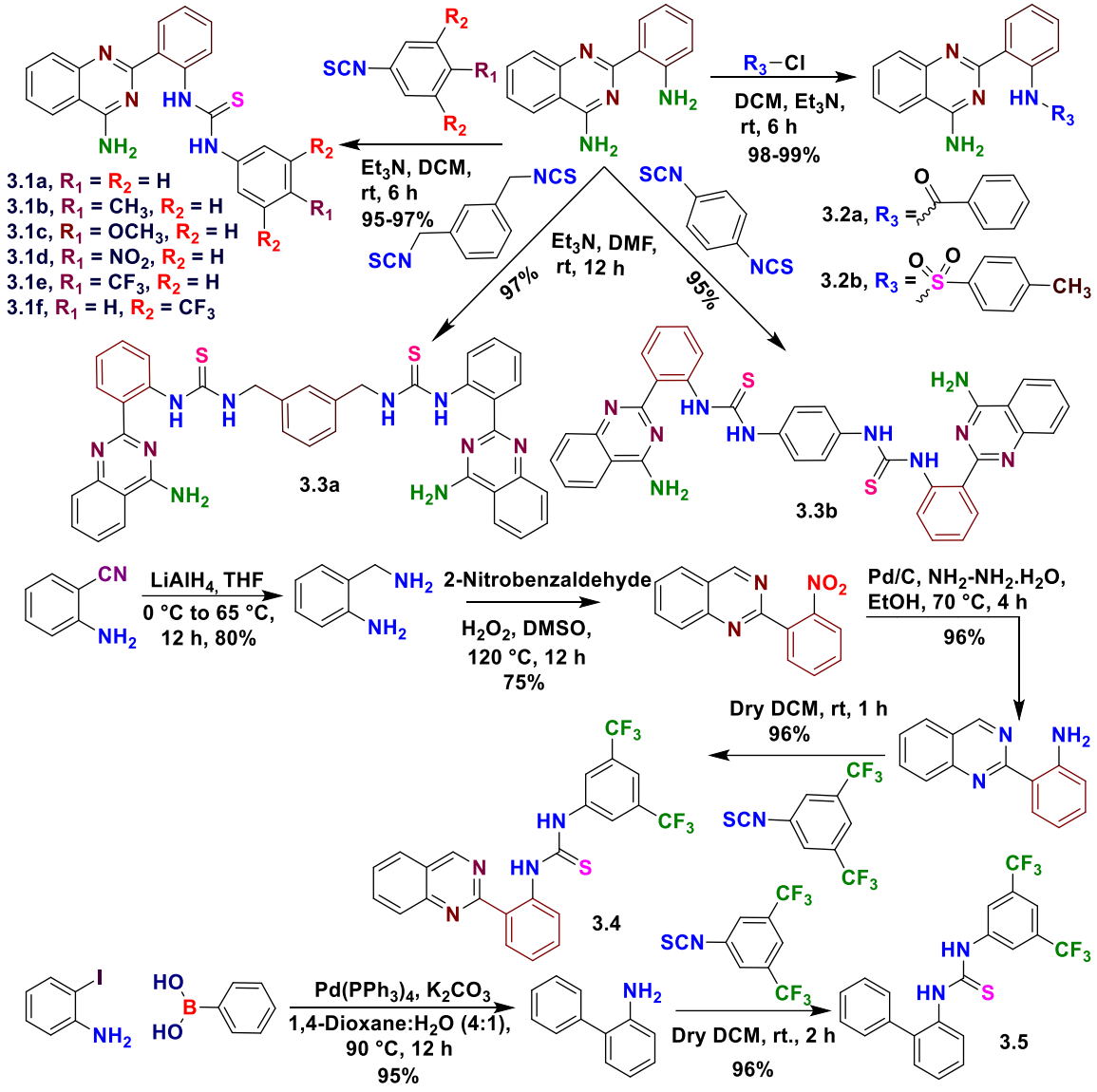

Scheme 3.1. Synthetic routes to 4-aminoquinazoline analogs.

3.2.2. Anion recognition methods

3.2.2.1. X-ray crystallographic analysis

Slow evaporation of a solution **3.1f** in acetonitrile/methanol (1:1) mixture provided a single orange crystal. The tetrabutylammonium chloride (TBACl) was used as a Cl^- source for co-crystallization with the **3.1f** in the presence of DMSO solvent. The X-ray solid-state structures of compound **3.1f** revealed that the amine and thiourea moieties adopt an anti-conformation. After complexation with Cl^-, the thiourea groups adopt a syn-conformation with respect to the amine group, which could be due to the strong intramolecular hydrogen bonding between the thiourea-N-H and the NH_2 protons with Cl^- (Figure 3.1A). The crystallographic data revealed

that the N_4-H…N hydrogen bond distance increases from 1.905 Å to 2.11 Å and the torsional angle of C_{14}-C_9-C_8-N_2 decreases from 179.28 to 25.64° (i.e., ± 153.64° rotation of the 4-aminoquinazoline moiety), and also the torsional angle of C_9-C_{14}-N_4-H increases from 14.98 to 38.45° (i.e., ± 23.47° rotation of H atom), and N_4-C_{15}-N_5-H changes from 162.95 to 9.61° (i.e., ± 153.34° rotation of the H atom and aryl ring) after Cl^- binding (Figure 3.1A).

3.2.2.2. Anion binding studies through ^{1}H NMR experiments

The ^{1}H NMR titration of **3.1f** in DMSO-d_6 solvent was performed with different concentrations of TBACl to investigate their interaction pattern in the solution phase (Figure 3.1B). A significant chemical shift of N-H_a and N-H_b protons of the thiourea groups and free amine NH_2 groups suggests the interaction of the compound with Cl^- via hydrogen bonding. The polarization of N-H_b and N-H_c protons could be prompted by the through-space effect due to the presence of Cl^-. This interaction is generally electrostatic and generates a partial positive charge on the proton, resulting in a deshielding effect leading to the downfield shift.[15] Interestingly, the N-H_a proton of **3.1f** showed an upfield chemical shift. The through-bond propagation could enhance the electron density in the aryl moiety in the presence of Cl^-, resulting in a shielding effect leading to the upfield shift.[16] Hence, these changes in the chemical shifts of the N-H protons could be due to structural switching upon Cl^- coordination. The binding analysis of the concentration-dependent chemical shifts revealed the formation of a 1:1 host-guest interaction-based complex with a binding affinity of 159.74 ± 7.81 M^{-1}, suggesting the Cl^- recognition aptitude of **3.1f** in the solution (Figure 3.1B), Similarly the association constant was measured in CD_3CN solvent and it was found 258.87 ± 0.1075 M^{-1} (Figure 3.7B). The difference in Ka values of compound 3.1f could be due to the competition of DMSO with TBACl in Cl^- ion recognition. The ^{1}H NMR titration of 3.1f with TBAF showed a strong binding affinity of 4323.64 ± 98.2 M^{-1} for F^- (Figure 3.8). In comparison, ^{1}H NMR titration of **3.1f** with TBABr, TBAI, and $TBANO_3$ showed a very low binding affinity for Br^-, I^-, and NO_3^- (Figure 3.9-3.12).

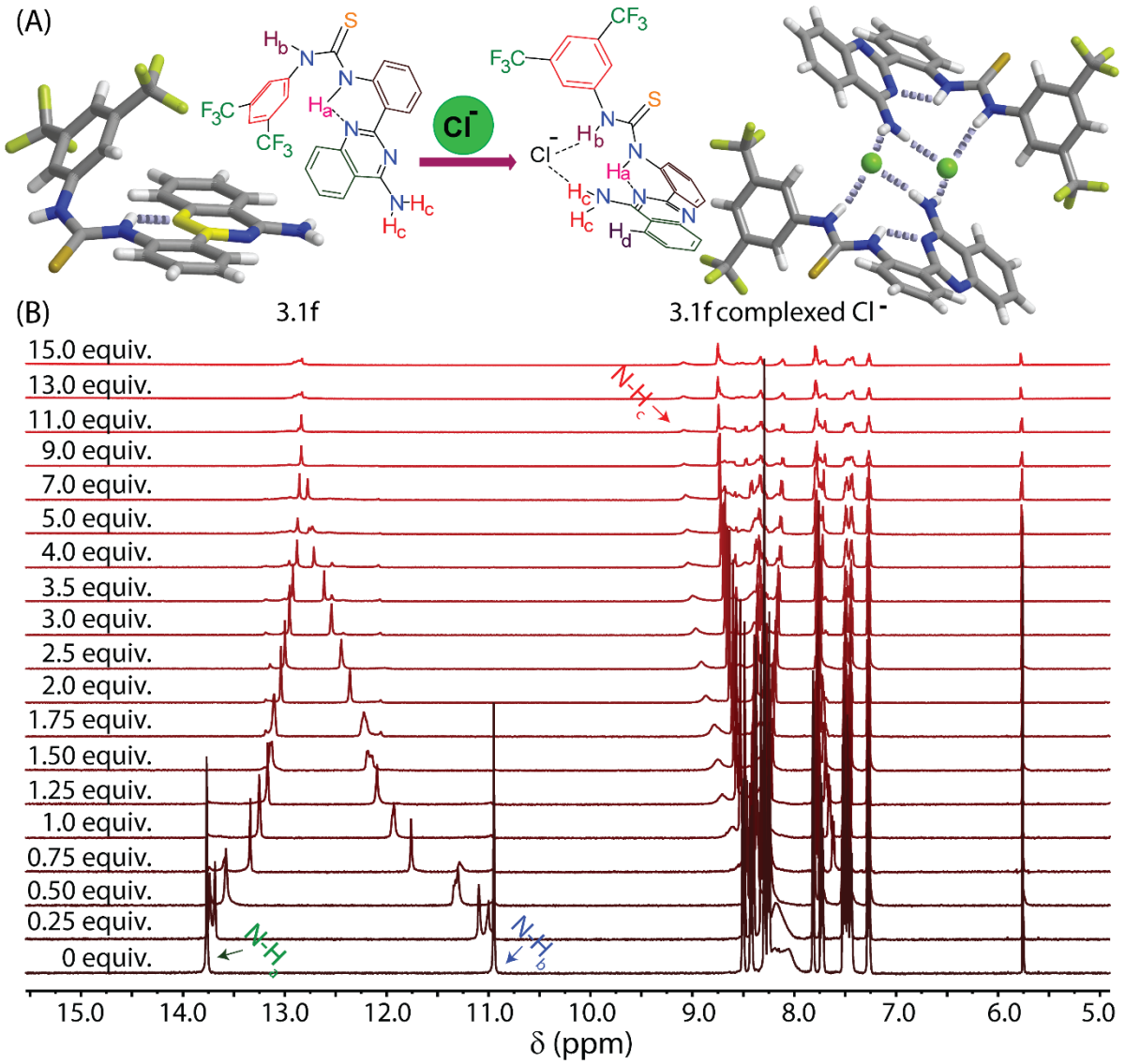

Figure 3.1. XRD-crystal structure of **3.1f** and **3.1f** complexed with Cl^- (A). The partially stacked plot of ^1H NMR titration experiment of **3.1f** (10.0 mM) with successive addition of TBACl in DMSO-d_6 solvent (B).

.

3.2.3. Conformational study

Further conformational analysis of **3.1f** in the presence of Cl^- by ^1H-^1H NOESY NMR revealed the interaction of the H_a proton with the H_b proton and that of the H_c proton with the H_d proton (Figure 3.2A, 3.2B). However, these interactions were not observed when NOESY NMR data of only **3.1f** was recorded in DMSO-d_6. Hence, the interactions of **3.1f** in the presence of Cl^- could be the consequence of the conformational alterations across the phenyl-quinazoline bond, indicating that **3.1f** remains in dynamic equilibrium with open and closed conformations, but

it folds into a closed conformation upon binding with Cl^-. Photographic image of **3.1f** in DMSO solvent under UV-Vis light (365 nm) showed an enhancement of fluorescence intensity with Cl^- concentration (Figure 3.2C), suggesting that Cl^- binding could restrict the access to the conical intersection to produce a fluorescence enhancement.[17] The concentration-dependent absorption studies did not show any significant alternation in the spectral properties of **3.1f** in the presence of TBACl (0-42 mM) (Figure 3.13A). In contrast, the concentration-dependent fluorescence studies showed a significant (over 4.2-folds) enhancement in fluorescence intensity of **3.1f** (λ_{ex} = 290/350 nm, λ_{em} = 420 nm) in the presence of TBACl (0-42 mM) (Figure 3.2D and 3.13B). This augmentation of fluorescence intensity of **3.1f** in the presence of TBACl could be due to the hydrogen-bond interaction with the Cl^-, which enhances the electron density of the NH fragment, reinforcing the electrical dipole on the aromatic moieties of **3.1f**. Hence, the charge-transfer transition is enhanced with the addition of Cl^-.

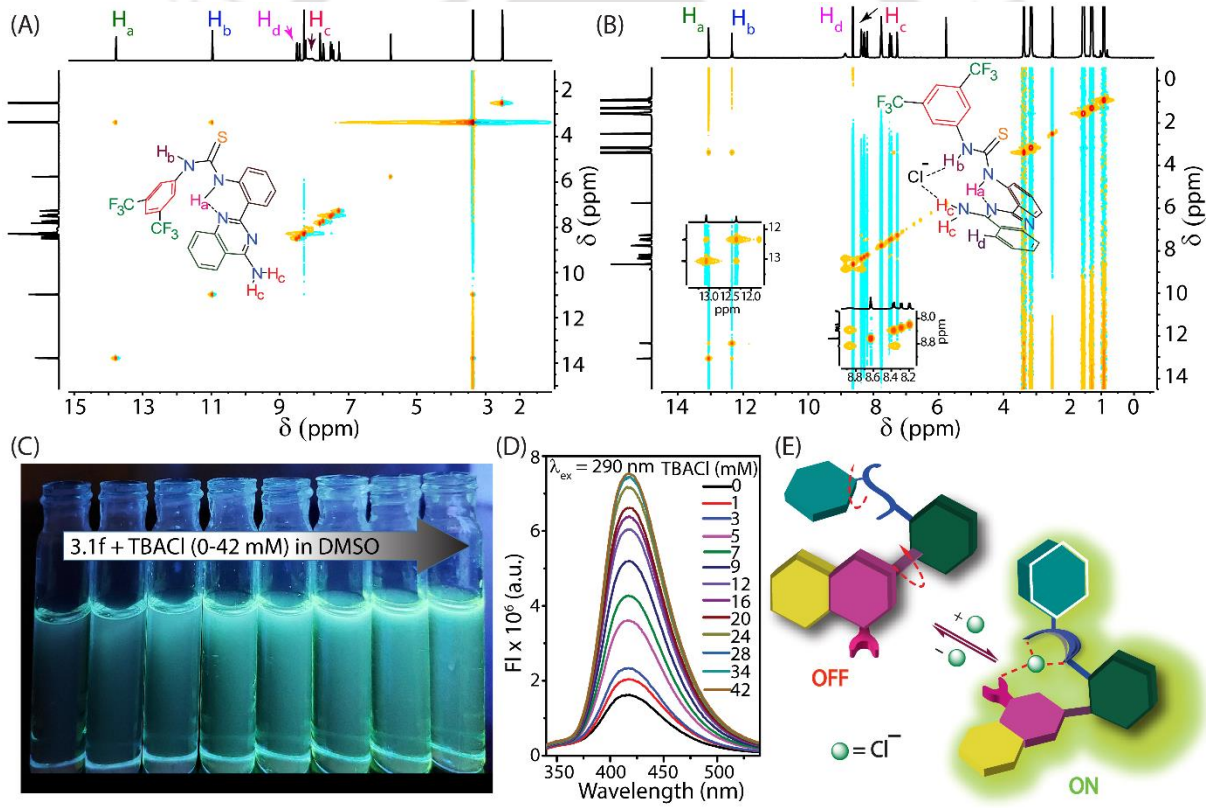

Figure 3.2. Partial ^1H-^1H NOESY NMR spectra of **3.1f** (10.0 mM) (A) and **3.1f** with TBACl (B) in DMSO-d_6 solvent. Image of **3.1f** in the presence of different concentrations of TBACl in DMSO solvent under UV-Vis (365 nm) light (C). Change in fluorescence intensity (λ_{ex} = 290 nm) of **3.1f** in the presence of different concentrations of TBACl in DMSO solvent. Schematic diagram of conformational change of **3.1f** in the presence of Cl^- (Figure 3.2E).

3.2.4. Chloride transport study

The transmembrane ion transport properties of these 4-aminoquinazoline derivatives were carried out using large unilamellar vesicles (LUVs). The vesicles were prepared using dipalmitoylphosphatidylcholine (DPPC), 1-palmitoyl-2-oleoyl-sn-glycero-3-phospho-L-serine (POPS), and cholesterol (CHOL) lipids with the molar ratio of 6:2:2 by entrapping lucigenin dye in the presence of 100 mM $NaNO_3$ in 20 mM of HEPES buffer at pH 7.2 and pH 5.4.[18] In the extravesicular medium, an isotonic solution of NaCl (100 mM), 20 mM HEPES was used. The compound pulse was given to initiate the transport of Cl^-, and the fluorescence intensity of lucigenin was monitored. The initial screening revealed that all 4-aminoquinazoline derivatives (20 μM at pH 7.2) proficiently enhanced the Cl^- influx rate, indicating their transmembrane transport aptitude. It also revealed that **3.1f** has the highest Cl^- transport efficacy among the tested compounds (Figure 3.3A).

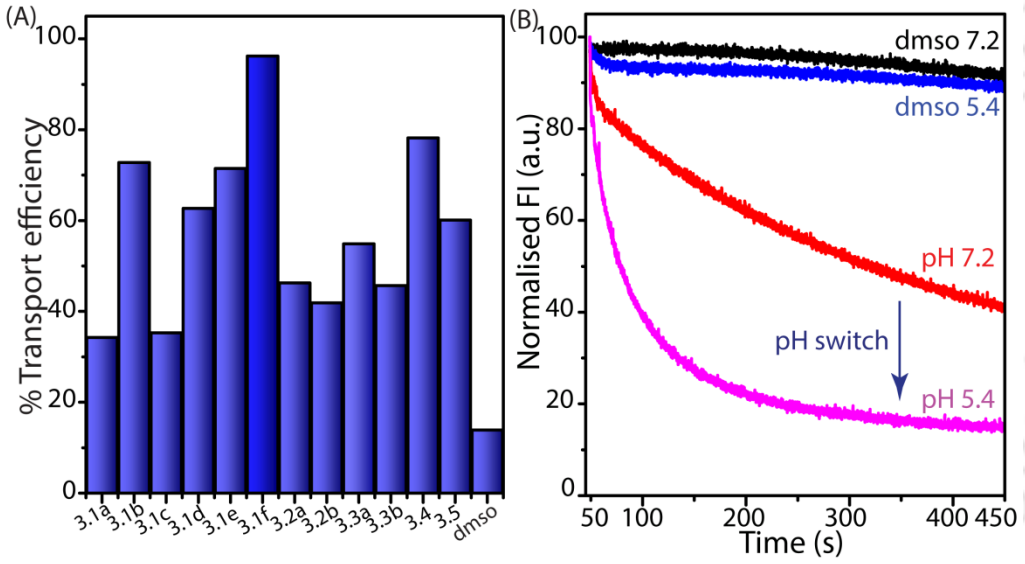

Figure 3.3. Assessment of Cl^- transport activity of the synthesized compounds (A). The pH-dependent Cl^- transport activity of **3.1f** (B).

The presence of the free amino group suggests that the protonation of the 4-aminoquinazoline moiety could significantly affect the anion-binding properties of the compounds. Hence, lucigenin-based Cl^- transport studies were performed at pH 5.4 and 7.2 (Figure 3.3B). The outcome of this assay showed that **3.1f** has superior Cl^- transport aptitude in an acidic medium (pH 5.4) compared to that under physiological conditions. The calculated EC_{50} values of the tested compound **3.1f** were 1.63 and 0.22 μM at pH 7.2 and 5.4, respectively (Figure 3.15,

3.16). Compound **3.1f** showed a 7.41-fold augmentation in Cl^- transport aptitude at pH 5.4 compared to that of pH 7.2, signifying pH-dependent Cl^- transport properties. The degree of protonation of the quinazoline moiety would be much higher in the acidic medium than under physiological conditions, resulting in higher Cl^- transport ability.[18] The chloride ion selective electrode (Cl-ISE)–based transport assay also showed the Cl^- transport aptitude of **3.1f** (Figure 3.21).

3.2.5. Ion selectivity study

The HPTS assay was used to investigate the effects of extravesicular anions on the Cl^- transport activities of **3.1f**.[18-20] In this assay, NaCl-containing buffer was used as the intravesicular solution, but isosmotic buffer solutions of different NaX salts (X = F^-, Cl^-, Br^-, I^-, NO_3^-, ClO_4^-, and SCN^-) were utilized as the extravesicular solution (Figure 3.20). Interestingly, significant differences in the anion transport properties were observed, with the highest transport ability for Cl^- among the other tested anions. Although **3.1f** showed stronger binding affinity for F^- over Cl^-, its transport efficacy is much lower for F^- over Cl^-, suggesting that very strong binding affinity restricted its releasing efficacy. A preferable transporter should have comparable binding and releasing affinity. This selective anion transport ability of **3.1f** could be due to its comparable recognition and release properties of the Cl^- through the cavity of the thiourea and 4-aminoquinazoline scaffolds. Similarly, the lucigenin assay was used to investigate the effects of extravesicular cations on the Cl^- transport activities of **3.1f**. Isosmotic buffer solutions of various monovalent metal chloride salts (Li^+, Na^+, K^+, Rb^+, and Cs^+) in the extravesicular solution were utilized to investigate the function of various cations in the Cl^- transport efficiency of the compounds (Figure 3.21).[18, 19, 21] Hence, the tested cations might have a minor effect on the transmembrane Cl^- transport activities of **3.1f**.

3.2.6. Mechanism of chloride ion transport activities

The transmembrane transport of Cl^- by **3.1f** could follow either a symport (H^+/A^-) or an antiport (OH^-/A^-) mechanism to maintain the overall charge neutrality. In this regard, we performed the HPTS assay in the absence and presence of 4-(trifluoromethoxy)phenylhydrazone (FCCP; a protonophore). The compound showed a similar Cl^- transport efficacy of **3.1f** both in the absence and presence of FCCP (Figure 3.4A). This observation suggests that the rate of dissipation of the pH gradient was not affected by the FCCP. Therefore, the association of Cl^-

is the rate-limiting step of the H^+/Cl^- symport process. In addition, the HPTS-based valinomycin (a potassium ionophore) assay was performed at pH 7.2. Simultaneous OH^- influx and/ or Cl^- efflux is anticipated to uphold the charge neutrality during the influx of K^+ by valinomycin.

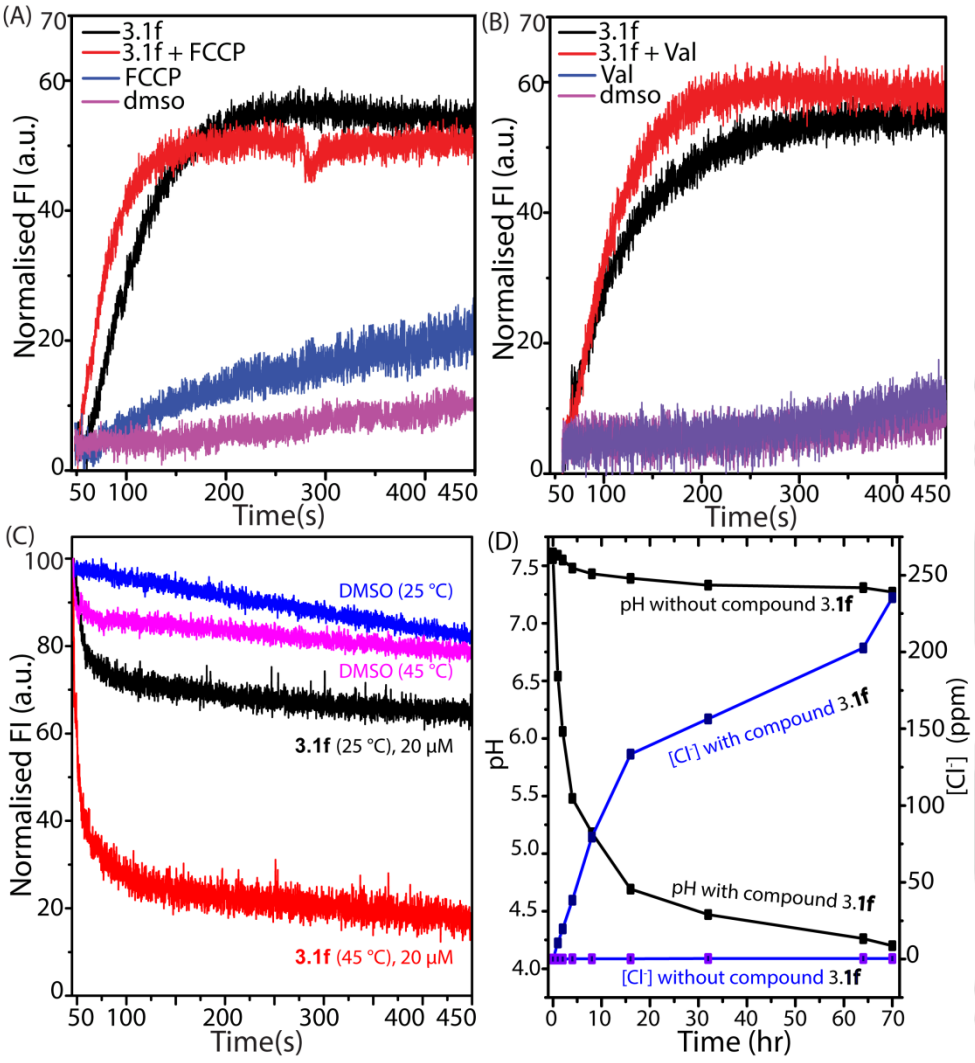

Figure 3.4. The Cl^- transport activity of **3.1f** in the absence and presence of FCCP (A) and valinomycin (Val) (B). Temperature-dependent Cl^- transport by **3.1f** (20 µM) using DPPC-LUV⊃lucigenin (C). Measurement of the H^+/ Cl^- transport efficacy by **3.1f** (20 µM) using Cl-ISE and pH-meter across a U-tube (D).

On the other hand, the similar transport rates in the presence and absence of valinomycin indicate higher transport efficacy of Cl^- over OH^- (Figure 3.4B). Therefore, both FCCP and valinomycin assays indicate the cotransport of H^+/Cl^- by the compound at physiological pH. The U-tube-based ion transport measurement was performed to investigate the evidence of the cotransport of H^+/Cl^- by **3.1f** in the acidic medium. The left and right sides of the U-tube contain

0.1M aqueous HCl solution (pH 1.2) and isotonic $NaNO_3$ solution, respectively. Chloroform (mimic of the lipid bilayer) separated these two aqueous solutions. The Cl^- and H^+ transport was recorded using Cl-ISE and pH meter (Figure 3.4D). The continuous increase in the Cl^- concentration and steady diminution in the pH value directly established the cotransport of H^+/Cl^- by the compound.

The temperature-dependent Cl^- transport assay was performed to distinguish whether the compound follows a carrier or channel mechanism. A sharp increase in the Cl^- transport efficiencies of **3.1f** was observed at 45 °C compared to that at 25 °C, suggesting that the Cl^- transport activity of **3.1f** is directly associated with the fluidity of the membrane (Figure 3.4C). The U-tube experiment also confirmed the transport of Cl^- across the lipid bilayer mimic (chloroform layer). Hence, **3.1f** transports Cl^- via a carrier pathway (Figure 3.4D). Meanwhile, the non-leaking ability of carboxyfluorescein from the vesicles in the absence and presence of the compound supports retaining vesicle integrity during the measurements (Figure 3.23).

The higher transmembrane Cl^- transport efficacy under an acidic media (pH 5.4), compared to that under physiological media (pH 7.2), suggests that the Cl^- transport aptitude of **3.1f** enhanced in the acidic medium.[18] The presence of CF_3 moiety in the benzene ring could make the neighboring nitrogen atoms more electron deficient, resulting in the N–H proton of the aryl ring being more electron deficient. This increase in the N–H proton acidity could provide a much stronger interaction with Cl^-. The CF_3 moiety also provides extra hydrophobicity to the compound, which would contribute to the higher Cl^- transport of **3.1f**. Additional studies showed that the 'apparent pK_a' value of **3.1f** was 6.8 (Figure 3.24), indicating that the pH of the surrounding media could be instrumental in Cl^- transport activity.[18]

3.2.7. Antibacterial activity study

The potent Cl^- transporter 3.1f was tested for its antibacterial activity against Gram-positive and Gram-negative bacterial strains to investigate its biological applicability.[7] Compound 3.1f exhibited strong antibacterial activity against the Staphylococcus aureus (S. aureus; MIC value of 2.34 ± 0.39 μM) and methicillin-resistant S. aureus (MRSA; MIC value of 2.50 ± 0.50 μM) (Table 3.2 and Figure 3.25-3.27). The minimal bactericidal concentration (MBC) calculation revealed that **3.1f** showed a bactericidal effect at a concentration as low as the MIC (Figure 3.25). However, **3.1f** failed to show any significant activity against E. Coli. The FESEM images revealed that there was a significant deformation in the S. aureus cells after the treatment with

3.1f (Figure 3.28). The S. aureus cells were also treated with MQAE dye, a cell-permeable fluorescence indicator of Cl^-.[22] The addition of **3.1f** resulted in a time-dependent drop in fluorescence intensity of MQAE dye, suggesting the **3.1f**-mediated Cl^- transport activity could modify the biological processes that rely on Cl^- cofactors, potentially resulting in bacterial cell death (Figure 3.28). Additional studies with 4-aminoquinazoline, control compounds 3.4 and 3.5, showed much lower antibacterial activity against the S. aureus cells, suggesting that bacteria damage was induced by the Cl^- transport activity of **3.1f**.

3.3. Conclusions

In conclusion, we established that potent 4-aminoquinazoline analog selectively transports Cl^- across the lipid bilayers via a carrier pathway. The solid-state crystal structure, NMR, and fluorescence studies validated the Cl^- binding mediated conformational change of **3.1f**. The outcomes also revealed that the quinazoline moiety has cooperative interactions of H^+ and Cl^- ions with the thiourea moiety, resulting in the transport of H^+/Cl^- across the membranes. The pH-dependent analysis revealed that the transport of Cl^- by the potent compound increased in the acidic environment. We hypothesize that such anion-induced molecular switch could be beneficial in exploring ion transport-mediated biological activities.

3.4. Experimental sections

3.4.1. General Information

The reagents and solvents used in the experiment were purchased from commercial sources such as Sigma-Aldrich and TCI. These were used without undergoing additional purification unless explicitly indicated. The monitoring of reactions was conducted through thin-layer chromatography (TLC) on silica gel 60 F254 (0.25 mm). Silica gel with a mesh size of 120-200 was utilized for the execution of column chromatography. The Bruker spectrometer was used to record the ^1H NMR and ^{13}C NMR at 600 MHz and 151 MHz, respectively. The chemical shifts were determined using internal solvents DMSO-d_6 and $CDCl_3$ and were expressed in parts per million (ppm). The values of the coupling constant (J) were expressed in hertz, and the corresponding abbreviations were provided as follows: s (representing singlet), d (representing doublet), t (representing triplet), q (representing quartet), m (representing multiple), and br (representing broadened). High-resolution mass spectra (HRMS) were acquired using an Agilent Q-TOF mass spectrometer equipped with a Z-spray source. The

obtained mass data were analyzed using the software integrated into the instrument. The chemical compounds utilized in the study, namely dipalmitoylphosphatidylcholine (DPPC), 1-palmitoyl-2-oleoyl-sn-glycero-3-phospho-L-serine (sodium salt) (POPS) and cholesterol (CHOL), were procured from Sigma Aldrich. The reagents utilized in this study, including HEPES buffer, 8-hydroxylysine-1, 3, 6-trisulfonic acid (HPTS), bis-*N*-methylacridinium nitrate (lucigenin), calcein, Triton X-100, and various inorganic salts, as well as their corresponding hydroxide bases, were procured from Sigma Aldrich. The buffers were prepared using ultrapure water sourced from the Milli-Q system manufactured by Millipore, located in Billerica, MA. The stock solutions of the compounds were prepared using spectroscopic grade DMSO of gas chromatographic grade, which was procured from Sigma.

3.4.2. Synthesis and characterization of compounds:

3.4.2.1. Synthesis of 2-(2-aminophenyl)quinazolin-4-amine ─ To the stirring suspension of sodium hydride (178 mg, 7.4 mmol) in THF (10 mL), 2-aminobenzonitril (500 mg, 4.23 mmol) in 10 mL THF was added dropwise under an N_2 atmosphere at 0 °C. After 2 hours, a dropwise solution of 2-aminobenzonitril (500 mg, 4.23 mmol) in dry THF was added and refluxed for additional 16 hours. After cooling down to room temperature, the reaction mixture was hydrolyzed with an acidic solution (1 equiv HCl in 10 mL of water). After that, the organic solvent was removed under reduced pressure, and 100 mL of water and 20 mL of dichloromethane were added to the resulting residue. The mixture was then neutralized with an aqueous NaOH (1.5 M) solution and three times extracted with 30 mL of dichloromethane. The combined organic layers were dried over sodium sulfate and evaporated to dryness. Then the crude reaction mixture was purified through column chromatography with a solvent gradient system using ethyl dichloromethane/ MeOH (5%) to furnish the target compound as a yellowish solid (75% yield).[1] The compound was characterized by ^{1}H NMR, ^{13}C NMR, and HRMS (ESI) analysis. **^{1}H NMR (400 MHz, DMSO-d_6):** δ 9.91-9.88 (m, 4H), 8.50 (d, *J* = 8.2 Hz, 1H), 8.17 (d, *J* = 8.4 Hz, 1H), 8.07 (d, *J* = 8.2 Hz, 1H), 8.00 (t, *J* = 7.6 Hz, 1H), 7.67 (t, *J* = 7.3 Hz, 1H), 7.32 (t, *J* = 7.7 Hz, 1H), 6.92 (d, *J* = 8.4 Hz, 1H), 6.69 (t, *J* = 7.6 Hz, 1H); **^{13}C NMR (151 MHz, DMSO-d_6):** δ 162.80, 158.59, 151.30, 140.52, 136.55, 134.42, 130.31, 127.55, 125.32, 120.02, 118.22, 115.81, 111.05, 110.67. **HRMS (ESI)** ***m/z*:** calculated for $C_{14}H_{12}N_4$ $(M + H)^+$: 237.1135, found: 237.1135.

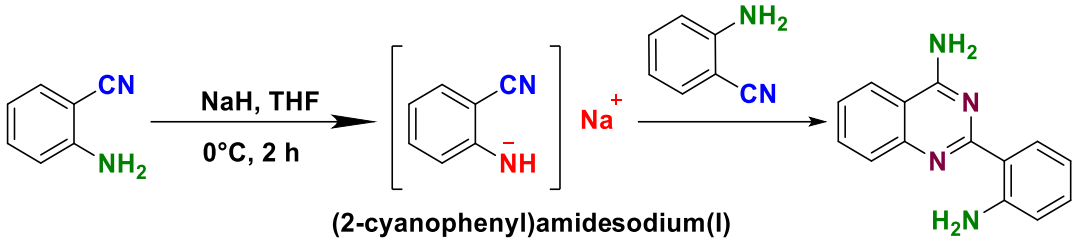

Scheme 3.2. Synthesis of 2-(2-aminophenyl)quinazolin-4-amine.

3.4.2.2. General procedure for the synthesis of thiourea derivatives (3.1a-3.1f) ─ To the stirring solutions of 2-(2-aminophenyl)quinazolin-4-amine (50 mg, 0.2 mmol, 1 equiv.) and triethylamine (30 µL, 0.2 mmol) in dichloromethane, a solution of respective phenyl isothiocyanate derivatives(0.2 mmol, 1 equiv.) in dichloromethane were added (dropwise) to the reaction mixture under an N_2 atmosphere at room temperature. Then the reaction mixture was allowed to stir for 6 hours at room temperature. After the completion of the reaction, precipitation happens. The crude precipitate was filtered and washed with dichloromethane and dried at 80 °C overnight, with a resulting yield of 95–98%.[2]

3.4.2.3. 1-(2-(4-aminoquinazolin-2-yl)phenyl)-3-phenylthiourea (3.1a) ─ The 1-(2-(4-aminoquinazolin-2-yl)phenyl)-3-phenylthiourea (**3.1a**) was synthesized according to the procedure as mentioned in the earlier section (3.4.2.2), using 2-(2-aminophenyl)quinazolin-4-amine (50 mg, 0.21 mmol), phenyl isothiocyanate (30 mg, 0.22 mmol) and triethylamine (30 µL, 0.2 mmol). The yellowish compound was isolated in 95% yield. The compound was characterized by ^{1}H NMR and ^{13}C NMR, HRMS (ESI) and melting point analysis. **^{1}H NMR (600 MHz, DMSO-*d*$_6$):** δ 13.47 (s, 1H), 10.41 (s, 1H), 8.44 (dd, *J* = 13.8, 8.0 Hz, 2H), 8.19 (d, *J* = 8.2 Hz, 1H), 8.11-7.87 (m, 2H), 7.61 (t, *J* = 7.4 Hz, 1H), 7.51 (d, *J* = 7.9 Hz, 2H), 7.46 – 7.45 (m, 4H), 7.26 (t, *J* = 7.3 Hz, 1H), 7.22 (t, *J* = 7.5 Hz, 1H), 6.70 (s, 1H); **^{13}C NMR (151 MHz, DMSO-*d*$_6$):** δ 178.93, 162.20, 160.64, 148.64, 140.43, 139.39, 133.65, 130.44, 129.69, 127.05, 126.50, 126.30, 125.41, 124.92, 124.06, 123.93, 123.45, 112.95. **HRMS (ESI)** ***m/z*:** calculated for $C_{21}H_{17}N_5S$ $(M + H)^+$: 372.1277, found: 372.1277. **Melting point:** 205 ± 2 °C.

3.4.2.4. 1-(2-(4-aminoquinazolin-2-yl)phenyl)-3-(p-tolyl)thiourea (3.1b) ─ The 1-(2-(4-aminoquinazolin-2-yl)phenyl)-3-(p-tolyl)thiourea (**3.1b**) was synthesized according to the procedure as mentioned in the earlier section (3.4.2.2), using 2-(2-aminophenyl)quinazolin-4-amine (40 mg, 0.17 mmol), 4-Methylbenzyl isothiocyanate (26 mg, 0.18 mmol) and

triethylamine (24 µL, 0.2 mmol). The yellowish compound was isolated in 95% yield. The compound was characterized by ^{1}H NMR and ^{13}C NMR, HRMS (ESI) and melting point analysis. **^{1}H NMR (600 MHz, CDCl$_3$ + DMSO-*d*$_6$):** δ 13.46 (s, 1H), 8.97 (s, 1H), 8.59 (d, *J* = 8.3 Hz, 1H), 8.44 (d, *J* = 7.9 Hz, 1H), 7.97 – 7.92 (m, 1H), 7.54 (t, *J* = 7.5 Hz, 1H), 7.45 (t, *J* = 1.8 Hz, 1H), 7.45 – 7.42 (m, 1H), 7.38 (d, *J* = 3.4 Hz, 2H), 7.36 (d, *J* = 2.4 Hz, 1H), 7.24 (d, *J* = 7.6 Hz, 2H), 7.20 (t, *J* = 7.6 Hz, 1H), 6.79 (s, 1H), 6.48 (s, 2H), 2.40 (s, 3H). **^{13}C NMR (151 MHz, CDCl$_3$ + DMSO-*d*$_6$)** δ 178.57, 161.46, 160.25, 148.91, 139.99, 136.17, 134.77, 132.68, 130.20, 129.69, 128.98, 127.16, 126.64, 125.41, 124.30, 123.87, 123.20, 122.96, 112.66, 20.81. **HRMS (ESI)** ***m/z*:** calculated for $C_{22}H_{19}N_5S$ $(M + H)^+$: 386.1434, found: 386.1438. **Melting point: 218 ± 2** °C.

3.4.2.5. 1-(2-(4-aminoquinazolin-2-yl)phenyl)-3-(4-methoxyphenyl)thiourea (3.1c) ─ The 1-(2-(4-aminoquinazolin-2-yl)phenyl)-3-(4-methoxyphenyl)thiourea (**3.1c**) was synthesized according to the procedure as mentioned in the earlier section (3.4.2.2), using 2-(2-aminophenyl)quinazolin-4-amine (40 mg, 0.17 mmol), 4-Methoxylbenzyl isothiocyanate (30 mg, 0.18 mmol) and triethylamine (24 µL, 0.2 mmol). The yellowish compound was isolated in 95% yield. The compound was characterized by ^{1}H NMR and ^{13}C NMR, HRMS (ESI) melting point analysis. **^{1}H NMR (600 MHz, CDCl$_3$ + DMSO-*d*$_6$):** δ 13.09 (s, 1H), 8.56 (s, 1H), 8.45 (d, *J* = 6.5 Hz, 1H), 7.75 (s, 1H), 7.67 (d, *J* = 8.0 Hz, 1H), 7.63 (t, *J* = 7.8 Hz, 1H), 7.51 (t, *J* = 7.7 Hz, 1H), 7.45 (t, *J* = 6.3 Hz, 1H), 7.38 (d, *J* = 8.9 Hz, 2H), 7.27 (m, 4H), 7.00 (d, *J* = 8.9 Hz, 2H), 3.87 (s, 3H). **^{13}C NMR (151 MHz, CDCl$_3$ + DMSO-*d*$_6$):** δ 178.87, 161.50, 160.34, 157.17, 148.99, 139.96, 132.70, 131.66, 130.19, 128.92, 127.21, 126.74, 125.74, 125.40, 124.34, 123.28, 122.90, 114.30, 112.68, 55.37. **HRMS (ESI)** ***m/z*:** calculated for $C_{22}H_{19}N_5OS$ $(M + H)^+$: 402.1382, found: 402.1378. **Melting point: 192 ± 2** °C.

3.4.2.6. 1-(2-(4-aminoquinazolin-2-yl)phenyl)-3-(4-nitrophenyl)thiourea (3.1d) ─ The 1-(2-(4-aminoquinazolin-2-yl)phenyl)-3-(4-nitrophenyl)thiourea (**3.1d**) was synthesized according to the procedure as mentioned in the earlier section (3.4.2.2), using 2-(2-aminophenyl)quinazolin-4-amine (40 mg, 0.17 mmol), 4-Nitrobenzyl isothiocyanate (30 mg, 0.18 mmol) and triethylamine (24 µL, 0.2 mmol). The orange color solid compound was isolated in 96% yield. The compound was characterized by ^{1}H NMR and ^{13}C NMR, HRMS (ESI) and melting point analysis. ^{1}H NMR (600 MHz, DMSO-*d*$_6$) δ 13.99 (s, 1H), 11.02 (s, 1H), 8.51 (m, 8.1 Hz, 2H), 8.24 (t, *J* = 7.6 Hz, 4H), 7.89 (d, *J* = 9.1 Hz, 2H), 7.66 (t, *J* = 7.6

Hz, 1H), 7.50 – 7.45 (m, 2H), 7.27 (t, *J* = 7.5 Hz, 1H), 7.18 (d, *J* = 8.3 Hz, 1H). **^{13}C NMR (151 MHz, CDCl$_3$ + DMSO-*d*$_6$):** δ 183.59, 166.46, 165.14, 154.00, 150.96, 147.56, 144.32, 137.96, 135.33, 134.27, 131.96, 131.45, 130.54, 129.32, 128.77, 128.51, 128.32, 126.45, 121.52, 117.77. **HRMS (ESI)** ***m/z*:** calculated for $C_{21}H_{16}N_6O_2S$ $(M + H)^+$: 417.1128, found: 4417.1126. **Melting point: 208 ± 2** °C.

3.4.2.7. 1-(2-(4-aminoquinazolin-2-yl)phenyl)-3-(4-(trifluoromethyl)phenyl)thiourea (3.1e) — The 1-(2-(4-aminoquinazolin-2-yl)phenyl)-3-(4-(trifluoromethyl)phenyl)thiourea (**3.1e**) was synthesized according to the procedure as mentioned in the earlier section (3.4.2.2), using 2-(2-aminophenyl)quinazolin-4-amine (40 mg, 0.17 mmol), 4-(Trifluoromethyl)phenyl isothiocyanate (35 mg, 0.18 mmol) and triethylamine (24 µL, 0.2 mmol). The yellow color solid compound was isolated in 97% yield. The compound was characterized by ^{1}H NMR and ^{13}C NMR, and HRMS (ESI) and melting point analysis. **^{1}H NMR (600 MHz, DMSO-*d*$_6$):** δ 13.84 (s, 1H), 10.74 (s, 1H), 8.61 – 8.29 (m, 3H), 8.22 (d, *J* = 8.2 Hz, 1H), 8.18 – 7.97 (m, 8H), 7.81 – 7.73 (m, 4H), 7.58 (t, *J* = 7.6 Hz, 2H), 7.47 (t, *J* = 7.6 Hz, 3H), 7.24 (t, *J* = 7.6 Hz, 1H), 6.78 (d, *J* = 7.9 Hz, 1H). **^{13}C NMR (151 MHz, CDCl$_3$ + DMSO-*d*$_6$):** δ 183.68, 166.36, 165.15, 153.82, 147.37, 144.48, 137.87, 135.32, 135.28, 134.24, 131.83, 131.48, 131.00, 130.52, 128.93, 128.89, 128.45, 128.41, 127.92, 127.88, 127.59, 127.55, 117.58. **HRMS (ESI)** ***m/z*:** calculated for $C_{22}H_{16}F_3N_5S$ $(M + H)^+$: 440.1151, found: 440.1154. **Melting point: 176 ± 2** °C.

3.4.2.8. 1-(2-(4-aminoquinazolin-2-yl)phenyl)-3-(3,5-bis(trifluoromethyl)phenyl)thiourea (3.1f) — The 1-(2-(4-aminoquinazolin-2-yl)phenyl)-3-(4-(trifluoromethyl)phenyl)thiourea (**3.1e**) was synthesized according to the procedure as mentioned in the earlier section (3.4.2.2), using 2-(2-aminophenyl)quinazolin-4-amine (40 mg, 0.17 mmol), 3,5-Bis(trifluoromethyl)phenyl isothiocyanate (48 mg, 0.18 mmol) and triethylamine (24 µL, 0.2 mmol). The yellow color solid compound was isolated in 97% yield. The compound was characterized by ^{1}H NMR and ^{13}C NMR, and HRMS (ESI) and melting point analysis. **^{1}H NMR (600 MHz, DMSO-*d*$_6$) δ:** 13.79 (s, 1H), 10.97 (s, 1H), 8.52 (d, *J* = 7.9 Hz, 1H), 8.44 (d, *J* = 8.2 Hz, 1H), 8.31 (s, 2H), 8.27 (d, *J* = 8.2 Hz, 1H), 8.21-8.08 (br, 2H), 7.83 (s, 1H), 7.74 (t, *J* = 7.6 Hz, 1H), 7.53 (t, *J* = 7.7 Hz, 1H), 7.50 (t, *J* = 7.7 Hz, 1H), 7.46 (d, *J* = 8.2 Hz, 1H), 7.28 (t, *J* = 7.5 Hz, 1H), 5.77 (s, 1H); **^{13}C NMR (151 MHz, DMSO-*d*$_6$):** δ 179.51, 162.23, 160.69, 148.88, 142.04, 139.71, 133.85, 130.94, 130.72, 130.14, 127.14, 126.58, 126.44, 124.56, 124.30, 124.13, 123.99, 123.88, 123.86, 123.83, 123.80, 122.76, 120.95, 117.51,

113.13. **HRMS (ESI) m/z:** calculated for $C_{23}H_{15}F_6N_5S$ $(M + H)^+$: 508.1025, found: 508.1025. **Melting point: 180 ± 2** °C.

3.4.2.9. Synthesis of *N*-(2-(4-aminoquinazolin-2-yl)phenyl)benzamide (3.2a) ─ To the stirring solutions of 2-(2-aminophenyl)quinazolin-4-amine (50 mg, 0.2 mmol, 1 equiv.) and triethylamine (30 µL, 0.2 mmol) in dichloromethane, a solution of benzoyl chloride (28.2 mg, 0.2 mmol) in dichloromethane were added (dropwise) to the reaction mixture under an N_2 atmosphere at room temperature. The reaction mixture was allowed to be stirred for 6 hours at room temperature. After the completion of the reaction, precipitation happens. The crude precipitate was filtered and washed with dichloromethane and dried at 80 °C overnight, with a resulting yield of 98%. The compound was characterized by ^{1}H NMR and ^{13}C NMR, and HRMS (ESI) and melting point analysis. **^{1}H NMR (600 MHz, $CDCl_3$ + DMSO-d_6):** δ 8.85 (d, *J* = 8.3 Hz, 1H), 8.71 (d, *J* = 8.0 Hz, 1H), 8.26 (d, *J* = 8.2 Hz, 1H), 8.12 (d, *J* = 7.4 Hz, 2H), 7.76 (d, *J* = 7.5 Hz, 1H), 7.72 (d, *J* = 8.3 Hz, 1H), 7.63 (d, *J* = 7.1 Hz, 2H), 7.59 (t, *J* = 7.4 Hz, 2H), 7.47 (q, *J* = 7.6 Hz, 2H), 7.19 (t, *J* = 7.6 Hz, 1H). **^{13}C NMR (151 MHz, $CDCl_3$ + DMSO-d_6):** δ 165.65, 161.86, 161.09, 148.54, 139.97, 136.13, 133.22, 131.61, 130.75, 130.70, 128.53, 127.45, 126.22, 125.68, 124.01, 123.83, 122.43, 120.06, 112.97. **HRMS (ESI)** *m/z***:** calculated for $C_{21}H_{16}N_4O$ $(M + H)^+$: 341.1397, found: 341.1397. **Melting point:** 165 ± 2 °C.

3.4.2.10. Synthesis of *N*-(2-(4-aminoquinazolin-2-yl)phenyl)-4-methylbenzenesulfonamide (3.2b) ─ To the stirring solutions of 2-(2-aminophenyl)quinazolin-4-amine (50 mg, 0.2 mmol, 1 equiv.) and triethylamine (30 µL, 0.2 mmol) in dichloromethane, a solution of benzoyl chloride (40 mg, 0.2 mmol) in dichloromethane were added (dropwise) to the reaction mixture under an N_2 atmosphere at room temperature. The reaction mixture was allowed to be stirred for 6 hours at room temperature. After the completion of the reaction, precipitation happens. The crude precipitate was filtered and washed with dichloromethane and dried at 80 °C overnight, with a resulting yield of 99%. The compound was characterized by ^{1}H NMR and ^{13}C NMR, and HRMS (ESI) and melting point analysis. **^{1}H NMR (600 MHz, $CDCl_3$ + DMSO-d_6**): δ 8.76 (d, *J* = 8.5 Hz, 1H), 8.01 (s, 1H), 7.85 (d, *J* = 8.2 Hz, 1H), 7.76 – 7.71 (m, 4H), 7.70 – 7.68 (m, 1H), 7.66 – 7.63 (m, 1H), 7.41 – 7.35 (m, 3H), 7.23 (t, *J* = 7.6 Hz, 1H), 7.10 (t, *J* = 7.3 Hz, 1H), 1.73 (s, 8H). **^{13}C NMR (151 MHz, $CDCl_3$ + DMSO-d_6):** δ 167.44, 162.12, 149.45, 148.42, 143.41, 141.78, 141.59, 141.09, 141.07, 140.85, 140.83, 138.17, 135.23, 134.25, 133.18, 131.38,

130.71, 130.01, 127.10, 116.22, 26.03. **HRMS (ESI)** *m/z***:** calculated for $C_{21}H_{18}N_4O_2S$ $(M + H)^+$: 391.1233, found: 391.1219. **Melting point:** 275 ± 2 °C.

3.4.2.11. Synthesis of bis(thiurea) derivative (3.3a) ─ To the stirring solutions of 2-(2-aminophenyl)quinazolin-4-amine (50 mg, 0.2 mmol, 1 equiv.) and triethylamine (30 µL, 0.2 mmol) in DMF, a solution of 1,4-phenylenediisocyanate (22 mg, 0.1 mmol, 0.5 equiv.) in DMF was added dropwise to the reaction mixture under an N_2 atmosphere at room temperature. The reaction mixture was allowed to be stirred for 12 hours at room temperature. After the completion of the reaction, the DMF solvent was removed under reduced pressure. The crude light yellowish solid was washed with dichloromethane and dried at 80 °C overnight, with a yield of 97%. The compound was characterized by ^{1}H NMR and ^{13}C NMR, and HRMS (ESI) and melting point analysis. **^{1}H NMR (600 MHz, DMSO-*d*$_6$):** δ 13.45 (s, 2H), 10.55 (s, 2H), 8.44 (t, *J* = 8.6 Hz, 4H), 8.22 (d, *J* = 8.2 Hz, 2H), 8.06 (m, 4H), 7.73 (t, *J* = 7.7 Hz, 2H), 7.61 (s, 4H), 7.47 – 7.44 (m, 4H), 7.23 (t, *J* = 7.6 Hz, 2H), 7.04 (s, 2H). **^{13}C NMR (151 MHz, DMSO-*d*$_6$):** δ 179.01, 162.24, 160.70, 148.75, 140.43, 136.26, 133.93, 130.46, 129.67, 127.29, 126.63, 126.25, 125.04, 124.55, 123.93, 123.43, 112.99. **HRMS (ESI)** *m/z***:** calculated for $C_{36}H_{28}N_{10}S_2$ $(M + H)^+$: 665.2013, found: 665.2013. **Melting point:** 188 ± 2 °C.

3.4.2.12. Synthesis of bis(thiurea) derivative (3.3b) ─ To the stirring solutions of 2-(2-aminophenyl)quinazolin-4-amine (50 mg, 0.2 mmol, 1 equiv.) and triethylamine (30 µL, 0.2 mmol) in DMF, a solution of 1,3-bis(isothiocyanatomethyl)benzene (25 mg, 0.1 mmol, 0.5 equiv.) in DMF was added dropwise to the reaction mixture under an N_2 atmosphere at room temperature. The reaction mixture was stirred for 12 hours at room temperature. After the completion of the reaction, the DMF solvent was removed under reduced pressure. The crude light yellowish solid was washed with dichloromethane and dried at 80 °C overnight, yielding 95 %. The compound was characterized by ^{1}H NMR and ^{13}C NMR, and HRMS (ESI) and melting point analysis. **^{1}H NMR (600 MHz, DMSO-*d*$_6$):** δ 12.93 (s, 2H), 9.27 (s, 2H), 8.45 (d, *J* = 8.0 Hz, 2H), 8.27-8.22 (m, 4H), 8.15 – 8.11 (m, 4H), 7.95 (s, 2H), 7.84 (t, *J* = 7.6 Hz, 2H), 7.55 – 7.51 (m, 2H), 7.43 – 7.37 (m, 4H), 7.28 – 7.25 (m, 2H), 7.18 (t, *J* = 7.7 Hz, 2H), 4.83 (d, *J* = 5.8 Hz, 4H). **^{13}C NMR (151 MHz, DMSO-*d*$_6$):** δ 181.65, 162.32, 159.99, 140.30, 139.48, 134.82, 130.61, 128.65, 126.93, 126.79, 126.20, 125.70, 124.53, 123.59, 112.55, 47.45, 45.94. **HRMS (ESI)** *m/z***:** calculated for $C_{38}H_{32}N_{10}S_2$ $(M + H)^+$: 693.2326, found: 693.2325. **Melting point:** 180 ± 2 °C.

3.4.2.13. Synthesis of 1-(3,5-bis(trifluoromethyl)phenyl)-3-(2-(quinazolin-2-yl)phenyl)thiourea (3.4) ─ The compounds 2-(aminomethyl)aniline and 2-(2-nitrophenyl)quinazoline were prepared according to literature procedure [1]. For the synthesis of 2-(quinazolin-2-yl)aniline, to the stirring solutions of 2-(2-nitrophenyl)quinazoline (100 mg, 0.398 mmol, 1 equiv.) and Pd/C (2.2 mg, 0.01 mmol) in EtOH, a solution of hydrazinehydrate (80 %) (100 µL, 1.6 mmol, 4 equiv.) was added dropwise to the reaction mixture under an N_2 atmosphere at room temperature. The reaction mixture was allowed to be stirred for 4 hours at 70 °C temperature. After the completion of the reaction. The reaction mixture was filtered through celite and dried under reduced pressure, with a resulting yellowish green solid yield of 95–98%. Subsequently 2-(quinazolin-2-yl)aniline directly use for the next step. Thereafter, to the stirring solutions of 2-(quinazolin-2-yl)aniline (20 mg, 0.2 mmol, 1 equiv.) in DCM, a solution of 3,5-Bis(trifluoromethyl)phenyl isocyanate (23 mg, 0.09 mmol, 1 equiv.) in DCM was added dropwise to the reaction mixture under an N_2 atmosphere at room temperature. The reaction mixture was allowed to be stirred for 1 hours at room temperature. After the completion of the reaction, precipitation happens. The crude precipitate was filtered and washed with dichloromethane and dried at 80 °C overnight, with a resulting compound **3.4**, yield of 95–98%. The compounds were characterized by ^{1}H NMR and ^{13}C NMR and HRMS (ESI) and melting point analysis. **^{1}H NMR (600 MHz, DMSO-d_6) δ:** 12.30 (s, 1H), 10.94 (s, 1H), 9.74 (s, 1H), 8.48 (d, *J* = 6.6 Hz, 1H), 8.25 (s, 2H), 8.22 (d, *J* = 7.9 Hz, 1H), 8.18 (d, *J* = 8.1 Hz, 1H), 8.04 (t, *J* = 8.2 Hz, 1H), 7.93 (d, *J* = 8.5 Hz, 1H), 7.80 (s, 1H), 7.78 (d, *J* = 7.8 Hz, 1H), 7.56 (t, *J* = 7.7 Hz, 1H), 7.39 (t, *J* = 7.6 Hz, 1H). **^{13}C NMR (151 MHz, DMSO-d_6) δ:** 179.96, 161.78, 160.68, 149.11, 142.03, 138.91, 135.67, 131.45, 130.88, 130.81, 130.59, 128.82, 128.41, 127.71, 125.88, 125.22, 124.53, 123.80, 123.12, 122.73. **HRMS (ESI)** ***m/z*:** calculated for $C_{23}H_{14}F_6N_4S$ $(M + H)^+$: 493.0911, found: 493.0911. **Melting point:** 174 ± 2 °C.

3.4.2.14. Synthesis of 1-([1,1'-biphenyl]-2-yl)-3-(3,5-bis(trifluoromethyl)phenyl)thiourea (3.5) ─ The compound [1,1'-biphenyl]-2-amine was synthesised according to literature procedure [2]. Thereafter, to the stirring solutions of [1,1'-biphenyl]-2-amine (20 mg, 0.12 mmol, 1 equiv.) in DCM, a solution of 3,5-Bis(trifluoromethyl)phenyl isocyanate (30 mg, 0.12 mmol, 1 equiv.) in DCM was added dropwise to the reaction mixture under an N_2 atmosphere at room temperature. The reaction mixture was allowed to be stirred for 2 hours at room temperature. After the completion of the reaction, precipitation happens. The crude precipitate was filtered

and washed with dichloromethane and dried at 80°C overnight, with a resulting compound **3.5,** yield of 95–98%. The compounds were characterized by ^{1}H NMR and ^{13}C NMR and HRMS (ESI) and melting point analysis. **^{1}H NMR (600 MHz, DMSO-*d*$_6$) δ:** 10.06 (s, 1H), 9.77 (s, 1H), 7.76 (s, 2H), 7.71 (broad, 1H), 7.46 – 7.36 (m, 8H), 7.32 (t, *J* = 7.2 Hz, 1H). **^{13}C NMR (151 MHz, DMSO-*d*$_6$) δ:** 180.78, 142.24, 139.39, 138.78, 135.80, 131.20, 129.02, 128.69, 128.02, 127.68, 124.55, 122.75, 117.32. **HRMS (ESI)** ***m/z*:** calculated for $C_{21}H_{14}F_6N_2S$ $(M + H)^+$: 441.0855, found: 441.0855. **Melting point:** 78 ± 2 °C.

3.4.3. Crystallographic Study:

Using SMART software, the crystallographic data were collected from the Bruker APEX-II CCD diffractometer equipped with a graphite monochromator and Apex CCD camera. All crystallographic data were refined using the SHELXL-2018/3 and or S-20 Olex2 1.2-alpha. Only **3.1f** was crystalized in an acetonitrile/methanol (1:1) mixture. The tetrabutylammonium chloride (TBACl) salt was used as a Cl^- source for co-crystallization with the **3.1f** in DMSO solvent.

Table 3.1. Crystal parameters and refinement data of the anion complex.

Parameters	**3.1f**	**3.1f complexed with Cl^-**
Emperical formula	C23 H15 F6 N5 S	C23 H15 F6 N5 S, C16 H31 N, Cl
Formula weight	507.46	779.32
Temperature (K)	293	293
Crystal system	Monoclinic	Monoclinic
Space group	C2/c	P-21/c
a (A^o)	26.509(6)	9.2259(11)
b (A^o)	8.6693(18)	17.758(2)
c (A^o)	19.550(4)	25.992(3)
α (deg)	90	90
β (deg)	102.969(5)	95.635(4)
γ (deg)	90	90
V (A^{o3})	4378.288	4237.7(9)
Z	8	4

λ	0.71073	0.71073
μ (mm^{-1})	0.222	0.200
Theta (max)	25	2561
h, k, l $_{max}$	31, 10, 23	10, 20, 30
F000	2064	1632
Density (g/cm^{-3})	1.54	1.221
R1, I > 2σ(I	0.1085	0.0879
wR_2	0.1654	0.2113
GooF	1.201	1.076
CCDC	2279459	2279460

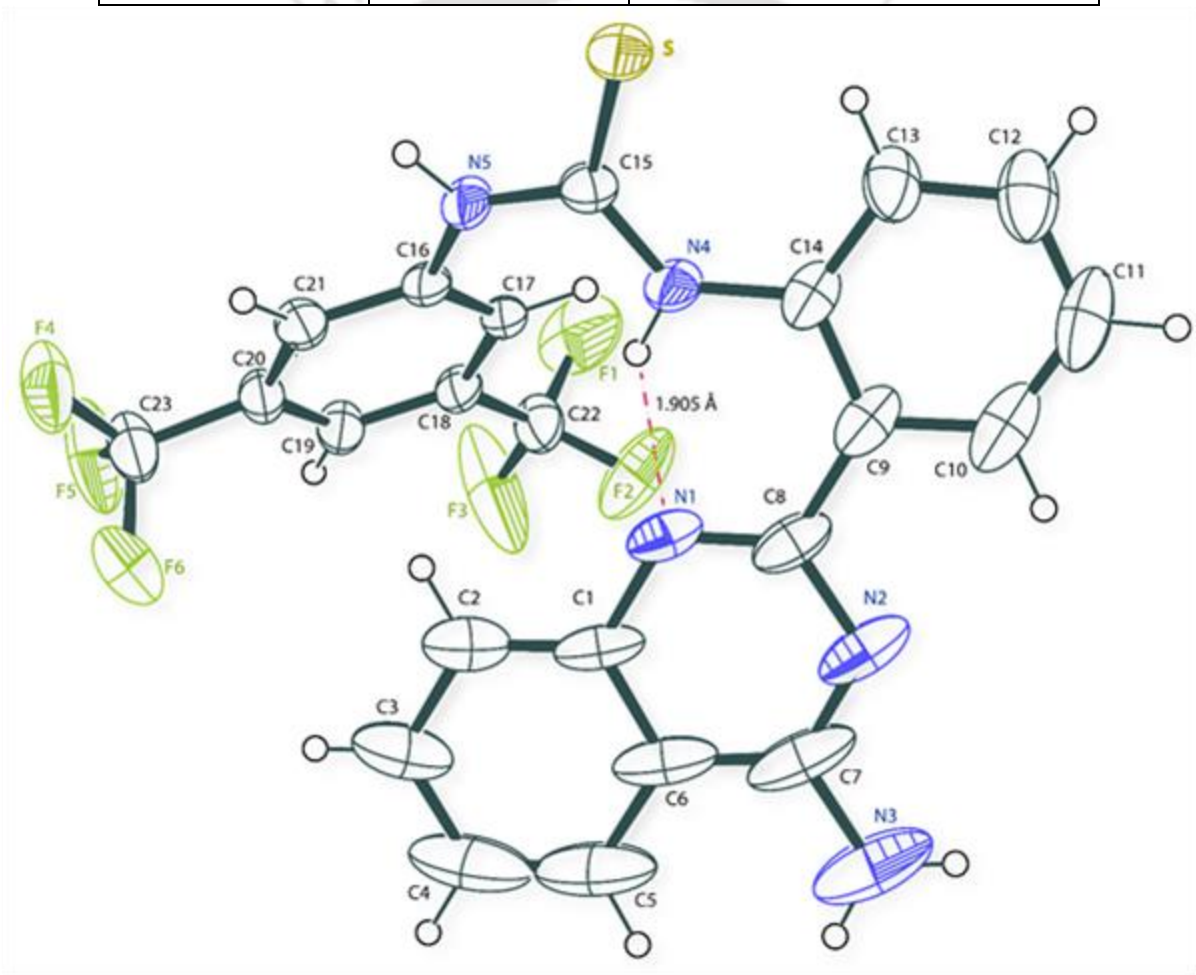

Figure 3.5. ORTEP diagram of **3.1f**.

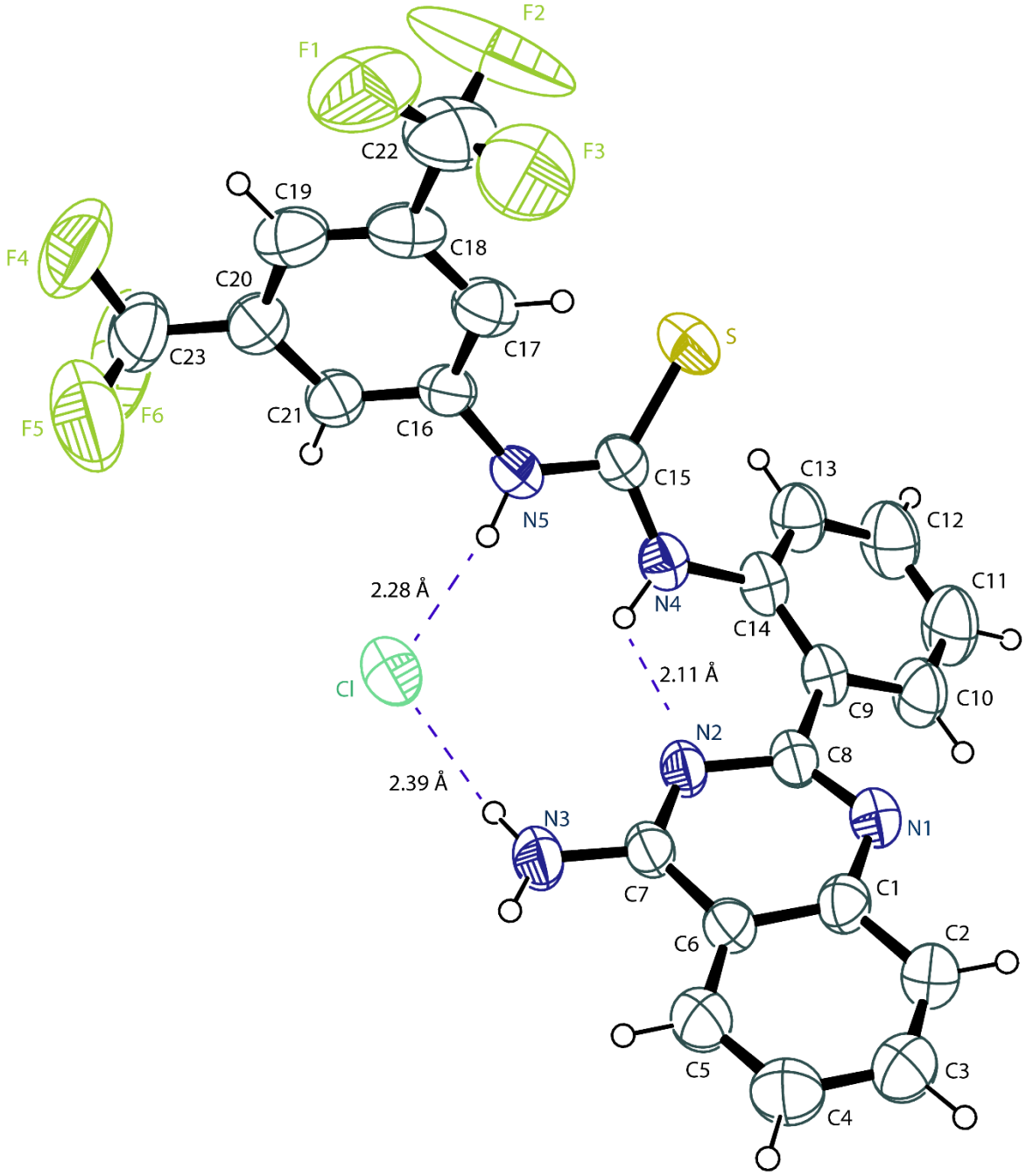

Figure 3.6. ORTEP diagram of complex **3.1f** with Cl^-.

3.4.4. Anion binding analysis by ^{1}H-NMR titration:

The ^{1}H NMR titration was performed for **3.1f** in DMSO-d_6. The stock solutions of the compound (10 mM) and TBACl, TBAF, TBABr, TBAI and $TBANO_3$ (1.5 M) were prepared in DMSO-d_6. The tetrabutylammonium or tetraethylammonium salts were used as the source of anions. The ^{1}H NMR titrations of compound in DMSO-d_6 were performed by the subsequent

addition of salt (0-15 equiv.). The changes in chemical shift (Δδ) values of the N-H protons of the compounds were analyzed. MestReNova software was used for the stacking of all the titration spectra. The BindFit v0.5 software fitted the changes in a chemical shift against the concentration of anions. The association constant (K_a) values were calculated using the BindFit v0.5 software (1:1 binding model).[2]

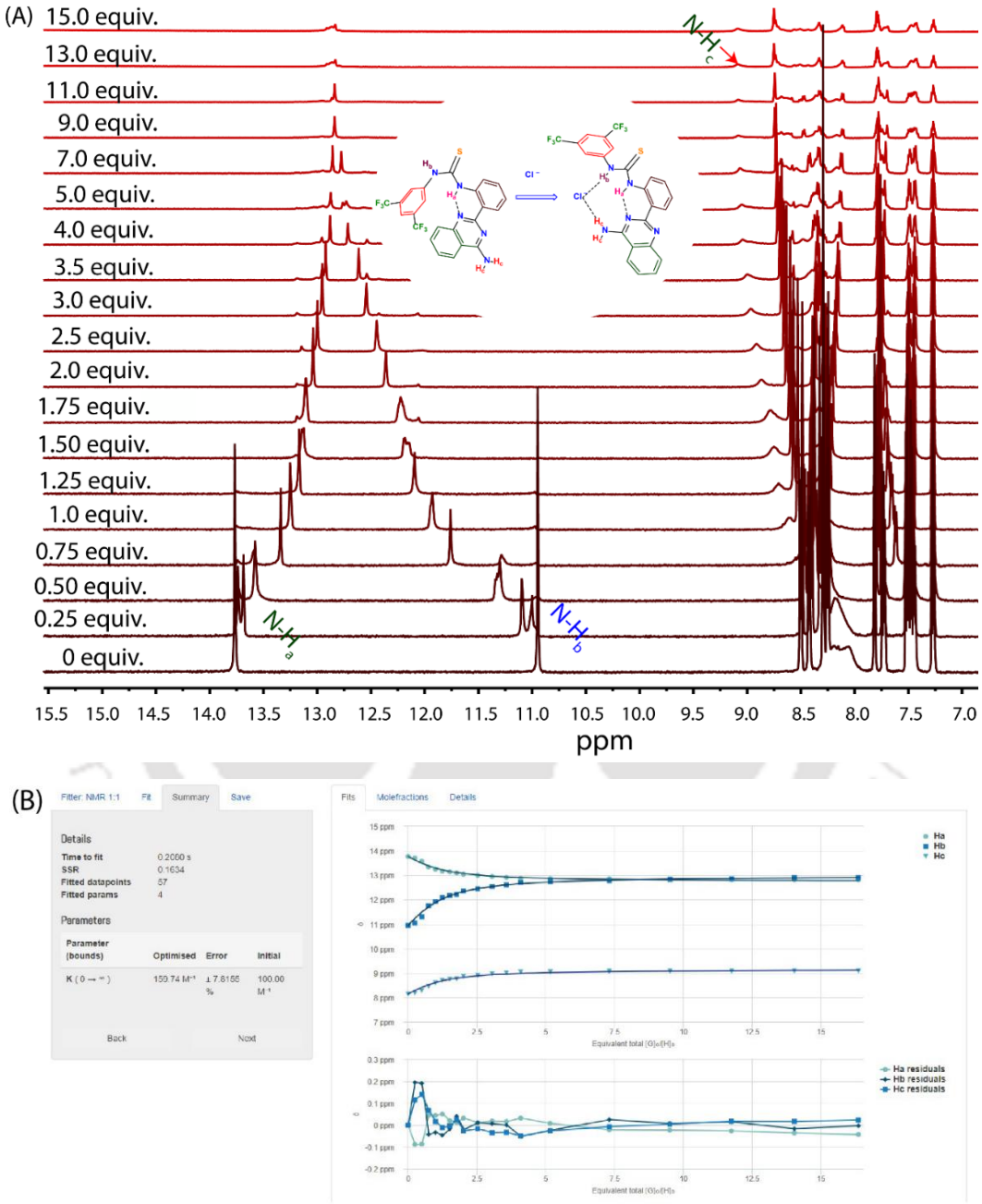

Figure 3.7. ^{1}H-NMR titration spectra for **3.1f** (10 mM) with the sequential addition of TBACl in DMSO-d_6 solvent. The amounts of added TBACl are shown on the spectra (**A**). The plot of chemical shift (δ) of N-H_a, N-

H_b and N-H_c protons vs. equivalent total ($[G]_0/[H]_0$) added, fitted to 1:1 binding model of BindFit v0.5 program (**B**). H = host = **3.1f** and G = guest = TBACl.

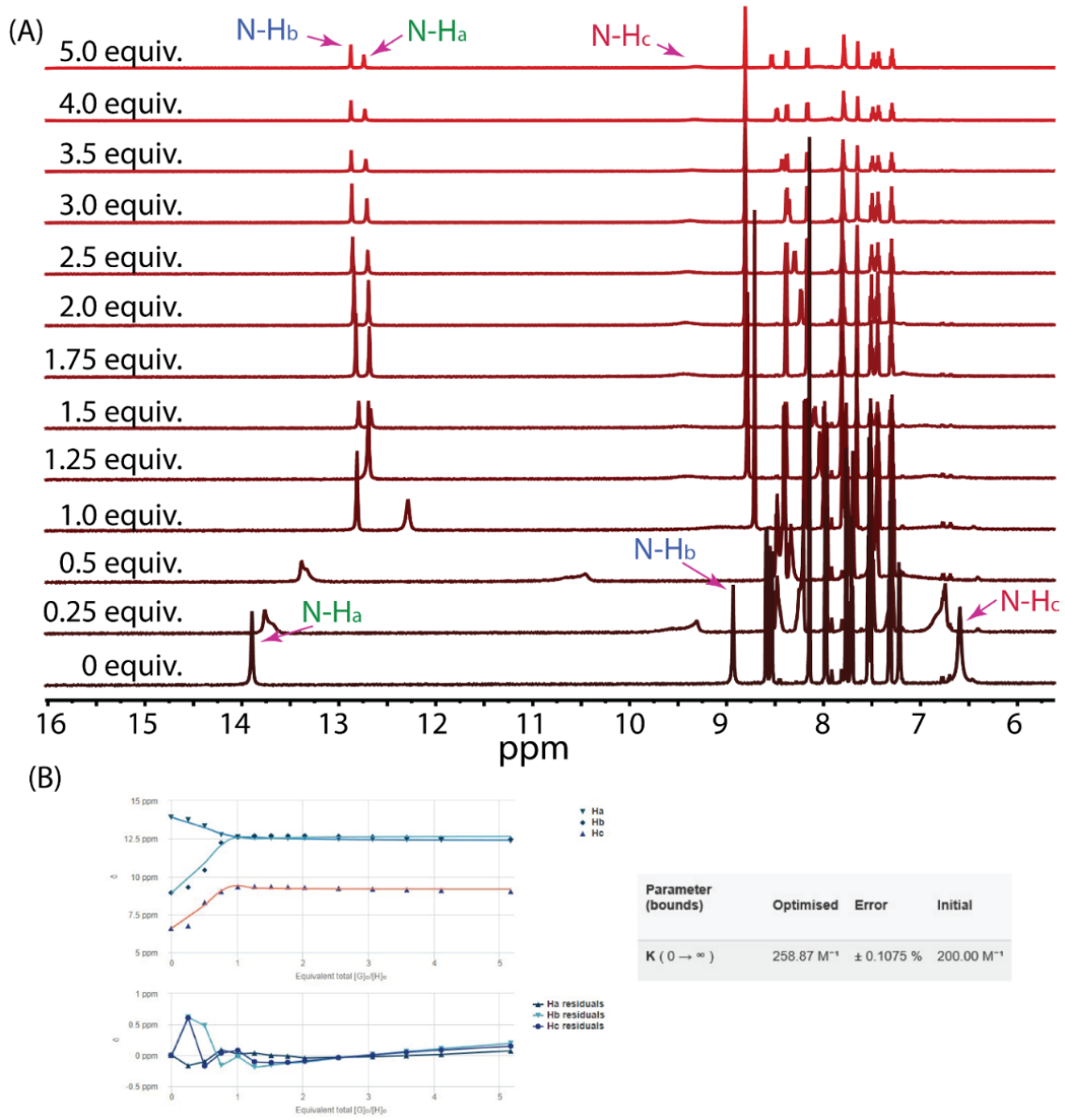

Figure 3.8. ^{1}H-NMR titration spectra for **3.1f** (10 mM) with the sequential addition of TBACl in CD_3CN solvent. The amounts of added TBACl are shown on the spectra (**A**). The plot of chemical shift (δ) of N-H_a, N-H_b and N-H_c protons vs. equivalent total ($[G]_0/[H]_0$) added, fitted to 1:1 binding model of BindFit v0.5 program (**B**). H = host = **3.1f** and G = guest = TBACl.

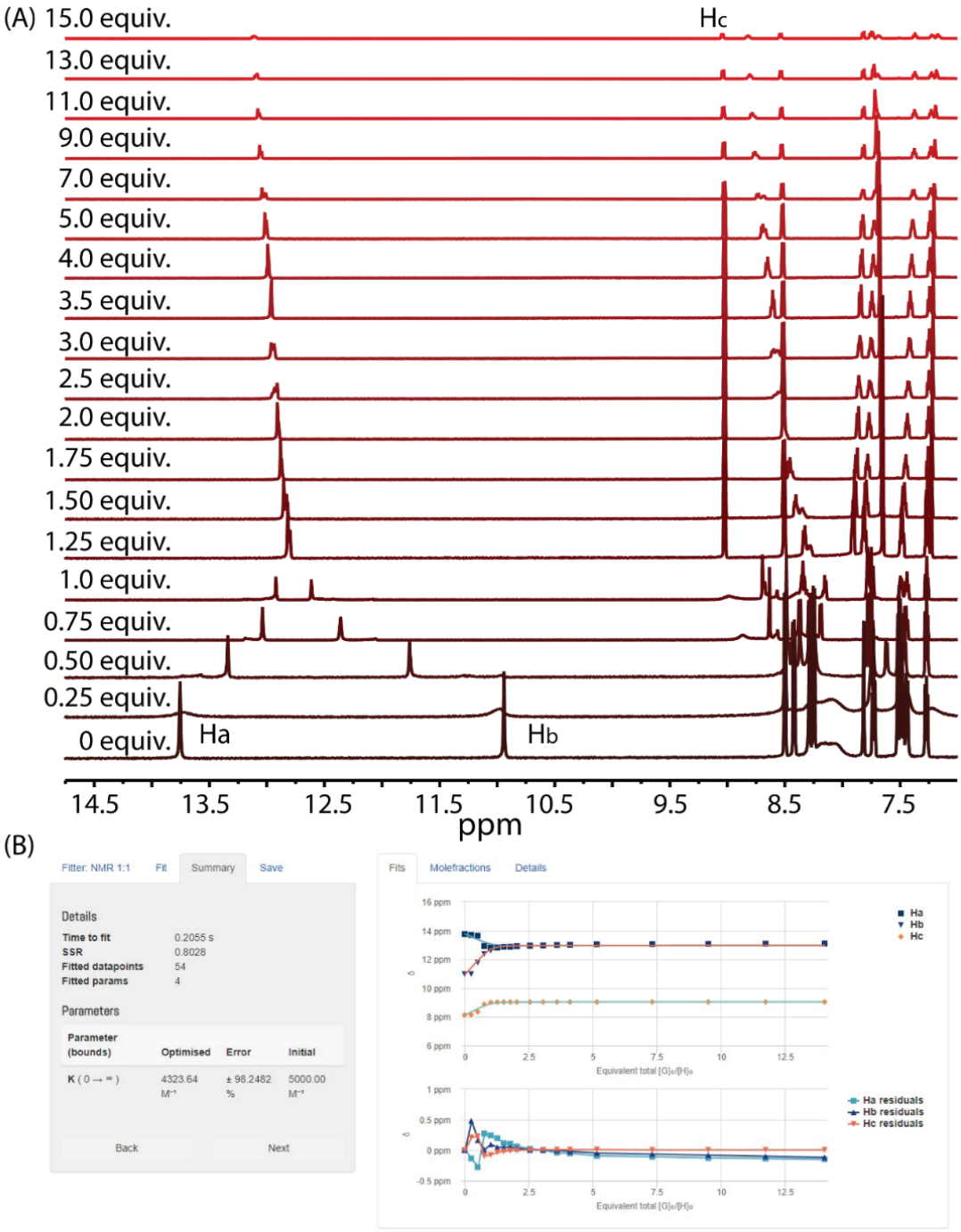

Figure 3.9. ^{1}H-NMR titration spectra for compound **3.1f (**10 mM) with the sequential addition of TBAF in DMSO-d_6 solvent. The amounts of added TBAF are shown on the spectra (A). The plot of chemical shift (δ) of N-Ha, N-Hb and N-Hc protons vs. equivalent total ($[G]_0/[H]_0$) added, fitted to 1:1 binding model of BindFit v0.5 program (B). H = host = **3.1f** and G = guest = TBAF.

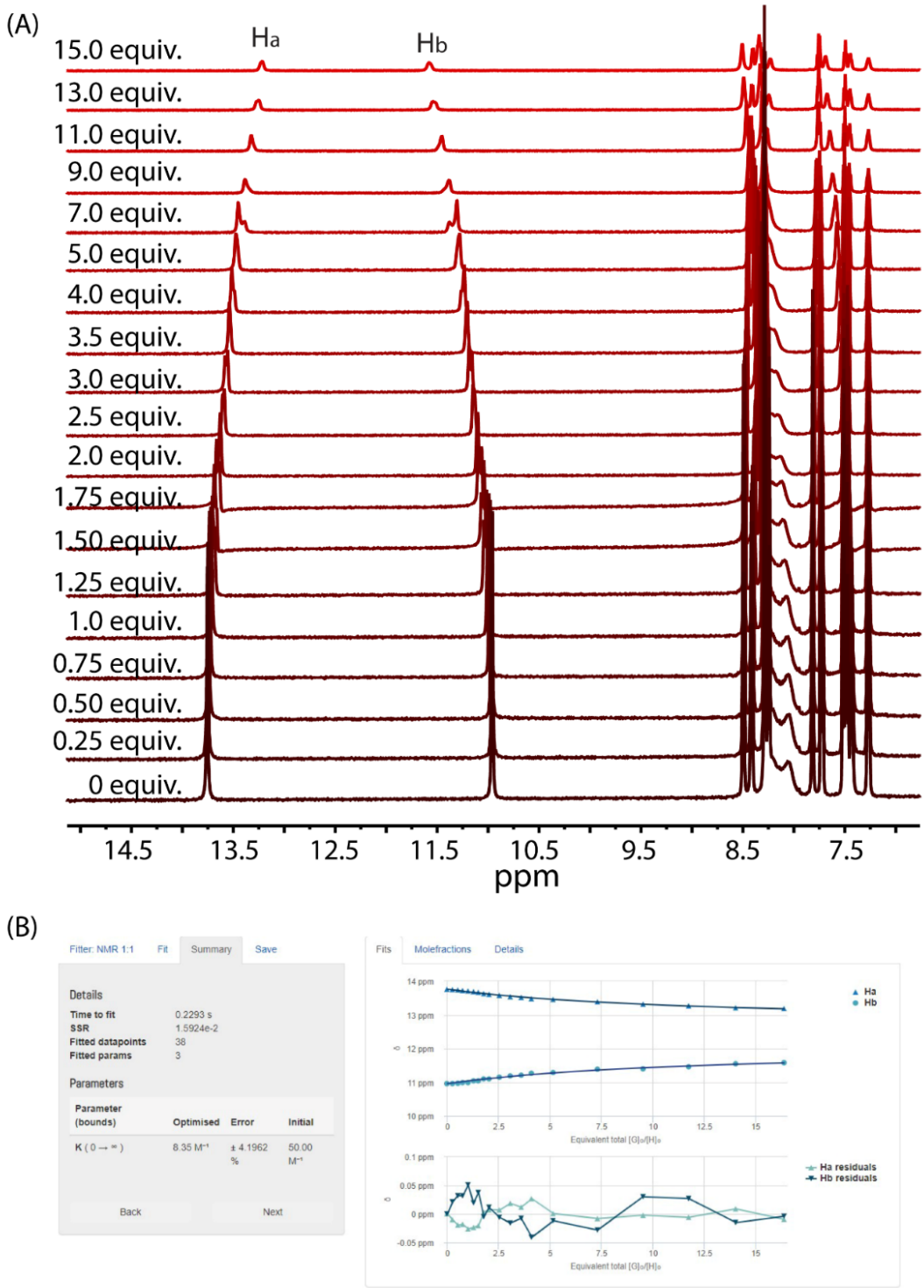

Figure 3.10. ^{1}H-NMR titration spectra for compound **3.1f (**10 mM) with the sequential addition of TBABr in DMSO-d_6 solvent. The amounts of added TBABr are shown on the spectra (A). The plot of chemical shift (δ) of N-H_a and N-H_b protons vs. equivalent total ($[G]_0/[H]_0$) added, fitted to 1:1 binding model of BindFit v0.5 program (B). H = host = **3.1f** and G = guest = TBABr.

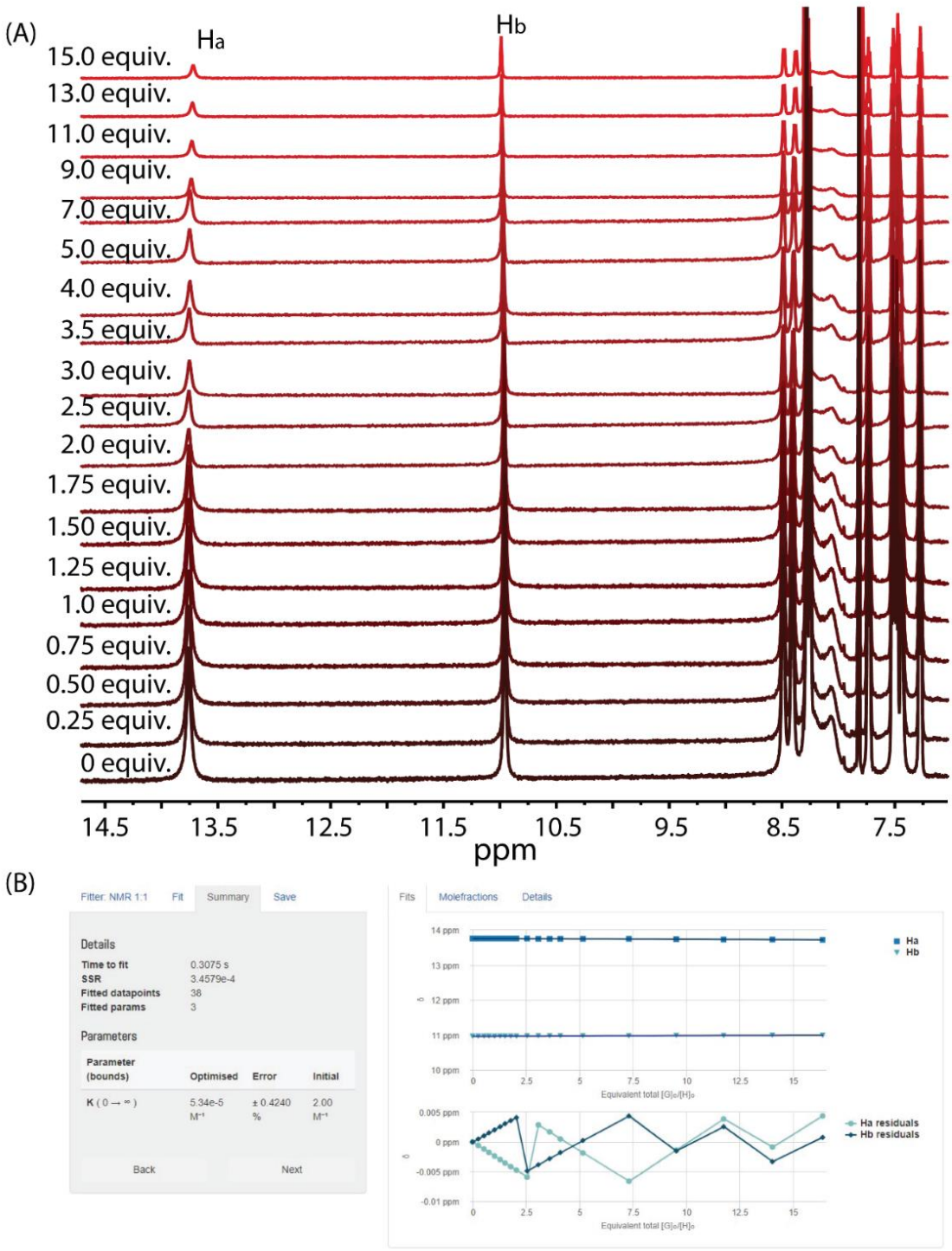

Figure 3.11. ^{1}H-NMR titration spectra for compound **3.1f (**10 mM) with the sequential addition of TBAI in DMSO-d_6 solvent. The amounts of added TBAI are shown on the spectra (A). The plot of chemical shift (δ) of N-H_a and N-H_b protons vs. equivalent total ($[G]_0/[H]_0$) added, fitted to 1:1 binding model of BindFit v0.5 program (B). H = host = **3.1f** and G = guest = TBAI.

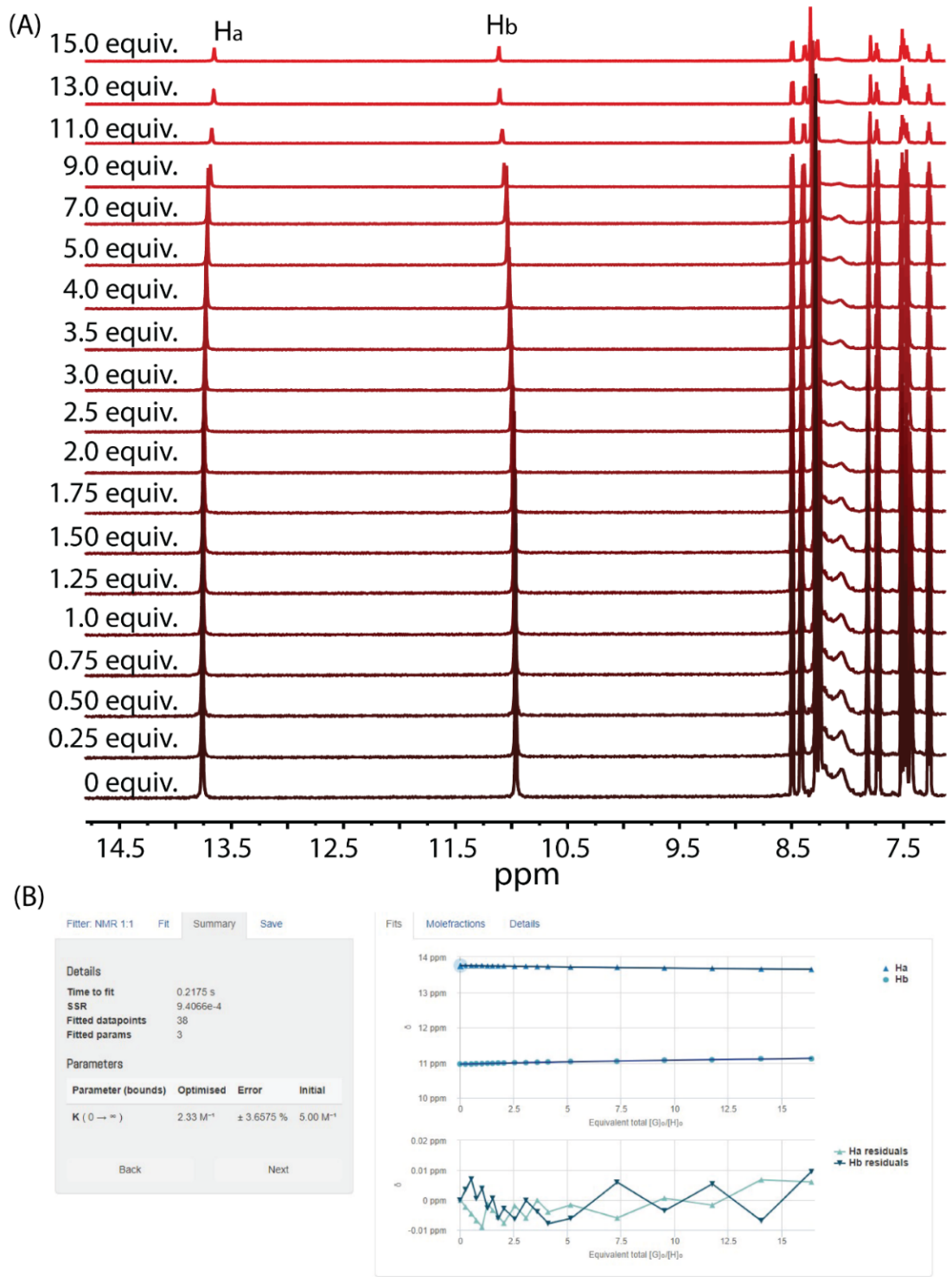

Figure 3.12. ^{1}H-NMR titration spectra for compound **3.1f (**10 mM) with the sequential addition of $TBANO_3$ in DMSO-d_6 solvent. The amounts of added $TBANO_3$ are shown on the spectra (A). The plot of chemical shift (δ) of N-H_a and N-H_b protons vs. equivalent total ($[G]_0/[H]_0$) added, fitted to 1:1 binding model of BindFit v0.5 program (B). H = host = **3.1f** and G = guest = $TBANO_3$.

3.4.5. Chloride binding study by using UV-Vis and fluorescence sensing:

To the Quartz fluorescence cuvette (1 mL), **3.1f** (10 µM) was taken in DMSO solvent. After that, the TBACl solution (stock concentration 1.5 M in DMSO) was added from 0 to 42 mM. In addition, the absorption and emission spectra of **3.1f** were also recorded.

In a quartz cuvette (2 mL) compound **3.1f** (10 mM) was taken in spectroscopic DMSO solvent, and different concentrations (from 0 to 42 mM) of tetrabutylammonium chloride (stock concentration 1.5 M in DMSO) were added. All fluorescence measurements were excited at 290 nm and 350 nm. After the saturation point, different amounts of Amberlite IRA-400 resin (1–6 mg) were added to the solution, and fluorescence spectra were taken at the excitation wavelength of 290 nm.

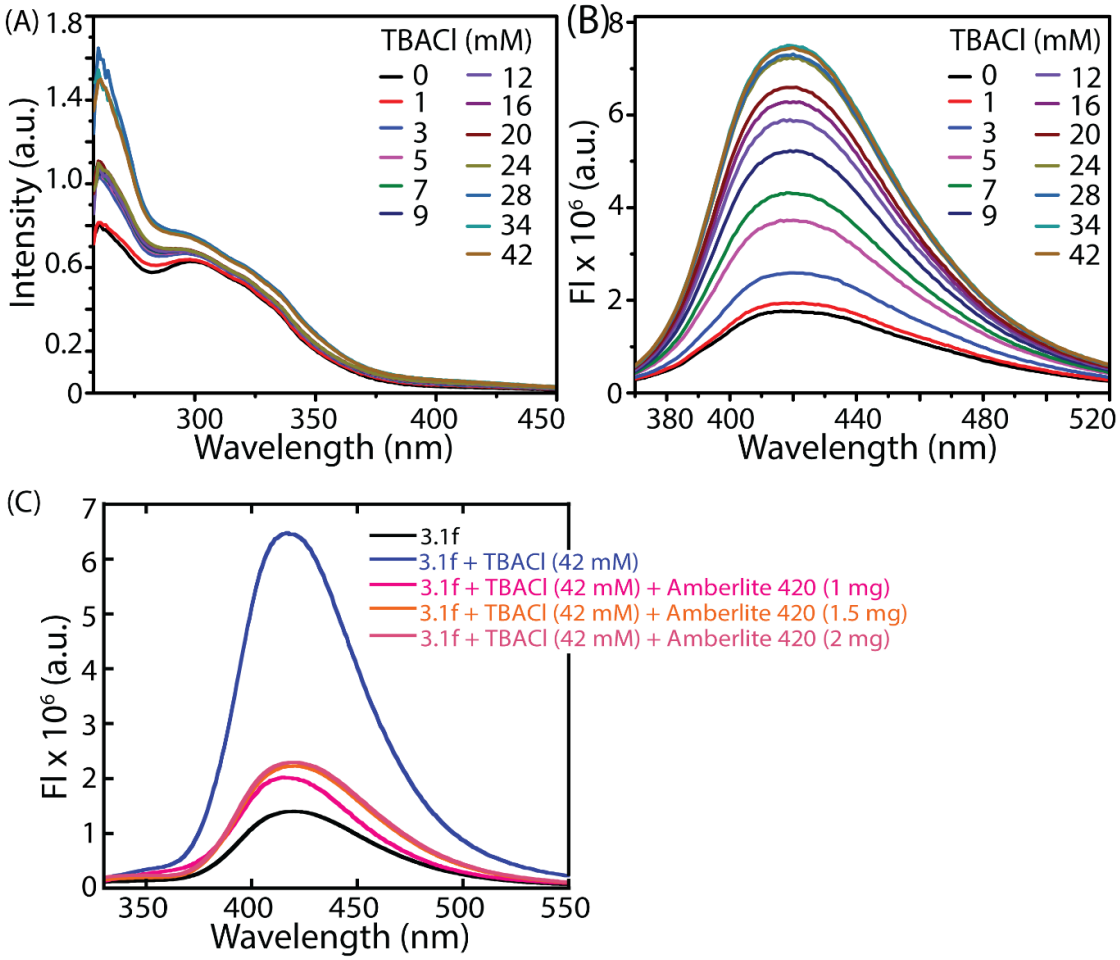

Figure 3.13. The UV-Vis spectra (A) of **3.1f** (10 µM) in DMSO solvent. Fluorescence spectra of **3.1f** with an excitation wavelength of 350 nm (B). The reversibility of Cl^- induced fluorescence enhance was tested using Amberlite 420 resin (C).

3.4.6. Ion transport activity studies:

3.4.6.1. Preparation of DPPC/POPS/CHOL-LUVs⊃lucigenin — In order to perform lucigenin-based ion transport studies, DPPC (50 mg/mL in deacidified $CHCl_3$), POPS (50

mg/mL in deacidified $CHCl_3$) and CHOL (25 mg/mL in deacidified $CHCl_3$) was taken in a clean sample vial in the molar ratio of 6:2:2. A thin lipid layer was formed when the fluid was continuously rotated for 6 hours under decreasing pressure. The thin lipid film was hydrated by the addition of 800 µL of 20 mM HEPES buffer containing 1 mM lucigenin and 100 mM $NaNO_3$ solution (pH 7.2 and 5.4). The resulting solution was vortexed 6-7 times for 1 h, subjected to 10-12 freeze-thaw cycles, and then sustained vortexing for 15 minutes to integrate lucigenin into the lipid bilayer. Using a mini-extruder, the lipid suspension was extruded through a polycarbonate membrane from Avanti Polar Lipids with a 200 nm pore size 19-21 times (must be an odd number). To achieve the final lipid content of 25 mM (assume 100% lipid regeneration), the unencapsulated lucigenin dye was removed using size exclusion column chromatography (Sephadex G-50), and a 20 mM HEPES buffer containing 100 mM $NaNO_3$ solution, pH 7.2 as the eluting solution.

3.4.6.2. Preparation of DPPC/POPS/CHOL-LUVs⊃HPTS — In order to prepare HPTS encapsulated LUVs, appropriate amounts of DPPC, POPS, and CHOL were combined in a clean, dry glass vial in the molar ratio of 6:2:2. A thin lipid layer was formed when the fluid was continuously rotated for 6 hours under decreasing pressure. The thin lipid film was hydrated by adding 800 µL of 20 mM HEPES, pH 7.2, 100 mM NaCl, and 1 mM HPTS. The resulting solution was vortexed 6-7 times for 1 hour and subjected to 10-12 freeze-thaw cycles. Finally, then sustained vortexing for 15 minutes to integrate HPTS within the lipid bilayer. Using a mini-extruder, the lipid suspension was extruded through a polycarbonate membrane from Avanti Polar Lipids with a 200 nm pore size 19-21 times (must be an odd number). To achieve the final lipid content of 25 mM (assume 100% lipid regeneration), the free unencapsulated HPTS dye was removed using size exclusion column chromatography (Sephadex G-50) and a 20 mM HEPES buffer containing 100 mM NaCl solution, pH 7.2 as the eluting solution.

3.4.6.3. Quantitative measurement of transport activity from lucigenin assay —

The fluorescence emission intensity of the Lucigenin dye, over the time range of t = 50 to t = 450 s, was adjusted to start all the kinetics spectra at 0. The transport capacity of the molecules was determined by measuring the fluorescence intensity (FI) at t = 450 s, prior to the inclusion of the Triton X-100 solution.

3.4.6.4. Quantitative measurement of transport activity from HPTS assay ─

The fluorescence emission intensity of the HPTS dye, over the time range of t = 50 to t = 450 s, was adjusted to start all the kinetics spectra at 0. The transport capacity of the molecules was determined by measuring the fluorescence intensity (FI) at t = 450 s, prior to the inclusion of the Triton X-100 solution.

3.4.6.5. Ion transport activity (lucigenin assay) ─ To perform the lucigenin assay, a 3 mL fluorescence cuvette was filled with 1950 µL of 20 mM HEPES buffer, pH 7.2, containing 100 mM NaCl, and 40 µL of the DPPC/POPS/CHOL-LUVs lucigenin. The cuvette was then placed in the fluorescence spectrophotometer under slow stirring conditions for 3-5 minutes to ensure a homogeneous solution. The kinetic experiment was initiated (at t = 0 s), and the excitation wavelength of lucigenin was 455 nm, with monitoring at 506 nm. After that, the cuvette was maintained in a stirring environment with the chamber temperature set to 25 ^{0}C. Compounds (final concentration 10 µM) were introduced to start the Cl^{-}inflow kinetics after 45 s. The vesicles were then lysed to end the kinetic experiment. At t = 450 s, the vesicles were finally lysed to end the kinetic experiment by adding 20% Triton X-100 (20 µL) to the cuvette, and fluorescence measurements were conducted for an additional 50 s (t = 500 s).

3.4.6.6. pH-dependent Cl^{-} transport activity across the DPPC/POPS/CHOL-LUVs⊃lucigenin ─ The vesicles were prepared following a similar procedure as the abovementioned method.

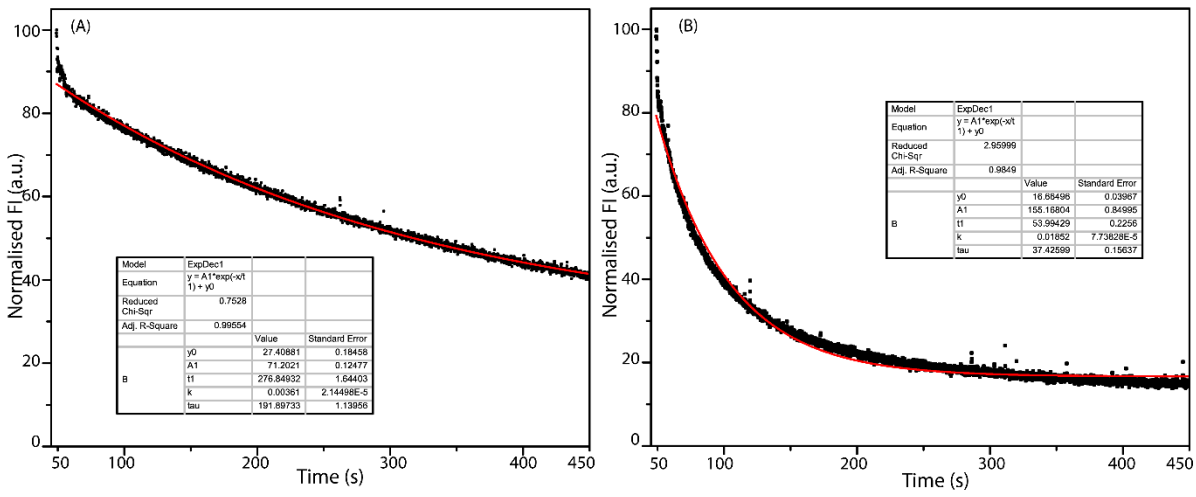

Figure 3.14. Normalized fluorescence quenching curves (F/F_0) were fitted to a first-order exponential decay equation.

3.4.6.7. Concentration-dependent lucigenin assay ─ Similar to the procedure mentioned above, the DPPC/POPS/CHOL-LUVs⊃lucigenin (pH 7.2 and 5.4) was created. The lucigenin dye's fluorescence signals (Y-axis) were scaled from 0 to 100 units [t = 50 to t = 500 s (X-axis)]. The transport activity of **3.1f** was determined using the normalized fluorescence intensity (FI) values obtained at t = 450 s (before the addition of Triton X-100). Using the earlier Eq.-S1, the transport activity (T) of chemical **3.1f** at a certain concentration was calculated. The transport activity values (Y-axis) were plotted versus concentration (X-axis) and fitted in the Hill equation to obtain the effective concentration (EC_{50}).[2]

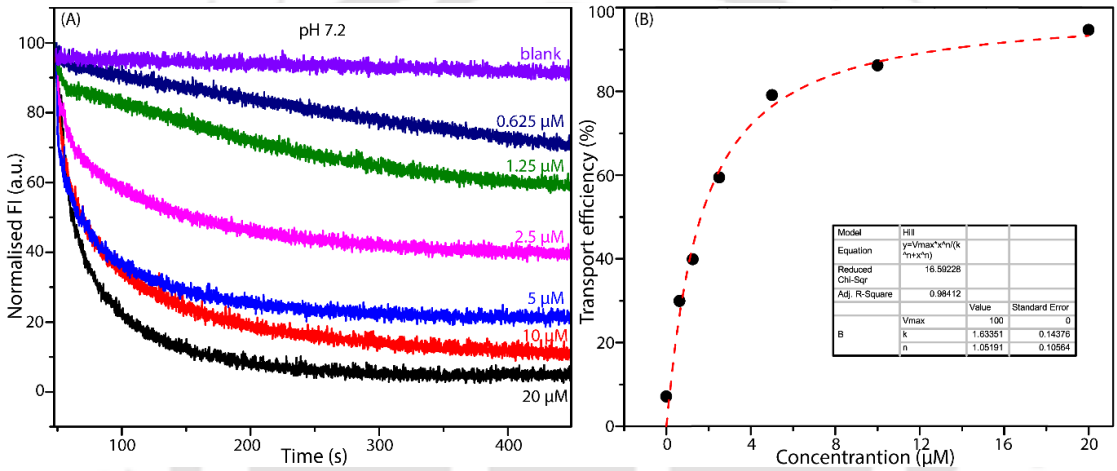

Figure 3.15. Concentration-dependent transmembrane transport of Cl^- in the presence of **3.1f** across the DPPC/POPS/CHOL-LUVs⊃lucigenin. The ion transport activity was measured by lucigenin fluorescence assay at pH 7.2. The EC_{50} value was calculated using the Hill equation (B). The compound concentration was varied from 20 to 0.625 µM.

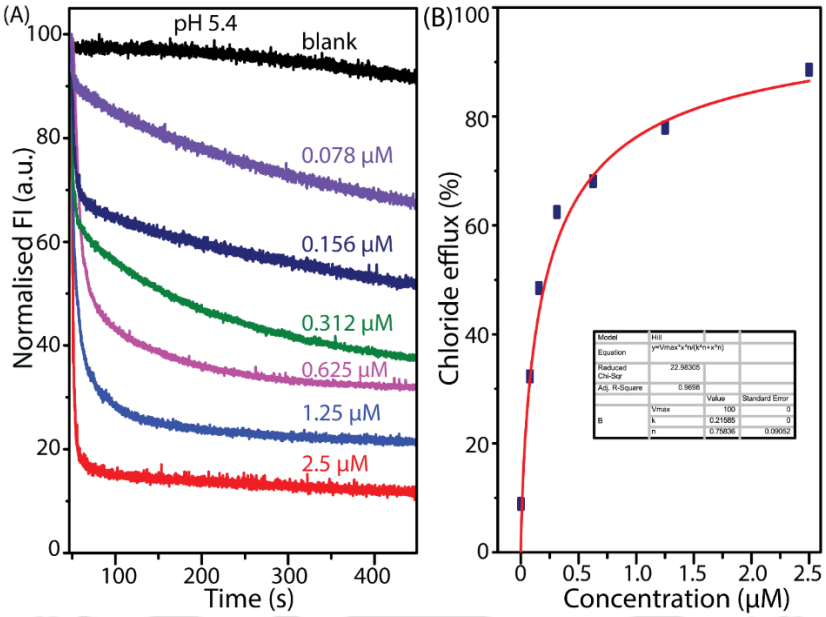

Figure 3.16. Concentration-dependent transmembrane transport of Cl^- ion in the presence of compound **3.1f** across the DPPC/POPS/CHOL-LUVs⊃lucigenin. The ion transport activity was measured by lucigenin fluorescence assay at pH 5.4. The EC_{50} value was calculated using the Hill equation (B). The compound concentration was varied from 2.5 to 0.078 μM.

3.4.6.8. Chloride transport activity of compound 1f, 4 and 5 across DPPC/POPS/CHOL-LUVs⊃lucigenin –

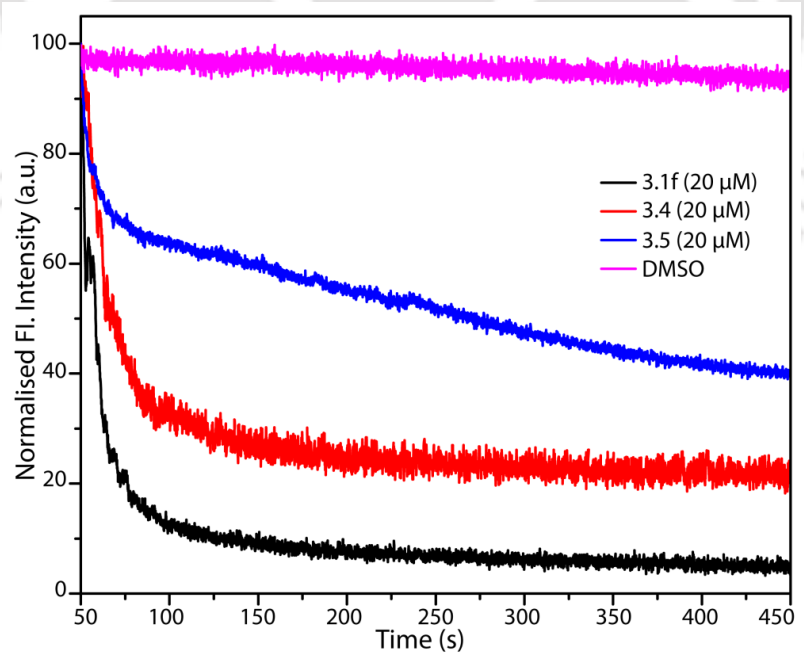

Figure 3.17. Cl^- transport activity of compound **3.1f**, **3.4** and **3.5** (20 μM) across DPPC/POPS/CHOL-LUVs⊃lucigenin.

3.4.6.9. Concentration dependent lucigenin assay of the compound 3.4 ─ Similar to the aforementioned procedure, the DPPC/POPS/CHOL-LUVs⊃lucigenin (pH 7.2) was prepared. The lucigenin dye's fluorescence signals (Y-axis) were scaled from 0 to 100 units [t = 50 to t = 500 s (X-axis)]. The transport activity of the compounds was determined using the normalised fluorescence intensity (FI) values obtained at t = 450 s (before the addition of Triton X-100). Using the earlier Eq.-S1, the transport activity (T) of compound **3.4** at a certain concentration was calculated. The transport activity in % (Y-axis) were plotted against concentration (X-axis) and fitted in the Hill 1 equation to obtain the effective concentration (EC_{50}) of the compound **3.4**.

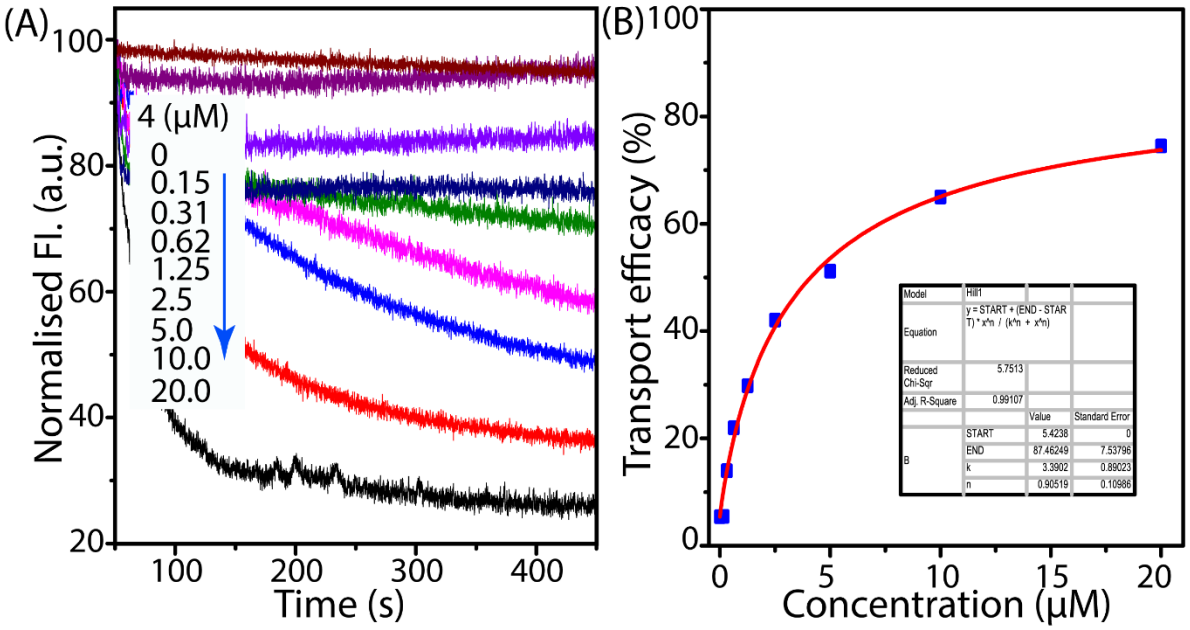

Figure 3.18. Concentration-dependent transmembrane transport of Cl^- ion in the presence of compound **3.4** across the DPPC/POPS/CHOL-LUVs⊃lucigenin (A). The ion transport activity was measured by lucigenin fluorescence assay at pH 7.2. The EC_{50} value was calculated using the Hill 1 equation (B). The compound concentration was varied from 20 to 0.15 μM. The EC_{50} of compound found 3.39 ± 0.89 μM.

3.4.6.10. Efflux study using chloride ion-selective-electrode (Cl-ISE) ─ Cl-ISE was used to assess the Cl^- efflux efficiency of the compound. Using 20 mM HEPES buffer with 100 mM NaCl and a different pH (pH 7.2), the DPPC/POPS/CHOL-LUVs were made in a manner similar to that described in the section above. The LUVs were first dialyzed against 100 mM

$NaNO_3$ in 20 mM HEPES buffer at a pH of 7.2 (iso-osmolar with the NaCl buffer). The Cl^- efflux efficiency of **3.1f** was assessed using the equation mentioned above.

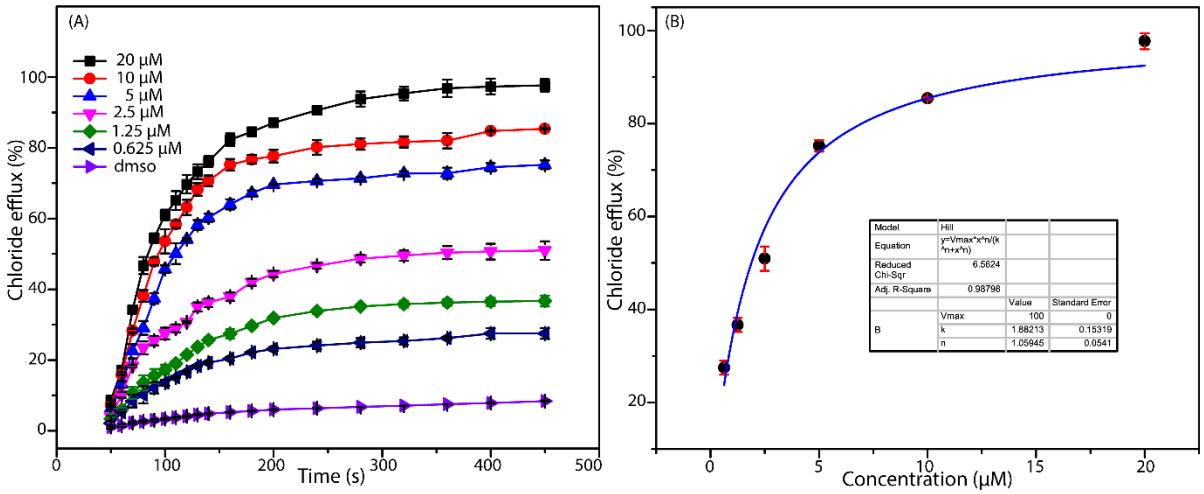

Figure 3.19. Concentration-dependent transmembrane transport of Cl^- in the presence of **3.1f** across the DPPC/POPS/CHOL-LUVs⊃lucigenin. The ion transport activity was measured by using Cl-ISE at pH 7.2 (A). The EC_{50} value was calculated using the Hill equation (B). The compound concentration was varied from 20 to 0.625 µM.

3.4.6.11. Ion transport activity (HPTS assay) ─ To prepare the solution for the HPTS assay, 1950 µL of 20 mM HEPES buffer, pH 7.2, with 100 mM NaCl, and 40 µL of the DPPC/POPS/CHOL-LUVs⊃HPTS was placed in a 3 mL fluorescence cuvette. The cuvette was then placed in the fluorescence spectrophotometer under slow stirring conditions for 3 to 5 minutes to ensure a homogeneous solution. HPTS fluorescence emission was measured at 506 nm (excited at 455 nm) when the kinetic experiment got underway (at t = 0 s). Following this, the cuvette was maintained in a stirring state with the chamber temperature set to 25 ºC. The compound (10 µL of 10 µM DMSO stock solution) was introduced after 45 s to start the Cl^- inflow kinetics. The vesicles were lysed by adding 20% Triton X-100 (20 L) to the cuvette at t = 450 s to end the kinetic experiment, and fluorescence measurements were conducted for an additional 50 s (t = 500 s).

3.4.6.12. Anion selectivity studies ─

Described in section 2.4.5.8.

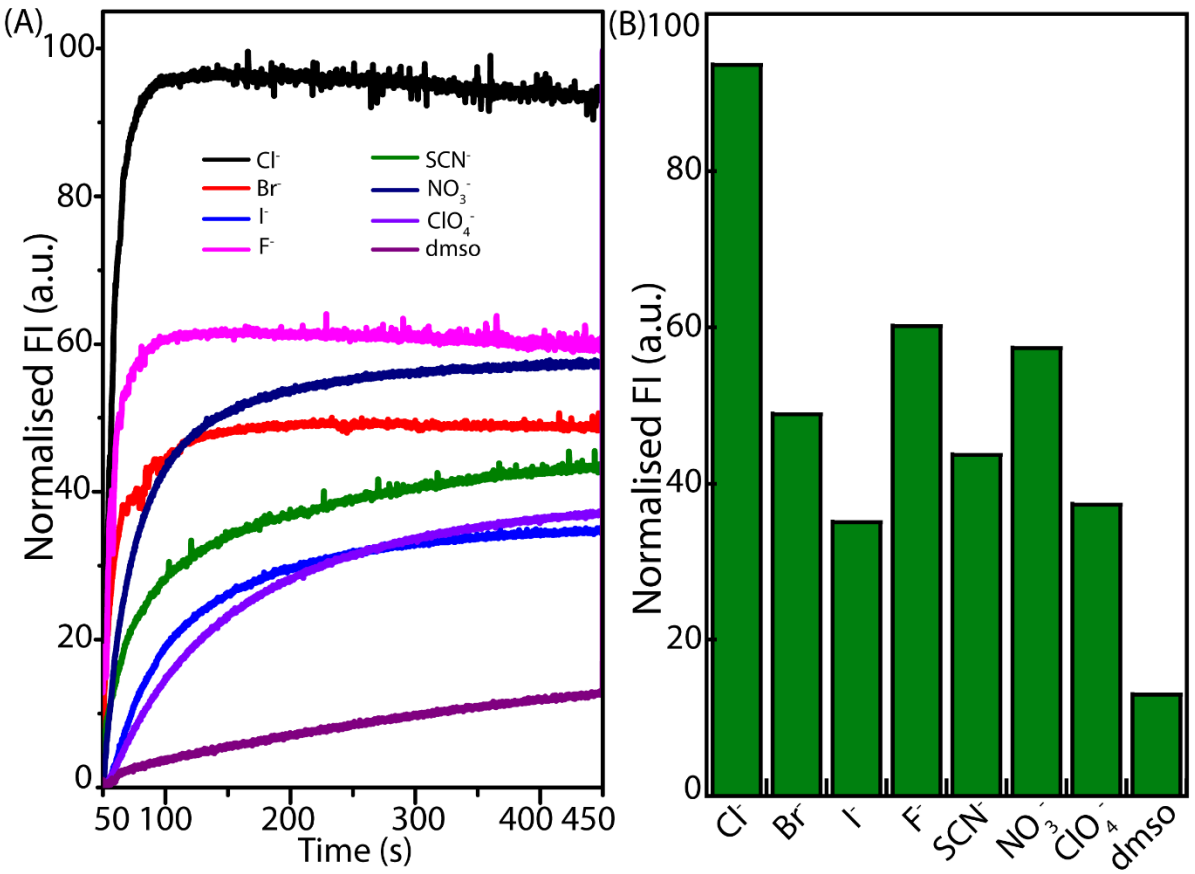

Figure 3.20. The anion transport selectivity of **3.1f** (20 μM) across the DPPC/POPS/CHOL-LUVs⊃HPTS (6:2:2 molar ratio) was measured at pH 7.2 (A), percentage of Cl^- efflux in the presence of different anions (B).

3.4.6.13. Cation selectivity assay across DPPC/POPS/CHOL-LUVs⊃lucigenin –

Described in section 2.4.5.8.

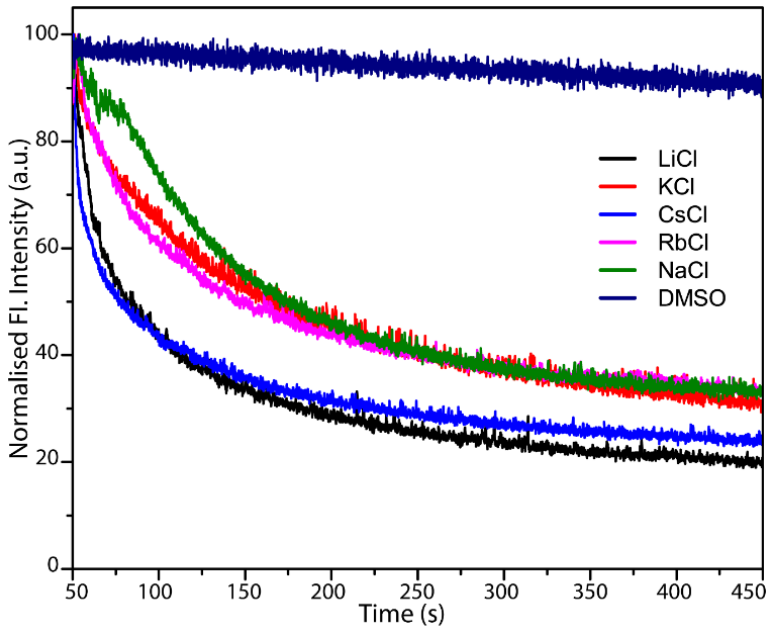

Figure 3.21. Cation selectivity of **3.1f** (5 μM) measured by varying external cations (M^+ = Li^+ , Na^+ , K^+ , Rb^+ , Cs^+) across DPPC/POPS/CHOL-LUVs⊃lucigenin.

3.4.7. Evidence for the mechanistic pathway for Cl^- transport:

3.4.7.1. Ion transport activity in the presence of FCCP (FCCP assay) ─ The ion transport activity was evaluated in the presence and absence of FCCP (H^+ selective transporter). In a 3 mL fluorescent cuvette, 1950 μL of 20 mM HEPES buffer, pH 7.2, including 100 mM NaCl, and 40 μL of the DPPC/POPS/CHOL-LUV⊃HPTS were placed. The cuvette was then placed into the fluorescence equipment and stirred for 3 minutes. The compound **3.1f** (8 μL of the stock solution in DMSO) and 2 μL of FCCP solution in DMSO (5 μM) were then added to the solution at t = 45 s. After 45 seconds, compound **3.1f** (final concentration) pulse was introduced to the cuvette to start the Cl^- transfer kinetics. After 450 s, the kinetic experiment was stopped by adding 20 μL of 20% Triton-X100 solution to the cuvette (to rupture the vesicular arrangements), and the fluorescence measurements were continued for another 45 s (t = 500 s). The control experiment was likewise conducted in the absence of FCCP.

3.4.7.2. Ion transport activity in the presence of Valinomycin (Valinomycin assay) ─ The vesicles were made using the same method described in the preceding section. The activity of ion transport was evaluated in the absence and presence of valinomycin. In a 3 mL fluorescent cuvette, 1950 μL of 20 mM HEPES buffer, pH 7.2, including 100 mM KCl, and 40 μL of the DPPC/POPS/CHOL-LUV⊃HPTS were placed. The cuvette was then placed into the

fluorescence equipment and stirred for 3 minutes. The intensity of the HPTS fluorescence was then measured (t = 0 s) at 510 nm (λ_{ex} = 450 nm). The compound (8 µL of the stock solution in DMSO) and 2 µL of valinomycin solution in DMSO (10 nM) were then added to the solution at t = 45 s to commence the Cl^- transport kinetics. After 450 seconds, the kinetic experiment was stopped by pouring 20 µL of 20% Triton-X100 solution into the cuvette (to break the vesicular arrangements), and the fluorescence measurements were continued for another 50 s (t = 500 s). The control experiment was likewise carried out in the absence of valinomycin.

3.4.7.3. U-tube experiment:

The U-tube experiment was carried out to verify this H^+/Cl^- co-transport (either inflow or efflux) mechanism of the compound in an acidic medium. The left arm of the U-tube was filled with 0.1 M aqueous HCl solution (pH 1.2), while the right arm was filled with isotonic $NaNO_3$ and separated by chloroform (organic layer). The chloroform layer is thought to be a lipid bilayer mimic. The transit of Cl^- and H^+ ions was monitored with a Cl-ISE and a pH meter, respectively. The **3.1f** (20 µM) was put in the chloroform layer, and measurements were taken for 70 hours.

3.4.8. Evidence for mobile carrier mechanism:

3.4.8.1. Transport activity across DPPC-lucigenin assay— The transport activity of the drugs was evaluated using a fluorescence spectrophotometer in this DPPC-lucigenin experiment. 1950 µL of 20 mM HEPES buffer, pH 7.2, including 100 mM NaCl, and 40 µL of DPPC-LUV⊃lucigenin were placed in a 3 mL fluorescence cuvette for this test. The kinetic experiment began (at t = 0 s), and the emission of lucigenin fluorescence was measured at 506 nm (excited at 455 nm). The cuvette was then stirred, and the chamber temperature was adjusted to 25 ºC. After 45 s, the compound (10 µL of DMSO stock solution) was introduced to begin the Cl^- inflow kinetics. Finally, at t = 450 s, the vesicles were lysed by adding 20% Triton X-100 (20 µL) to the cuvette, and fluorescence measurements were continued for another 50 s (t = 500 s). A comparable measurement was carried out to assess the transport efficiency at 45 ºC. To calculate the half-life and starting rate at different temperatures, the time-dependent lucigenin fluorescence plot was fitted with a first order exponential decay equation.

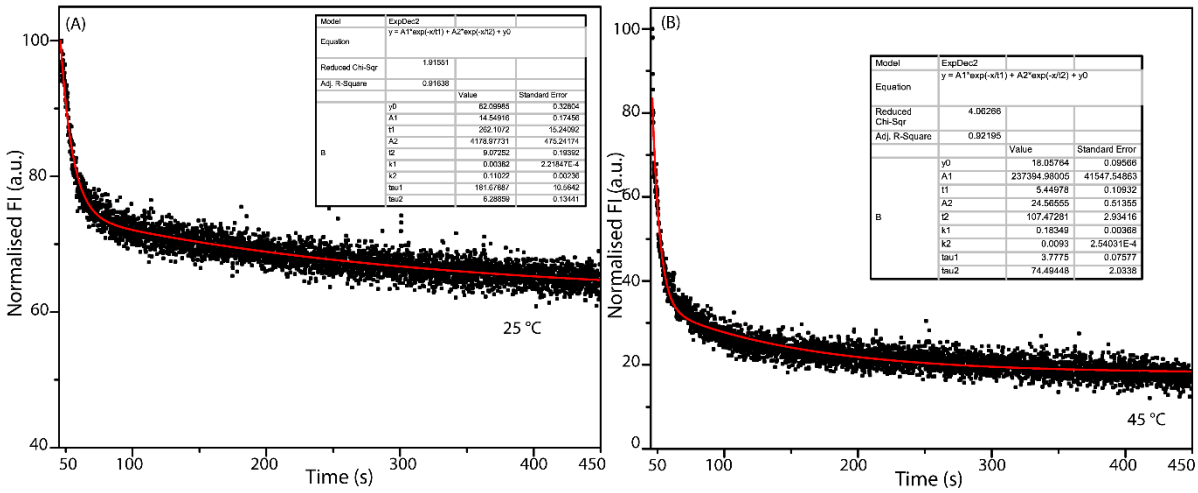

Figure 3.22. Normalized fluorescence quenching curves (F/F_0) were fitted to an exponential decay 2 equation.

3.4.9. Preparation of DPPC/POPS/CHOL-LUV⊃CF:

A thin lipid film was prepared by evaporating a solution of DPPC/POPS/CHOL in 0.5 ml $CHCl_3$ in vacuum for 4 h. After that lipid film was hydrated with 0.5 mL buffer (20 mM HEPES, 100 mM NaCl, 50 mM Carboxyfluorescein (CF), pH 7.2) for 1 hour with occasional vortexing of 3-5 times and then subjected to freeze-thaw cycle (≥ 15 times). The vesicle solution was extruded through a polycarbonate membrane with 200 nm pores 19-21 times (it must be an odd number) to give vesicles with a mean diameter of ~ 200 nm. Size exclusion chromatography (Sephadex G-50) with 20 mM HEPES buffer (100 mM NaCl, pH 7.2 final) was used to remove the extracellular dye. Final concentration: ~25 mM lipid; intravesicular solution: 20 mM HEPES, 100 mM NaCl, 50 mM CF, pH 7.2; extravesicular solution: 20 mM HEPES, 100 mM NaCl, pH 7.2.

3.4.10. Carboxyfluorescein (CF) leakage assay — In a clean and dry fluorescence cuvette, 40 µL of the aforementioned lipid solution and 1950 µL of 20 mM HEPES buffer (100 mM NaCl, pH 7.2) were mixed slowly by a magnetic stirrer fitted with the fluorescence equipment (at t = 0 s). The temporal path of CF fluorescence emission intensity, F_t, was recorded at λ_{em} = 517 nm (λ_{ex} = 492). The compound was added at t = 50 s, and finally, at t = 450 s, 20 µL of 20% Triton X-100 was injected to lyse those vesicles for 100% Cl^- inflow. Fluorescence intensities (F_t) were normalized to fractional emission intensity (IF) using Eq. S2. This investigation demonstrated that neither the bilayer membranes damaged nor large transmembrane pores were generated by **3.1f.**

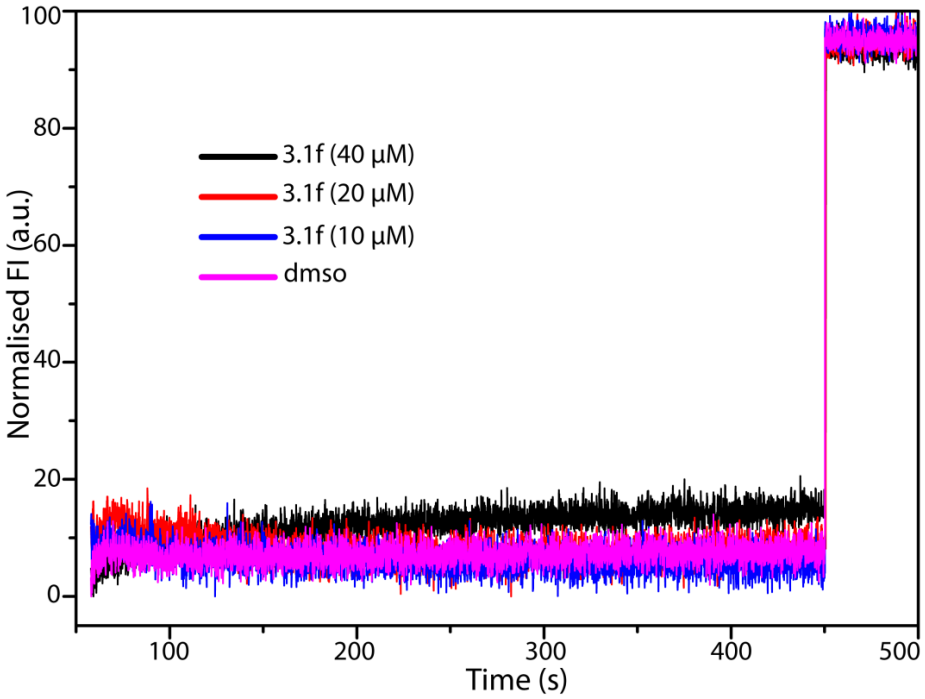

Figure 3.23. The carboxyfluorescein leakage assay of **3.1f** across DPPC/POPS/CHOL-LUV⊃CF.

3.4.11. pKa determination of by UV-Visible titration:

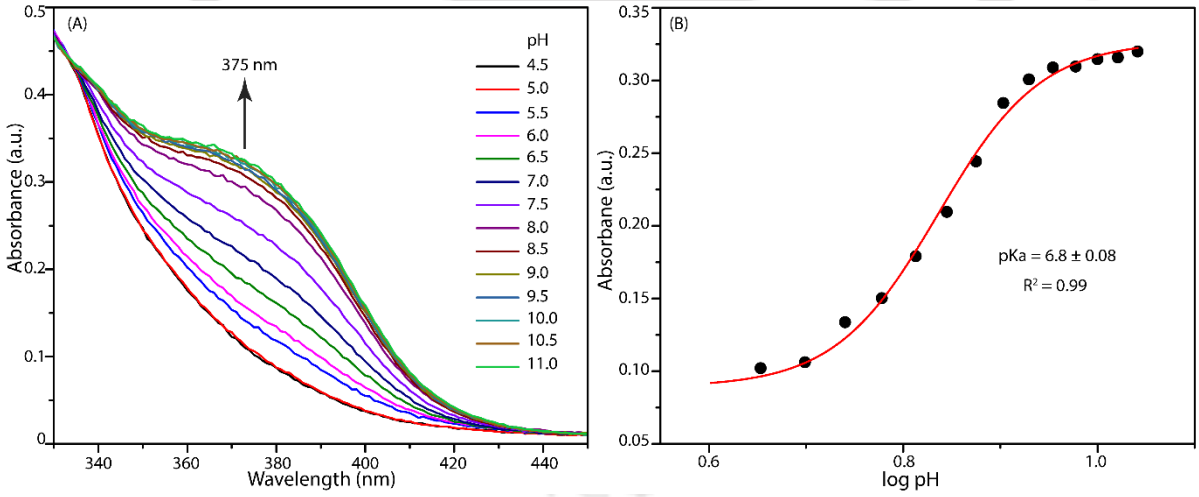

Figure 3.24. Absorbance spectra of **3.1f** (20 μM) at different pH in 9:1 DMSO/H_2O (v/v) solution containing 0.1 M NaCl (A). Comparison plots of absorbance at 375 nm at different pH (B).

3.4.12. Antibacterial activity studies:

Using the micro broth dilution method, the antibacterial efficacy of the compound was assessed against gram-positive (*S. aureus* (MTCC 96) and MRSA) and gram-negative strains (*E. coli* (MTCC 1687)). The MIC values were calculated as its lowest concentration at which visible

growth of the microorganism is inhibited. The assay was performed according to the CLSI guidelines. At 37 °C and 180 rpm, the bacteria were grown in an LB medium (Luria Bertani Broth). As soon as the desired optical density had been attained, the bacteria were centrifuged and washed with distilled water before being diluted to 10^6 CFU/mL in an LB medium. Serial dilution of the compound was performed in a 96-well plate using a micropipette. The cells were added to the serially diluted solution of the compound and incubated at 37 °C for 14-16 hours. Following incubation, the OD_{600} was measured with a BioTek Epoch microplate reader to determine the MIC. In order to obtain the most accurate MIC values, this assay was repeated at different concentration ranges. The error value was calculated as the standard deviation obtained through the mean of the repeated assay results.

To assess the bactericidal activity, 10 µL of the culture from MIC wells exhibiting visibly inhibited growth were subsequently transferred into 100 µL of a fresh medium within neighbouring wells. The 96 well-plate was then incubated at 37 °C for duration of 24 hrs, following which the optical density was determined at a wavelength of 600 nm. Simultaneously, 10 µL of culture was taken from the well with the MIC concentration and plated on an agar plate for the duration of 24 hours to determine the bactericidal activity.

Table 3.2. Antibacterial activity of the compounds.

MIC (µM)			
Compounds	*S. aureus* (MTCC 96)	MRSA (ATCC 33592)	*E. coli* (MTCC1687)
3.1a	>50	-	-
3.1b	>50	-	-
3.1c	>50	-	-
3.1d	>50	-	-
3.1e	20.0 ± 5.00	10.0 ± 2.50	>100
3.1f	2.34 ± 0.39	2.50 ± 0.50	>100
3.2a	>50	-	-
3.2b	>50	-	-
3.4	12.75 ± 1.25	-	-
3.5	15.625 ± 3.125	-	-

2-(2-aminophenyl)quinazolin-4-amine	>75	-	-
2-(quinazolin-2-yl)aniline	>75	-	-

Note: The **3.1f** was tested for its antibacterial activity against gram-negative and gram-positive strains. The compound showed enhanced antibacterial activity against Gram-positive strains. However, the poor antibacterial activity of the compound was observed activity against gram-negative strain (*E. coli*). This may be because gram-negative bacteria have an extra outer membrane shielding them from such compounds (**Table 3.2**). Compounds **3.1a-f, 3.2a-b, 3.4, 3.5, 2-(2-aminophenyl)quinazolin-4-amine and 2-(2-aminophenyl)quinazolin-4-amine** were also tested against *S. aureus* (gram-positive bacteria). It should be noted that only compounds **3.1e and 3.1f** showed antibacterial activities with **3.1f** being better antibacterial compound. This data correlates with the Cl^- transport activity of the mentioned compounds (**Figure 3.3A)**.

The **3.1f** showed a bactericidal effect at a concentration as low as the MIC. Thus, it can be inferred that the compound is highly potent and is able to kill Gram-positive bacteria at a very low dose. This finding is conspicuous as it suggests that this chemical entity has promising potential in the treatment of bacterial infection, primarily caused by drug-resistant strains. The efficacy of **3.1f** in achieving a bactericidal effect demonstrates its robust and precise mode of action against the bacteria and indicates its potential significance in altering essential physiological and biological pathways necessary for the organism's survival. Moreover, the ability of **3.1f** to transport Cl^- ions across membranes suggests its potential role in disrupting the Cl^- homeostasis, potentially resulting in bacterial cell death.

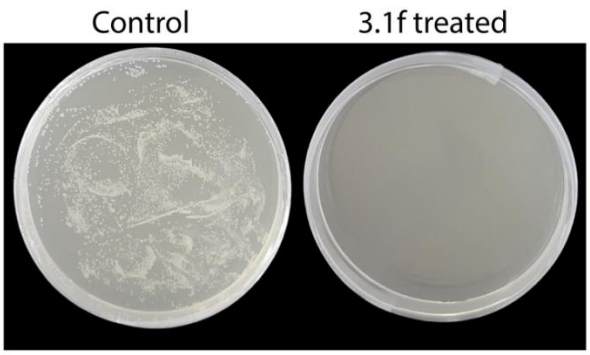

Figure 3.25. Minimum bactericidal concentration of **3.1f** at MIC concentration.

3.4.12.1. Time-kill assay:

This study aimed to evaluate the antibacterial activity of the tested compound over the specified duration. The *S. aureus* (MTCC 96) cells were cultured until they had reached the mid-logarithmic phase of their growth. The inoculum was prepared by diluting the culture in LB medium to obtain an optical density of 0.1. The compound was prepared in PBS buffer together with LB medium in a final concentration of 10 × MIC (20 μM). After the addition of the inoculum, samples were incubated at 37 °C and 180 rpm. Samples were collected at different time points (0, 1, 2, 4, 8, and 12 hours) and stored at -20 °C. Once all samples were collected, they were centrifuged at 5000 rpm for 5 minutes, and the supernatant was removed. The samples were then diluted three-fold and inoculated onto agar plates using a spreader. The plates were then incubated overnight at 37 °C, and the resulting colonies were counted manually to determine the colony-forming units per milliliter (CFU/mL).

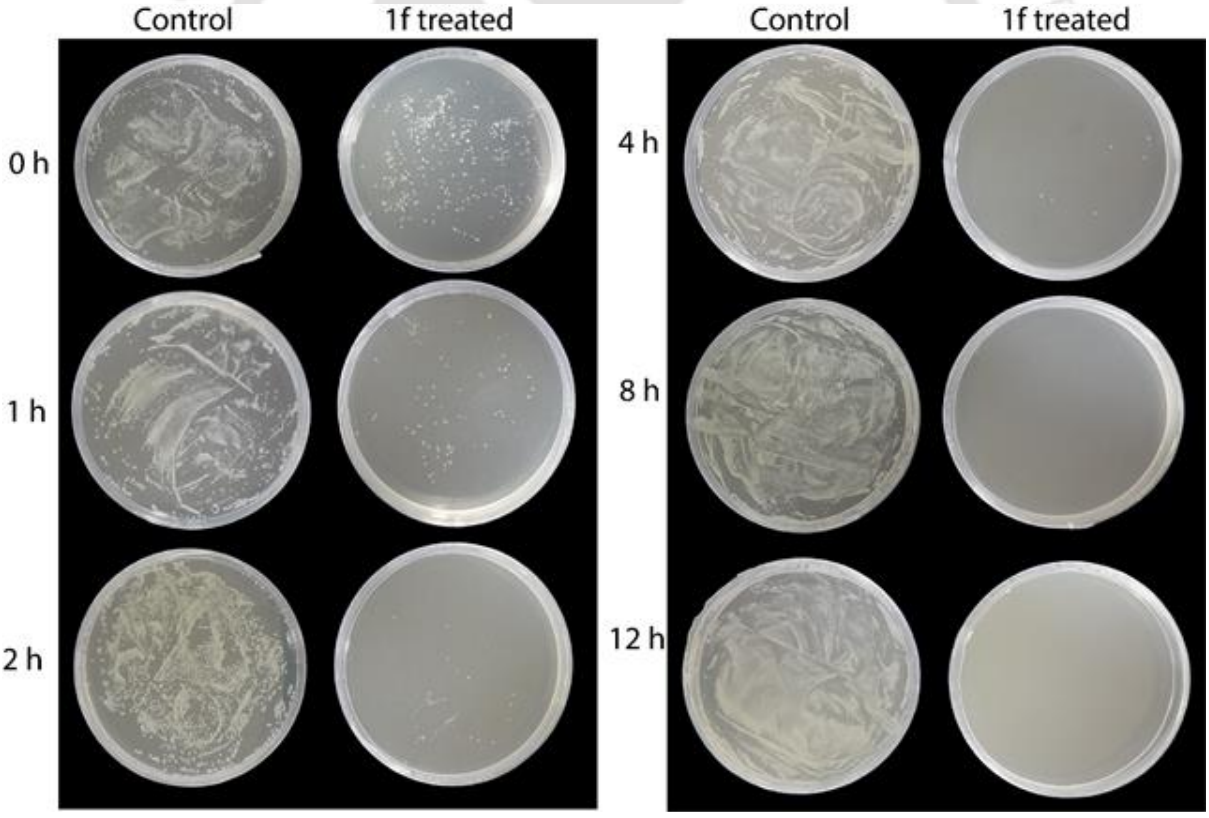

Figure 3.26. Bacterial growth on agar plates after a differential period of time.

Note: The viability of *S. aureus* cells was measured at different time intervals in order to determine the bactericidal effect of the compound. Figure 3.25 revealed that the compound

exhibited bactericidal activity after 8 hours of incubation. The CFU/mL (colony forming units per milliliter) were calculated while taking the dilution factor into consideration. The dilution factor is the proportion of the original sample volume to the volume plated on the agar plate.

$$CFU/mL = \frac{No.of\ colonies \times dilution\ factor}{Volume\ of\ culture\ plated\ (in\ mL)} \qquad Eq.\ 3.1$$

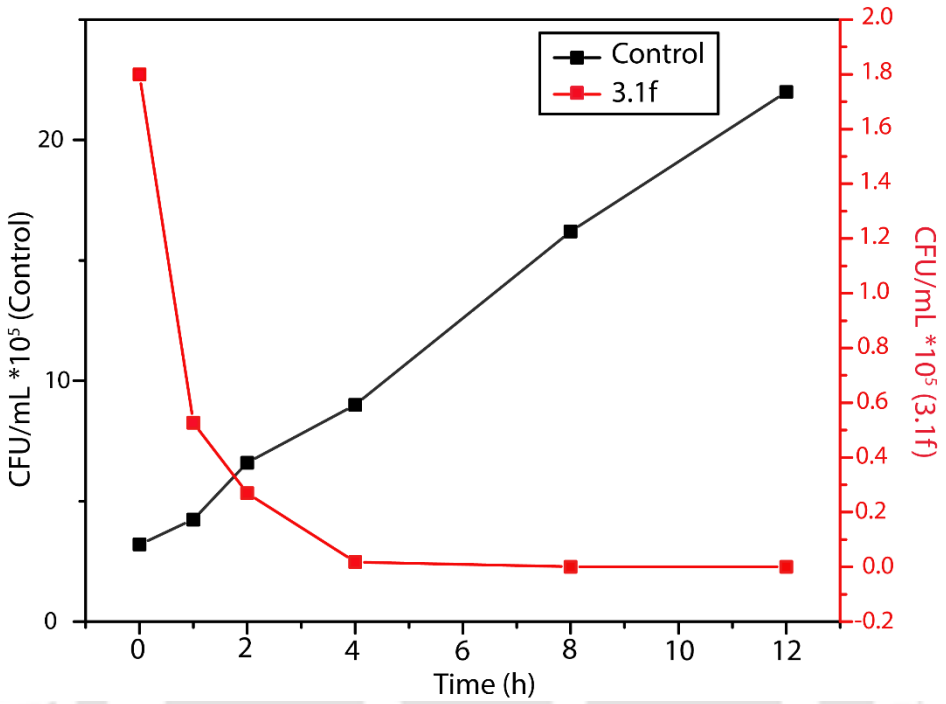

Figure 3.27. Time-kill curve showing changes in CFU of control and compound treated bacteria culture over time.

3.4.12.2. Morphological study:

Morphological analysis of bacterial cells treated with the compound was performed using a field emission scanning electron microscope (FESEM). To prepare the samples for FESEM imaging, *S. aureus* cells were cultured until they reached the mid-logarithmic growth phase and then harvested by centrifugation at 5000 rpm for 5 minutes. The cells were then washed and treated with **3.1f** (at MIC concentration). A bacterial culture without treatment with the compound was retained as a control. After 3 hours of incubation, the cell pellets were collected by centrifugation, washed with PBS buffer, and dropped onto a glass grid covered with aluminium foil. A laminar airflow was used to air dry the sample. The drop cast sample was then mounted on a metal FESEM grid held in place with carbon tape. The sample was gold-plated twice before FESEM analysis. This preparation process facilitated the study of the

morphology of the bacterial cells using FESEM. It allowed for a detailed characterization of any structural changes induced by the compound treatment.

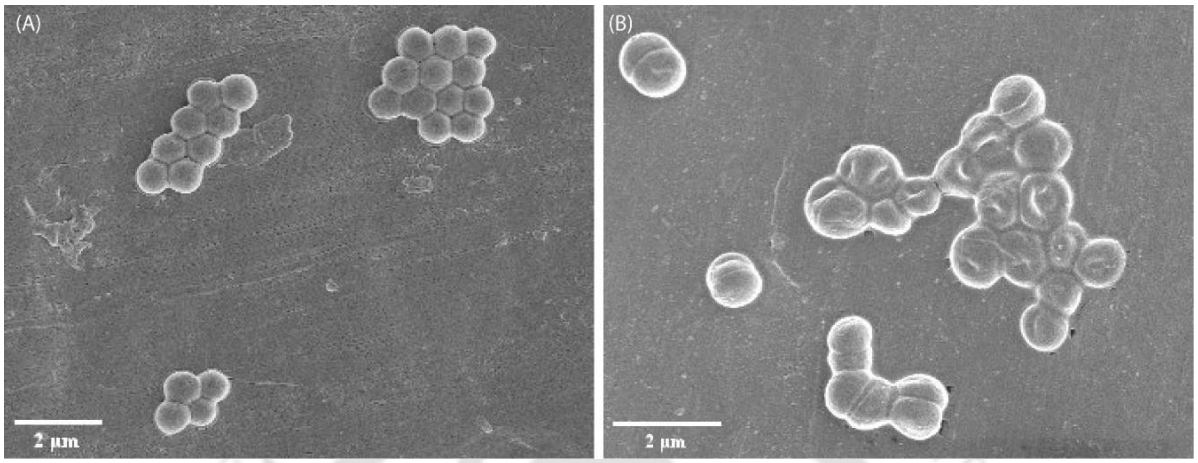

Figure 3.28. Morphological analysis of *S. aureus* cells. Control (A) and **3.1f** (B) treated *S. aureus* cells.

Note: The morphological study using FESEM showed a significant deformation in the bacterial cell in bacterial cell morphology after being treated with **3.1f**. By H^+/Cl^- cotransport across membrane as established in transport studies, it is evident that the transport of H^+ across membrane leads to the change in bacterial membrane pH and accumulation of Cl^- ions inside the bacterial cells, together, leads to the bacterial cell damage.

3.4.12.3. MQAE Assay:

This assay has been performed to analyze Cl^- transport in bacterial cells. The MQAE dye (N-(ethoxycarbonylmethyl)-6-methoxyquinolinium bromide) is a specific Cl^--sensing dye used to analyze Cl^- transport in cells due to its cell permeability.[3] *S. aureus* cells were grown in LB medium in the presence of MQAE (1 mM) in an incubator shaker at 37 °C and 180 rpm for 14-16 hours. The cells were then washed, collected, and resuspended in 10 mM HEPES and 50 mM NaCl buffer (pH: 7.2) to estimate intracellular Cl^- transport. For this assay, 150 µL of resuspended bacterial culture was mixed in 1850 µL of buffer (10 mM HEPES and 50 mM NaCl, pH 7.2) in a clean and dry fluorescence cuvette and kept under slow stirring conditions, and the fluorescence intensity of MQAE within the cells was monitored at 450 nm (λ_{ex}: 350 nm). At t = 100s, **3.1f** was added at a concentration of 20 µM, and the MQAE fluorescence intensity was monitored for a further 900s. The same was performed for the control; 0.5% DMSO was added.

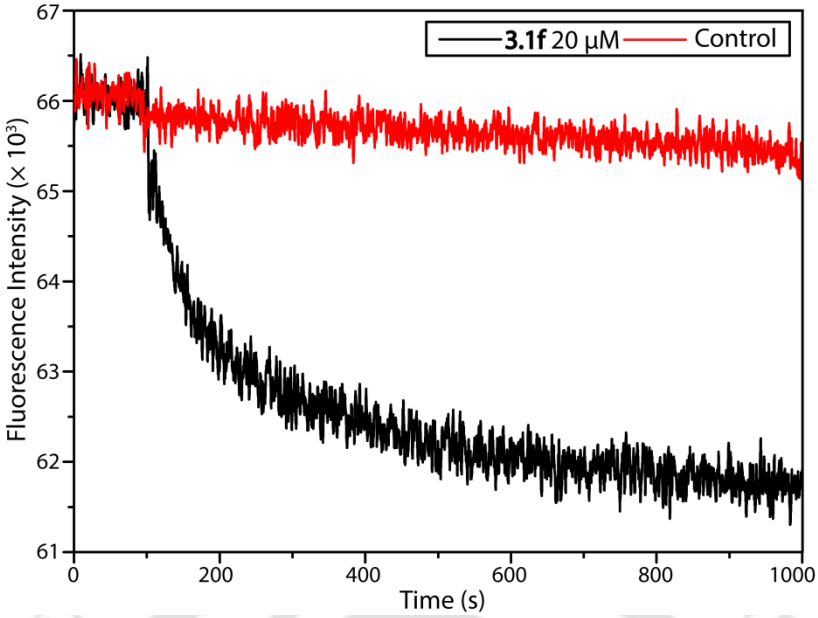

Figure 3.29. MQAE-based fluorescence assay. At t = 100s, the compound was the bacterial cells, and a decrease in fluorescence intensity was observed.

Note: This study aimed at assessing transmembrane Cl^- transport properties of the bacterial cells in the presence of **3.1f** using the MQAE (cell permeable) dye.[3] Bacterial cells were exposed to the dye, which was internalized by the cells. As Cl^- was transported into the cytoplasm of the bacterial cells, the fluorescence intensity of the dye was quenched. The addition of **3.1f** enhanced the rate of Cl^- transport within the cells, resulting in a time-dependent drop in fluorescence intensity. This result suggests that **3.1f** could rapidly transport Cl^- across bacterial cell membranes, as evidenced by a decrease in fluorescence intensity.

3.4.13. NMR spectra of synthesized compounds:

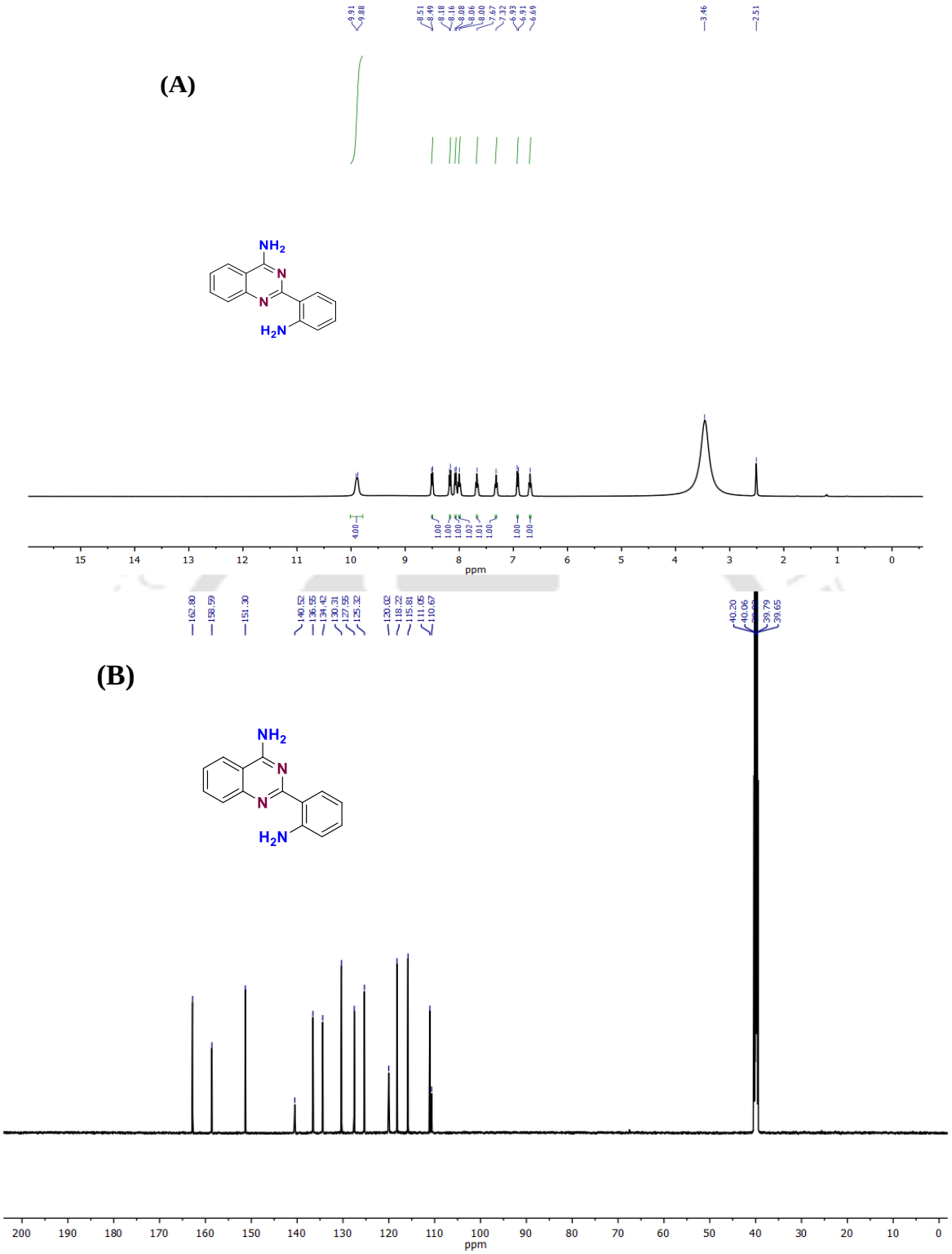

Figure 3.30. ^{1}H NMR (A) and ^{13}C NMR (B) spectra of 2-(2-aminophenyl)quinazolin-4-amine in the DMSO-d_6 solvent.

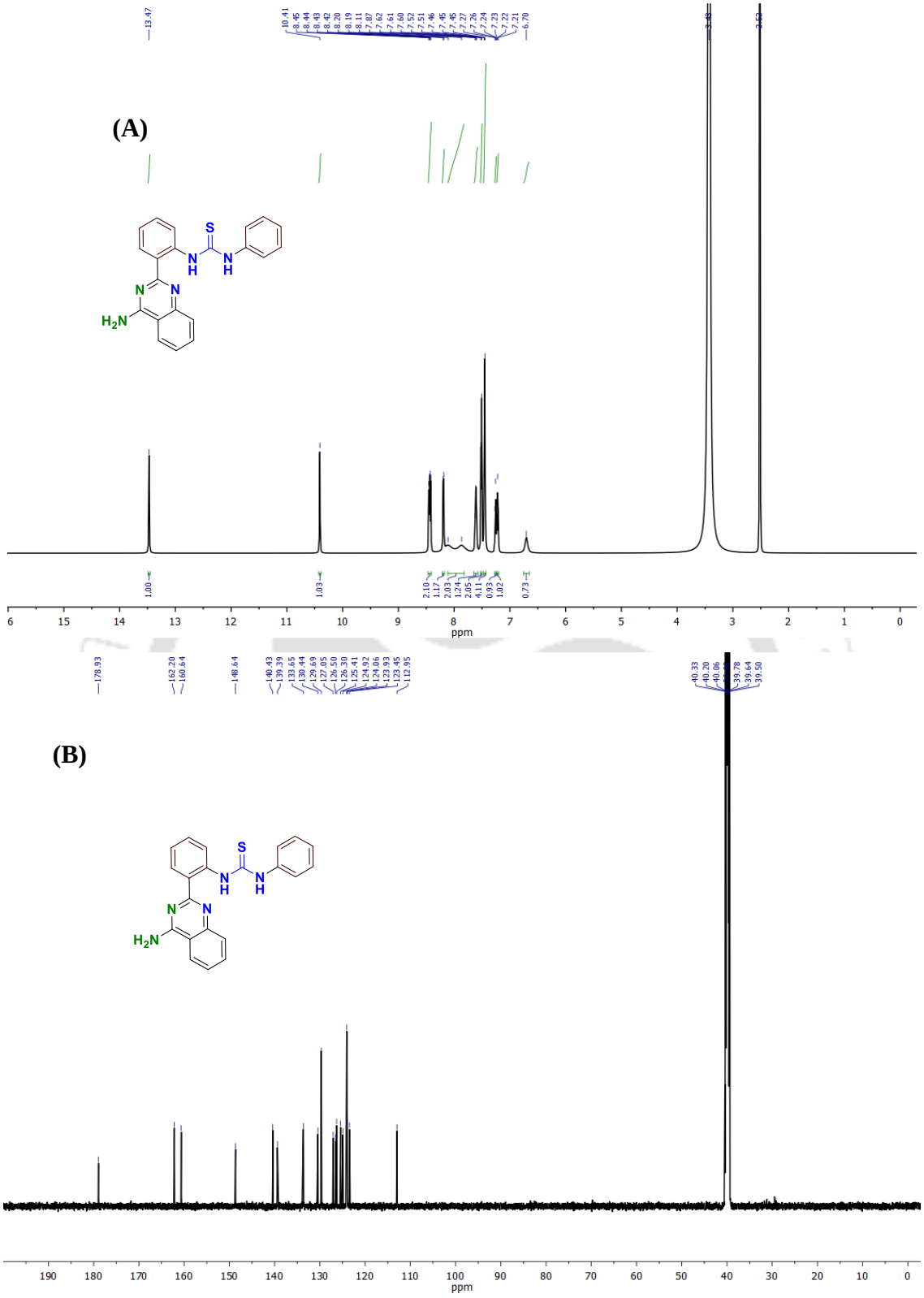

Figure 3.31. ^{1}H NMR (A) and ^{13}C NMR (B) spectra of **3.1a** in the DMSO-d_6 solvent.

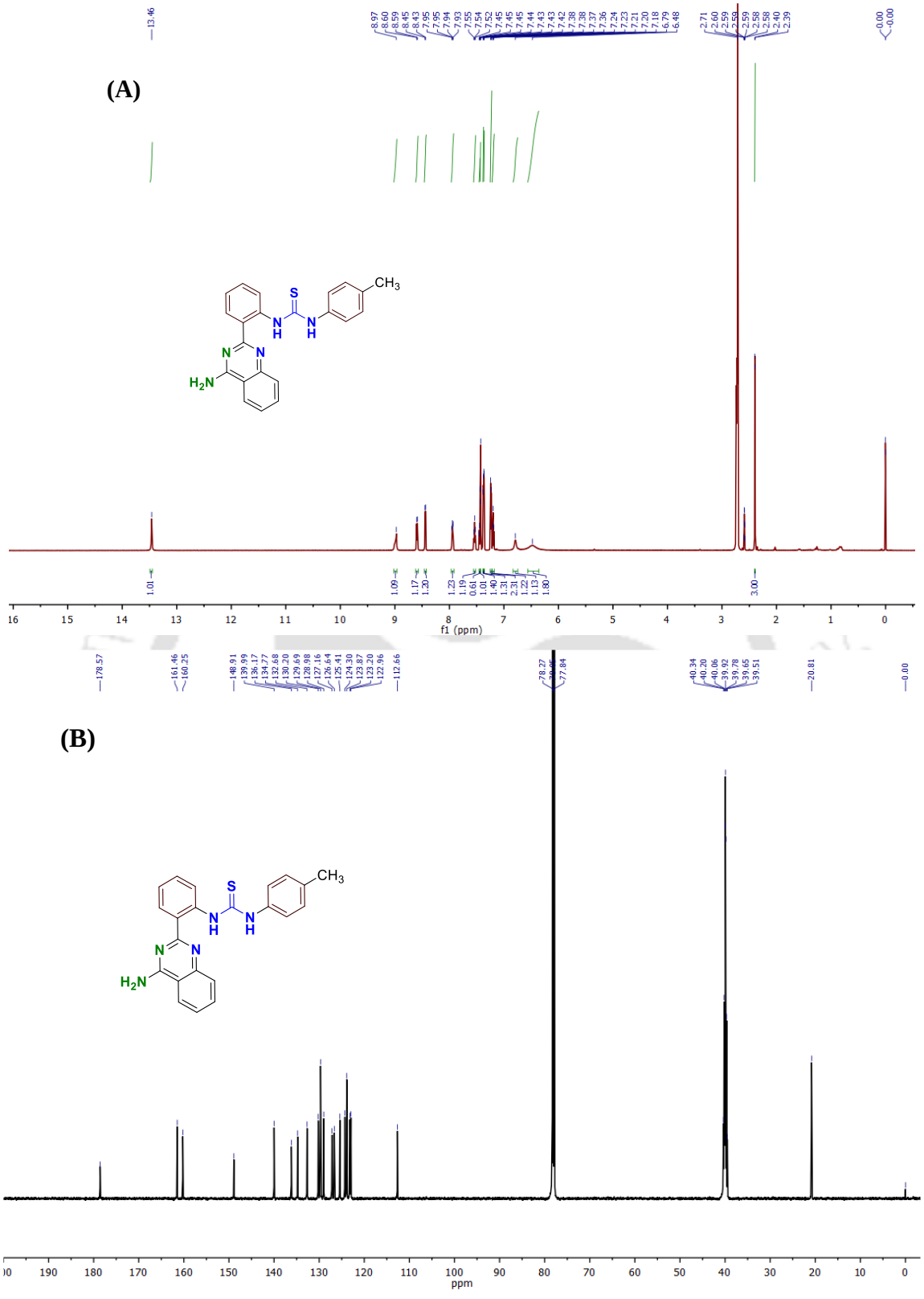

Figure 3.32. ^{1}H NMR (A) and ^{13}C NMR (B) spectra of **3.1b** in the $CDCl_3$ + DMSO-d_6 solvent.

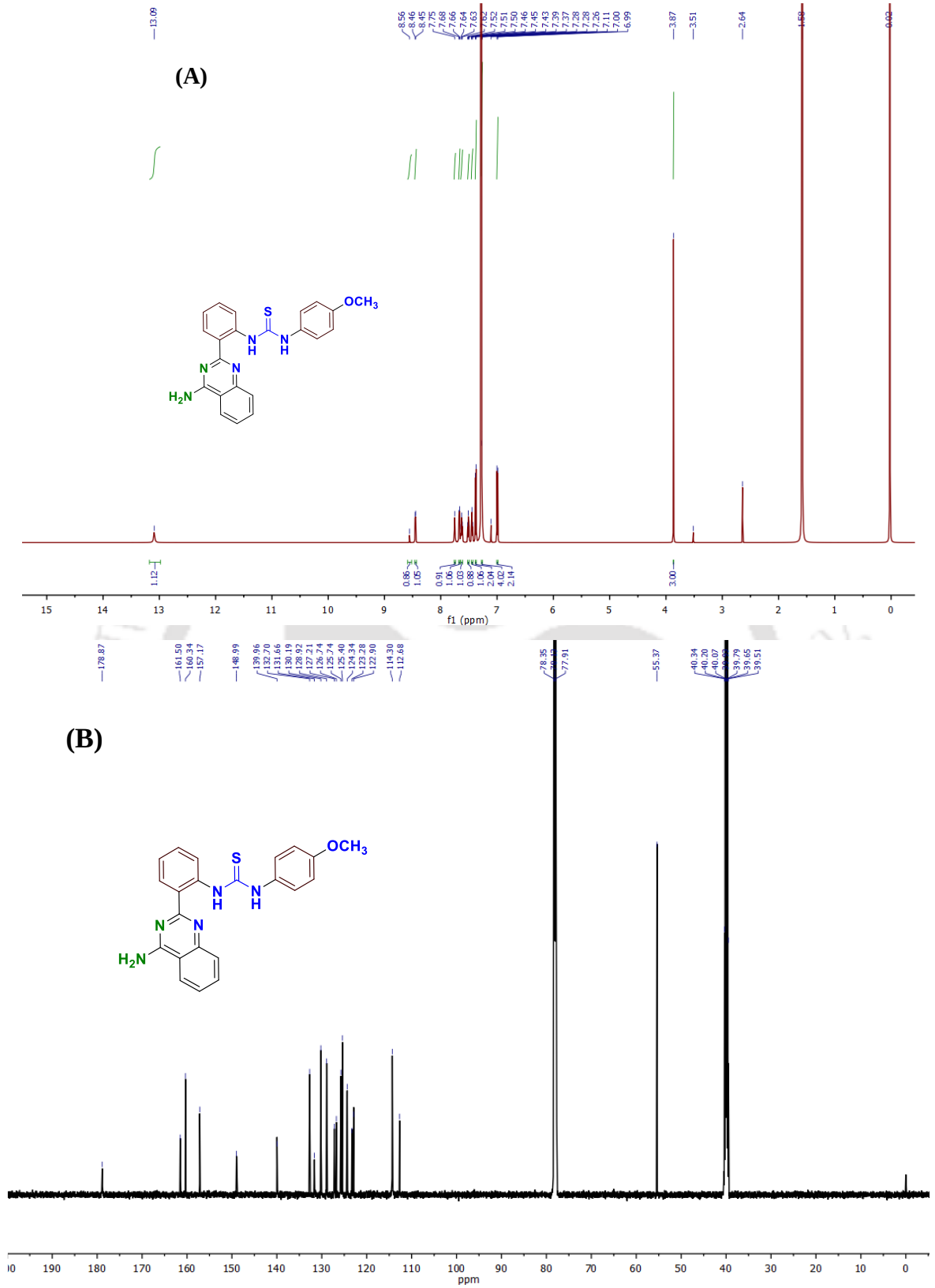

Figure 3.33. ^{1}H NMR (A) and ^{13}C NMR (B) spectra of **3.1c** in the $CDCl_3$ + DMSO-d_6 solvent.

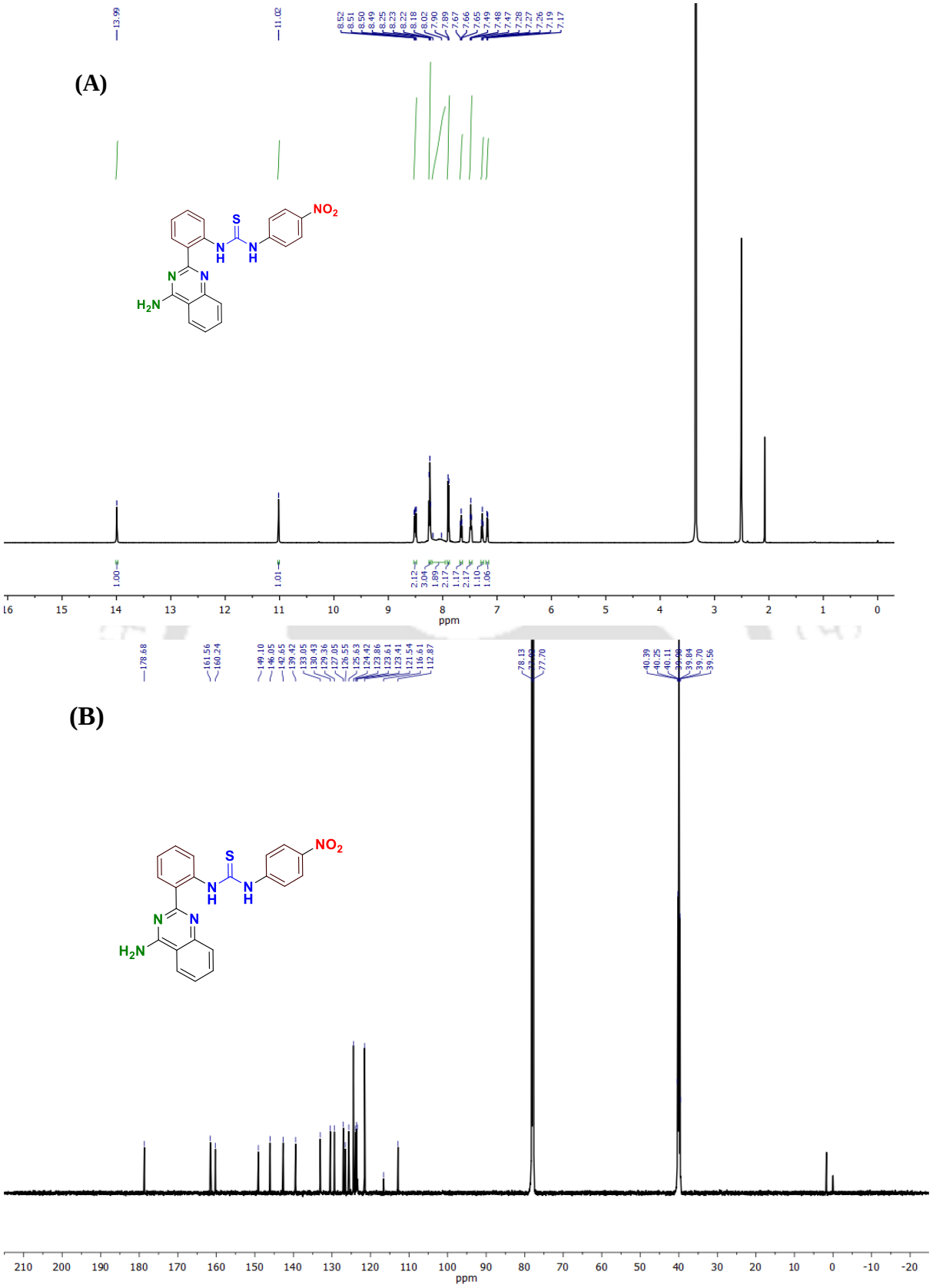

Figure 3.34. ^{1}H NMR (A) and ^{13}C NMR (B) spectra of **3.1d** in the $CDCl_3$ + DMSO-d_6 solvent.

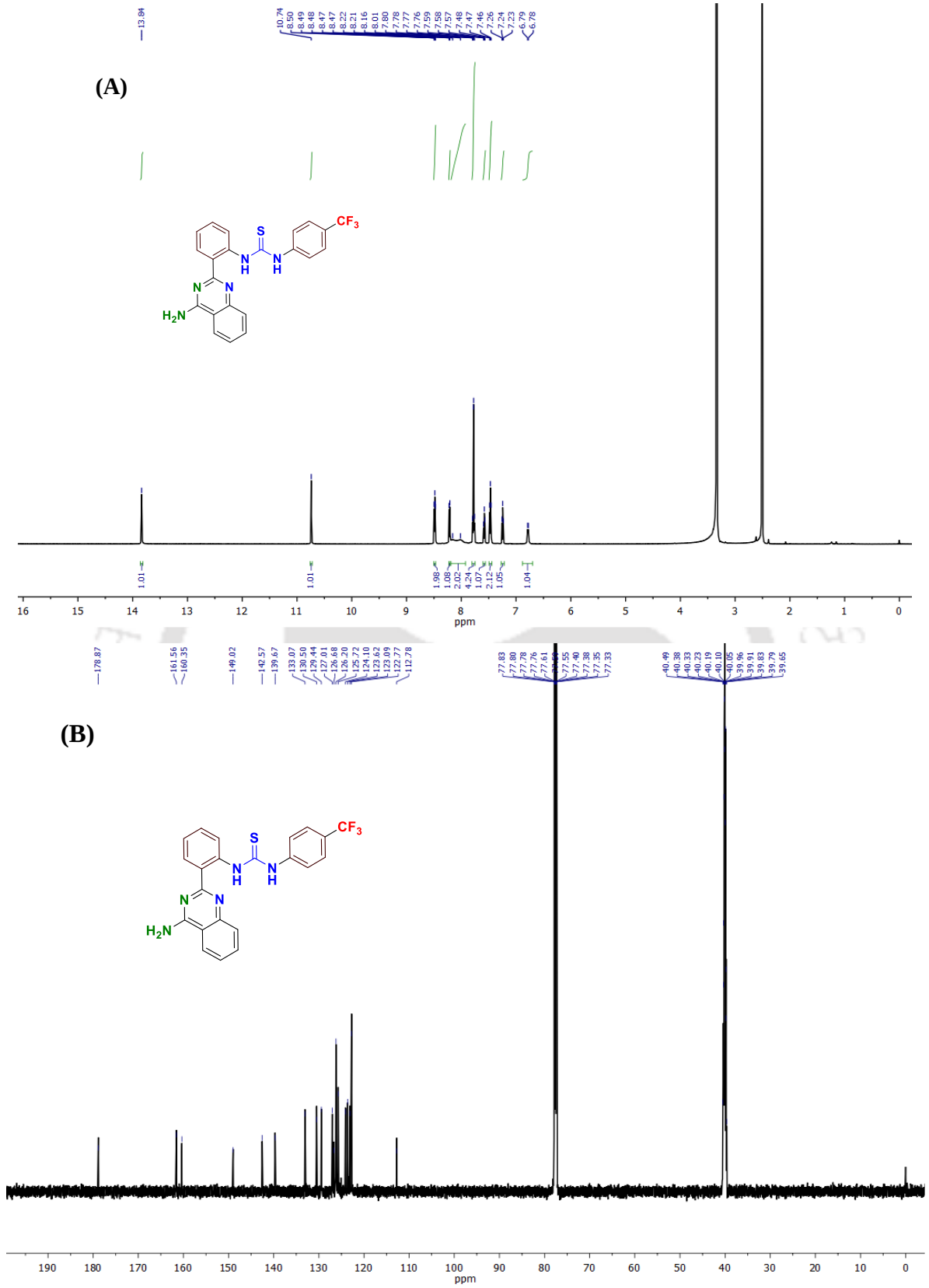

Figure 3.35. ^{1}H NMR (A) and ^{13}C NMR (B) spectra of **3.1e** in the DMSO-d_6 solvent.

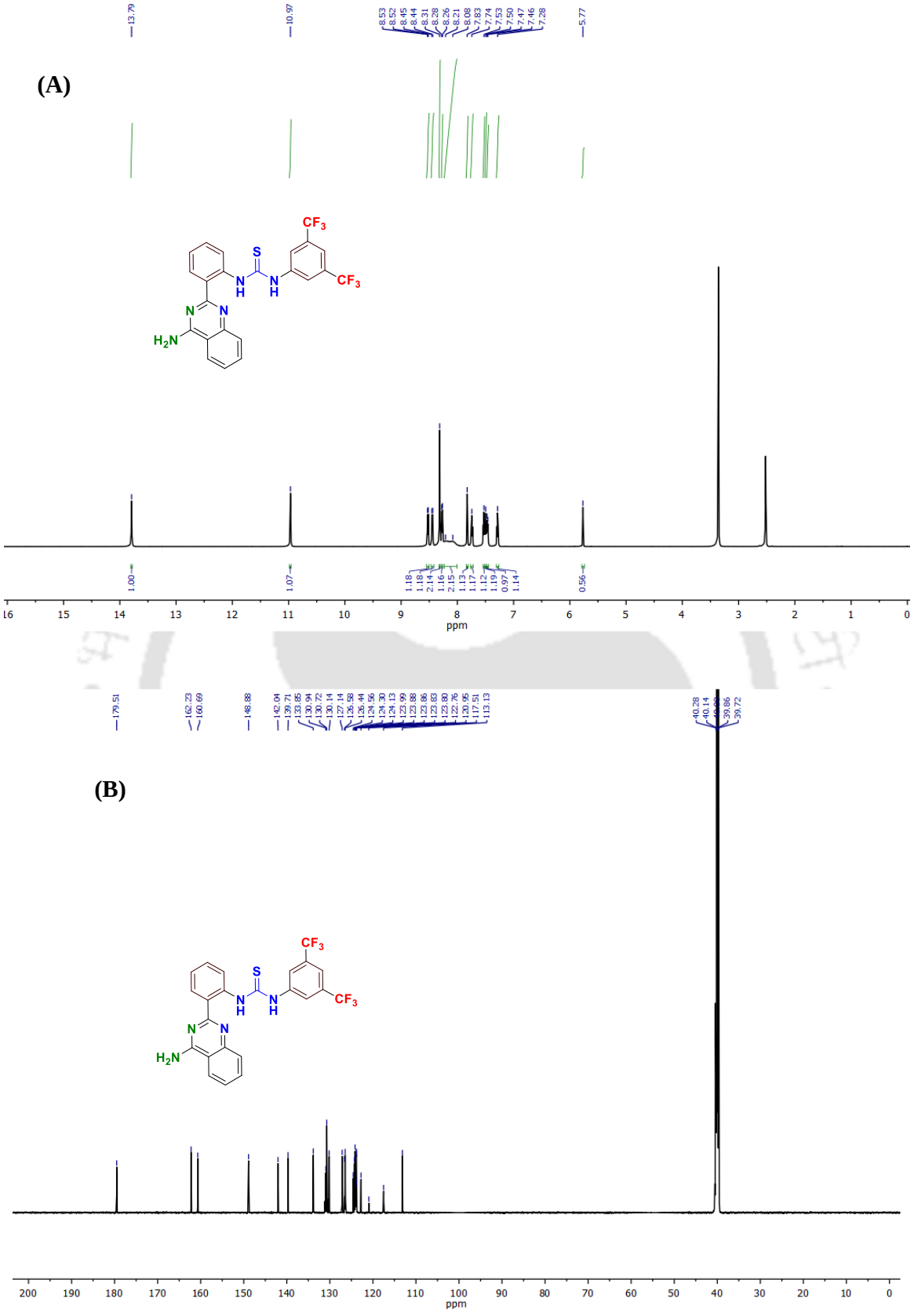

Figure 3.36. ^{1}H NMR (A) and ^{13}C NMR (B) spectra of **3.1f** in the DMSO-d_6 solvent.

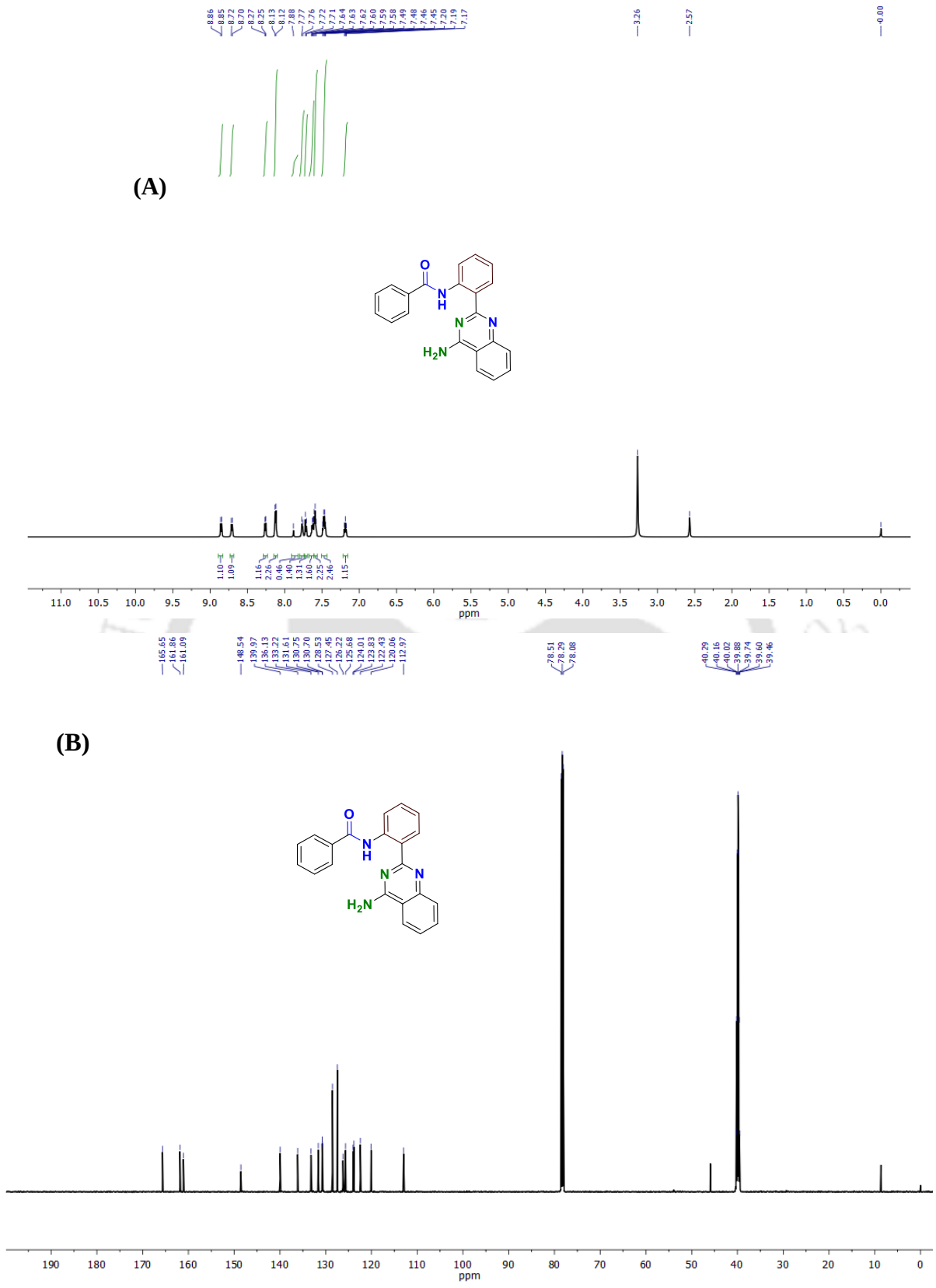

Figure 3.37. ^{1}H NMR (A) and ^{13}C NMR (B) spectra of **3.2a** in the $CDCl_3$ + DMSO-d_6 solvent.

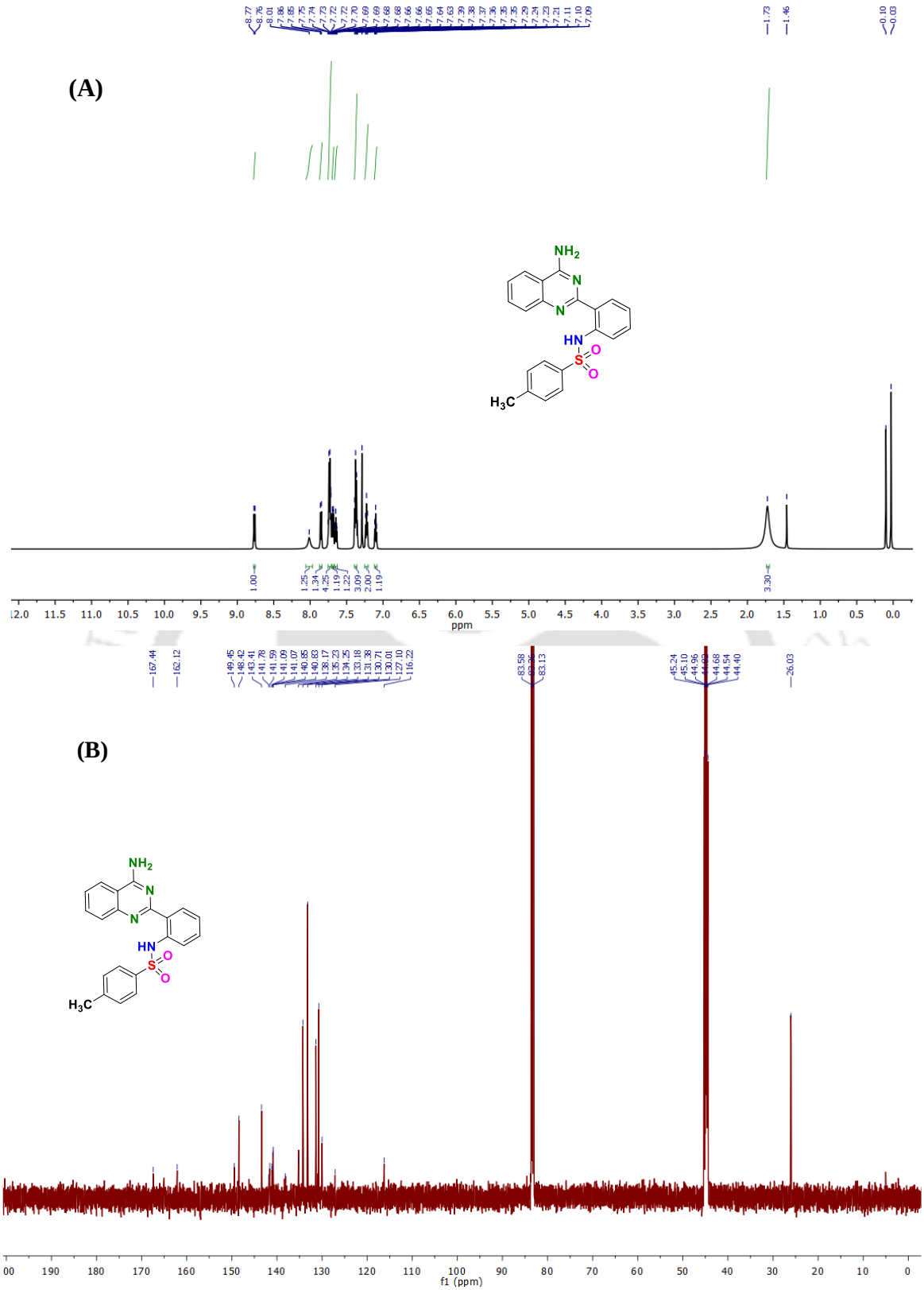

Figure 3.38. ^{1}H NMR (A) and ^{13}C NMR (B) spectra of **3.2b** in the $CDCl_3$ + DMSO-d_6 solvent.

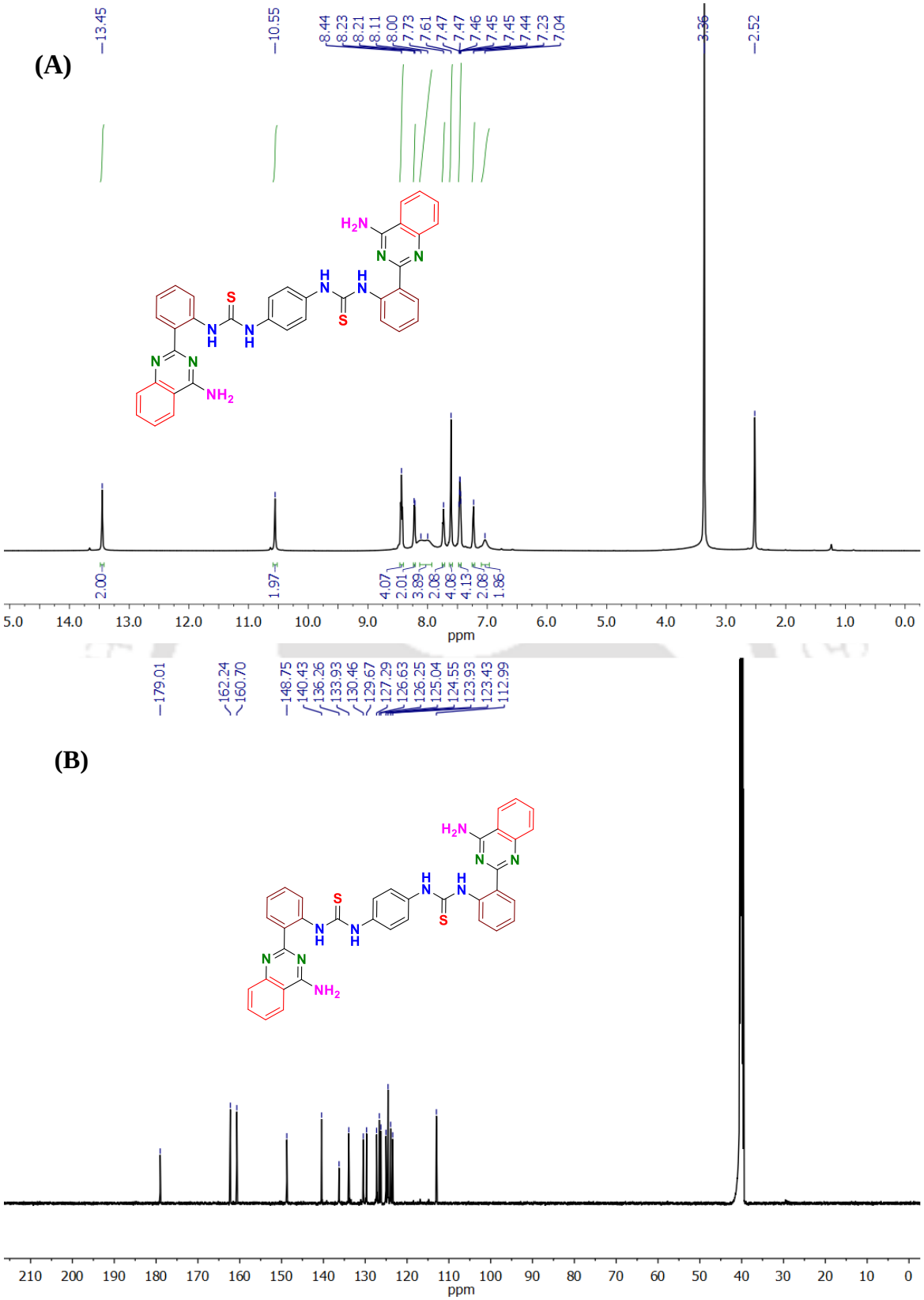

Figure 3.39. ^{1}H NMR (A) and ^{13}C NMR (B) spectra of **3.3a** in the DMSO-d_6 solvent.

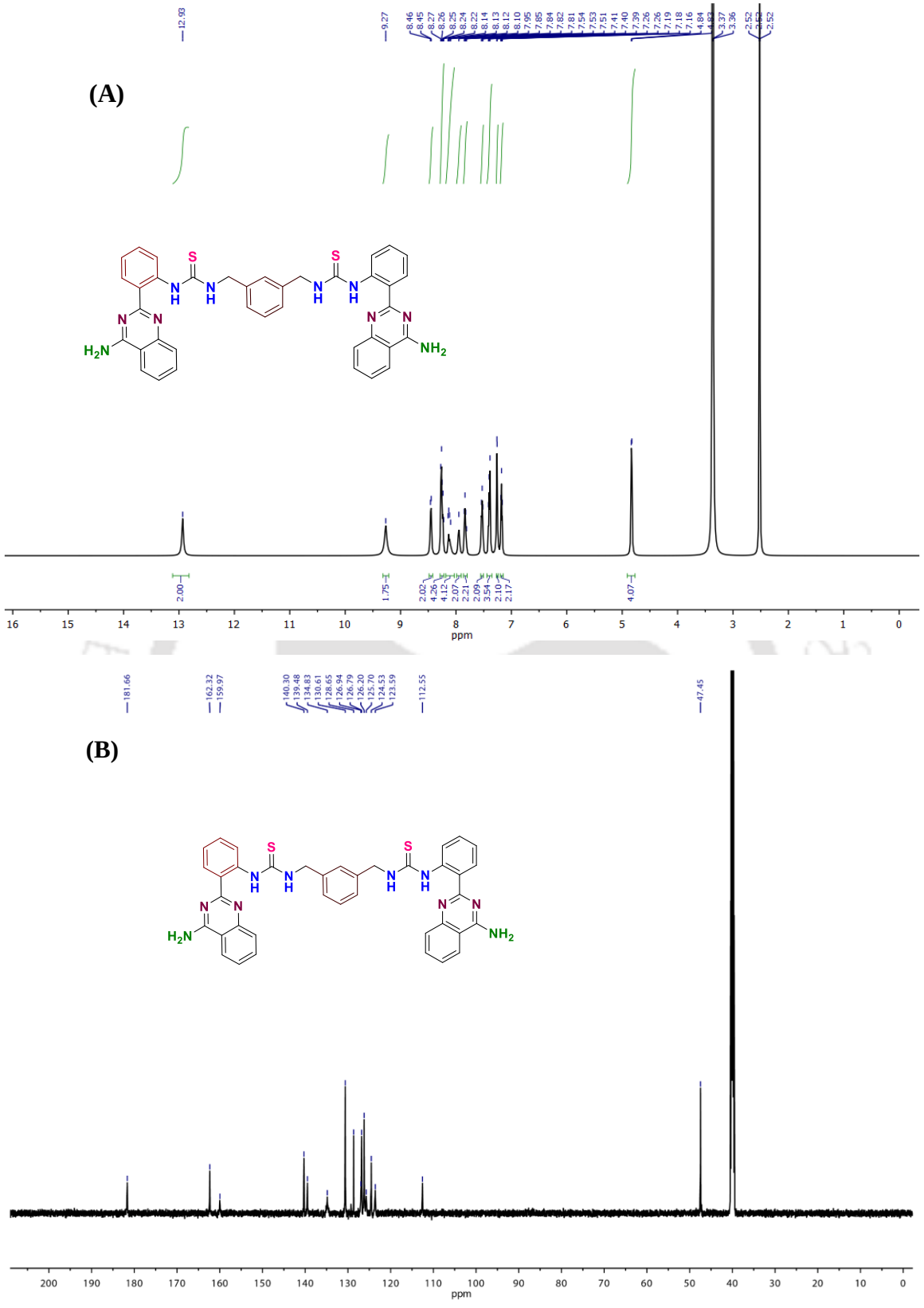

Figure 3.40. ^{1}H NMR (A) and ^{13}C NMR (B) spectra of **3.3b** in the DMSO-d_6 solvent.

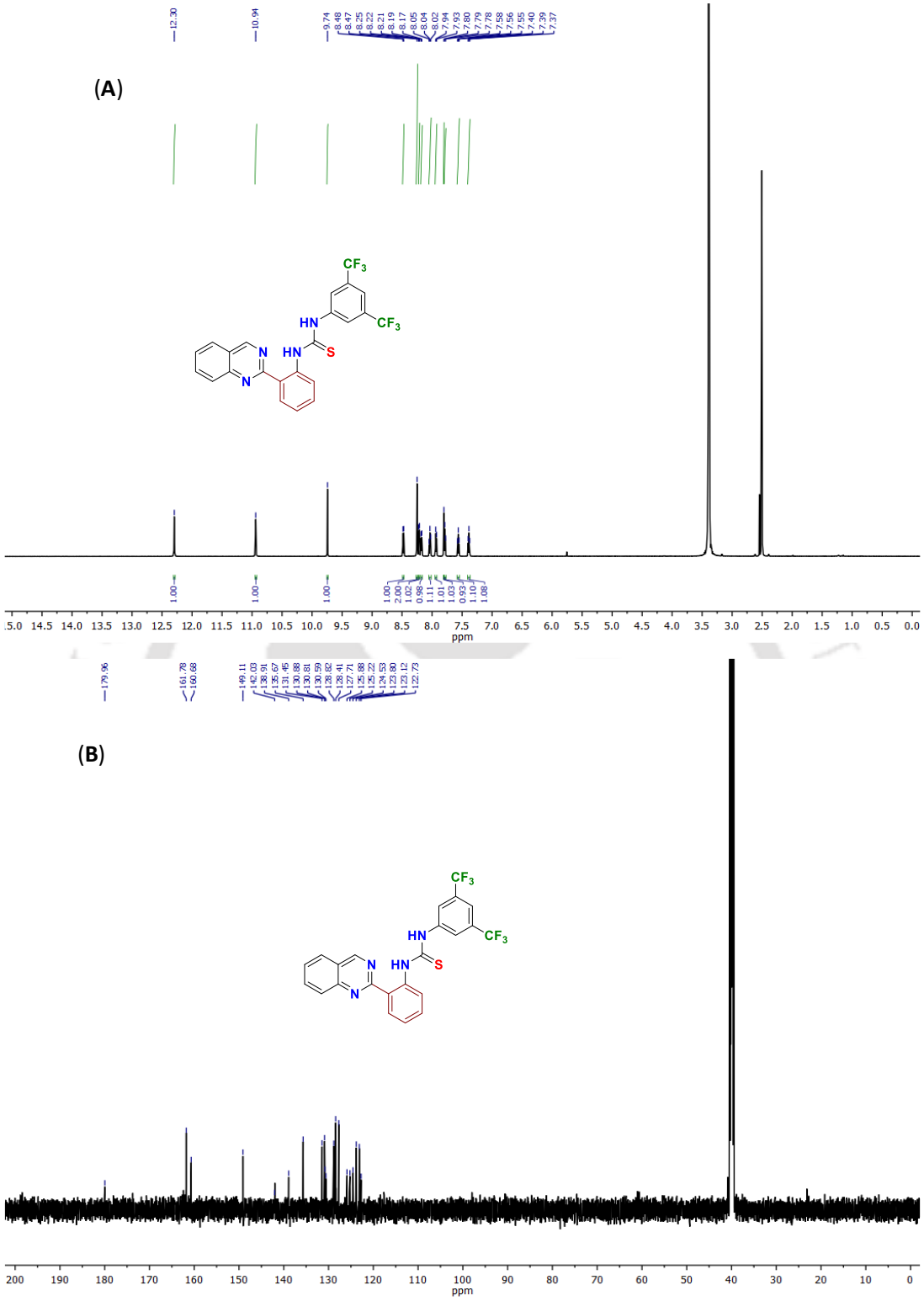

Figure 3.41. ^{1}H and ^{13}C NMR spectrum of compound **3.4** in DMSO-d_6 solvent.

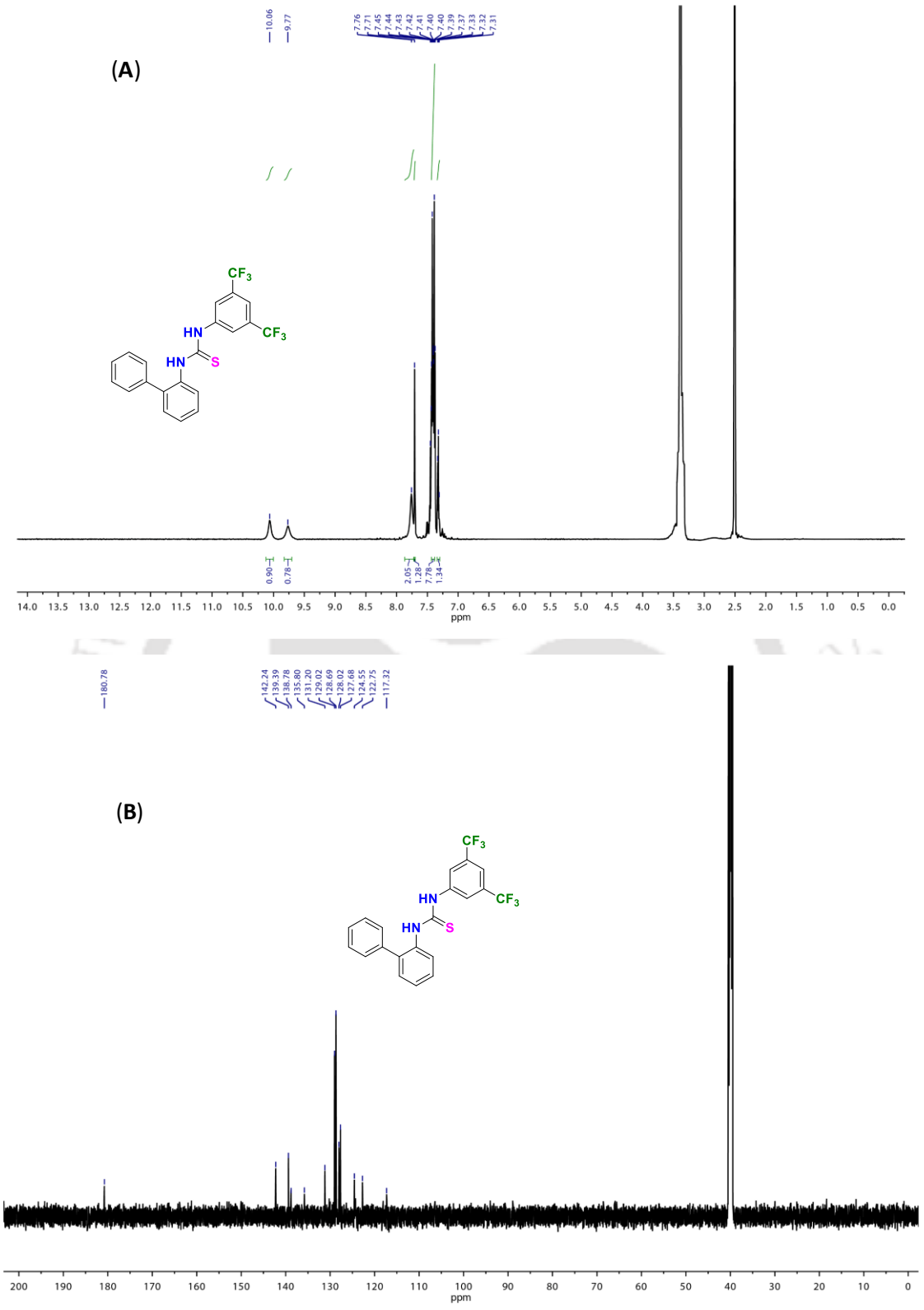

Figure 3.42. ^{1}H and ^{13}C NMR spectrum of compound **3.5** in DMSO-d_6 solvent.

3.5. References

1. Yang, J.; Yu, G. C.; Sessler, J. L.; Shin, I.; Gale, P. A.; Huang, F. H., Artificial transmembrane ion transporters as potential therapeutics. *Chem-Us* **2021,** *7*, 3256-3291.

2. Zilahi, G.; Artigas, A.; Martin-Loeches, I., What's new in multidrug-resistant pathogens in the ICU? *Ann Intensive Care* **2016,** *6*, 96.

3. Carreira-Barral, I.; Rumbo, C.; Mielczarek, M.; Alonso-Carrillo, D.; Herran, E.; Pastor, M.; Del Pozo, A.; Garcia-Valverde, M.; Quesada, R., Small molecule anion transporters display in vitro antimicrobial activity against clinically relevant bacterial strains. *Chem Commun* **2019,** *55*, 10080-10083.

4. Gavette, J. V.; Evoniuk, C. J.; Zakharov, L. N.; Carnes, M. E.; Haley, M. M.; Johnson, D. W., Exploring anion-induced conformational flexibility and molecular switching in a series of heteroaryl-urea receptors. *Chem Sci* **2014,** *5*, 2899-2905.

5. Akhtar, N.; Biswas, O.; Manna, D., Biological applications of synthetic anion transporters. *Chem Commun* **2020,** *56*, 14137-14153.

6. Roy, A.; Talukdar, P., Recent Advances in Bioactive Artificial Ionophores. *Chembiochem* **2021,** *22*, 2925-2940.

7. Dey, S.; Patel, A.; Haloi, N.; Srimayee, S.; Paul, S.; Barik, G. K.; Akhtar, N.; Shaw, D.; Hazarika, G.; Prusty, B. M.; Kumar, M.; Santra, M. K.; Tajkhorshid, E.; Bhattacharjee, S.; Manna, D., Quinoline Thiourea-Based Zinc Ionophores with Antibacterial Activity. *J. Med. Chem.* **2023,** *66*, 11078–11093.

8. Share, A. I.; Patel, K.; Nativi, C.; Cho, E. J.; Francesconi, O.; Busschaert, N.; Gale, P. A.; Roelens, S.; Sessler, J. L., Chloride anion transporters inhibit growth of methicillin-resistant Staphylococcus aureus (MRSA) in vitro. *Chem Commun* **2016,** *52*, 7560-7563.

9. Elie, C. R.; David, G.; Schmitzer, A. R., Strong Antibacterial Properties of Anion Transporters: A Result of Depolarization and Weakening of the Bacterial Membrane. *J Med Chem* **2015,** *58*, 2358-2366.

10. Maslowska-Jarzyna, K.; Korczak, M. L.; Chmielewski, M. J., Boosting Anion Transport Activity of Diamidocarbazoles by Electron Withdrawing Substituents. *Front Chem* **2021,** *9*, 690035.

11. Valkenier, H.; Judd, L. W.; Li, H.; Hussain, S.; Sheppard, D. N.; Davis, A. P., Preorganized Bis-Thioureas as Powerful Anion Carriers: Chloride Transport by Single Molecules in Large Unilamellar Vesicles. *J Am Chem Soc* **2014,** *136*, 12507-12512.

12. Auti, P. S.; George, G.; Paul, A. T., Recent advances in the pharmacological diversification of quinazoline/quinazolinone hybrids. *Rsc Adv* **2020,** *10*, 41353-41392.

13. Docker, A.; Shang, X. B.; Yuan, D. H.; Kuhn, H.; Zhang, Z. Y.; Davis, J. J.; Beer, P. D.; Langton, M. J., Halogen Bonding Tetraphenylethene Anion Receptors: Anion-Induced Emissive Aggregates and Photoswitchable Recognition. *Angew Chem Int Edit* **2021,** *60*, 19442-19450.

14. van Muijlwijk-Koezen, J. E.; Timmerman, H.; van der Goot, H.; Menge, W. M. P. B.; Kunzel, J. F. V.; de Groote, M.; IJzerman, A. P., Isoquinoline and quinazoline urea analogues as antagonists for the human adenosine A(3) receptor. *J Med Chem* **2000,** *43*, 2227-2238.

15. Mondal, D.; Ahmad, M.; Panwaria, P.; Upadhyay, A.; Talukdar, P., Anion Recognition through Multivalent C-H Hydrogen Bonds: Anion-Induced Foldamer Formation and Transport across Phospholipid Membranes. *J Org Chem* **2022,** *87*, 10-17.

16. Boiocchi, M.; Del Boca, L.; Gomez, D. E.; Fabbrizzi, L.; Licchelli, M.; Monzani, E., Nature of urea-fluoride interaction: Incipient and definitive proton transfer. *J Am Chem Soc* **2004,** *126*, 16507-16514.

17. Shi, J. Q.; Suarez, L. E. A.; Yoon, S. J.; Varghese, S.; Serpa, C.; Park, S. Y.; Luer, L.; Roca-Sanjuan, D.; Milian-Medina, B.; Gierschner, J., Solid State Luminescence Enhancement in a pi-Conjugated Materials: Unraveling the Mechanism beyond the Framework of AIE/AIEE. *J Phys Chem C* **2017,** *121*, 23166-23183.

18. Saha, A.; Akhtar, N.; Kumar, V.; Kumar, S.; Srivastava, H. K.; Kumar, S.; Manna, D., pH-Regulated anion transport activities of bis(iminourea) derivatives across the cell and vesicle membrane. *Org Biomol Chem* **2019,** *17*, 5779-5788.

19. Akhtar, N.; Pradhan, N.; Barik, G. K.; Chatterjee, S.; Ghosh, S.; Saha, A.; Satpati, P.; Bhattacharyya, A.; Santra, M. K.; Manna, D., Quinine-Based Semisynthetic Ion Transporters with Potential Antiproliferative Activities. *Acs Appl Mater Inter* **2020,** *12*, 25521-25533.

20. Wu, X.; Gale, P. A., Measuring anion transport selectivity: a cautionary tale. *Chem comm* **2021,** *57*, 3979-3982.

21. Srimayee, S.; Badajena, S. R.; Akhtar, N.; Kar, M. K.; Dey, S.; Mohapatra, P.; Manna, D., Stimuli-responsive release of active anionophore from RGD-peptide-linked proanionophore. *ChemComm* **2023**.

22. Mondal, A.; Save, S. N.; Sarkar, S.; Mondal, D.; Mondal, J.; Sharma, S.; Talukdar, P., A Benzohydrazide-Based Artificial Ion Channel that Modulates Chloride Ion Concentration

in Cancer Cells and Induces Apoptosis by Disruption of Autophagy. *J Am Chem Soc* **2023,** *145*, 9737-9745.

Chapter 4

Development of multi-stimuli controlled release of a transmembrane chloride ion carrier from a sulfonium-linked procarrier

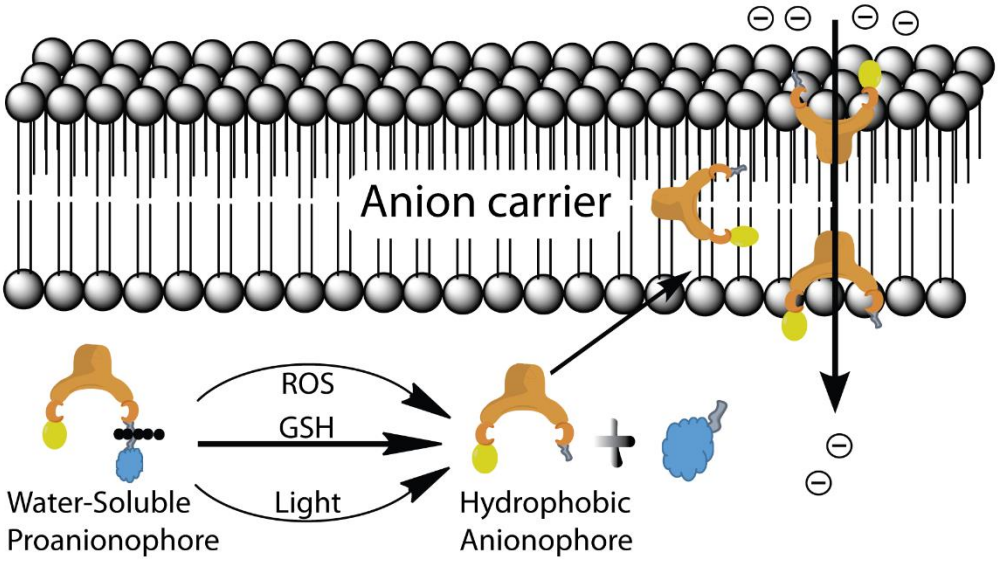

4.1. Background and objectives of the present work

Several synthetic ionophores have been developed as potential anticancer agents.[4, 5, 7-18] The lipid-soluble synthetic ionophore catalyzes the transport of ions across the hydrophobic membranes to promote apoptosis. These molecules generally do not bind to any target specific proteins or genetic materials. Therefore, it is postulated that the synthetic ion transporters can overcome the resistance associated with the overexpression and mutations of genes and proteins. However, the lipophilicity of these synthetic ion carriers precluded their target specific cellular delivery and in vivo applications. The poor aqueous solubility is one of the reasons for the clinical trial failure of obatoclax, the Cl^- ion carrier and inhibitor of Bcl-2 family of antiapoptotic proteins.[19-21] Therefore, an additional delivery system is required to accomplish the expected biological effects of these lipophilic ion carriers. Hence, a novel strategy is needed to mitigate the challenges of selective cellular uptake and target specific deliverability of the hydrophobic anionophores.

In this chapter, we introduced GSH, ROS, and photo-responsive anion transport strategy to regenerate lipophilic anionophores from the water-soluble proanionophores and endorse controlled transport of Cl^- ion across the lipid bilayers. The use of only external stimuli, like the light, has several limitations as it has lower tissue penetration ability.[24] The smaller change in pH gradient between cancerous and normal cells may not be even adequate in obtaining reliable in vivo results.[10, 11, 15] We hypothesize that this multi-stimuli-responsive anion transport strategy could be beneficial in targeting different types of cancer cells. The higher intracellular levels of GSH and ROS in cancer cells in comparison with that of normal healthy cells would preferentially release the anionophores within the cancer cells leading to the induction of apoptosis by perturbing the ion homeostasis. The GSH-mediated cleavage of sulfonium moieties is used in several applications, including drug delivery, selective protein, and peptide modifications.[25-27] The installation of sulfonium moiety also improves the viabilities, cellular uptake than the other onium based moieties and undergoes facile reductive cleavage under physiological conditions.[25] We hypothesized that the installation of a 4-carboxy-2-nitrobenzyl sulfonium moiety would increase the aqueous solubility of the corresponding anionophore and allow its removal at high GSH and ROS concentrations or in the presence light (Figure 4.1). Therefore, we installed a 4-carboxy-2-nitrobenzyl

group linked via sulfonium moiety, as the group is responsive to its linking to membrane-active anionophore. Substituted aryl groups were attached at the other end of the 1, 3-phenylenedimethanamine scaffold to optimize the ion transport efficiency. The outcome of our studies revealed that the water-soluble proanionophore successfully release the membrane active ionophore in the presence of stimuli like GSH, ROS, and light, and transports Cl^- ion across the model lipid bilayers.

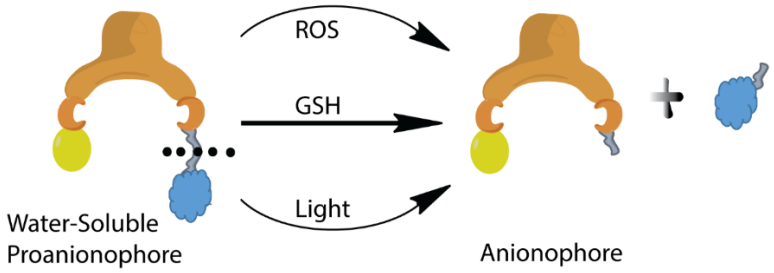

Figure 4.1. Schematic diagram representing the stimuli-responsive release of an anionophore from its proanionophore.

4.2. Results and discussions

4.2.1. Synthesis of the anionophores and proanionophore

The compounds **4.1a**–**4.1d** were synthesized from 1-(3-(isothiocyanatomethyl)benzyl)-3-(2-(methylthio)ethyl)thiourea via condensation with the corresponding amines. The 4-carboxy-2-nitrobenzyl sulfonium appended compound **4.2** was synthesized by reacting compound **4.1c** with 4-bromomethyl-3-nitrobenzoic acid (Scheme 4.1). Several thiourea based dipodal ionophores were already described,[8, 19] but the presence of methylthioethyl moiety allows these synthesized compounds to generate water-soluble proanionophore. All the synthesized compounds were purified by column chromatography and characterized by ^{1}H NMR, ^{13}C NMR, and HRMS or LCMS analysis.

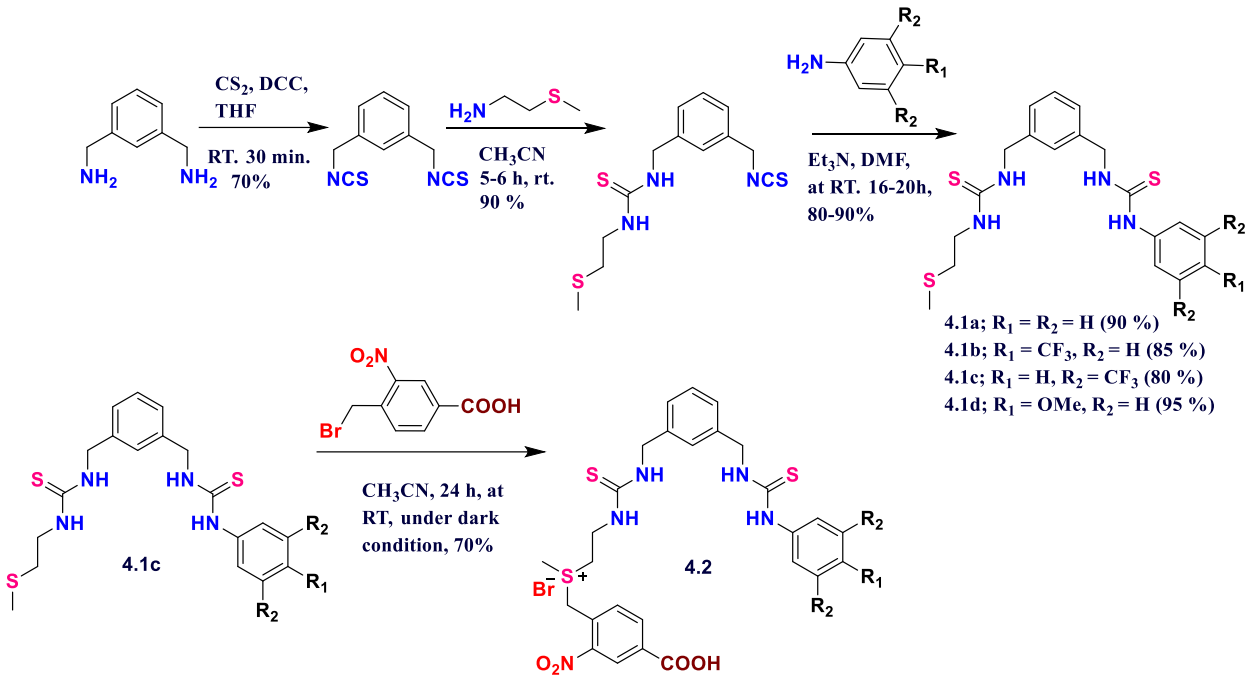

Scheme 4.1. Synthesis of anionophores **4.1a-4.1b** and proanionophore **4.2.**

4.2.2. Anion binding analysis by ^{1}H-NMR titrations

The ^{1}H NMR titration experiment was conducted to investigate the Cl^- ion recognition competences of the compounds.[7-10, 19, 22] The tetrabutylammonium chloride (TBACl) was used as the source of Cl^- ion. The downfield chemical shifts of N–H signals suggest the interaction with Cl^- ion with the compounds through hydrogen bonding. The strength of interactions was scrutinized by calculating the binding affinities (K_a) from the chemical shifts ($\Delta\delta$) values for the N-H signals, using the BindFit v0.5 program. The inbuilt 1:1 binding model provided the best fit for the titration curves. The calculated K_a values revealed that the compounds **4.1b** and **4.1c** have higher Cl^- ion binding capabilities (Table 4.1 and Figure 4.2, 4.7-4.9). The ^{1}H NMR titration experiment was also performed in CD_3CN solvent to investigate the effect of solvent on Cl^- ion recognition properties of the compounds. The calculated K_a values of compound **4.1c** was 69.08 (Figure 4.9) and 105.21 M^{-1} (Figure 4.10) in DMSO-d_6 and CD_3CN solvent, respectively. The difference in K_a values of compound **4.1c** could be due to the competition of DMSO solvent in Cl^- ion recognition.

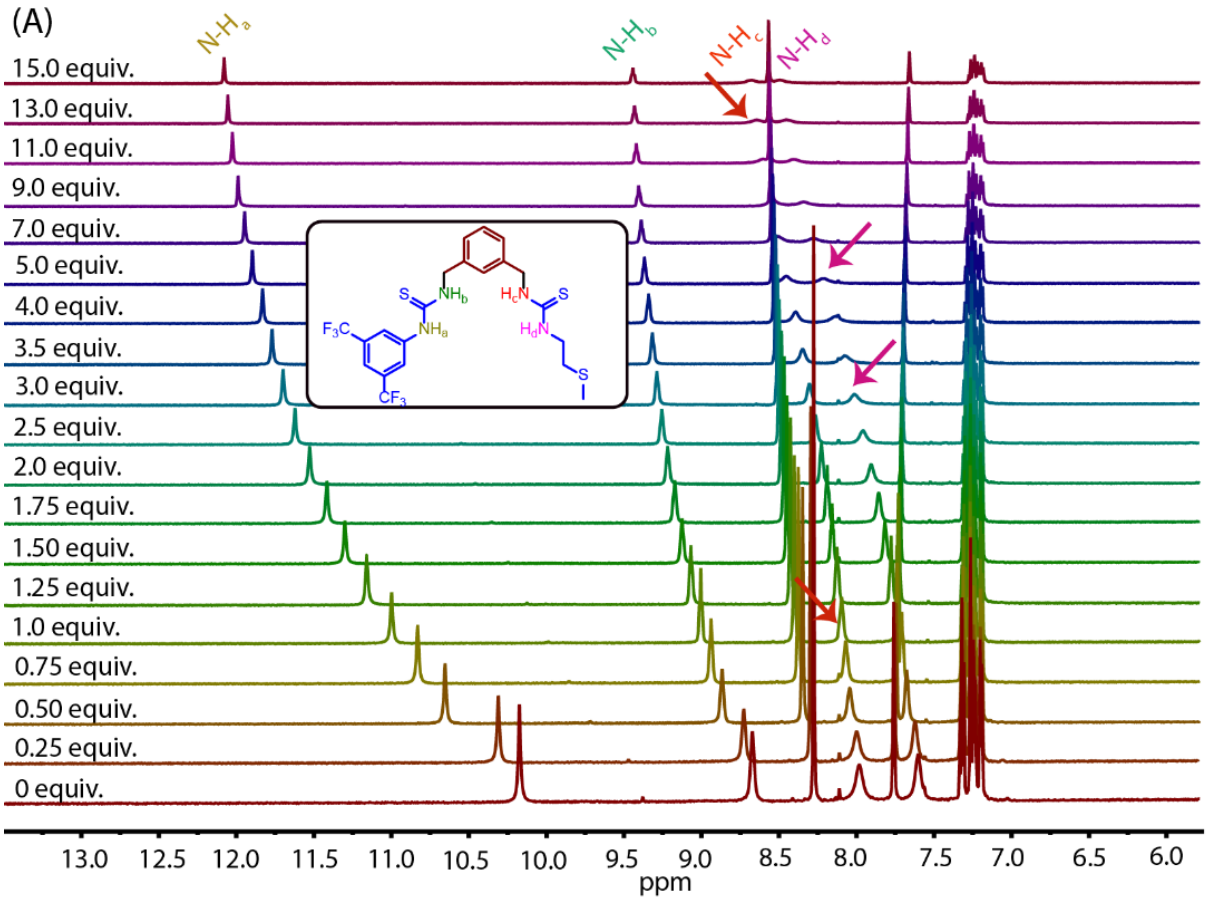

Figure 4.2. ^{1}H-NMR (600MHz) titration spectra for compound **4.1c** with the sequential addition of TBACl in DMSO-d_6 solvent. The amounts of added TBACl are shown on the spectra (**A**).

4.2.3. Ion transport activity across the vesicles

The ion transport activities of compounds **4.1a**–**4.1d** and **4.2** were evaluated by fluorescence assay using model large unilamellar vesicles (LUVs). The pH-sensitive ratio-metric fluorophore, 8-hydroxypyrene-1,3,6-trisulfonate (HPTS, pK_a = 7.3), was encapsulated within the LUVs of egg-yolk phosphatidylcholine (EYPC) and cholesterol (CHOL) lipids with internal and external pH 7.2. The transmembrane ion transport activities of the compounds were measured by applying a pH gradient with the addition of NaOH in the extravesicular buffer (pH_{in} = 7.2, pH_{out} = 7.8).[7-10, 19, 22] The alternation of internal pH in the presence of compounds was examined by the change in fluorescence intensity of HPTS at 510 nm (λ_{ex} = 450 nm). The initial screening revealed that compounds **4.1b** and **4.1c** efficiently transport Cl^- ion across the lipid bilayer (Figure 4.3A). The compounds **4.1a-4.1d** showed very similar Cl^- ion binding capabilities in DMSO-d_6 solvent but higher Cl^- ion transport abilities of compounds

4.1b and **4.1c** in comparison to **4.1a** and **4.1d**, which could be due to the difference in their lipophilicity (logP values < 5 for compounds **4.1a** and **4.1d**), which is considered as one of the essential criteria for their effective permeability to the biological membranes and transmembrane Cl^- ion transport ability (Table 4.1). The poor Cl^- ion transport efficiency of the sulfonium-based compound **4.2** could be due to its higher aqueous solubility. The dose-dependent HPTS assay showed that the compounds **4.1b** and **4.1c** have over 45 and 88-fold higher Cl^- ion transport efficacy than that of compounds **4.1a** and **4.1d**, respectively, under similar experimental conditions (Figure 4.11-4.14). The Hill analysis revealed that the effective concentration at 50 % (EC_{50}) Cl^- ion transport activity was 79.45 and 37.98 nM for compounds **4.1b** and **4.1c**, respectively (Table 4.1). Accordingly, the HPTS assay revealed that compound **4.1c** has higher Cl^- ion transport abilities than the other synthesized compounds. Consequently, further biophysical studies were carried out with compound **4.1c** and its derivatives.

Table 4.1. Physical properties of the thiourea derivatives.

Compound	Clog P	K_a (M^{-1})	EC_{50} (μM) (n)
4.1a	4.18	32.07 ± 0.31	3.66 ± 0.36 (0.59)
4.1b	5.07	49.51 ± 0.27	0.08 ± 0.01 (0.63)
4.1c	5.95	69.08 ± 0.40	0.04 ± 0.02 (1.04)
4.1d	3.93	24.58 ± 0.37	3.35 ± 0.69 (0.81)
4.2	-	-	

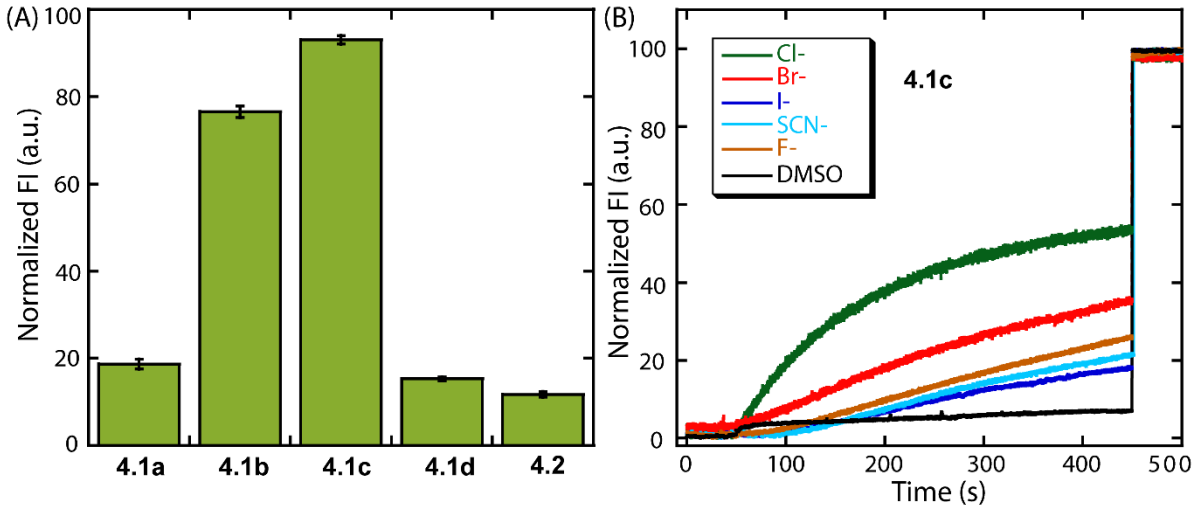

Figure 4.3. Transmembrane Cl^- ion transport activity of the compounds (**4.1a-4.1d** and **4.2**) across EYPC/CHOL-LUV⊃HPTS by applying pH gradient (A; pH_{in} = 7.2 and pH_{out} = 7.8). The compound concentration was 0.038 μM. Anion transport selectivity of compound **4.1c** (B) under similar experimental conditions.

4.2.4. Ion selectivity study

To examine the role of other anions or cations on the Cl^- ion transport activity of the compound **4.1c**, the HPTS assay was conducted in the presence of a pH gradient (pH_{in} = 7.2, pH_{out} = 7.8) across EYPC/CHOL-LUV⊃HPTS.[7-10, 19, 22] A substantial variance in the extent of anion transport abilities of compound **4.1c** (Figure 4.3B) was achieved when ion transport activity was measured with intravesicular NaCl and an iso-osmolar extravesicular NaX salts (Cl^-, Br^-, I^-, F^-, and SCN^-). Whereas, the use of intravesicular NaCl and an iso-osmolar extravesicular M^+/Cl^- salt (M^+ = Li^+, Na^+, K^+, Rb^+, and Cs^+) displayed comparable Cl^- ion transport efficiencies, but their pattern of Cl^- ion transport properties could be different (Figure 4.15). The outcome of the ion transport selectivity experiments revealed that the compound has Cl^- ion transport selectivity over the other investigated anions. However, the tested metal cations may not have any significant role in the ion transport process.

4.2.5. Evidence for the transport mechanism and pathways

The HPTS assay in the absence and presence of 4-(trifluoromethoxy)phenylhydrazone (FCCP; a protonophore) and valinomycin (a selective K^+ transporter) was also performed to get direct experimental evidence of the preferential Cl^- ion transport mechanism of the potent compound.[7-10, 19, 22] An increase in the Cl^- ion transport rate in

the presence of FCCP suggests a supportive effect between the compound and FCCP, eliminating the possibility of H^+ ion transport by the compound (Figure 4.4A). Similarly, the HPTS assay was also executed in the absence and presence of valinomycin. The valinomycin-mediated transport of K^+ ions from the extravesicular to intravesicular solution could induce the efflux of Cl^- ion and/or influx of OH^- ions to maintain the pH gradient. A substantial improvement in the Cl^- ion transport in the presence of valinomycin suggests the OH^-/Cl^- antiport mechanism (Figure 4.4B). The cooperative effect of compound **4.1c** and valinomycin suggest the preferential transport of OH^- ion over Cl^- ion. In the meantime, the cholesterol concentration-dependent transport (Figure 4.4C) and U-tube assay (Figure 4.4D) established that compound **4.1c** transport Cl^- ion via a carrier pathway.

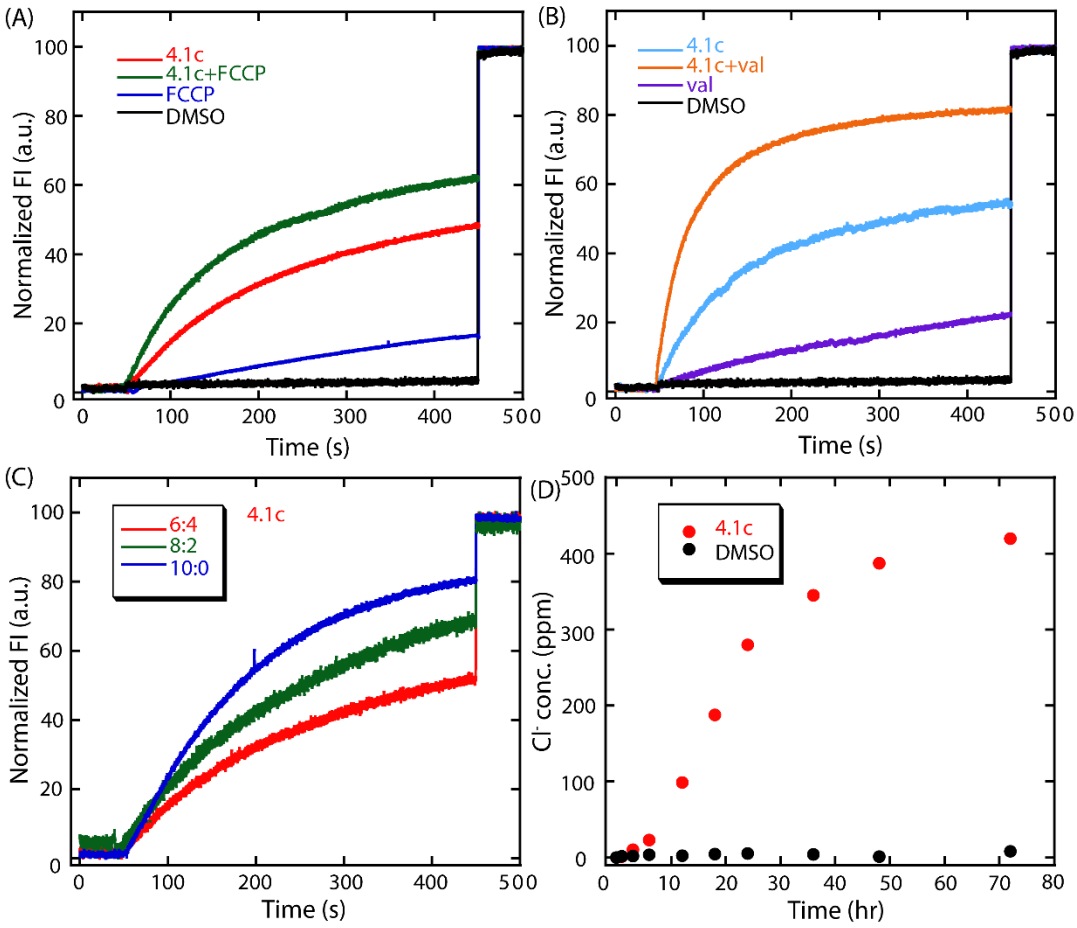

Figure 4.4 Assessment of ion transport activity of compound **4.1c** (0.038 µM) in the absence and presence of FCCP (4 µM) (A) and valinomycin (Val; 2.5 pM) (B). A pH gradient (pHin = 7.2, pHout = 7.8) was applied to initiate the transport of Cl^- ion. The effect of cholesterol concentration on the transport of Cl^- ion in the presence of compound **4.1c** (0.038 µM) (C). The Cl^- ion transport efficacy of compound **4.1c** (2 mM) was recorded across a U-tube by utilizing the Cl^- ion gradient, using chloride ion-selective electrode (D).

4.2.6. Regeneration study

The stimuli mediated dealkylation ability of proanionononophore **4.2** was investigated by HPLC and NMR analyses in the absence and presence of GSH, ROS, and light.

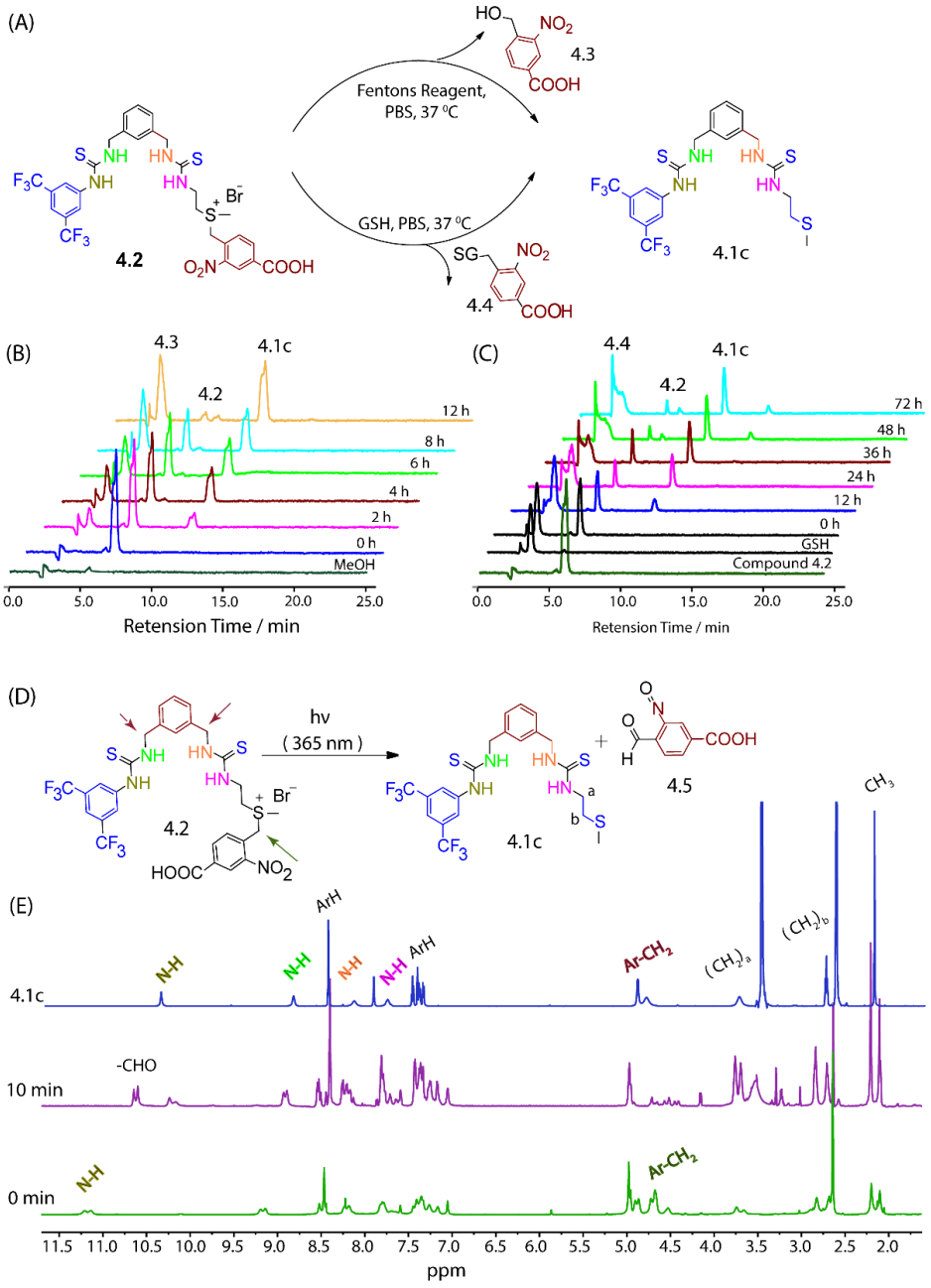

Figure 4.5. Proposed mechanisms of ROS and GSH mediated cleavage of proanionophore **4.2** (A). HPLC traces at different time intervals in the absence and presence of Fenton's Reagent (B) and GSH (C). Proposed mechanism of photo-mediated cleavage of proanionophore **4.2** (D). ^{1}H NMR spectra of proanionophore **4.2** at different time intervals (E).

The GSH, ROS mediated dealkylation of water-soluble proanionononophore **4.2,** and the in situ production of the active ion carrier **4.1c** was investigated by HPLC analysis (Figure 4.5A-B). The water solubility of compound **4.2** was 2.8 mg/mL in water. However, to avoid any solvent effect on the transport efficiency, all compounds (including compound **4.2**) were initially dissolved in DMSO and then diluted in buffer (so that final DMSO concentration is less than 3% (v/v)). The dealkylation of proanionononophore **4.2** (1 mmol) was performed in the presence of GSH (2 mM) in 10 mM PBS (pH 7.4) at 37 °C. The HPLC analysis revealed the time-dependent dealkylation of proanionononophore **4.2** and the regeneration of the active hydrophobic carrier **4.1c** along with intermediate **4.3** in the presence of GSH. Similarly, the dealkylation of proanionononophore **4.2** (1 mmol) was performed in the presence of Fenton's reagent (1 mM Fe^{2+} and 5 mM H_2O_2) in 10 mM PBS (pH 7.4) at 37 °C. The time-dependent dealkylation of proanionononophore **4.2** and hydrophobic carrier **4.1c** along with intermediate **4.4** in the presence of Fenton's reagent was analyzed by HPLC. The HRMS analyses further confirmed the generation of intermediates **4.3**, **4.4**, and active anionophore **4.1c** (Figure 4.17 and 4.18). The photolytic conversion of proanionononophore **4.2** to the active carrier **4.1c** was investigated by ^{1}H NMR in DMSO-d_6 solvent (Figure 4.5D and 4.5E). The solution was irradiated by LED lamps (365 nm wavelength) for 10 min. The presence of a new signal at δ = 10.6 ppm that corresponds to the aldehyde proton indicates the release of 4-formyl-3-nitrosobenzoic acid and regeneration of compound **4.1c** from **4.2.** The photolytic generation of 4-formyl-3-nitrosobenzoic acid was also confirmed by FT-IR and HRMS analyses (Figure 4.19 and 4.20).

The successful regeneration of active lipophilic carrier **4.1c** from water-soluble proanionononophore **4.2** in the presence of GSH, ROS, and light encouraged us to study stimuli-activated transmembrane ion transport efficiency.[19] The time-dependent improvement of the Cl^- ion transport aptitude also proved the generation of the active carrier **4.1c** in the presence of GSH, ROS, and light (Figure 4.6 A-C). The photo-irradiation rate of dealkylation was quite faster in comparison with that in the presence of GSH and ROS, which is advantageous for their bio-applicability. The photo-activated strategy can be applied for only surface phenomena due to the lack of tissue penetration ability of the light. The higher levels of intracellular GSH and ROS in cancer cells could

be sufficient enough to release the active carrier and promote ion transport mediated apoptosis. However, the structural integrity of proanionophore **4.2** was intact in the absence of GSH, ROS, and light.

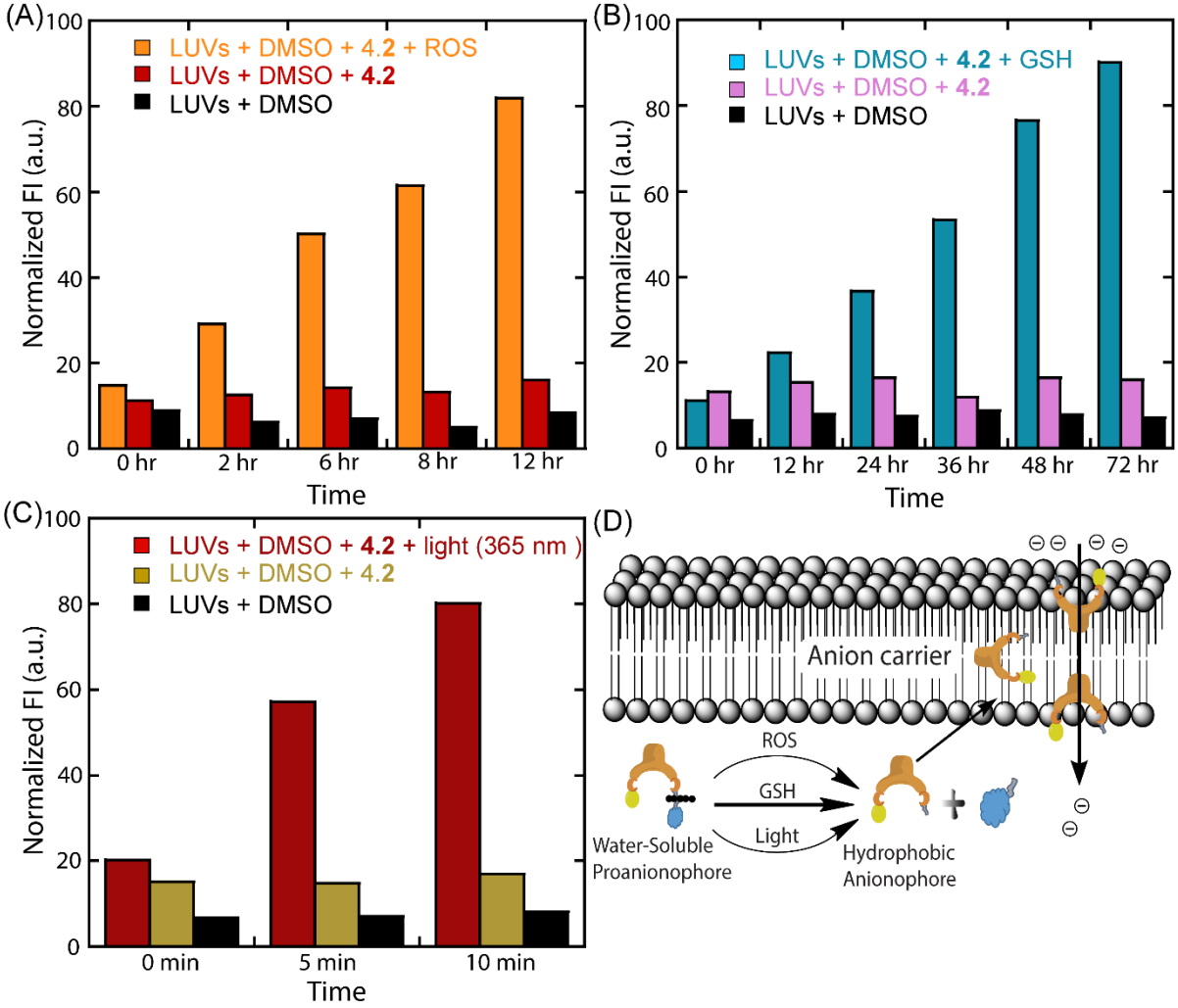

Figure 4.6. Chloride ion transport measurement of the Fenton's reagent (A), glutathione (B) and light (365 nm) (C) mediated release of the active transporter **4.1c** from proanionophore **4.2** in the presence of LUVs. Schematic diagram representing the stimuli-mediated regeneration of the active anionophore from its proanionophore and its transmembrane anion transport properties (D).

4.3. Conclusions

Herein, we demonstrated a multistimuli-responsive approach to regenerate the active lipophilic ionophore from the water-soluble proanionophore. The sulfonium-based proanionophore was successfully cleaved in the presence of stimuli like ROS, GSH, and light. The ^{1}H NMR titration experiments confirmed the binding of dithiourea derivative to the Cl^{-} ion. The fluorescence-based assay confirmed that the dithiourea derivative

selectively transports Cl^- ion across the lipid bilayer. The U-tube and cholesterol concentration-dependent assays suggest the transport of Cl^- ion via carrier pathway. The FCCP and valinomycin assays showed that Cl^-/ OH^- antiport mechanism is the operative pathway of Cl^- ion transport. The regenerated active carrier also successfully transports Cl^- ion under similar experimental conditions. Overall, this investigation revealed that the multistimuli-responsive strategy could be applied for the treatment of ion transport associated diseases.

4.4. Experimental Section

4.4.1. General information

All the chemicals were purchased from commercial sources like Sigma Aldrich and Alfa Aesar and directly used without further purification. Thin-layer chromatography (TLC) on silica gel 60 F254 (0.25 mm) was used to monitor completion of the reactions, and column chromatography was performed using the silica gel of 120-200 mesh (Merck). The ^1H NMR and ^{13}C NMR were recorded at 600 MHz and 151 MHz, respectively, by Bruker spectrometer. The chemical shifts were reported in parts per million (δ) using DMSO-d_6, $CDCl_3$, as the internal solvent. The coupling constant (J) values were reported in Hz, and the abbreviation was stated as follows: s (singlet), d (doublet), t (triplet), q (quartet), and m (multiple). High-resolution mass spectra (HRMS) were recorded at Agilent Q-TOF mass spectrometer with a Z-spray source using built-in software for the analysis of the documented mass data. Egg yolk phosphatidylcholine (EYPC) and cholesterol used for the biophysical assays were purchased from Sigma Aldrich. HEPES buffer, 8- hydroxypyrene-1, 3, 6-trisulfonic acid (HPTS), calcein, Triton X-100, and inorganic salts were also obtained from Sigma Aldrich. Ultrapure water (Milli-Q system, Millipore, Billerica, MA) was used for the preparation of all the buffers, and stock solutions of all the compounds were prepared in gas chromatographic grade DMSO which also purchased from Sigma.

4.4.2. Synthesis of compounds

4.4.2.1. Synthesis of 1,3-bis(isothiocyanatomethyl)benzene — The compound, 1,3-bis(isothiocyanatomethyl)benzene was synthesized according to literature procedure.[19] In brief, to a stirring solution of 1,3-phenylenedimethanamine (500 mg, 3.67 mmol) and N,N'-dicyclohexylcarbodiimide (DCC; 1.5 g) in dry THF, dropwise CS_2 (2.3 mL, 36

mmol) was added at room temperature under N_2 atmosphere. The reaction mixture was allowed to stir for 30 min at room temperature, and the progress of the reaction was monitored by thin-layer chromatography (TLC) analysis. After that, the reaction mixture was filtered through the filter paper. The filtrate was concentrated under reduced pressure. Then the crude reaction mixture was purified through column chromatography with a solvent gradient system using ethyl acetate/hexane (0-10%) to furnish the target compound as a yellowish liquid (70% yield). The compound was characterized by ^{1}H NMR and ^{13}C NMR analysis. ^{1}H NMR (600 MHz, $CDCl_3$): δ 7.34-7.30 (m, 1H), 7.21-7.19 (m, 2H), 7.15 (s, 1H), 4.64 (s, 4H); ^{13}C NMR (151 MHz, $CDCl_3$): δ 129.9, 127.6, 124.4, 121.6, 120.0, 43.2.

4.4.2.2. Synthesis of 1-(3-(isothiocyanatomethyl)benzyl)-3-(2-(methylthio)ethyl)thiourea — The compound, 1-(3-(isothiocyanatomethyl)benzyl)-3-(2-(methylthio)ethyl)thiourea was synthesized according to literature procedure.[19] In brief, to a stirring solution of 1,3-bis(isothiocyanatomethyl)benzene (500 mg, 2.27 mmol) in dry CH_3CN, was added 2-(methylthio)ethan-1-amine (186.2 mg, 2.04 mmol) at room temperature under N_2 atmosphere. Then the reaction mixture was continued to stir for 5-6 h at room temperature, and the progress of the reaction was monitored by TLC analysis. After the competition of the reaction, the mixture was concentrate under reduced pressure. Then the crude reaction mixture was purified through column chromatography with a solvent gradient system using ethyl acetate/hexane (0-10%) to give the target compound as a white solid (90% yield). The compound was characterized by ^{1}H NMR and ^{13}C NMR analysis. ^{1}H NMR (600 MHz, $CDCl_3$): δ 7.32-7.28 (m, 1H), 7.24-7.22 (m, 1H), 7.19-7.17 (m, 2H), 4.64 (m, 2H), 4.57 (s, 2H), 3.67-3.62 (m, 2H), 2.63-2.60 (m, 2H), 1.98 (s, 3H); ^{13}C NMR (151 MHz, $CDCl_3$): δ 182.2, 135.0, 129.6, 126.4, 126.0, 48.6. 47.8, 42.7, 33.3, 14.9.

4.4.2.3. Synthesis of bis(thiourea) derivatives (4.1a-4.1d) — To a stirring solution of 1-(3-(isothiocyanatomethyl)benzyl)-3-(2-(methylthio)ethyl)thiourea (200 mg, 0.64 mmol) in dry DMF, corresponding aromatic amine (0.77 mmol) and triethylamine (89 mL, 0.64 mmol) were added at room temperature under N_2 atmosphere. Then, the reaction mixture was stirred for 16-22h at room temperature, and the reaction was monitored by TLC analysis. After completion of the reaction, the maximum DMF

solvent was removed through ethyl acetate/ice water workup (minimum five times) using 100 mL separating funnel. The collected organic layers were dried over the anhydrous Na_2SO_4, filtered, and concentrated under reduced pressure. The crude reaction mixture was purified through the column chromatography with a solvent gradient system using ethyl acetate/hexane (0-10%) to give the corresponding yellowish compound. For compounds **4.1a, 4.1b, 4.1c,** and **4.1d,** the yields were 90%, 85%, 80%, and 95% respectively.

4.4.2.4. Synthesis of sulfonium derivative (4.2) — To a stirring solution of compound **4.1c** (200 mg, 0.37 mmol) in dry CH_3CN was added 4-bromomethyl-3-nitrobenzoic acid (106 mg, 0.41 mmol) at room temperature under N_2 atmosphere. Then, the reaction mixture was stirred for 24h under dark condition. The progress of the reaction was monitored by TLC analysis. After completion of the reaction, the solvent was removed under reduced pressure. The crude product was purified by preparative HPLC using the solvent system water/methanol (0-95%) to give the yellowish solid compound **4.2** (70% yield).

4.4.3. Characterization of the synthesized compounds

4.4.3.1. 1-(3-((3-(2-(methylthio)ethyl)thioureido)methyl)benzyl)-3-phenylthiourea (4.1a) — Following the general procedure as mentioned in earlier section 4.4.2.3, using 1-(3-(isothiocyanatomethyl)benzyl)-3-(2-(methylthio)ethyl)thiourea (200 mg, 0.64 mmol), aniline (71.15 mg, 0.77 mmol) and triethylamine (89 mL, 0.64 mmol). The yellowish compound was isolated with 90% yield. The compound was characterized by the HRMS (ESI), ^{1}H NMR and ^{13}C NMR analysis. ^{1}H NMR (600 MHz, DMSO-d_6): δ 9.61 (s, 1H), 8.14 (s, 1H), 7.98 (s, 1H), 7.60 (s, 1H), 7.74 – 7.43 (m, 2H), 7.35 – 7.32 (m, 2H), 7.31 – 7.29 (m, 1H), 7.25 (s, 1H), 7.23 – 7.22 (m, 1H), 7.19 – 7.17 (m, 1H), 7.14 – 7.11 (m, 1H), 4.73 – 4.66 (m, 4H), 3.61 (m, 2H), 2.64 – 2.62 (t, J = 7.0 Hz, 2H), 2.08 (s, 3H); ^{13}C NMR (151 MHz, $CDCl_3$): δ 181.3, 139.6, 139.4, 129.4, 128.7, 126.8, 126.5, 126.4, 124.8, 123.8, 47.8, 43.3, 32.93, 15.1; HRMS (ESI) m/z: calculated for $C_{19}H_{24}N_4S_3$ $(M+H)^+$: 405.1236, found: 405.1236.

4.4.3.2. 1-(3-((3-(2-(methylthio)ethyl)thioureido)methyl)benzyl)-3-(4-(trifluoromethyl)phenyl)thiourea (4.1b) — Following the general procedure as mentioned in earlier section 4.4.2.3, using 1-(3-(isothiocyanatomethyl)benzyl)-3-(2-(methylthio)ethyl)thiourea (200 mg, 0.64 mmol) and 4-(trifluoromethyl)aniline (124.07 mg, 0.77 mmol) and triethylamine (89 mL, 0.64 mmol). The crude yellowish compound was isolated with 85% yield. The compound was characterized by the HRMS (ESI), ^{1}H NMR and ^{13}C NMR analysis. ^{1}H NMR (600 MHz, DMSO-d_6): δ 9.97 (s, 1H), 8.47 (s, 1H), 8.00 (s, 1H), 7.75 – 7.73 (m, 2H), 7.68 – 7.66 (m, 2H), 7.6 (s, 1H), 7.33 – 7.30 (m, 1H), 7.26 (s, 1H), 7.24 – 7.23 (m, 1H), 7.20 - 7.19 (m, 1H), 4.74-4.67 (m, 4 H), 3.61 (m, 2H), 2.63 – 2.61 (t, J = 7.0 Hz, 2H), 2.08 (s, 3H); ^{13}C NMR (151 MHz, $CDCl_3$): δ 182.4, 181.0, 140.8, 137.9, 129.1, 126.8, 126.7, 126.0, 124.8, 122.9, 122.5, 121.2, 48.3, 48.1, 42.9, 32.9, 14.9; HRMS (ESI) m/z: calculated for $C_{20}H_{23}F_3N_4S_3$ $(M + H)^+$: 473.1110, found: 473.1110.

4.4.3.3. 1-(3,5-bis(trifluoromethyl)phenyl)-3-(3-((3-(2-(methylthio)ethyl)thioureido)methyl)benzyl)thiourea (4.1c) — Following the general procedure as mentioned in earlier section 4.4.2.3, using 1-(3-(isothiocyanatomethyl)benzyl)-3-(2-(methylthio)ethyl)thiourea (200 mg, 0.64 mmol), 3,5-bis(trifluoromethyl)aniline (416.26 mg, 0.77 mmol) and triethylamine (89 mL, 0.64 mmol). The crude yellowish compound was isolated with 90% yield. The compound was characterized by the ES-MS, ^{1}H NMR and ^{13}C NMR analysis. ^{1}H NMR (600 MHz, DMSO-d_6): δ 10.17 (s, 1H), 8.67 (s, 1H), 8.28 (s, 2H), 7.98 (s, 1H), 7.76 (s, 1H), 7.60 (s, 1H), 7.56 – 7.31 (t, J = 7.6 Hz, 1H), 7.26 (s, 1H), 7.25 – 7.23 (m, 1H), 7.20 – 7.19 (m, 1H), 4.77 – 4.66 (m, 4H), 3.61 (m, 2H), 2.63 – 2.61 (t, 2H), 2.07 (s, 3H); 13C NMR (151 MHz, CDCl3): δ 181.3, 139.8, 131.8, 131.6, 129.1, 126.9, 126.8, 123.8, 122.0, 121.9, 120.2, 118.1, 50.9, 48.2, 42.9, 32.9, 14.6; HRMS (ESI) m/z: calculated for $C_{29}H_{22}F_6N_4O_4S_3$ $(M + H)^+$: 541.0984, found: 541.0961.

4.4.3.4. 1-(4-methoxyphenyl)-3-(3-((3-(2-(methylthio)ethyl)thioureido)methyl)benzyl)thiourea (4.1d) — Following the general procedure as mentioned in earlier section 4.4.2.3, using 1-(3-(isothiocyanatomethyl)benzyl)-3-(2-(methylthio)ethyl)thiourea (200 mg, 0.64 mmol), 4-methoxyaniline (94.89 mg, 0.77 mmol) and triethylamine (89 mL, 0.64 mmol). The

crude yellowish compound was isolated with 95% yield. The compound was characterized by the ES-MS, ^{1}H NMR and ^{13}C NMR analysis. ^{1}H NMR (600 MHz, DMSO-d6): δ 9.46 (s, 1H), 8.01 (s, 1H), 7.96 (s, 1H), 7.62 (s, 1H), 7.30 – 7.28 (m, 1H), 7.26 – 7.24 (m, 2H), 7.22 (s, 1H), 7.20 – 7.19 (m, 1H), 7.17 – 7.16 (m, 1H), 6.92 – 6.90 (m, 2H), 4.70 - 4.69 (m, 4H), 3.74 (s, 3H), 2.64 – 2.62 (m, 2H), 2.08 (s, 3H); ^{13}C NMR (151 MHz, CDCl3): δ182.3, 181.5, 158.9, 138.3, 137.8, 129.6, 128.4, 127.6, 126.9, 126.7, 126.0, 115.3, 55.6, 48.8, 48.1, 42.9, 33.3, 14.9; HRMS (ESI) m/z: calculated for $C_{20}H_{26}N_4OS_3$ $(M + H)^+$: 435.1342, found: 435.1316.

4.4.3.5. (2-(3-(3-((3-(3,5-bis(trifluoromethyl)phenyl)thioureido)methyl)benzyl)thioureido)ethyl)(4-carboxy-2-nitrobenzyl)(methyl)sulfonium bromide (4.2) — Following the general procedure as mentioned as mentioned in earlier section 4.4.2.4, using **4.1c** (200 mg, 0.37 mmol) and 4-bromomethyl-3-nitrobenzoic acid (106 mg, 0.41 mmol). The crude compound was isolated with 70% yield. The compound was characterized by the ES-MS, 1H NMR and 13C NMR analysis. ^{1}H NMR (600 MHz, DMSO-d_6): δ 11.15 – 11.08 (m, 1H), 9.13 - 9.07 (m, 1H), 8.44 (s, 1H), 8.39 – 8.37 (m, 2H), 8.14 – 8.10 (m, 1H), 7.74 – 7.70 (m, 1H), 7.51(s, 1H), 7.36 – 7.27 (m, 3H), 7.17(s, 1H), 7.08 (s, 1H), 6.96 (s, 1H), 4.87 - 4.84 (m, 2H), 4.79 – 4.75 (m, 2H), 4.61 – 4.56 (m, 2H), 3.62 – 3.54 (m, 2H), 2.69 (m, 2H), 2.06 (s, 3H); ^{13}C NMR (151 MHz, CDCl3): δ181.4, 165.7, 163.6, 148.2, 142.6, 134.6, 133.2, 132.6, 130.6, 129.0, 127.1, 126.3, 126.0, 124.6, 123.1, 122.8, 121.5, 116.4, 47.0, 46.2, 43.7, 32.1, 31.6, 15.2; HRMS (ESI) m/z: calculated for $C_{29}H_{28}F_6N_5O_4S_3^+$ (M): 720.1280, found: 720.1249.

4.4.4. Anion binding analysis by ^{1}H-NMR titration:

The ^{1}H NMR titration was performed for compounds **4.1a**, **4.1b**, **4.1c**, and **4.1d** and the procedure is previously outlined in section 2.4.4 with few alterations. The association constant (Ka) values were calculated using the BindFit v0.5 software (1:1 binding model).

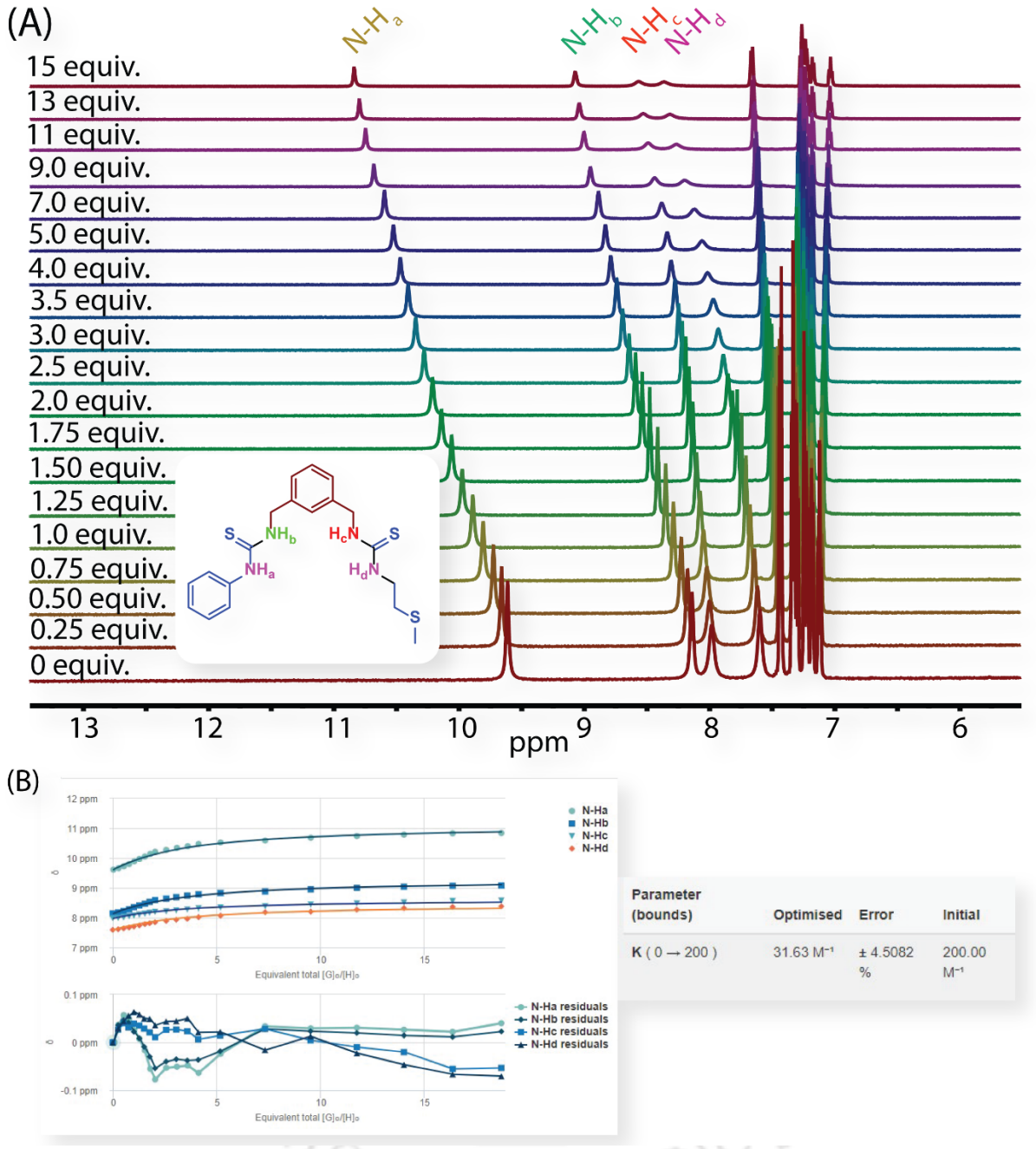

Figure 4.7. ^{1}H-NMR titration spectra for compound **4.1a** (10 mM) with the sequential addition of TBACl in DMSO-d_6 solvent. The amounts of added TBACl are shown on the spectra (A). The plot of chemical shift (δ) of N-H_a and N-H_b protons vs. equivalent total ($[G]_0/[H]_0$) added, fitted to 1:1 binding model of BindFit v0.5 program (B). H = host = **4.1a** and G = guest = TBACl.

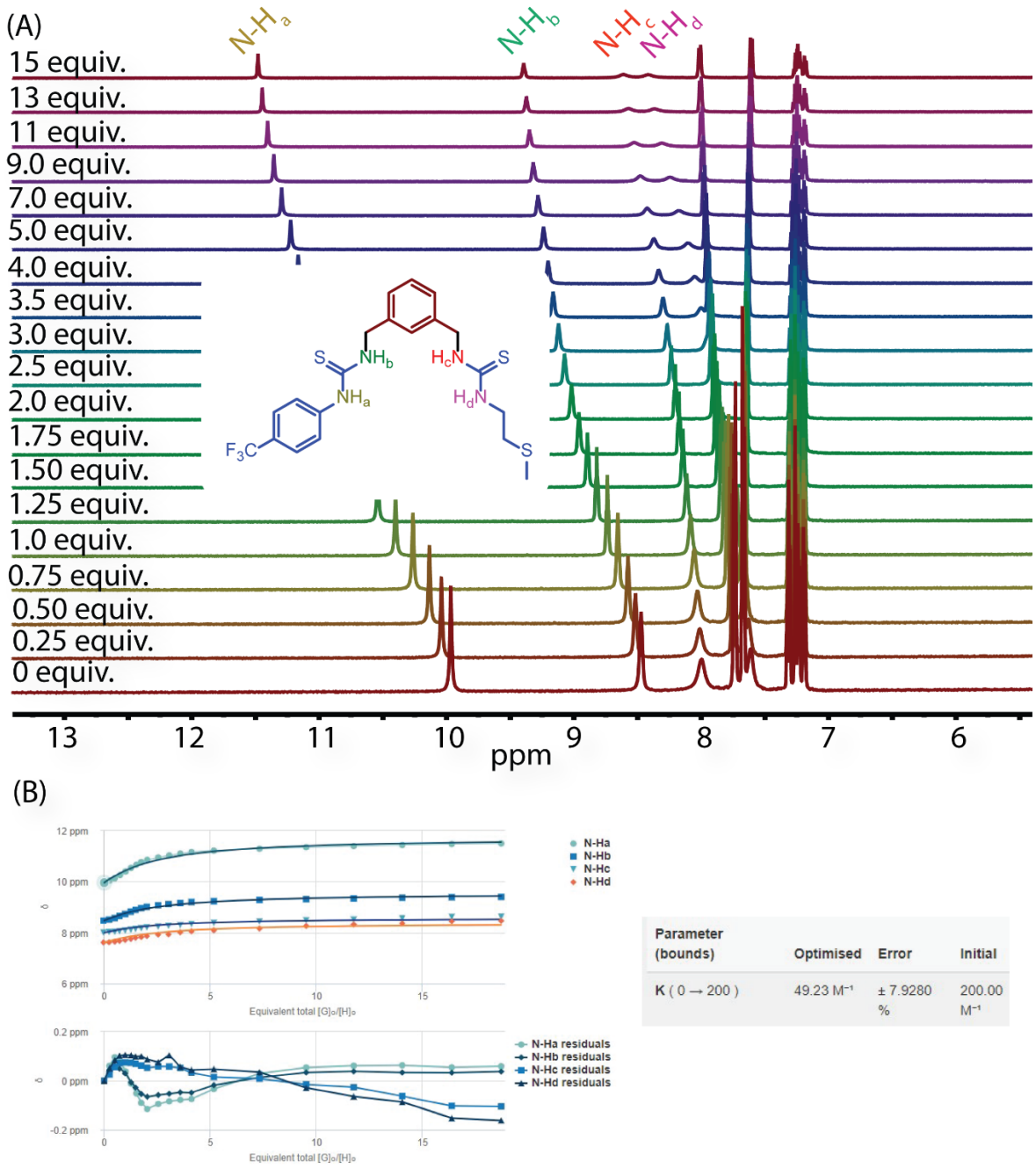

Figure 4.8. ^{1}H-NMR titration spectra for compound **4.1b** (10 mM) with the sequential addition of TBACl in DMSO-d_6 solvent. The amounts of added TBACl are shown on the spectra (A). The plot of chemical shift (δ) of N-H_a and N-H_b protons vs. equivalent total ($[G]_0/[H]_0$) added, fitted to 1:1 binding model of BindFit v0.5 program (B). H = host = **4.1b** and G = guest = TBACl.

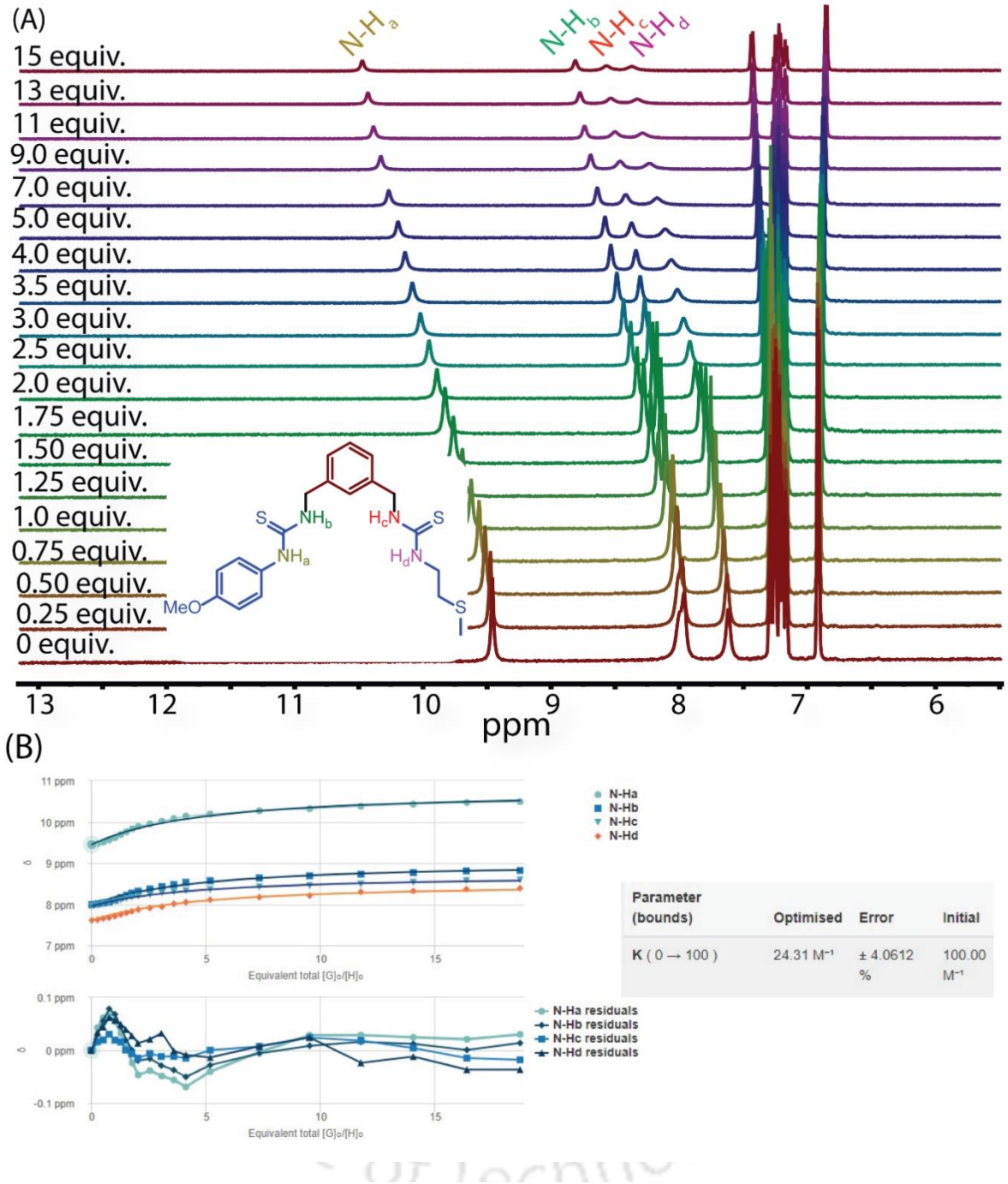

Figure 4.9. ^{1}H-NMR (600MHz) titration spectra for compound **4.1d** (10 mM) with the sequential addition of TBACl in DMSO-d_6 solvent. The amounts of added TBACl are shown on the spectra (A). The plot of chemical shift (δ) of N-H_a and N-H_b protons vs. equivalent total ($[G]_0/[H]_0$) added, fitted to 1:1 binding model of BindFit v0.5 program (B). H = host = **4.1d** and G = guest = TBACl.

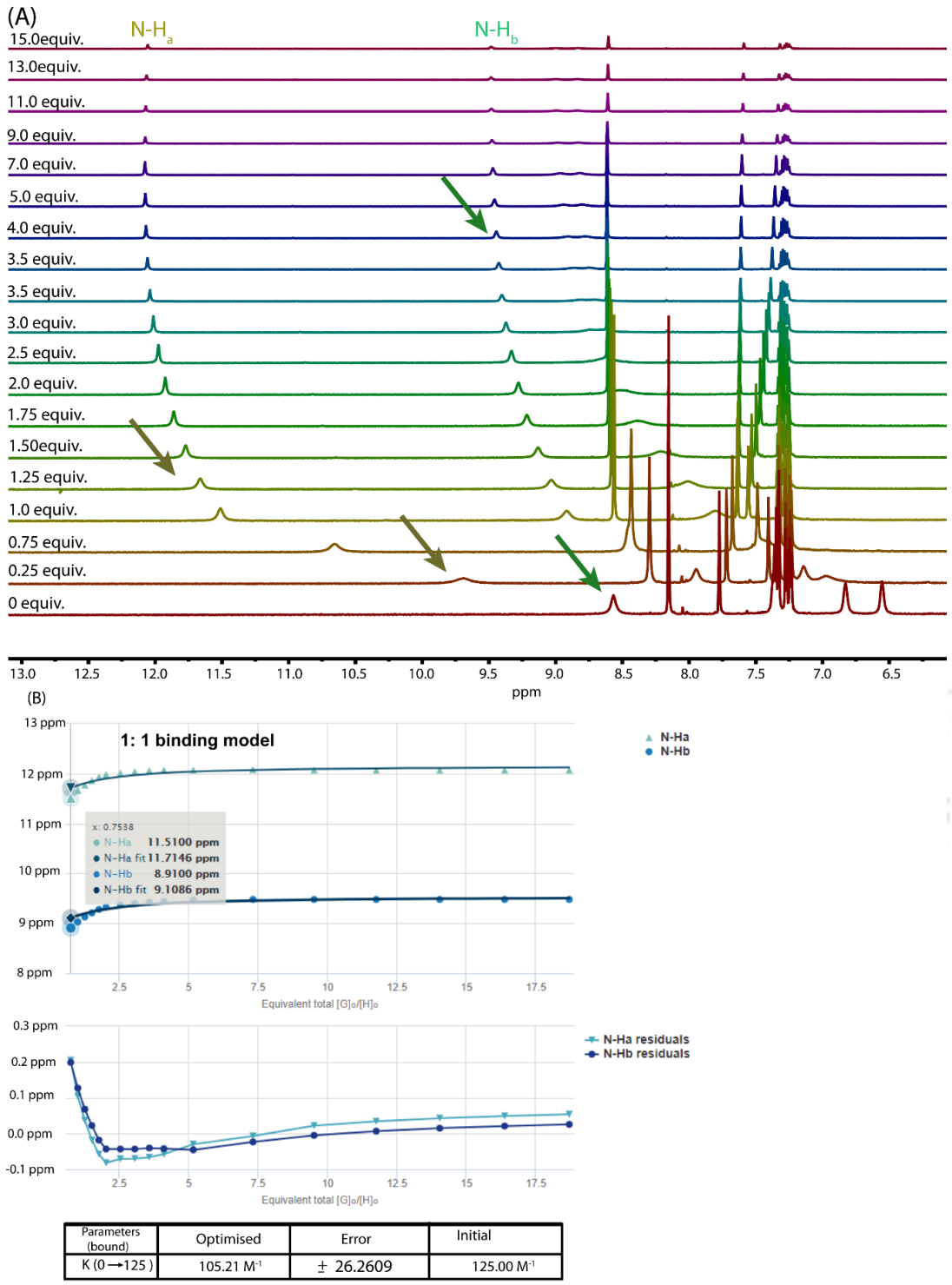

Parameters (bound)	Optimised	Error	Initial
K (0→125)	105.21 M^{-1}	± 26.2609	125.00 M^{-1}

Figure 4.10. ^{1}H-NMR titration spectra for compound **4.1c** (10 mM) with the sequential addition of TBACl in CD_3CN solvent. The amounts of added TBACl are shown on the spectra (A). The plot of chemical shift (δ) of N-H_a and N-H_b protons vs. equivalent total ($[G]_0$ / $[H]_0$) added, fitted to 1:1 binding model of BindFit v0.5 program (B). H = host = **4.1c** and G = guest = TBACl.

Table 4.2: Binding constant

Compound	Binding constant (M^{-1})			Average(M^{-1})	Standard deviation(M^{-1})
	Set 1	Set 2	Set 3		
4.1a	31.63	32.35	32.23	32.07	0.31496
4.1b	49.23	49.88	49.43	49.5133	0.27183
4.1c	68.57	69.1	69.56	69.0767	0.4045
4.1d	24.31	25.1	24.32	24.5767	0.37008

Table 4.3: Solubility of the compounds

Compound	Aqueous solubility (mg/mL)
4.1a	Insoluble
4.1b	Insoluble
4.1c	Insoluble
4.1d	Insoluble
4.2	2.8

4.4.5. Ion transporting activity studies

4.4.5.1. Preparation of EYPC-LUVs⊃HPTS –

Described in section 2.4.5.2.

4.4.5.2. Ion transport activity across EYPC / CHOL-LUV⊃ HPTS –

The HPTS fluorescence assay was done by adding 2890 µL of buffer solution (20 mM HEPES buffer, pH 7.2, containing 100 mM NaCl), 50 µL of EYPC / CHOL-LUV ⊃ HPTS and 50 µL of 0.5 M NaOH in a clean and dry 3 mL fluorescence cuvette placed in the fluorescence spectrophotometer (Fluoromax-4 spectrofluorometer) at room temperature under the slow stirring condition for around 3 minutes. During this time, a pH gradient of ~ 0.6 between the extra- and intravesicular systems was generated. The HPTS fluorescence intensity was monitored (at t = 0 s) at λem = 510 nm (λex = 450 nm). The kinetics was initiated at t = 50 s by adding 10 µL of the respective compound from their DMSO stock solution. The vesicles

were lysed at t = 450 s by adding 20 µL 20% Triton X-100 solution, and the fluorescence measurement was continued for an additional 50 s (t = 500 s).

4.4.5.3. Quantitative measurement of transport activity from HPTS assay ─

Mentioned in section 2.4.5.4.

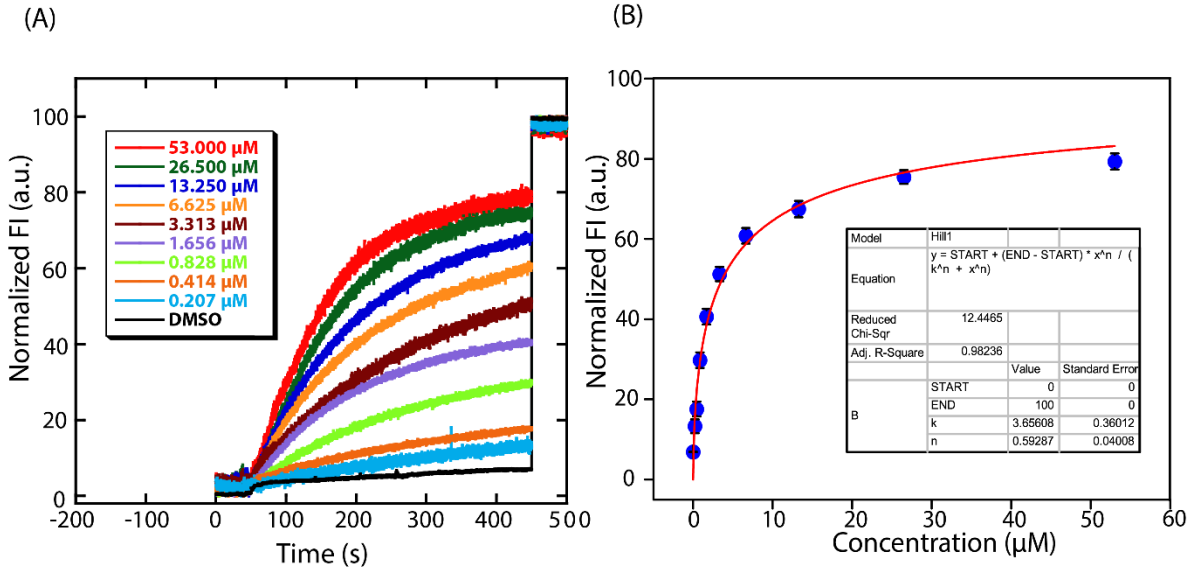

Figure 4.11. Concentration-dependent transmembrane transport of Cl^- ion in the presence of compound **4.1a** across the EYPC/CHOL-LUV⊃HPTS. The ion transport activity was measured by HPTS fluorescence assay using a pH gradient (pH_{in} = 7.2, pH_{out} = 7.8; A). The EC_{50} value was calculated using the modified Hill equation (B).

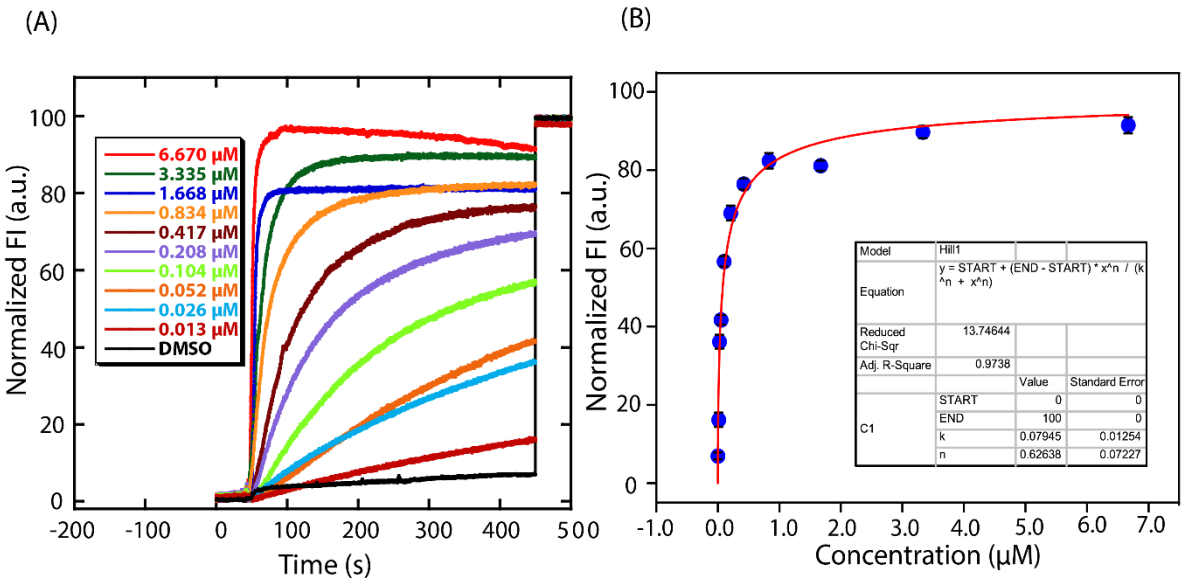

Figure 4.12. Concentration-dependent transmembrane transport of Cl^- ion in the presence of compound **4.1b** across the EYPC/CHOL-LUV⊃HPTS. The ion transport activity was measured by HPTS fluorescence assay using a pH gradient (pH_{in} = 7.2, pH_{out} = 7.8; A). The EC_{50} value was calculated using the modified Hill equation (B).

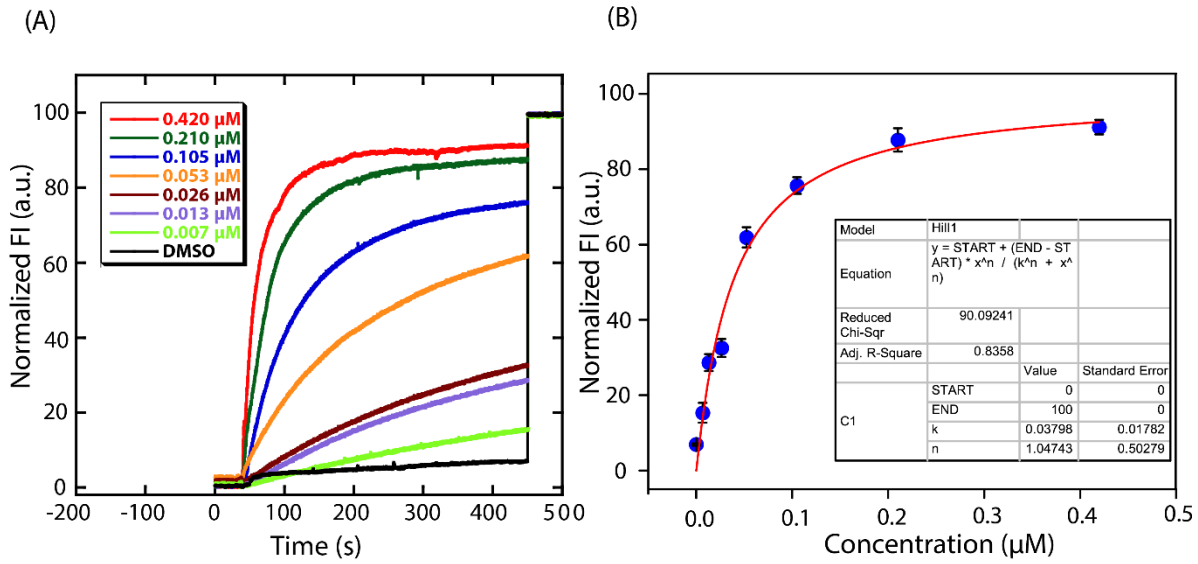

Figure 4.13. Concentration-dependent transmembrane transport of Cl^- ion in the presence of compound **4.1c** across the EYPC/CHOL-LUV⊃HPTS. The ion transport activity was measured by HPTS fluorescence assay using a pH gradient (pH_{in} = 7.2, pH_{out} = 7.8; A). The EC_{50} value was calculated using the modified Hill equation (B).

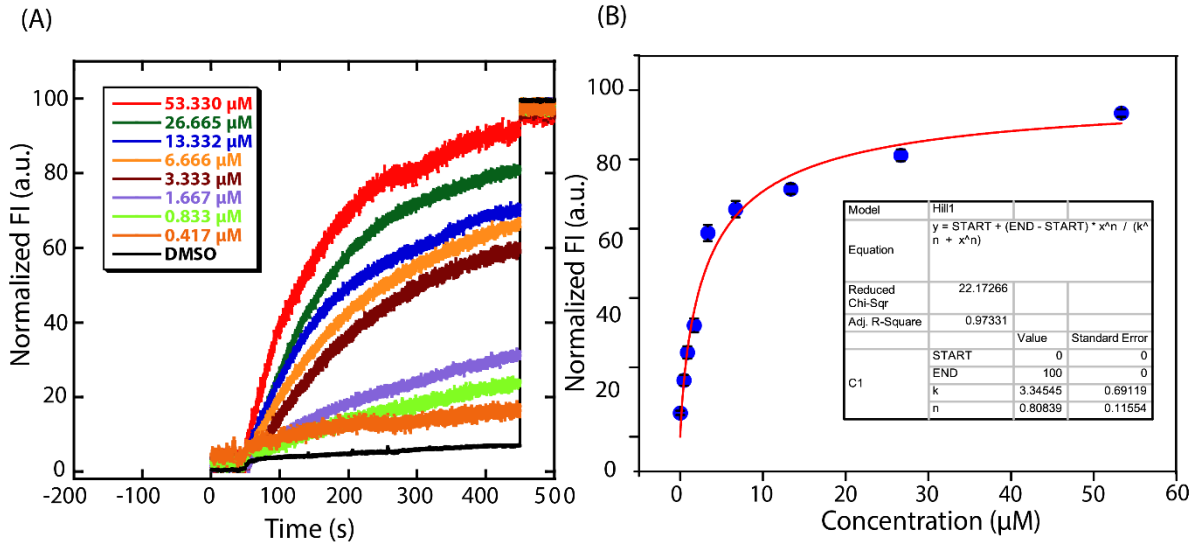

Figure 4.14. Concentration-dependent transmembrane transport of Cl^- ion in the presence of compound **4.1d** across the EYPC/CHOL-LUV⊃HPTS. The ion transport activity was measured by HPTS fluorescence assay using a pH gradient (pH_{in} = 7.2, pH_{out} = 7.8; A). The EC_{50} value was calculated using the modified Hill equation (B).

4.4.5.4. Ion Selectivity Studies

4.4.5.4.1. Buffer and stock solution preparation ─ Requisite amount of HEPES and MCl or Na_xA salt (LiCl, NaCl, KCl, RbCl, CsCl, NaBr, NaI, $NaNO_3$ and NaOAc) were added and

dissolved in MilliQ water to attain a final concentration of 20 mM HEPES and 100 mM of the respective salt.

4.4.5.4.2. Cation selectivity studies ─ The HPTS fluorescence assay was done by adding 2890 µL of buffer solution (20 mM HEPES buffer, pH 7.2, containing 100 mM of MCl salt), 50 µL of EYPC/CHOL-LUV⊃HPTS and 50 µL of 0.5 M NaOH in a clean and dry 3 mL fluorescence cuvette placed in the fluorescence spectrophotometer (Fluoromax-4 spectrofluorometer) at room temperature under the slow stirring condition for around 3 minutes. During this time, a pH gradient of ~ 0.6 between the extra- and intravesicular systems was generated. The HPTS fluorescence intensity was monitored (at t = 0 s) at λem = 510 nm (λex = 450 nm). The kinetics was initiated at t = 50 s by adding 10 µL of the respective compound from their DMSO stock solution. The vesicles were lysed at t = 450 s by adding 20 µL 20% Triton X-100 solution, and the fluorescence measurement was continued for an additional 50 s (t = 500 s).

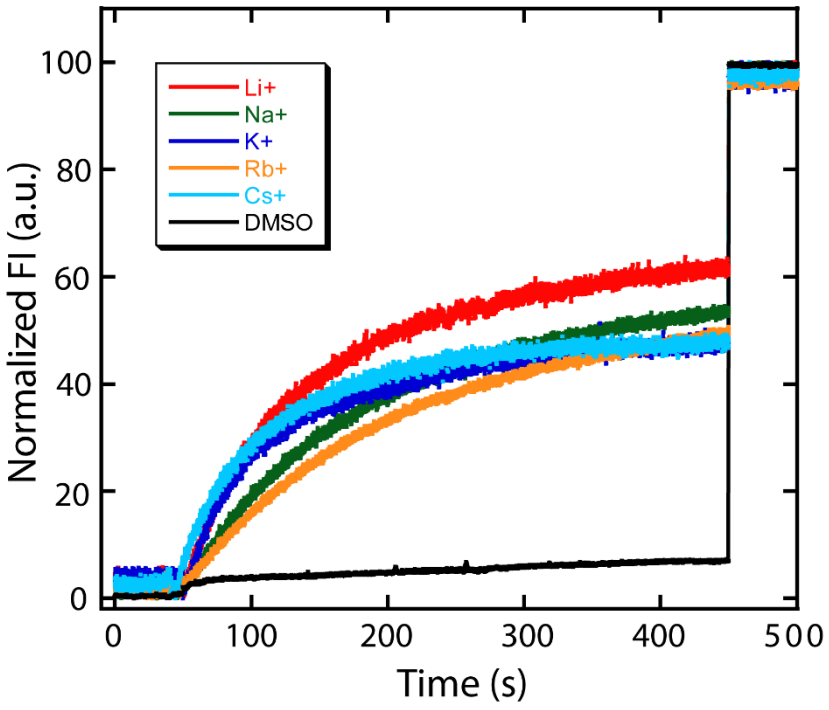

Figure 4.15. cation selectivity of compound **4.1c** (0.038 µM), as measured by HPTS assay in the presence of pH gradient.

4.4.5.4.3. Anion selectivity studies ─ Similar procedure was followed according to the earlier section except that here HEPES buffer (20 mM), pH 7.2 containing Na_xA (100 mM) solutions were used where A = Cl^-, Br^-, I^-, F^-, and SCN^- for anion selectivity.

4.4.5.5. Evidence for the mechanistic pathway for chloride ion transport

4.4.5.5.1. Ion transport activity in the presence of FCCP ─ The vesicles were prepared by following a similar procedure, as discussed in earlier section 4.4.5.1. The ion transport activity was measured in the presence as well as in the absence of FCCP dye. The HPTS fluorescence assay was done by adding 2890 µL of buffer solution (20 mM HEPES buffer, pH 7.2, containing 100 mM NaCl), 50 µL of EYPC/CHOL-LUV⊃HPTS and 50 µL of 0.5 M NaOH in a clean and dry 3 mL fluorescence cuvette placed in the fluorescence spectrophotometer (Fluoromax-4 spectrofluorometer) at room temperature under the slow stirring condition for around 3 minutes. During this time, a pH gradient of ~ 0.6 between the extra- and intravesicular systems was generated. The HPTS fluorescence intensity was monitored (at t = 0 s) at λem = 510 nm (λex = 450 nm). The kinetics was initiated at t = 50 s by adding 10 µL of a solution containing 8 µL compound and 2 µL FCCP from their respective DMSO stock solution. The vesicles were lysed at t = 450 s by adding 20 µL 20% Triton X-100 solution, and the fluorescence measurement was continued for an additional 50 s (t = 500 s). A similar experiment was carried out by adding 10 µL of the compound solution only without FCCP at t = 50 s.

4.4.5.5.2. Ion transport activity in the presence of valinomycin ─ The vesicles were prepared by following a similar procedure, as discussed in earlier section 3.1. The HPTS fluorescence assay was done by adding 2890 µL of buffer solution (20 mM HEPES buffer, pH 7.2, containing 100 mM NaCl), 50 µL of EYPC/CHOL-LUV⊃HPTS and 50 µL of 0.5 M NaOH in a clean and dry 3 mL fluorescence cuvette placed in the fluorescence spectrophotometer (Fluoromax-4 spectrofluorometer) at room temperature under the slow stirring condition for around 3 minutes. During this time, a pH gradient of ~ 0.6 between the extra- and intravesicular systems was generated. The HPTS fluorescence intensity was monitored (at t = 0 s) at λem = 510 nm (λex = 450 nm). The kinetics was initiated at t = 50 s by adding 10 µL of a solution containing 8 µL compound and 2 µL valinomycin from their respective DMSO stock solution. The vesicles were lysed at t = 450 s by adding 20 µL 20% Triton X-100 solution, and the fluorescence measurement was continued for an additional 50 s (t = 500 s). A similar experiment was carried out by adding 10 µL of the compound solution only without valinomycin at t = 50 s.

4.4.5.6. Evidence for mobile carrier mechanism

4.4.5.6.1. Cholesterol dependency assay ─ The LUVs were prepared in a similar manner as described in the earlier section, only the molar ratios of EYPC and cholesterol were varied as 10:0, 8:2 and 6:4 to explore the effect of cholesterol on Cl^- ion transport activity of the compounds. Increasing the concentration of cholesterol is known to slow the diffusion process, which will be more prominent in the case of a mobile carrier mechanism. At the same time, not much significant difference is expected in the case of an ion channel mechanistic pathway. A similar experimental procedure was followed, as mentioned in the earlier section, except that here, for each experiment, a different liposome solution was used, having a different concentration of cholesterol.

4.4.5.6.2. U-tube experiment ─

Mentioned in section 2.4.5.10.2.

4.4.5.7. Test for the leaching-out of the compounds from the membrane bilayer environment ─ The assay was performed to prove the membrane bilayer location of the compounds over the course of the different experiments being performed. If the compounds are in the membrane bilayer, then with the dilution of the lipid solution, the transport rate should remain the same. For this assay, various concentrations of EYPC/CHOL-LUV⊃HPTS in 20 mM HEPES buffer at pH 7.2, containing 100 mM NaCl (final concentration of the vesicles were 300 µM, 400 µM, 500 µM, and 600 µM) were taken in a 3 mL fluorescence cuvette followed by addition of the compound **4.1c** (10 µL from the stock solution to maintain a fixed ionophore/lipid ratio in all cases). The cuvette was then placed under the stirring conditions for maximum incorporation of the compounds into the lipid bilayer. The HPTS fluorescence intensity was monitored (at t = 0 s) at λ_{em} = 510 nm (λ_{ex} = 450 nm). The kinetics was initiated at t = 50 s by adding 10 µL of the compound solution **4.1c** from the respective DMSO stock solution. The vesicles were lysed at t = 450 s by adding 20 µL 20% Triton X-100 solution, and the fluorescence measurement was continued for an additional 50 s (t = 500 s). Four lipid concentrations were used for this assay, and the transport efficacy was found to be the same in all these four cases suggesting that the compounds were in the lipid bilayer during the course of all the experiments.

4.4.6. Regeneration of the active transporter by dealkylation of the proanionophore

4.4.6.1. Regeneration by using GSH ─ The bromosulfonium salt of compound **4.2** (1 mM) was dissolved in methanol, and 10 mM PBS, pH 7.4, containing 2 mM reduced glutathione GSH, and the mixture was incubated at 37 °C. At different time points, an aliquot of the reaction solution was removed and monitored by HPLC analysis. The aliquots were dissolved in methanol before its injection to the analytical HPLC (Ultimate 3000, Thermo Fisher Scientific) system. The Hypersil GOLD™ C18 Selectivity LC Column and a Charged Aerosol Detector (CAD) were used for the analysis. Methanol/water gradient (95% methanol and 5% water) was used as the mobile phase at a flow rate of 0.5 mL/minute for 25 minutes run time.

4.4.6.2. Regeneration by using Fenton's reagent ─ The bromosulfonium salt of compound **4.2** (1 mM) was dissolved in methanol, and 10 mM PBS, pH 7.4 containing Fenton's reagent (1 mM Fe^{2+} and 5 mM H_2O_2). The mixture was then incubated at 37 °C. At different time points, an aliquot of the reaction solution was collected, and the dealkylation efficiency was monitored by HPLC analysis.

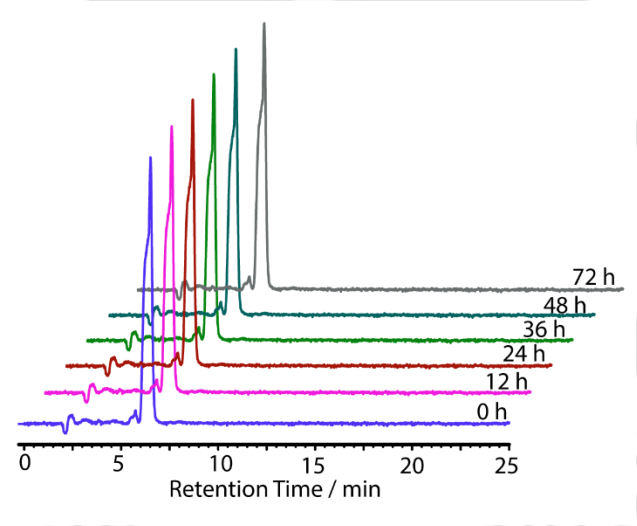

Figure 4.16. HPLC traces of proanionophore **4.2** at different time intervals in the absence of Fenton's reagent. A similar spectral pattern was observed in the absence of GSH.

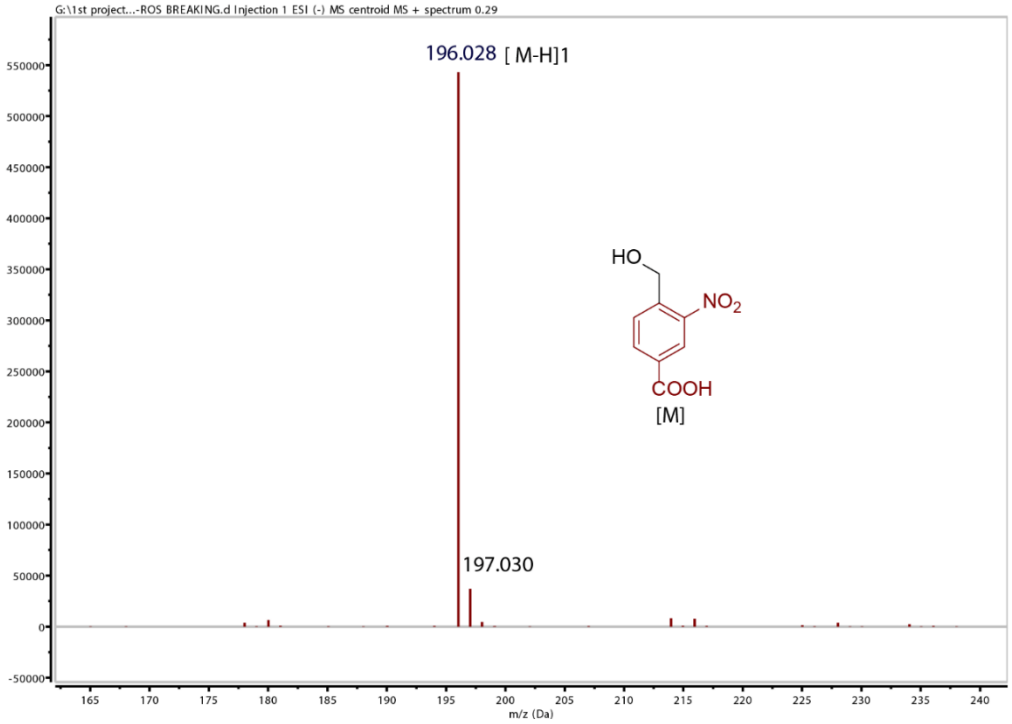

Figure 4.17. Mass spectra of the intermediate **4.3** generated due to the cleavage of proanionophore **4.2** in the presence of Fenton's reagent.

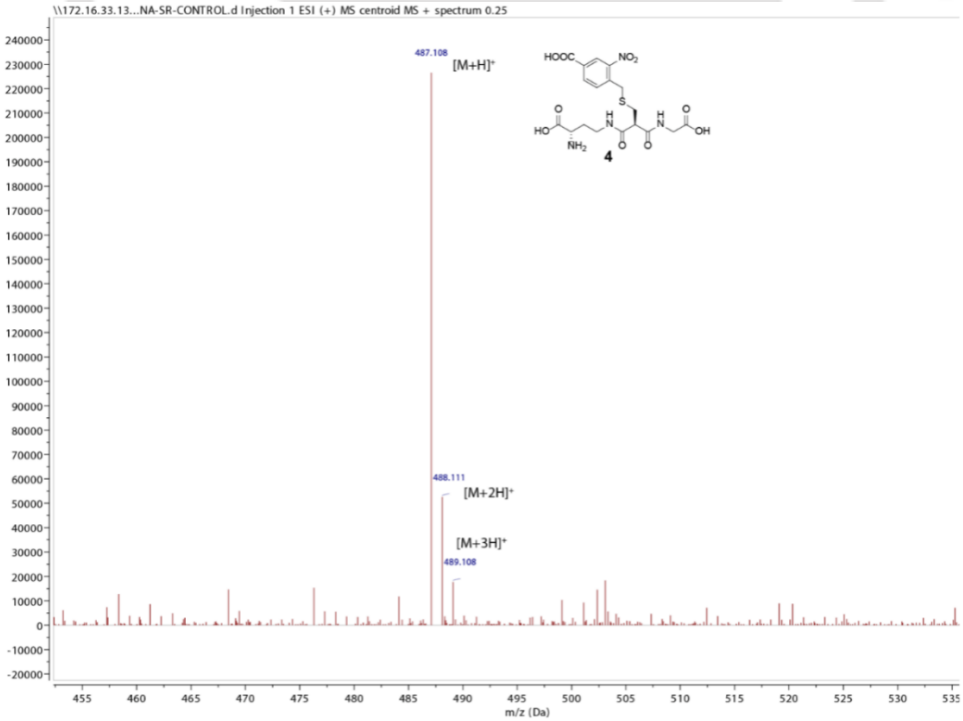

Figure 4.18. Mass spectra of the glutathione derivative **4.4**.

4.4.6.3. Photolysis Studies ─ In a clean and dry NMR tube, the solution of proanionophore **4.2** (5 mg in 0.5 mL) was taken in DMSO-d_6. The ^{1}H NMR spectrum of the sample was recorded first (t = 0 min). Then, the tube was kept in a photoreactor and irradiated with UV light (3×3 Watt LEDs, λ = 365 nm) for 10 min, and ^{1}H NMR spectrum of the irradiated sample was recorded. The ^{1}H NMR spectra were processed using MestReNova 6.0 by considering residual solvent peak as an internal reference. We have also performed the FT-IR experiment, the sulfonium salt **4.2** was dissolved in methanol, and it was kept in a photoreactor and irradiated with UV light for 10 min, and the FTIR spectrum was recorded. Therefore, upon photoirradiation, the appearance of the new aldehyde proton peak signal was generated, and the photolytic conversion of proanionophore **4.2** to carrier **4.1c** was confirmed by ^{1}H NMR and FT-IR spectrum.

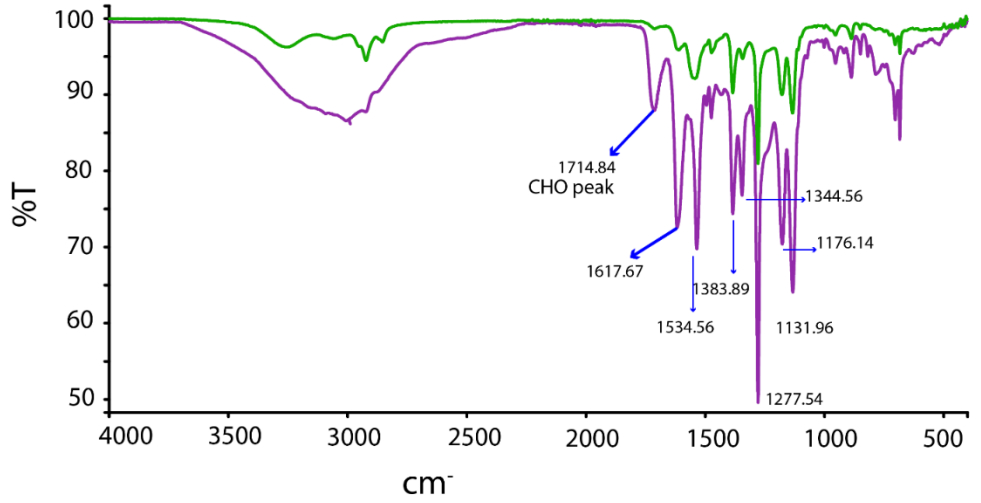

Figure 4.19. FT-IR spectrum of sulfonium salt **4.2** in the absence of 365 nm UV light (green line) and after 10 min (violet line) irradiated with 365 nm light.

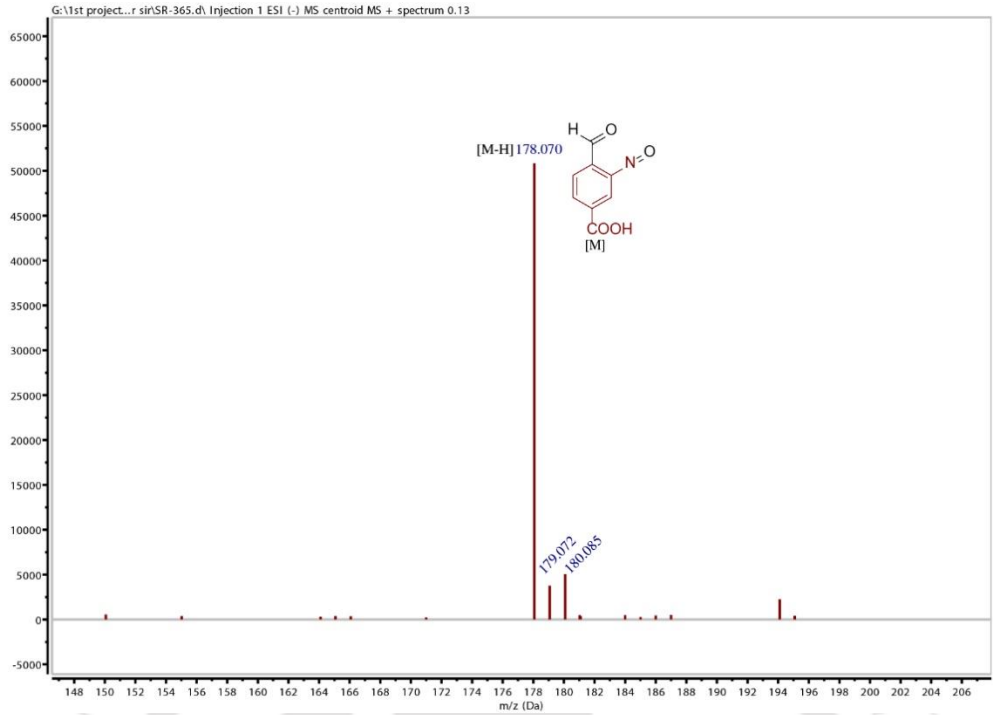

Figure 4.20. Mass spectra of intermediate **4.5** upon photoirradiation of compound **4.2**.

4.4.7. Ion transport activity of regenerated anionophore by fluorescence-based assay

4.4.7.1. Ion transport activity of glutathione mediated regenerated anionophore ─ The bromosulfonium salt **4.2** (1 mM) was dissolved in methanol, and 10 mM PBS, pH 7.4, containing 2 mM reduced GSH, and the mixture was incubated at 37 °C. At different time points (0 h, 12 h, 24 h, 36 h, 48 h, 72 h), an aliquot of the reaction solution was removed. Using similar fluorescence based assay as reported in the earlier section, the Cl^- ion transport efficiency of the aliquots was tested. A control experiment was done by adding DMSO instead of bromosulfonium salt **4.2**, and similarly, the aliquots were tested.

4.4.7.2. Fenton's reagent mediated regeneration of carrier from proanionophore ─ Regeneration by using the bromosulfonium salt **4.2** (1 mM) was dissolved in methanol and 10 mM PBS, pH 7.4 containing Fenton's reagent (1 mM Fe^{2+} and 5 mM H_2O_2) and the mixture was incubated in 37 °C. At different time points (0h, 2h, 4h, 6h, 8h, 12h), an aliquot of the reaction mixture was removed, and the Cl^- ion efficiency was analyzed by the fluorescence-based method as reported in the earlier section.

4.4.7.3. Light mediated regeneration of carrier from proanionophore ─ In a clean and dry 3 mL fluorescence cuvette 2890 µL of buffer solution (20 mM HEPES buffer, pH 7.2, containing 100 mM NaCl), 50 µL of EYPC/CHOL-LUV⊃HPTS and 50 µL of 0.5 M NaOH were taken and placed in the fluorescence spectrophotometer (Fluoromax-4 spectrofluorometer) at room temperature under the slow stirring condition for around 3 minutes. During this time, a pH gradient of ~ 0.6 between the extra- and intravesicular systems was generated. While in a clean glass sample vial, 63 µM of the proanionophore **4.2** was taken and irradiated with UV light (3 × 3 Watt LEDs, λ = 365 nm) for 5 minutes and 10 minutes and the two aliquots were taken. The HPTS fluorescence intensity was monitored (at t = 0 s) at λem = 510 nm (λex = 450 nm). The kinetics was initiated at t = 50 s by adding 10 µL of the respective aliquots. The vesicles were lysed at t = 450 s by adding 20 µL 20% Triton X-100 solution, and the fluorescence measurement was continued for an additional 50 s (t = 500 s).

4.5. NMR spectra of the synthesized compounds

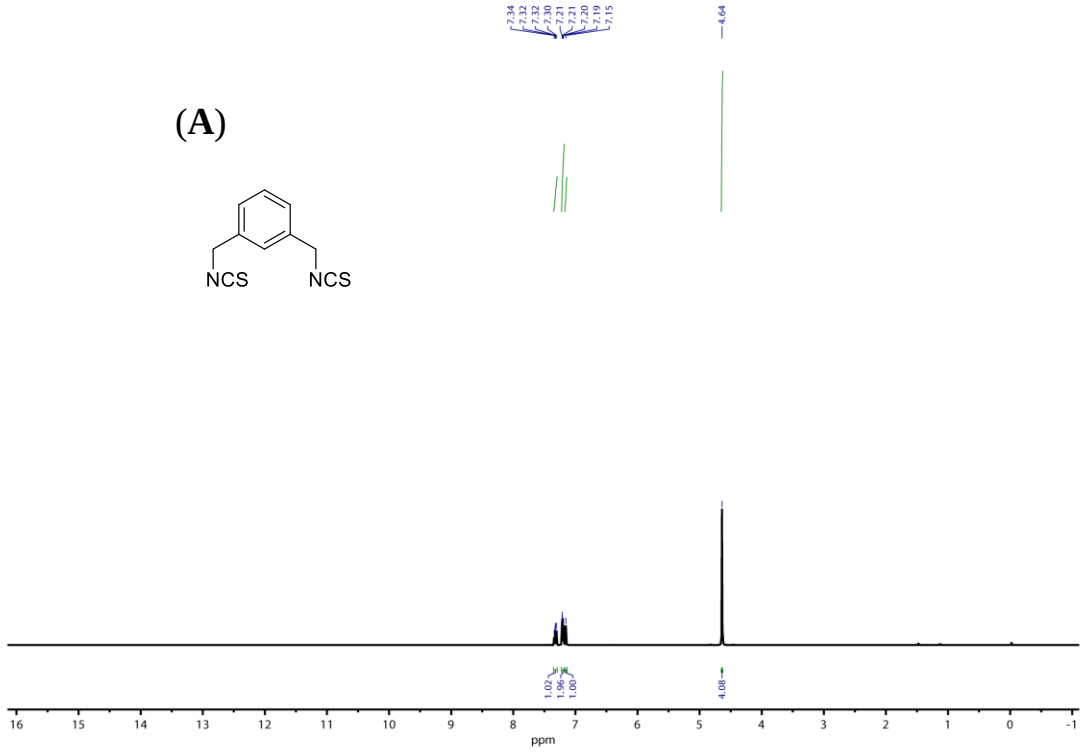

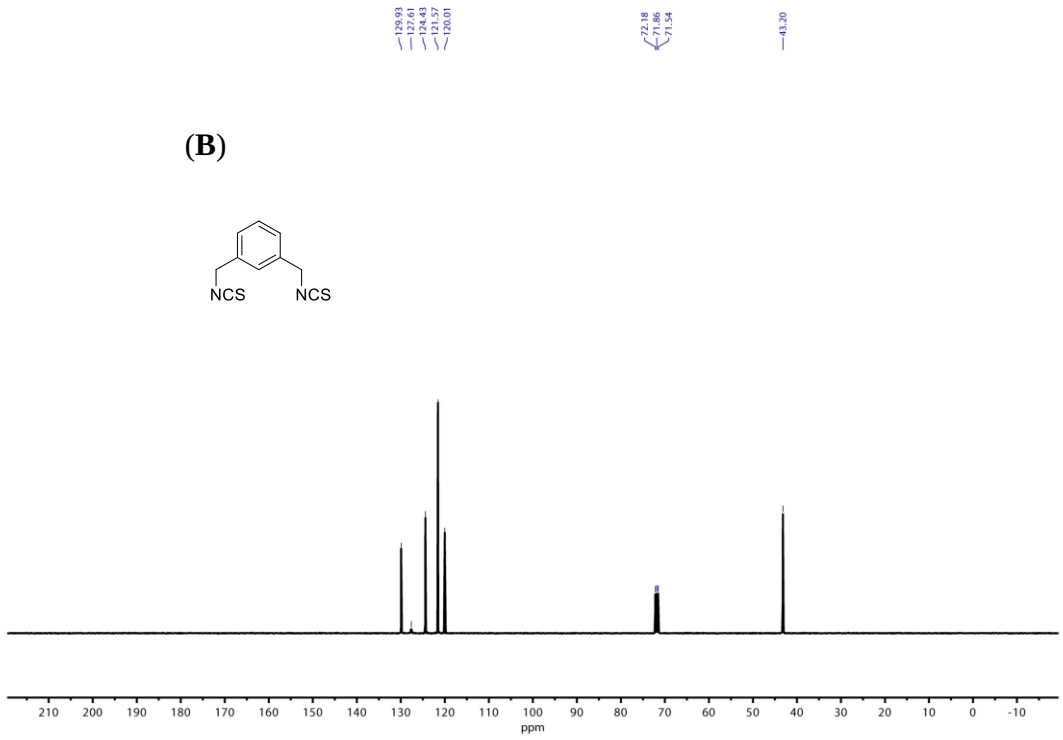

Figure 4.21. ^{1}H NMR (A) and ^{13}C NMR (B) spectra of 1,3-bis(isothiocyanatomethyl)benzene in the $CDCl_3$ solvent.

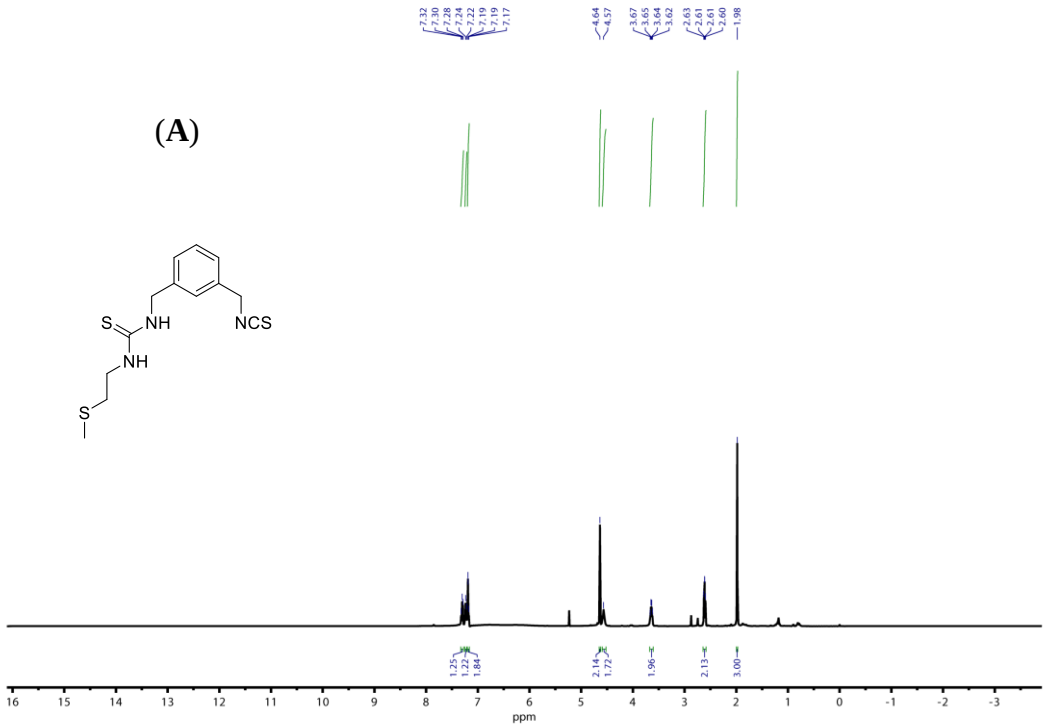

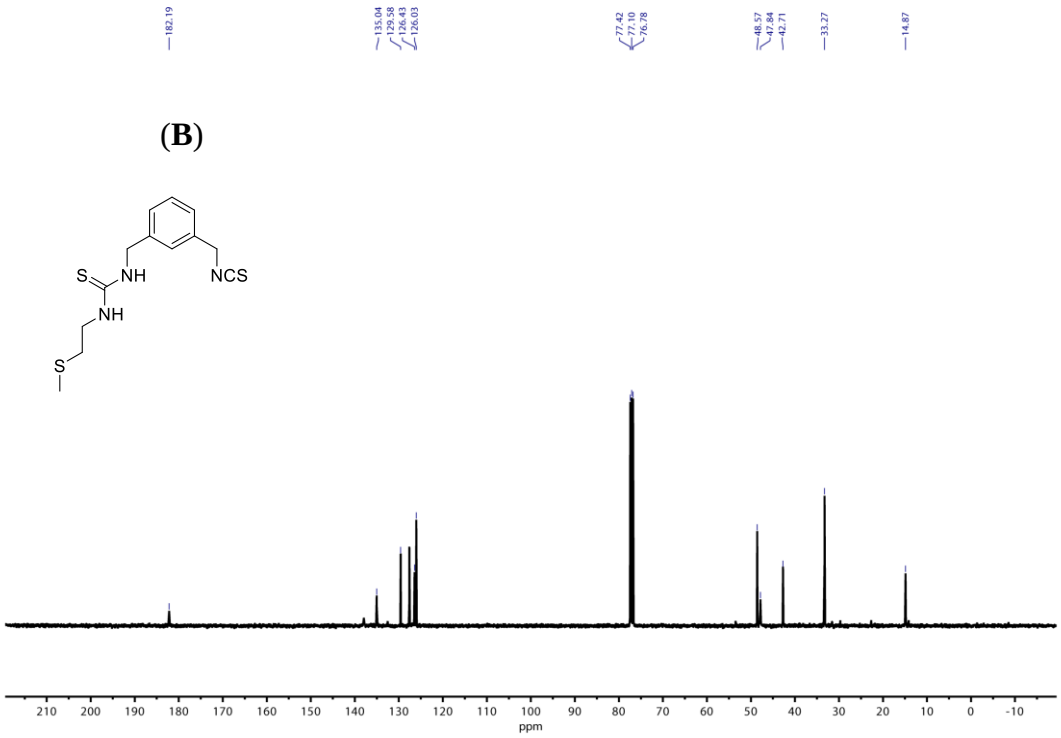

Figure 4.22. ^{1}H NMR (A) and ^{13}C NMR (B) spectra of compound 1-(3- (isothiocyanatomethyl)benzyl)-3-(2-(methylthio)-ethyl)-thiourea in the $CDCl_3$ solvent.

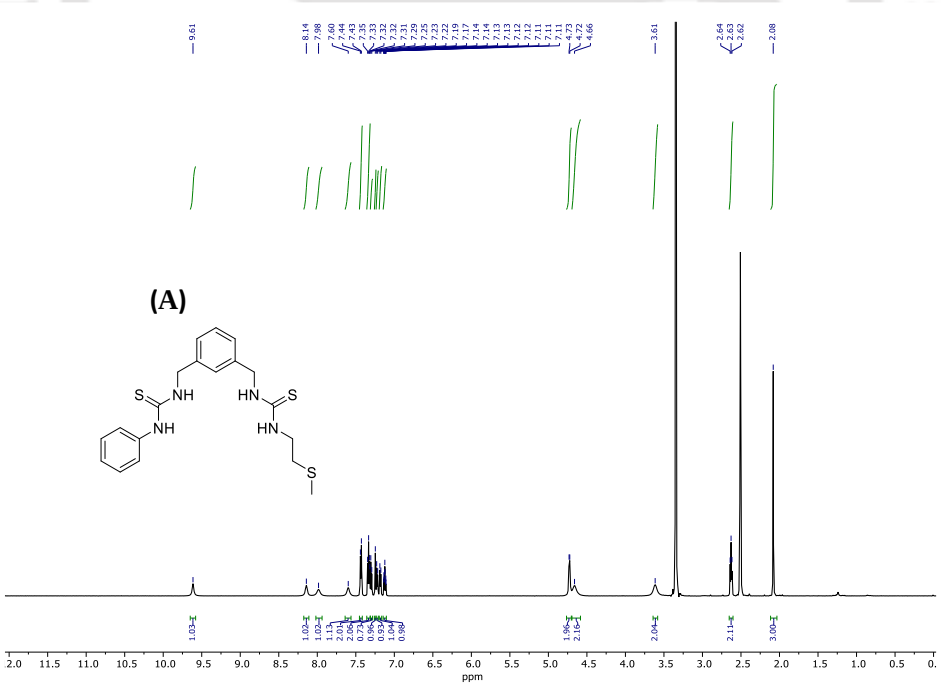

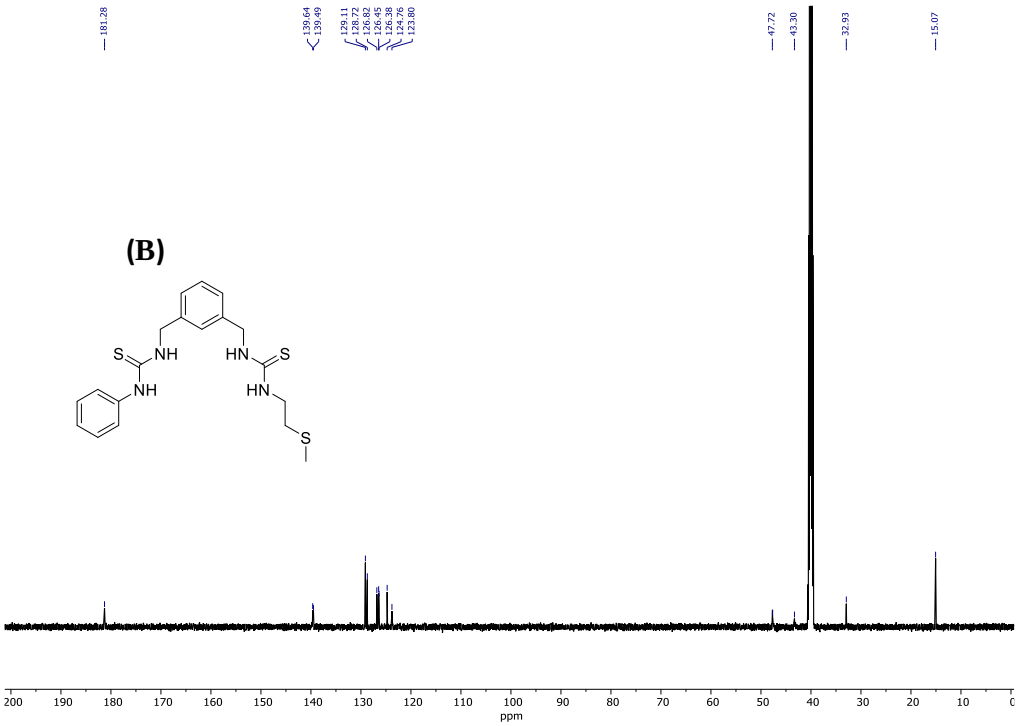

Figure 4.23. ^{1}H NMR (A) and ^{13}C NMR (B) spectra of compound **4.1a** in $CDCl_3$ solvent.

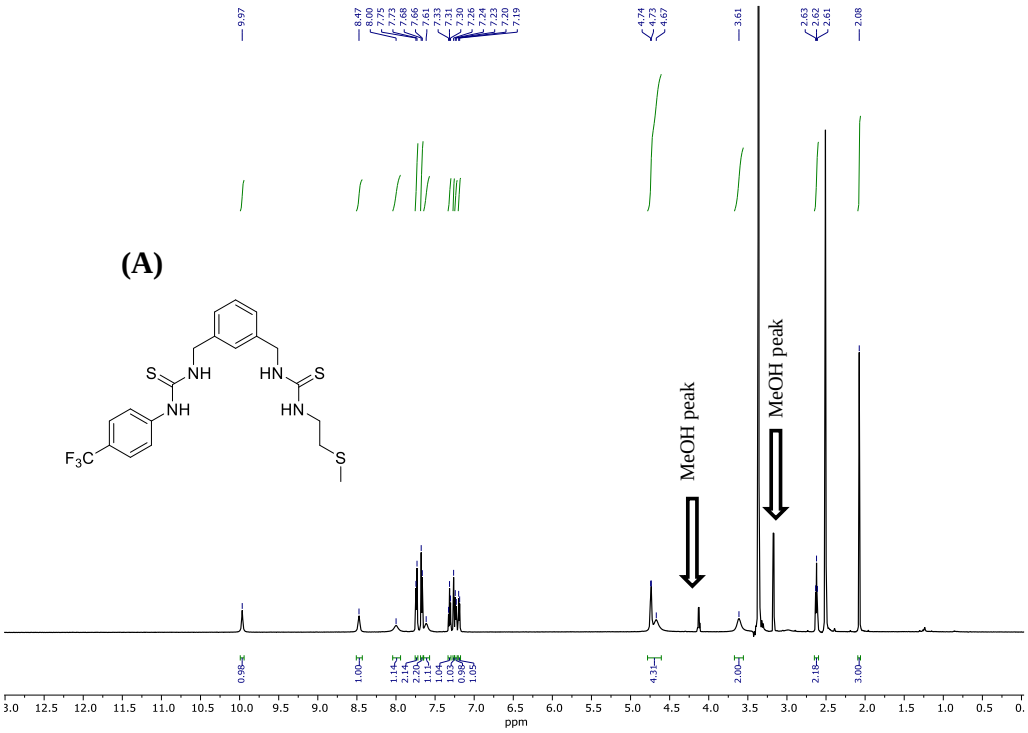

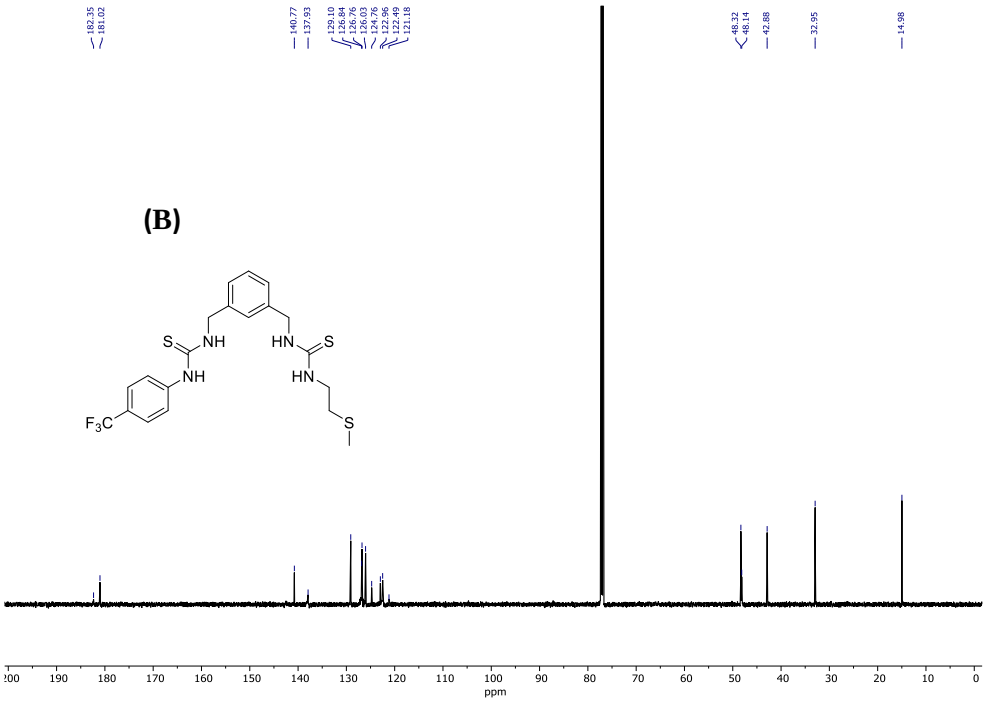

Figure 4.24. ^{1}H NMR (A) in DMSO-d_6 and ^{13}C (B) spectra of compound **4.1b** in $CDCl_3$ solvent.

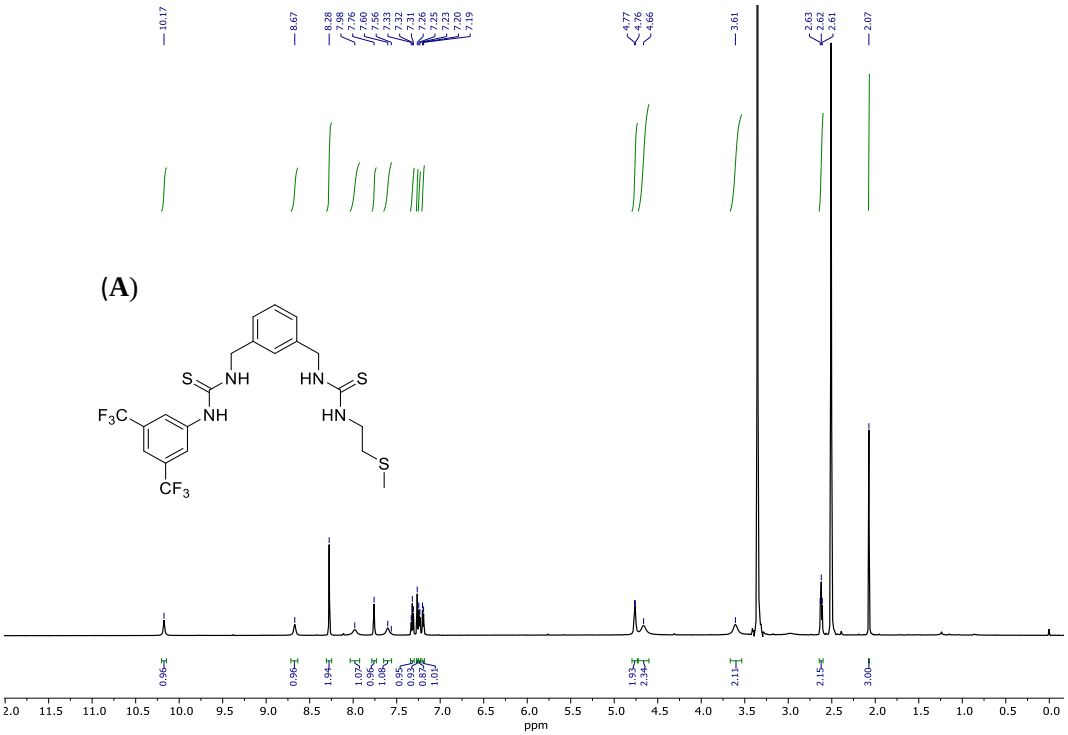

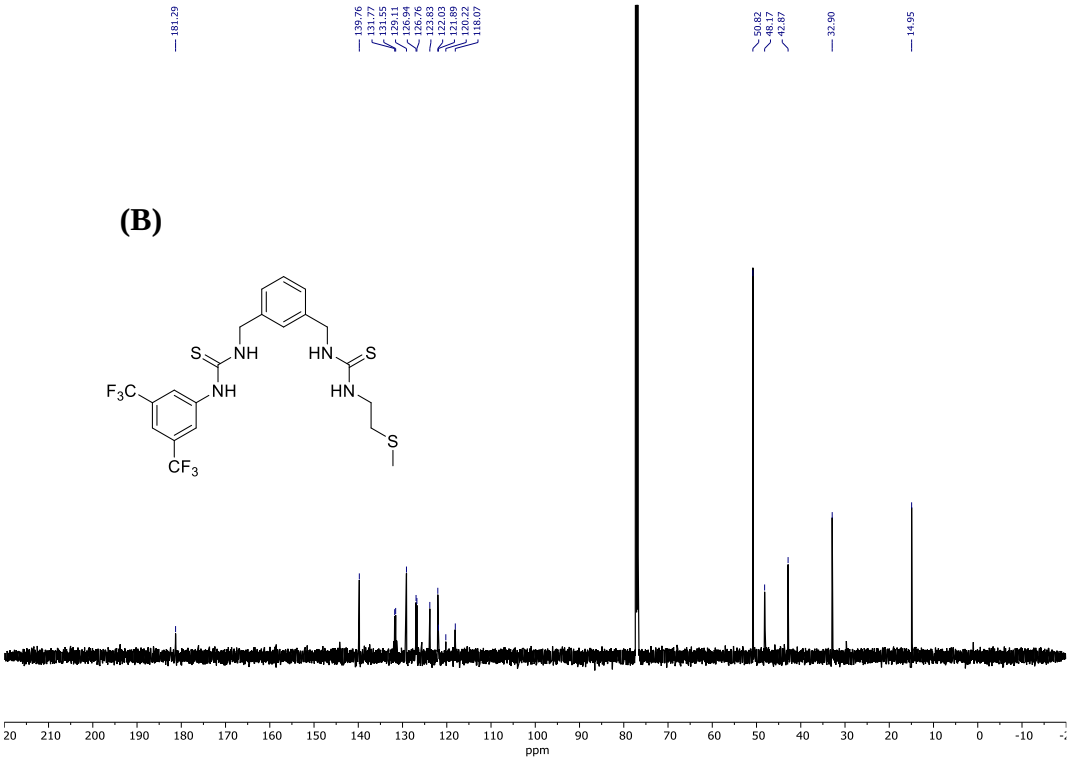

Figure 4.25. ^{1}H NMR (A) in DMSO-d_6 and ^{13}C (B) spectra of compound **4.1c** in $CDCl_3$ solvent.

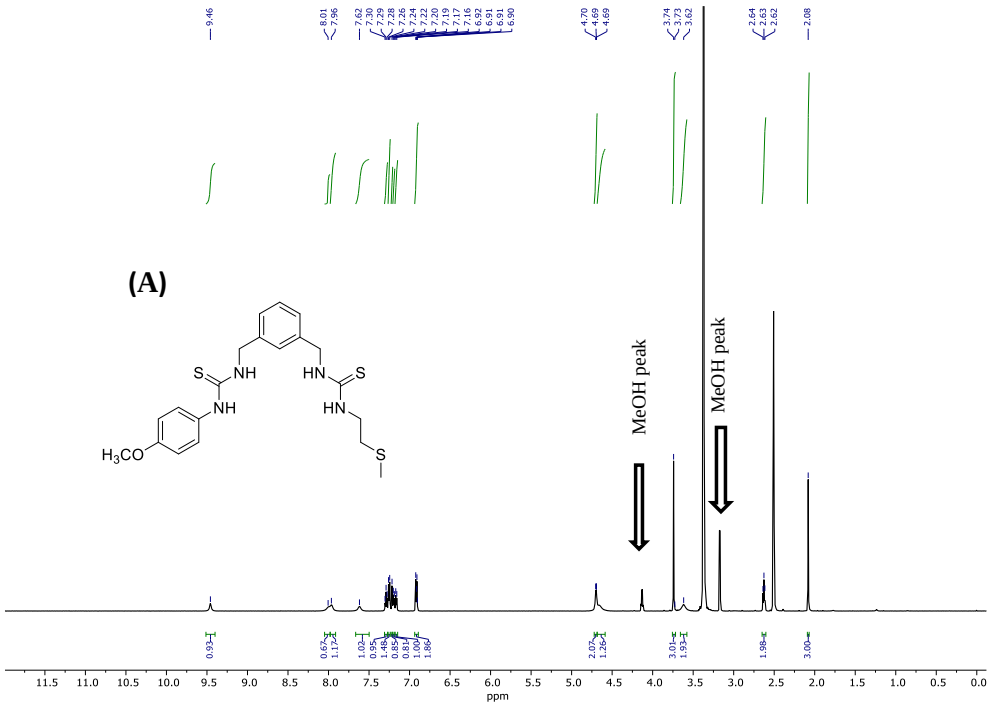

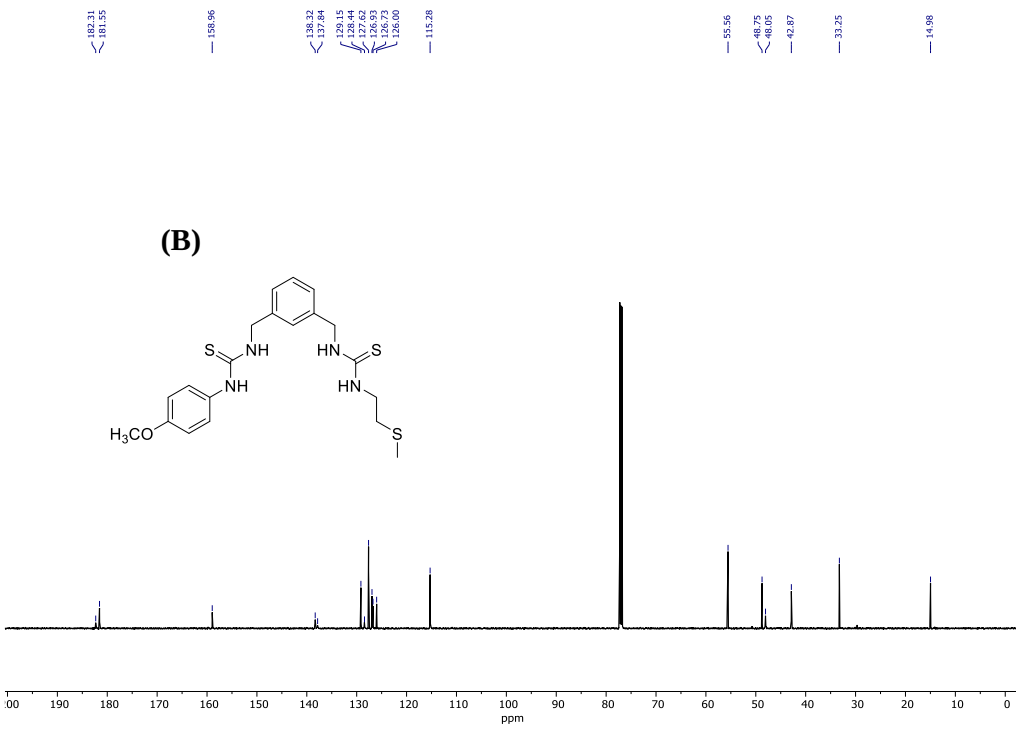

Figure 4.26. ^{1}H NMR (A) in DMSO-d_6 and ^{13}C NMR (B) spectra of compound **4.1d** in $CDCl_3$ solvent.

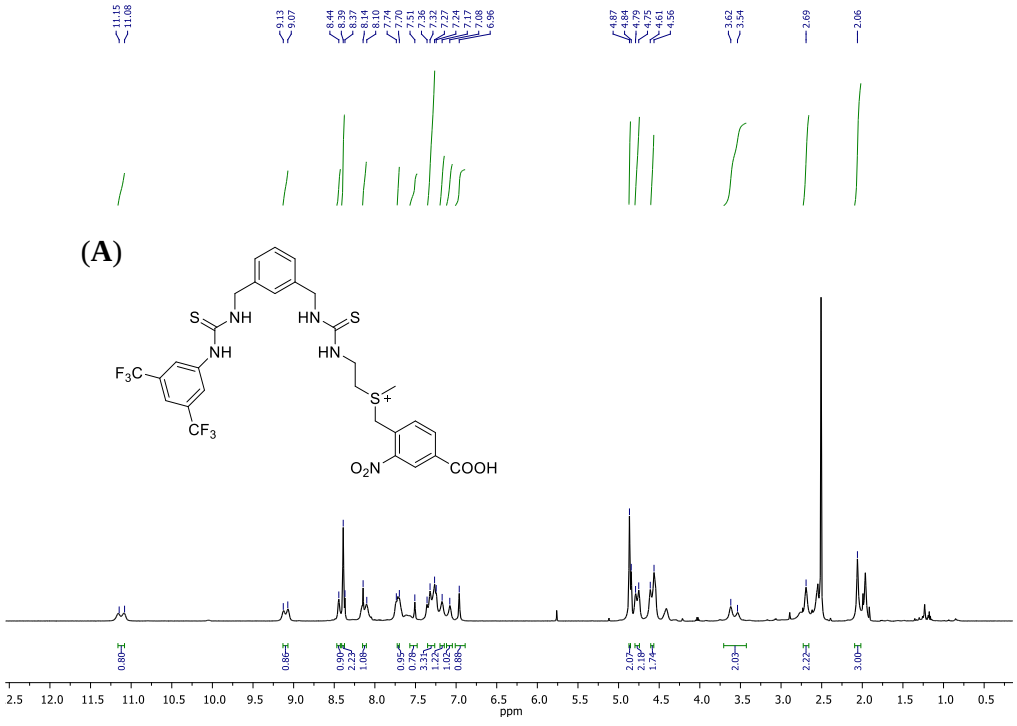

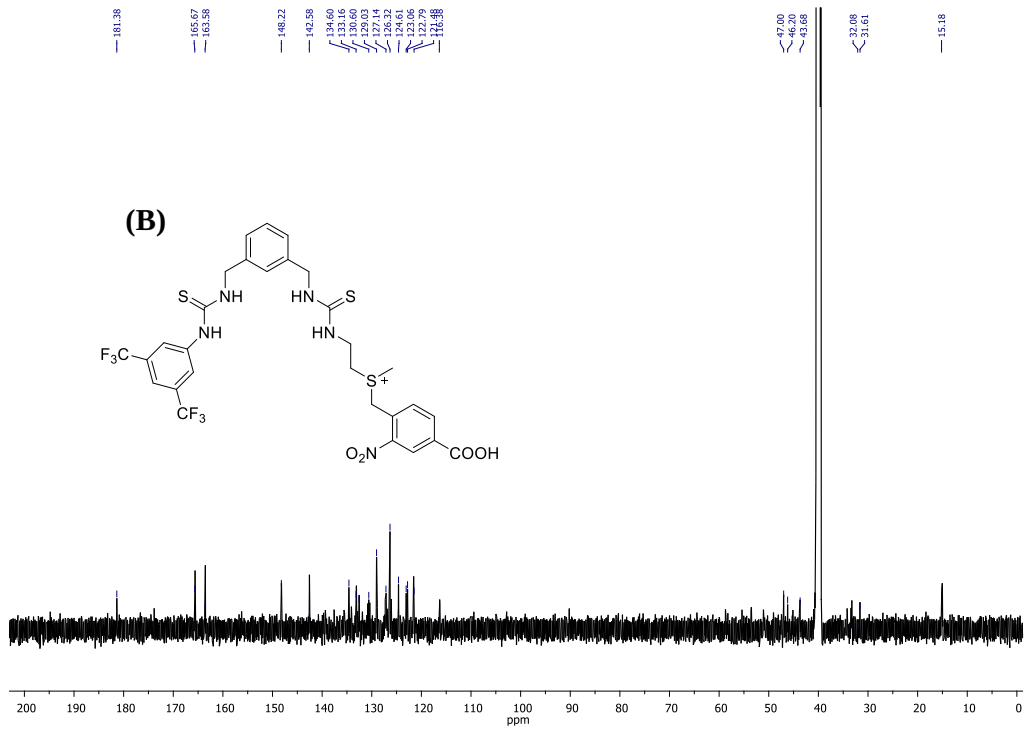

Figure 4.27. ^{1}H NMR (A) and ^{13}C (B) spectra of compound **4.2** in DMSO-d_6.

4.6. References

1. K. Fernald and M. Kurokawa, *Trends Cell Biol.*, 2013, **23**, 620-633.
2. V. Labi and M. Erlacher, *Cell Death Dis.*, 2015, **6**, 1675.
3. S. Fulda, *Int. J. Cell Biol.*, 2010, **2010**, 370835.
4. N. Akhtar, N. Pradhan, G. K. Barik, S. Chatterjee, S. Ghosh, A. Saha, P. Satpati, A. Bhattacharyya, M. K. Santra and D. Manna, *ACS Appl. Mater. Interfaces*, 2020, **12**, 25521-25533.
5. N. Akhtar, O. Biswas and D. Manna, *Chem. Commun.*, 2020, DOI: 10.1039/D0CC05489E
6. A. Bansal and M. C. Simon, *J. Cell Biol.*, 2018, **217**, 2291-2298.
7. N. Akhtar, A. Saha, V. Kumar, N. Pradhan, S. Panda, S. Morla, S. Kumar and D. Manna, *ACS Appl. Mater. Interfaces*, 2018, **10**, 33803-33813.
8. T. Saha, M. S. Hossain, D. Saha, M. Lahiri and P. Talukdar, *J. Am. Chem. Soc.*, 2016, **138**, 7558-7567.
9. S. B. Salunke, J. A. Malla and P. Talukdar, *Angew. Chem. Int. Ed.*, 2019, **58**, 5354-5358.

10. S. V. Shinde and P. Talukdar, Org. Biomol. *Chem.*, 2019, **17**, 4483-4490.

11. E. N. W. Howe and P. A. Gale, J. Am. *Chem. Soc.*, 2019, **141**, 10654-10660.

12. H. Li, H. Valkenier, A. G. Thorne, C. M. Dias, J. A. Cooper, M. Kieffer, N. Busschaert, P. A. Gale, D. N. Sheppard and A. P. Davis, *Chem. Sci.*, 2019, **10**, 9663-9672.

13. R. Montis, A. Bencini, S. J. Coles, L. Conti, L. Fusaro, P. A. Gale, C. Giorgi, P. N. Horton, V. Lippolis, L. K. Mapp and C. Caltagirone, *Chem. Commun.*, 2019, **55**, 2745-2748.

14. M. J. Spooner, H. Li, I. Marques, P. M. R. Costa, X. Wu, E. N. W. Howe, N. Busschaert, S. J. Moore, M. E. Light, D. N. Sheppard, V. Felix and P. A. Gale, *Chem. Sci.*, 2019, **10**, 1976-1985.

15. X. Wu, J. R. Small, A. Cataldo, A. M. Withecombe, P. Turner and P. A. Gale, *Angew. Chem. Int. Ed.*, 2019, **58**, 15142-15147.

16. S. Zhang, Y. Wang, W. Xie, E. N. W. Howe, N. Busschaert, A. Sauvat, M. Leduc, L. C. Gomes-da-Silva, G. Chen, I. Martins, X. Deng, L. Maiuri, O. Kepp, T. Soussi, P. A. Gale, N. Zamzami and G. Kroemer, *Cell Death Dis.*, 2019, **10**, 242.

17. O. Biswas, N. Akhtar, Y. Vashi, A. Saha, V. Kumar, S. Pal, S. Kumar and D. Manna, *ACS Appl. Bio. Mater.*, 2020, **3**, 935-944.

18. A. Saha, N. Akhtar, V. Kumar, S. Kumar, H. K. Srivastava, S. Kumar and D. Manna, *Org. Biomol. Chem.*, 2019, **17**, 5779-5788.

19. N. Akhtar, N. Pradhan, A. Saha, V. Kumar, O. Biswas, S. Dey, M. Shah, S. Kumar and D. Manna, *Chem. Commun.*, 2019, **55**, 8482-8485.

20. B. Diaz de Grenu, P. Iglesias Hernandez, M. Espona, D. Quinonero, M. E. Light, T. Torroba, R. Perez-Tomas and R. Quesada, *Chem.*, 2011, **17**, 14074-14083.

21. S. Cournoyer, A. Addioui, A. Belounis, M. Beaunoyer, C. Nyalendo, R. Le Gall, P. Teira, E. Haddad, G. Vassal and H. Sartelet, *BMC cancer*, 2019, **19**, 1018.

22. J. A. Malla, R. M. Umesh, S. Yousf, S. Mane, S. Sharma, M. Lahiri and P. Talukdar, *Angew. Chem. Int. Ed.*, 2020, **59**, 7944-7952.

23. M. A. Inlay, V. Choe, S. Bharathi, N. B. Fernhoff, J. R. B. Jr., I. L. Weissman and S. K. Choi, *Chem. Commun.*, 2013, **49**, 4971-4973.

24. C. Fowley, N. Nomikou, A. P. McHale, B. McCaughan and J. F. Callan, *Chem. Commun.*, 2013, **49**, 8934-8936.

25. S. Dey, A. Patel, K. Raina, N. Pradhan, O. Biswas, R. P. Thummer and D. Manna, *Chem. Commun.*, 2020, **56**, 1661-1664

26. D. Wang, M. Yu, N. Liu, C. Lian, Z. Hou, R. Wang, R. Zhao, W. Li, Y. Jiang, X. Shi, S. Li, F. Yin and Z. Li, *Chem. Sci.*, 2019, **10**, 4966-4972.

27. R. Nathani, P. Moody, M. E. Smith, R. J. Fitzmaurice and S. Caddick, *Chembiochem*, 2012, **13**, 1283-1285.

5. Thesis conclusions

In this thesis, we have fruitfully defined various prospects of anionophore research. Additionally, concise literature on the biologically active anionophores has also been documented in **Chapter 1**. Inspired by the numerous prospects of anionophore, the artificial anionophores have shown effectiveness in specifically targeting both cancerous and non-cancerous cells, in **Chapter 2** we developed a new class of amino acid based (tryptophan-based) derivatives and we hypothesize that the amino acid scaffold already a biologically relevant molecule which may mute the toxicity towards the normal cells. The tryptophan based receptors selectively transport the Cl^- ions across the lipid bilayer. The tryptophan-based transporters have valuable insights into the development of novel therapeutic agents, especially in addressing ion transport-related challenges. We propose that these tryptophan-based transporters hold significant promise for designing innovative solutions to ion transport-related disorders. In **Chapter 3**, to overcome the limitation of classical anionophores we developed a 4-aminoquinazoline analogue selectively transports Cl^- across the lipid bilayers via a carrier pathway. The outcomes also revealed that the quinazoline moiety has cooperative interactions of H^+ and Cl^- ions with the thiourea moiety, resulting in the transport of H^+/Cl^- across the membranes. The pH-dependent analysis revealed that the transport of Cl^- by the potent compound increased in the acidic environment. We hypothesize that such anion-induced molecular switch could be beneficial in exploring ion transport-mediated biological activities. But still, the classical anionophores are having the problems such as deliverability and cellular uptake due to the lipophilic nature of the anionophore. So in this regard, in chapter 4, the primary motivation has been given to overcome all these traditional difficulties related with anionophore and we came up with the concept of sulphonium-based proanionophore, where the sulphonium-based proanionophore compound have been synthesized and explored their transport activity, and release studies.

Despite of significant advancements over the past two decades in the development of synthetic anionophores, challenges regarding selectivity and toxicity remain pervasive. In Chapters 2 and 3, we introduced a series of hydrophobic receptors; however, the primary drawback of these receptors was their hydrophobic nature, which limits their practical applicability. Although in Chapter 4 we addressed the solubility issues by designing a molecule responsive to glutathione (GSH), reactive oxygen species (ROS),

and light, this solution is not without its limitations. The use of GSH and ROS as internal stimuli presents a significant challenge due to their ubiquitous presence in physiological systems, which inherently lacks spatiotemporal control and thus compromises selectivity. Furthermore, the reliance on 365 nm light as an external stimulus poses another limitation. This wavelength primarily affects surface phenomena and lacks the penetrative ability to influence deeper tissues, restricting the molecule's efficacy to superficial applications.

7. Future perspectives

Research on anion transport has made significant progress in the last two decades, with potential therapeutic applications in treating cancer, cystic fibrosis, and channelopathies. However, conventional anionophores face challenges such as inadequate transportability, cellular absorption, and discrimination between cancerous and healthy cells. Scientists are now working on stimuli-responsive proanionophores to overcome these challenges. Extensive research has been conducted on molecules that transport chloride anions for potential therapeutic applications. However, it is crucial to focus on creating and investigating additional molecules that transport other ions to explore their biological functions and discover more therapeutic possibilities. It is possible for monovalent anions to fight different viruses, and it is also possible for artificial chloride ion transporter molecules to help with diseases like arrhythmogenesis, cardiac ischemia preconditioning, and heart failure. Artificial molecules that transport anions could manage anionic imbalances and prevent chronic kidney disease. Changes in the genes of some cation-chloride cotransporters (CCCs) channels can throw off the balance of chloride ions, which can cause health problems like ischemia, newborn seizures, temporal lobe epilepsy, and neuropathic pain.

Multi-stimuli controlled release of a transmembrane chloride ion carrier from a sulfonium-linked procarrier

S. Das, O. Biswas, N. Akhtar, A. Patel and D. Manna, *Org. Biomol. Chem.*, 2020, **18**, 9246 **DOI:** 10.1039/D0OB00938E

A chloride-responsive molecular switch: driving ion transport and empowering antibacterial properties

S. Das, R. Karn, M. Kumar, S. Srimayee and D. Manna, *Org. Biomol. Chem.*, 2024, **22**, 114 **DOI:** 10.1039/D3OB01826A

Publications

1. **Das, S.**; Biswas, O.; Akhtar, N.; Patel, A.; Manna, D., Multi-stimuli controlled release of a transmembrane chloride ion carrier from a sulfonium-linked procarrier. *Org. Biomol. Chem.* **2020**, 18 (45), 9246-9252.

2. Dey, S.; [+] **Das, S.;** [+] Patel, A.; [+] Raj, K. V.; Vanka, K.; Manna, D., Antimicrobial two-dimensional covalent organic nanosheets (2D-CONs) for the fast and highly efficient capture and recovery of phosphate ions from water. J. Mater. Chem. A **2022**, 10 (9), 4585-4593. (+ = Equal contribution).

3. Das, S.; Hazarika, G.; Manna, D., Guanidine-Functionalized Fluorescent sp2 Carbon-Conjugated Covalent Organic Framework for Sensing and Capture of Pd (II) and Cr (VI) Ions. *Chem. Eur. J.* **2023,** *29* (15), e202203595.

4. Patel, A.; Paul, S.; Akhtar, N.; **Das, S.**; Kar, S.; Bhattacharjee, S.; Manna, D., Onium-and Alkyl Amine-Decorated Protein Nanoparticles as Antimicrobial Agents and Carriers of Antibiotics to Promote Synergistic Antibacterial and Antibiofilm Activities. *ACS Appl. Nano Mater.* **2022,** *5* (11), 16602-16611.

5. Das, S.; Karn, R.; Kumar, M.; Srimayee, S.; Manna, D., A chloride-responsive molecular switch: driving ion transport and empowering antibacterial properties. *Org. Biomol. Chem.* **2024,** *22* (1), 114-119.

6. Hazarika, G.; **Das, S.**; Das, N. M.; Manna, D., A pH-responsive covalent organic network: morphology change leads to capture and removal of phosphate ions from water. *J. Mater. Chem. A* **2024**, 12 (30), 19559-19566.

7. Hazarika, G.; **Das, S.**; Patel, A.; Manna, D., Guanidine-Modified Cellulose Enhances Capturing and Recovery of Phosphates from Wastewater. *Available at SSRN 4731893*.

8. **Das, S.**; Manna, D., Harnessing Tryptophan-Based Molecular Vehicles for Facilitated Chloride Ion Transport across the lipid bilayers. (*Under review*).